# SYNTHESIS, MODIFICATION AND CATALYTIC EVALUATION OF MESOPOROUS MOLECULAR SIEVES

**BY**

Mr. PRASHANT RAMKRISHNA KARANDIKAR

DOCTOR OF PHILOSOPHY

(IN CHEMISTRY)

Dr. (Mrs.) ASHA J. CHANDWADKAR

(RESEARCH GUIDE)

AUGUST 2006

1

# SYNTHESIS, MODIFICATION AND CATALYTIC EVALUATION OF MESOPOROUS MOLECULAR SIEVES

A THESIS

**SUBMITTED TO THE**

UNIVERSITY OF PUNE

**FOR THE DEGREE OF**

DOCTOR OF PHILOSOPHY

**(IN CHEMISTRY)**

**BY**

Mr. PRASHANT R. KARANDIKAR

CATALYSIS DIVISION

NATIONAL CHEMICAL LABORATORY

PUNE 411008

INDIA

Dr. (Mrs.) ASHA J. CHANDWADKAR

(RESEARCH GUIDE)

AUGUST 2006

*Dedicated to*

*Mother and*

*Deodhar grandparents…*

# CERTIFICATE

Certified that the work incorporated in the thesis **"Synthesis, modification and catalytic evaluation of mesoporous molecular sieves",** submitted by **Mr. Prashant Ramkrishna Karandikar,** for the degree of **Doctor of Philosophy,** was carried out by the candidate under my supervision in Catalysis Division, National Chemical Laboratory, Pune, India. Materials obtained from other sources have been duly acknowledged in the thesis.

Dr. (Mrs.) Asha J. Chandwadkar

   (Research Guide)

# DECLARATION

I hereby declare that the thesis entitled**, "Synthesis, modification and catalytic evaluation of mesoporous molecular sieves",** submitted for the Degree of Doctor of Philosophy to the University of Pune, has been carried out by me at the National Chemical Laboratory, Pune under the supervision of Dr. (Mrs.) Asha J. Chandwadkar (Research guide). The work is original and has not been submitted in part or full by me for any other degree or diploma to this or any other University.


**(**Mr. Prashant R. Karandikar**)**

## *Acknowledgements*

*I take this opportunity to express my deep sense of gratitude to my research guide Dr. (Mrs.) Asha J. Chandwadkar, Scientist F, Inorganic and Catalysis Division, NCL, for her stimulating and invaluable guidance throughout this work. Madam's constant striving for excellence coupled with her quest for knowledge will always remain a source of inspiration for me. This thesis would not have taken its shape without her continuous efforts to encourage me towards perfection.*

*I express my profound gratitude to, Dr. Rajiv Kumar, Head of Inorganic and Catalysis Division, NCL, for providing me all the facilities required for my work.*

*It gives me a great pleasure to express my deep sense of gratitude and indebtedness to Dr. S. Sivasanker Emeritus Scientist and former Head, Inorganic and Catalysis Division, NCL, for his expert and inspiring guidance and suggestions in carrying out the research work.*

*I sincerely acknowledge Miss Mangal Agashe retired Scientist for her valuable help and suggestions in my research work.*

*I take this opportunity to thank Dr. Jeevan G. Chandwadkar for his fruitful suggestions and guidance during the presentation of scientific data in graceful manner.*

*I owe my special thanks to Dr. Srinivas, Dr. Singh, Dr. Satyanarayana, Dr. Halligudi, Dr. Dongare, Dr. Waghmare, Violet, Mrs. Jacob, Dr. Umbarkar, Dr. Belhekar, Dr. Deshpande, Dr. Pardhy, Dr. Mirajkar, Dr. Awate,, Dr. Kamble, Mr. Jha, Dr. Manikandan and my college teachers. I also thank M Purushottam, Mr. Milind, Mr. Madhu, Mr. Katti Mr. Kashinath technical staff for their help.*

*I would like to thank my friends, Bennur, Pai, Vasu, Shanbhag, Suresh, Rohit, Devu, Atul, Sachin Attarde, Ankur, Lakshi, Reddy, Rajendra, Sanker, Ganesh, Sachin, Surendran, Thiru, Kumbar, Shrikant, Santosh, Mahesh, Biju, Amit, Sangamesh, Pradeep, Upendra, Shivram, Sriprashant, Chidam, Shylesh, Ankush, Vijayraj, Pranjal,Jayprakash, Surekha, Nisha, Kala, Trissa, Dhanashri, Maitri, Suman Nevin, Neelam, Smita, Suhas and many others for their co-operation, encouragement, invaluable help and moral support rendered by them.*

*The words are not enough to express all my love and thankfulness towards my mother who was behind me at every good and bad time and inspiring me all the way. I would like to express my deep felt gratitude to my relatives. I could not have completed my research work without their help and blessings. I also like to thank my friends Sachin, Satish, Mahesh, Sadanand and Sukhada for their presence in my life.*

*I take this opportunity to thank Dr. S. Sivaram, Director, NCL, Pune, for allowing me to carry out research and providing all infrastructural facilities at NCL and to submit the work in the form of the thesis for the award of the Ph.D. degree. Finally, I would like to thank Council of Scientific and Industrial Research (CSIR), New Delhi for awarding me the research fellowship.*

*Prashant R. Karandikr*

CONTENTS

i

List of Figures:

**List of Tables:**

# Chapter-1

# Introduction and Literature Review

## 1.1 GENERAL BACKGROUND AND INTRODUCTION

During the past few decades enormous amount of reports on the synthesis, characterization and application of different types of zeolites and related microporous materials have formed an important part of material science, inorganic chemistry and heterogeneous catalysis [1]. Different architectural features of zeolites and related materials generate different types of shape selectivity e.g. product, reactant and transition state shape selectivity [2], besides, zeolites possess relatively high stability. This has lead to their wide use in the production of fine and specialty chemicals. Moreover, microporous zeolite materials have earned the reputation of environmentally benign catalysts due to several factors like waste minimization, simple operations, easy work-up and recyclibility of the catalysts [3].

Till 1990, heterogeneous catalysts developed with zeolite base were of pore size less than 10 Å and consequently the reactant molecules trapped and transformed inside them were also small. Hence, there has been an ever-growing interest in expanding the pore sizes of these zeolite materials from the micropore region to mesopore region. In order to maintain the remarkable catalytic properties of the zeolites while expanding their use to process bulkier molecules, new synthesis routes have been undertaken to increase the pore diameters.

According to IUPAC definition [4] porous materials may be divided in to three types based on their pore dimensions:

| Type | | Pore diameter (Å) |
|------|---|-------------------|
| Microporous | : | < 20 |
| Mesoporous | : | 20-500 |
| Macroporous | : | > 500 |

Researchers have taken significant efforts to synthesize mesoporous materials such as silicas [5] transitional aluminas [6] or pillared clays and silicates [7, 8] but the pores in these materials are generally irregularly spaced and broadly distributed in size.

The synthesis of surfactant-templated mesostructure is one of the most exciting discoveries in the field of materials research in the last decade [9]. The discovery of hexagonally ordered mesoporous silicate structures by Mobil Corporation M41S materials [9a, b] and by Kuroda et al. (FSM-16 materials) [9c, d] pioneered a new era in materials science. The M41S type mesoporous materials are classified in to three categories: MCM-

41, MCM-48 and MCM-50, with hexagonal, cubic and lamellar structures, respectively [9 a, b]. These mesoporous silicate and aluminosilicate materials, are of great interest because they have well defined pore size of 20-100 Å, very high surface area (> 800 $m^2$/g) and the pore size can be controlled effectively. The understanding about the synthesis of these materials and the corresponding mechanism has opened up a new era of molecular engineering. The outstanding feature of the preparation of these materials is the role of self-assembled surfactant molecular array around which the main structure is built up. These surfactants are large organic molecules having a long hydrophobic tail of variable length [e.g. alkyltrimethylammonium cations with formula $C_nH_{2n+1}(CH_3)_3N^+$, where n > 8] and a hydrophilic head.

## 1.2. FORMATION MECHANISM OF MESOPOROUS SILICA

A number of models have been proposed to rationalize the mechanism of formation of mesoporous materials by various synthesis routes. All these models are based on the role of surfactants in solution to direct the formation of silicate mesostructures. The surfactants have a hydrophilic head group and a long chain hydrophobic tail group within the same molecule. In solution, these will aggregate and self organize in such a way as to minimize the contact between the incompatible ends. Different types of interactions between the surfactant and the inorganic precursor under different synthesis conditions leads to different postulates for the mechanism of formation of mesoporous materials.

### 1.2.1. Liquid Crystal Templating (LCT) Mechanism

The researchers of Mobil Corporation proposed a 'liquid crystal templating (LCT) mechanism' to explain the formation of M41S type mesoporous materials [9a, b]. The mesostructure formation depends on the hydrocarbon chain length of the surfactant tail group [10], the effect of variation of surfactant concentration and the additional organic swelling agents. The lowest concentration at which surfactant molecules aggregate to form spherical isotropic micelles is called critical micelle concentration (CMC1). Further increase in the surfactant concentration initiates aggregation of spherical into cylindrical or rod-like micelles (CMC2). There are three main liquid crystalline phases with hexagonal, cubic and lamellar structure. The hexagonal phase is the result of hexagonal packing of cylindrical

micelles, the lamellar phase corresponds to the formation of surfactant bilayers and the cubic phase regarded as a bicontinuous structure.

Two possible pathways have been proposed [9 b] for the LCT mechanism which is schematically shown in Fig. 1.1. In the first pathway, it is considered that first there is a formation of surfactant hexagonal liquid crystal phase around which the growth of the inorganic materials is directed. The $C_nH_{2n+1}(CH_3)_3N^+$ surfactant micelles aggregate to form hexagonal arrays of rods. Silicate anions present in the reaction mixture interact with surfactant cationic head groups. Condensation of the silicate species leads to the formation of an inorganic polymer.

On calcination, the organic template is burnt off, leaving inorganic hollow cylinders in hexagonal arrangement. However, this pathway did not get much support in the literature. It has been observed that at lower concentrations only micelles exist in solution [11]. Moreover, in situ $^{14}$N NMR spectra revealed that the hexagonal liquid crystalline phase of CTMA ions was not present at any time during MCM-41 formation. Thus the first synthesis scheme proposed by Beck et al. [9 a] has been abandoned (Fig. 1.1.)
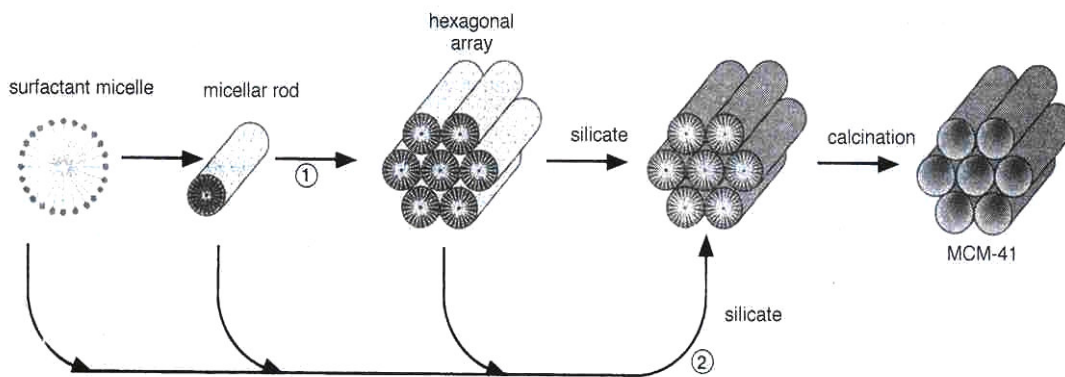


Fig. 1.1. Two possible pathways for the LCT mechanism.

In the second pathway, it has been proposed that the randomly ordered rod like micelles interact with silicate species by coulombic interaction in the reaction mixture to produce approximately two or three monolayers of silicate around the external surface of the micelles. These randomly ordered composite species spontaneously pack in to highly ordered mesoporous phase with an energetically favorable hexagonal arrangement, accompanied by silicate condensation. With the increase in heating time, the inorganic wall continues to condense. The investigation on the formation mechanism [12, 13] using XRD,

^{29}Si NMR, in situ ^{14}N NMR and thermogravimetric analysis (TGA) proves the absence of hexagonal liquid crystalline mesophase, either in the synthesis gel or in the surfactant solution used as template. It was therefore concluded that the formation of MCM-41 phase is possibly via pathway 2 rather than pathway 1 (Fig. 1.1.).

### 1.2.2. Silicate Rod Assembly

Davis and co-workers [12] found that the hexagonal liquid crystalline phase did not develop during MCM-41 synthesis, based on in situ ^{14}N NMR spectroscopy. They proposed that, under the synthesis condition reported by Mobil, the formation of MCM-41 began with the deposition of two to three monolayer of silicate precursor on to isolated surfactant miceller rods (Fig. 1.2.). The silicate–encapsulated rods were randomly ordered, eventually into a hexagonal mesostructure. Heating and aging completed the condensation of the silicates into the as-synthesized MCM-41 mesostructure.
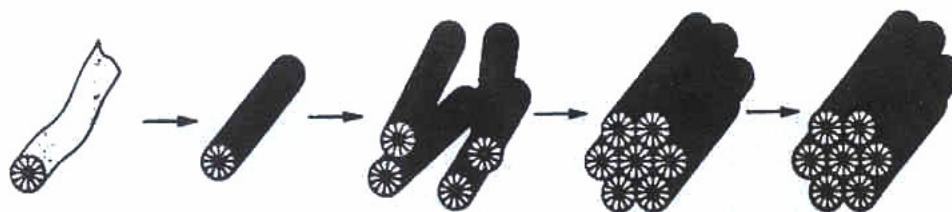


Fig. 1.2. Assembly of silicate encapsulated rods [Source Ref. 12].

### 1.2.3. Folded Sheet Mechanism

Yanagisawa et.al [9 c] and Inagaki et.al [9 d] synthesized crystalline mesoporous silicate and aluminosilicate materials designated as FSM-16 (Folded Sheet Mesoporous Materials). They proposed a folded sheet mechanism for the formation of mesostructure derived from kanemite, a type of hydrated Na silicate composed of single-layered silica sheets.

After the surfactants were ion- exchanged into the layered structure, the silicate sheets were thought to fold around the surfactants and condense into a hexagonal mesostructure (Fig. 1.3). The final product was claimed to be very similar to MCM-41, with no resemblance to the original kanemite structure.
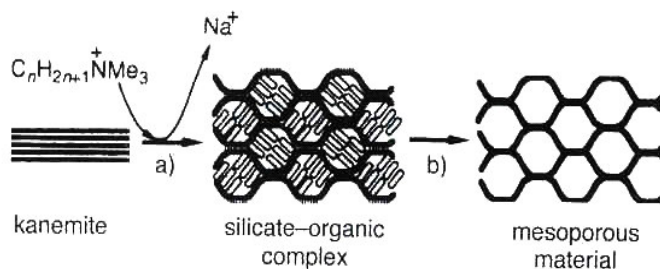
Fig. 1.3. Folding of silicate sheets around intercalated surfactant molecules. a) Ion-exchange, b) Calcination [Source Ref. 9 c].

## 1.3. SYNTHESIS OF MESOPOROUS MOLECULAR SIEVES OF THE TYPE M41S

Different synthesis strategies have been proposed and successfully used to prepare mesostructures with a unique pore size distribution. Similar to zeolite and molecular sieve synthesis, mesoporous molecular sieves can be synthesized hydrothermally by mixing surfactants, silica and/or silica-alumina source to form a gel while maintaining the mixture at a temperature between 70-150$^{\circ}$ C for a fixed period of time. Surfactant molecules function as templates forming an ordered organic-inorganic composite material [10]. The product obtained after crystallization is filtered, washed with water and dried at ambient temperature. Surfactant molecules are removed by calcination leaving a porous silicate/aluminosilicate network.

The structure and pore diameter of mesoporous materials can be altered by varying the surfactant/$SiO_2$ ratio [9 b]. It has been found that as the surfactant/$SiO_2$ molar ratio is increased, different siliceous products are obtained which could be grouped in to four categories [14]:

Table 1.1. Classification of Mesoporous Molecular Sieves.

| Surfactant/Silica | Phase |
|---|---|
| <1.0 | Hexagonal |
| 1.0-1.5 | Cubic (MCM-48) |
| 1.2-2.0 | Thermally unstable materials |
| 2.0 | Cubic octamer $[(CTMA)SiO_{2.5}]_8$ |

The pore diameter (20 to 100 Å) of MCM-41 materials can be controlled by three different methods: (i) by varying the chain length of alkyl group (8-22 C atoms) of surfactants [9 b, 15], (ii) by adding auxiliary chemicals (viz. 1,2,5 trimethyl benzene) which dissolve in the hydrophobic region of the micelles, thus increasing their size or (iii) by varying aging conditions (viz. temperature and aging period) [16]. The pore diameter of MCM-41 also depends on other factors such as temperature, pH and crystallization time [17, 18].

Since the first report of MCM-41 synthesis in alkaline medium appeared, [9 a, b, 15] a number of patents and publications on the synthesis of MCM-41 have been reported [18-23]. Huo et al. [24, 25] reported the synthesis of mesoporous silica under acidic conditions, while Tanev and Pinnavaia [26] proposed a neutral templating synthesis mechanism based on hydrogen bonding between primary amines and neutral inorganic species (Table 1.1.). Mesoporous materials obtained from neutral templating mechanism are named as 'hexagonal mesoporous silica' (HMS).

## 1.4. MODIFICATION OF MESOPOROUS SILICA

Pure siliceous MCM-41 (Si-MCM-41) mesoporous materials are electrically neutral, which limits their catalytic applications. In order to provide a specific catalytic activity to the chemically inert silicate framework, researchers have incorporated a variety of metals complexes and metal nanoparticles into the walls of mesostructures either by direct synthesis, ion exchange, impregnation or grafting.

### 1.4.1. Immobilization of transition metal complexes

The selective oxidation of aromatic compounds is still a challenge in chemical industry and catalysis research. The oxidation of aromatic compounds by chromate and permanganate oxidants leads to severe environmental problems [27]. The development of catalytic methods involving clean oxidants to carry out selective oxidation of aromatics is thus of great practical interest. Several homogeneous catalytic methods including methyltrioxorhenium [28, 29] and metalloporphyrin catalysts [30] have been developed.

Enzymes are natural catalysts, well known for their high selectivity and mild operating temperature. This has lead to a growing interest in their utilization as catalysts in the chemical processes. Due to the similarity with the active centers of oxidation enzymes like cytochrome P-450, transition metal porphyrin and phthalocyanine complexes are useful industrial homogeneous catalysts. $Cu^{n+}$ and $Fe^{n+}$ are predominantly contained in metalloenzymes that play an important role in biological dioxygen metabolism [31]. Several model complexes containing porphyrin and schiff base ligands have been synthesized and studied for their oxygen uptake and oxidative catalysis [32-34]. The fixation of biologically active species on to inorganic materials combines the high selectivity of enzymatic reactions with the chemical and mechanical properties of the support. When compared to homogenous catalysts, heterogeneous systems present many advantages such as easy separation and recovery of the catalyst from the reaction media, increase in the stability of catalytic species and protection against catalyst destruction. Hence the combination of the versatile metalloporphyrin homogenous system with the advantages of heterogeneous catalysis has enabled major advances in this area [35-38].

### 1.4.1.1. Grafting of the transition metal complexes

Grafting refers to post synthesis modification of the pores of mesoporous silica, where the organic functional groups are introduced as terminal groups of an organic monolayer [39]. The large concentration of surface silanol groups $[(-SiO)_3Si-OH]$ present in mosoporous silica can be utilized as convenient moieties for anchoring of organic functional groups [40]. At typical calcination temperatures ($\sim 500$ $^oC$), several surface silanol groups are lost after condensation of unreacted silanol groups. However, it is necessary to maintain a large concentration of surface silanol groups after calcination, if a high coverage of organic functional groups on the surface is desired. There are varieties of methodologies by which silica can be modified with organic functionalities. Three main

methods can be mentioned in which functional groups are attached to the silica surface: (i) through reaction between organosilanes or organic molecules and silica surface functions, (ii) chlorination of silica surface followed by reaction of the –(Si-Cl) moiety with an appropriate functional molecule/reactant, (iii) incorporation of functional groups via. sol-gel methodology followed by post modification.

The modification of surface silanol groups using organo functionalized silanes and forming a Si-O-Si bond can be achieved by two ways. In the first, trialkoxy silanes react with the silanol groups liberating the corresponding alcohol [41]. In the second method developed by Kirkland and DeStefano, [42] 3-chloropropylsilane moiety reacts with the silanol functional group, thus liberating HCl.

Over the past decade there have been several significant developments in the use of organically modified silicas as catalysts in the variety of organic synthesis. Macquarrie and coworkers developed solid based catalysts which use simple aminopropyl functionalized silica materials [43, 44]. The modified silica surface of mesopores has a covering of organic nonfunctional part (functioning as a spacer) to which transition metal complexes can be attached. These exhibit good oxidative character [45-47]. Chisem et al. developed a catalyst which uses silica supported schiff base chromium complex. The schiff base ligand is formed using aminopropyltriethoxy silane and salicyaldehyde [47]. The catalyst exhibits high rates of ethylbenzene oxidation. Sutra and Brunel [48] attached Mn(III) Schiff-base complex (Mn-salen) to an MCM-41 surface modified with 3-chloropropylsilane moiety. In this type of reaction, HCl is produced and quaternization of amine can occur as side reaction. Liu et al. [49] anchored ruthenium porphyrene on the aminomodified MCM-41 and found high product turnover for the oxidation of alkenes. Balkus and co-workers [50] functionalized MCM-41 with cobalt complexing ligands [ethylenediamine, diethylenetriamine and ethylenediaminetriacetic acid (EDT)] and EDT complexed metal centers were shown to be redox active. Dimeric μ-oxo iron tetrasulphophthalocyanine grafted on to amino modified MCM-41 proved to be selective catalyst for the oxidation of 2-methylnaphthalene to 2-methylnaphthaquinone [43].

### 1.4.1.2. Impregnation of transition metal complexes

During 1970's extensive research was devoted to impregnating insoluble solid support with homogeneous catalysts. Adsorption of Mn(III) tetra cationic porphyrin on silica was first reported by Battion et al. [51] and the resulting adsorbed transition metal complex phase was found more effective for olefin oxidation and alkane hydroxylation than the corresponding soluble Mn-porphyrin emphasizing the beneficial effect of silica support.

The metal complexes are known to be very active homogeneous catalysts but when immobilized in to the zeolite materials acquire special properties due to the site isolation. Moreover in zeolite voids the complex has a unique configuration, which may differ from that existing in solution and acquire new catalytic properties. For example in order to obtain a better isolation of catalytic sites, Romanovsky performed the immobilization of transition metal phthalocyanine inside the microporous system of zeolites using the ship-in bottle procedure [52]. This approach has been then widely followed by several authors for other macrocyclic tetradentate or pentadentate ligands such as salen- and salophen- type ligands [53, 54]. The physical encapsulation of metal complexes in the zeolite super cages could also be performed by templating the zeolite along with the metal complex as reported by Balkus et al. [55].

Due to restricted size of pores and cavities in these zeolites, the maximum size of the complexes which can be accommodated seems to be limited [56]. But MCM-41 type materials with their tunable pore size offer the potential of immobilizing larger size metal phthalocyanine. Ernst et al. [57] reported immobilization of catalytically active transition metal complexes viz. CuPc and FePc in the pores of MCM-41 and the catalyst was used for oxidation of n-hexane.

### 1.4.1.3. Incorporation of metal nanowires

During the last few decades a substantial amount of research has been aimed towards the synthesis and size-dependent physicochemical properties of nanoparticles because of their enormous importance in a variety of applications, viz. catalysis, [58], optoelectronics [59], biomineralization [60], as electron microscopy markers [61] and DNA sequence determination [62]. A number of reports are available on the synthesis of nanoparticles by different methods like sol-gel method [63], sonochemical method [64], reflux method [65], γ-irradiation method [66], chemical reduction method [67] and pulse sonoelectrochemical method [68]. It is observed that, bare metal nanoparticles are unstable.

Therefore, stabilizers like polymer matrix are added to improve their stability for further applications [69].

Today, advanced technology requires preparation of nanosystems with specified size and morphology of particles. Controlled synthesis of nanomaterial could be performed by several techniques, and all of them involve use of confined geometry system as nanoreactors. Usually, a nanoreactor is formed by colloidal species, such as in Langmuir-Blodgett films, self-assembling multilayer, reversed micelles etc. Another approach involves synthesis in solid state nanoreactors [70]. In this case nanoparticles are protected from external influence and aggregation. This method also provides high monodispersity of the particles. Mesoporous silica is commonly used as a nanoreactor due to its homogenous, regular structure of pores and high chemical resistance [9b].

Ryoo et al. [71] have prepared platinum (Pt) nanoclusters and nanowires inside the channels of mesoporous silica through consecutive ion exchange, impregnation and thermal reduction of Pt(II). Schuth et al. [72] have synthesized monodispersed palladium (Pd) nanoclusters by reduction of Pd (II) in presence of phenanthroline stabilizers, followed by incipient wetness impregnation in to the mesoporous host. Advantage of template method is that it provides good control over the size and shape of the nanowires and can be used to prepare the nanomaterials with desired aspect ratio [73]. Optical properties of germanium semiconducting nanowires and GaAs confined in pores of MCM-41 have been well studied by Leon et al. [74] and Srdanov et al. [75]. These quantum wires are well ordered and separated by silica walls of MCM-41. Due to optical transparency of host material such inclusion of metal or semiconductor in matrix can produce good material for optoelectronic devices. Similar to semiconducting nanowires, there are also reports on formation of metallic nanowires inside zeolite matrix [76]. Noble metal nanowires inside cubic MCM-48, hexagonal MCM-41 [77] and SBA-15 [78] have also been reported. These highly ordered mesoporous materials due to their distribution of pore sizes can control the growth, direction and the diameters of nanowires. Isolated nanowires can be easily obtained by treating the mesoporous silicas with HF.

## 1.5. SYNTHESIS OF MESOPOROUS SILICA THROUGH ECO-FRIENDLY, ECONOMICAL ROUTE

The synthesis of mesoporous silica materials using surfactants as templates has been studied extensively since 1992 [9a, 79]. So far surfactants, ionic [9b, 24] or neutral [80, 81] have been the most commonly used templates for directing the formation of mesopores. All the ionic pathways are based on charge matching between the ionic surfactants and ionic inorganic precursors through electrostatic interactions. For the neutral surfactants, it is suggested that hydrogen bonding between the surfactants and the precursors directs the formation of mesostructures. The preparation of mesoporous silica via neutral route has advantage over electrostatic route because of the easy removal of the surfactants by solvent extraction and the tendency to form material with thicker walls and smaller particle size. The second advantage is that these are relatively inexpensive, environmentally compatible and biodegradable.

A general non-surfactant route for the preparation of mesoporous silica materials with the large surface area and pore volumes via sol-gel route is reported by Wei et al. [82] and Pang et al. [83]. The optically active non-surfactant organic compounds such as D-glucose, D-maltose, dibenzoyl L-tartaric acid etc. were used as templates or pore forming agents and TEOS as source of silica. The aggregation of the template molecules and their hydrogen bonding interactions with the inorganic precursor and its sol-gel intermediates might be playing an important role in directing the mesostructure formation.

In the preparation of mesoporous silica via this neutral route, alkoxysilanes (TEOS) have usually been used as silicon source, which is rather an expensive silica precursor. In view of the diversity of real and potential applications of these materials [84-86], the design of low cost successful synthesis strategies became a challenging task. Indeed Chen and coworkers reported for the first time the use of low cost sodium silicate (as silica source) in the surfactant assisted procedure yielding mesoporous silica with an interconnected channel system MCM-48 [87]. Subsequently the use of sodium silicate as reagent has been described in a diversity of synthesis of mesoporous silicas MCM-41 [88, 89], MCM-48 [90-92], SBA-n [93, 94], MSU-X [95, 96], MSU-H [97, 98] etc. These mesoporous silica's prepared by using inexpensive silica source can be used as templates to design the mesoporous carbon material of tunable porosity.

## 1.6. SYNTHESIS OF MESOPOROUS CARBON USING MESOPOROUS SILICA AS TEMPLATE

Porous carbon with high surface areas, large pore volumes and chemical inertness are useful in many materials application areas, including water and air purification, adsorption, as a catalytic support, chromatographic columns and capacitors for energy storage [100, 101]. One way of preparing mesoporous carbon with the narrow pore size distribution involves the use of inorganic materials as templates. Ryoo et al. [102, 103] reported the first synthesis of new type of mesoscopically ordered mesoporous carbon molecular sieve CMK-1 and CMK-3 (cubic and hexagonal respectively), by carbonizing sucrose inside the pores of the cubic MCM-48 and hexagonal SBA-15 mesostructured silica materials. Fig. 1.4 shows the Schematic presentation of synthesis strategy for ordered mesoporous carbon.
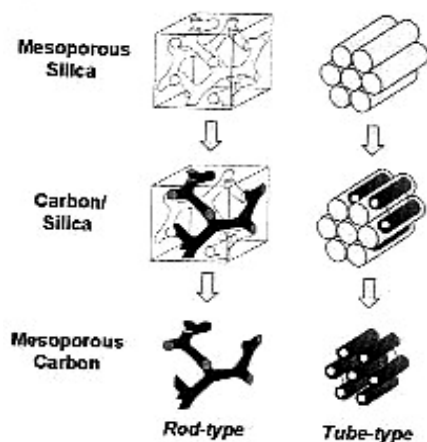


Fig. 1.4. Schematic diagram of synthesis strategy for ordered mesoporous carbon.

Furfuryl alcohol was found to be suitable as carbon precursor to synthesize hollow or fully filled cage-like silica-carbon mesostructures from SBA-16 [104] and wormhole [105], foam like [106] mesostructured carbons and mesoporous carbons with high textural porosity [107] were fabricated using mesoporous aluminosilicate, organic colloids and mesostructured HMS silica materials as templates respectively. However the materials applications of MCM-48, SBA-15 etc. have been limited partly due to relatively high costs of the reagents needed to assemble these mesophase. One of the most important research areas in the mesoporous materials is developing an inexpensive and environmentally benign

route for the fabrication of three dimensionally interconnected mesoporous materials containing large amount of textural mesopores. Because the synthesis of mesoporous carbon involves sacrificing the mesoporous silica templates the establishment of low cost for producing these mesoporous silica templates would open the way for cheap production of mesoporous carbon [108, 109].

Porous carbon has been widely used to prepare electrodes for energy storage in double layer capacitors [110-112]. The small pore size of activated carbon has imposed serious problems relating to the rate of molecule transport through the pores and thus limited the application of the carbon as electrodes in electrochemical system such as electric double layer capacitors [111, 112]. Therefore high surface area carbon materials containing regularly interconnected mesopores (> 20 Å) are highly desirable for electric double layer capacitors. In fact some compromise must be found in the meso/micro ratio as the micropores determine the high surface area on which ions are adsorbed and mesopores are essential for ion transportation [113].

## 1.7. PHYSICO-CHEMICAL CHARACTERIZATION

The inorganic-organic hybrid mesostructured materials can be characterized by various techniques, which provide important information about different physicochemical features. The most extensively used techniques can be categorized as follows;

1. Spectroscopic techniques:

(a) Powder X-ray diffraction (XRD), (b) UV-Vis. spectroscopy, (c) Fourier transform infrared spectroscopy (FTIR), (d) Solid state nuclear magnetic resonance spectroscopy (NMR), (e) X-ray photoelectron spectroscopy (XPS), (f) Atomic absorption spectroscopy (AAS).

2. Volumetric techniques:

(a) Porosity measurements by nitrogen adsorption (BET method)

3. Gravimetric techniques:

(a) Thermogravimetric analysis (TGA), (b) Differential thermal analysis (DTA)

4. Microscopic techniques:

(a) Scanning electron spectroscopy (SEM), (b) Transmission electron spectroscopy (TEM)

### 1.7.1. X-ray diffraction

It is well recognized that X-ray diffraction, based on wide angle elastic scattering of X-rays, has been the single most important tool to determine the structure of the materials. The X-ray diffraction patterns are obtained by measurement of the angle at which an X-ray beam is diffracted by the sample. From the diffraction patterns, the uniqueness of mesoporous structure [115], phase purity [116], degree of crystallinity [116] and unit cell parameters [115] of the crystalline/semicrystalline hybrid materials can be determined.

X-ray patterns of mesoporous phases exhibit peaks in the low angle region. The most intense peak being (100) reflection. In the case of MCM-41 the wall thickness of hexagonal channels is usually calculated by subtraction of the inside pore diameters (obtained by nitrogen adsorption) from the unit cell dimensions determined by XRD.

### 1.7.2. Diffuse Reflectance UV-Vis Spectroscopy

UV-Vis spectroscopy deals with the study of electronic transitions between orbital or bands of atoms, ions or molecules in gaseous, liquid and solid state. In the case of transition metal ions or atoms, any change in their coordination sphere may affect their optical properties and therefore can be characterized by UV-Vis study [117]. For solid substances like transition metal containing mesoporous materials, diffuse reflectance UV-Vis spectroscopy (DRUV-Vis) is applied to determine the ligand field symmetry and oxidation state of the metal inside the solid matrices. Thus DRUV-Vis is a sensitive probe to examine the type of the sites, framework or extra-framework, in which that metal ion or cluster exist [118].

### 1.7.3. Fourier Transform Infrared Spectroscopy

IR spectroscopy identifies the vibration of chemical bonds in a molecule at various frequencies depending on the elements and types of bonds. The energy corresponding to these transitions corresponds to the infrared region (4000–400 cm$^{-1}$) of the electromagnetic spectrum. The term Fourier transform (FT) refers to the manner in which the data are collected and converted from an interference pattern to an infrared absorption spectrum that is unique like a molecular "fingerprint" [119].

The mid-infrared region from 1300-400 cm$^{-1}$ contains vibrations due to the framework structure of zeolite [120]. Similarly, mesoporous molecular sieves also show a series of bands that are characteristic of the $SiO_4$ tetrahedral unit. The spectra show two

main absorption bands between the regions 1245-1210 cm$^{-1}$ and 1090-1055 cm$^{-1}$. These are assigned to asymmetric stretching mode of $SiO_4$ units in the silicate structures containing five membered rings. The IR bands around 3600-3700 cm$^{-1}$ confirm the presence of the silanol groups [121, 122] .

### 1.7.4. Solid state Nuclear magnetic resonance spectroscopy (NMR)

Nuclear magnetic resonance (NMR) spectroscopy is one of the most powerful tools to investigate structure and dynamics of a molecular system in liquid phase. Atomic nuclei consisting of odd number of protons and/or neutrons possess a nuclear spin $I \neq 0$ and consequently a magnetic moment $\mu = \gamma h I$ ($\gamma$ = gyromagnetic ratio), when placed in a magnetic field of strength $B_0$. Zeeman interaction results in quantized orientations of the nuclear magnetic moments [123]. The nucleus can adopt $2I + 1$ eigen states with energies $E(m) = -m\gamma h B_0$, where m = ($I$, $I$–1,…., –$I$). Transitions between neighboring energy states ($m = \pm 1$) can be induced by electromagnetic radiation (energy $E = h\nu$) of frequency $\nu_0 = \gamma B_0/2\pi$.

With the advent of sophisticated solid-state NMR techniques, it has become possible to obtain NMR spectra of solids with spectral resolution comparable to that of liquids [124]. Modern high-resolution solid-state NMR spectroscopy allows to elucidate the chemical and structural environment of several atoms (*e.g.* $^{13}$C, $^{27}$Al, $^{29}$Si, $^{31}$P *etc.*) in a solid matrix like that of porous materials [125]. The most popular technique to get high-resolution NMR spectra with narrow line width is the magic angle spinning (MAS), where the solid sample is fast rotated about an axis inclined at a "magic" angle $\theta = 54°44'$ to the direction of $B_0$ [126]. Cross-polarization (CP) technique does not affect the line width of the spectra, but is applied to improve the sensitivity, *i.e.*, the signal to noise ratio (SNR) of the spectra of nuclei with low natural abundance (*e.g.* $^{13}$C, $^{29}$Si, $^{31}$P *etc.*), and to monitor the spatial proximity of nuclei [126]. CP involves indirect excitation of the less abundant nucleus through magnetization transfer from an abundant spin system (*e.g.* $^1$H).

### 1.7.5. X-ray photoelectron spectroscopy (XPS)

X-ray photoelectron spectroscopy is widely used for probing the electronic structure of atoms, molecules and condensed matter. When an X-ray photon of energy $h\nu$ is incident on a solid matter, the kinetic energy ($E_k$) and the binding energy ($E_b$) of the ejected photoelectrons can be related as follows: $E_k = h\nu - E_b$.

16

This kinetic energy distribution of the photoelectrons is fabricated by a series of discrete bands, which symbolizes for the electronic structure of the sample [127]. The core level binding energies of all the elements (other than H and He) in all different oxidation states are unique, which provides instant detection of the chemical composition of the sample after a full range scan [128]. However, to account for the multiplet splitting and satellites accompanying the photoemission peaks, the photoelectron spectra should be interpreted in terms of many-electron states of the final ionized state of the sample, rather than the occupied one-electron states of the neutral species [129].

### 1.7.6. Atomic absorption spectroscopy (AAS)

The principle of atomic absorption is based on energy absorbed during transitions between electronic energy levels of an atom. When heat energy is provided to an atom in ground state by a source such as a flame (temperature ranging from 2100–2800 °C), outer-shell electrons are promoted to a higher energy excited state. The radiation absorbed as a result of this transition between electronic levels can be used for quantitative analysis of metals and metalloids present in solid matrices, which have to be dissolved by appropriate solvents before analysis. The basis of quantitative analysis depends on measurement of radiation intensity and the assumption that radiation absorbed is proportional to atomic concentration. Analogy of relative intensity values for reference standards is used to determine elemental concentrations [130].

### 1.7.7. Adsorption measurements

Molecular sieves have ability to adsorb probe molecules of different sizes. Sorption capacities for probe molecules such as n-hexane, water, benzene, nitrogen etc. yield information about the hydrophylicity/hydorphobicity, pore dimensions and pore volume of the molecular sieves.

The Brunaure-Emmett-Teller (BET) method is the most widely used method for the evaluation of surface area, pore volume and pore size distributions of porous solids from nitrogen physisorption isotherm data. The BET equation can be represented as follows:

$$\frac{p}{v(p_0 - p)} = \frac{1}{v_m c} + \frac{c-1}{v_m c} \frac{p}{p_0},$$

where $v$ = volume of $N_2$ adsorbed by the sample under pressure $p$, $p_o$ = saturated vapor pressure at the same temperature, $v_m$ = volume of $N_2$ adsorbed when the surface is covered with a unimolecular layer, and c = constant for a given adsorbate [131].

$N_2$-adsorption-desorption isotherms of MCM-41, MCM-48 and FSM-16 are of the type IV. The steep increase in $N_2$ adsorption (in the $P/P_0$ range of 0.2 to 0.4) corresponds to capillary condensation within uniform pores. The sharpness and the height of peak reflect the uniformity of the pore size and the pore volume respectively. The wall thickness of hexagonally packed silicate was determined as the difference between the repeat distance $a_0$ = $2d_{100}/\sqrt{3}$ (from XRD) and the average pore diameter obtained from Horvath-Kawazoe equation [132].

### 1.7.8. Thermal analysis

Thermal analysis is widely used to study the structural stability of as-synthesized forms of molecular sieves. It provides information about the temperature required for the removal of adsorbed water, decomposition of the occluded organic cations in the pores and channels of molecular sieves and dehydroxylation at higher temperatures to produce Lewis acid sites. Data obtained from TG, DTA and DTG study are useful in evaluating the thermal properties of molecular sieves. The shape and splitting of the endotherms (low temperature) helps to identify the location of water molecules and also helps in studying the kinetics of dehydration. The temperature at which an exotherm appears in the DTA after the loss of water molecules, gives helpful information about the temperature required to remove the template molecules from the pores of the molecular sieves during calcination. Phase transformations (if any) can also be understood from the exotherms obtained at higher temperatures.

### 1.7.9. Scanning electron microscopy (SEM)

Scanning electron microscopy is an important tool for morphological characterization of mesoporous molecular sieve materials. A scanning electron microscope can generate an electron beam scanning back and forth over a solid sample. The interaction between the beam and the sample produces different types of signals providing detailed information about the surface structure and morphology of the sample. When an electron from the beam encounters a nucleus in the sample, the resultant Coulombic attraction leads to a deflection in the electron's path, known as Rutherford elastic scattering. A fraction of

these electrons will be completely back scattered, reemerging from the incident surface of the sample. Since the scattering angle depends on the atomic number of the nucleus, the primary electrons arriving at the given detector position can be used to produce images containing topological and compositional information [133].

### 1.7.10. Transmission electron microscopy (TEM)

TEM is used to elucidate the pore structure of mesoporous molecular sieves [9b, 15, 134]. It provides topographic information of materials at near atomic resolution. However, the exact analysis of pore sizes and thickness of the pore walls is very difficult and not possible without additional simulations because of the 'focus' problem. More than one model with a hexagonal array of large cylindrical pores with thin walls gives a similar XRD pattern, but TEM gives a direct, precise and simultaneous measurement of the pore diameter and pore thickness. HRTEM can be successfully used to examine the microstructural feature of mesoporous molecular sieves [132, 135]. In addition to structural characterization, it can also be used to detect the location of metal clusters and heavy cations in the framework [135].

### 1.8. CATALYTIC APPLICATIONS AND PROSPECTS

The commercialization of some of the homogeneous catalytic systems consisting of transition metal complexes is difficult due to some inherent shortcomings, viz., (i) complicated work-up of the reaction mixture, (ii) preparation of the pure products not contaminated with catalysts or constituents thereof, (iii) isolation of the valuable catalyst or its constituents, which can be achieved only with high technical complexity and expenditure [136].

During the last few years, hybrid mesoporous solids have been considered for a wide range of heterogeneous catalysis reactions [137, 138]. Heterogenization of active centers can improve the overall efficiency of the catalytic processes because: 1) it is easier to retain the solid catalyst in the reactor or to separate it from the liquid process stream by filtration (compared to extraction or distillation requirements for homogeneous processes); 2) often the catalyst can be regenerated and recycled; and 3) confinement of the catalyst within mesopores provides a means of introducing size and/or shape selectivity and thus greater specificity to a reaction. In contrast to organic polymers, mesoporous silicates used in

organic solvents do not swell or dissolve. If functional groups are covalently attached to the surface, leaching is minimized.

### 1.8.1. Selective oxidation of alkenes and alkanes

Epoxides are important intermediates for the preparation of oxygen containing natural products, fine chemicals as well as for the production of epoxy resins. The direct epoxidation of alkenes generally uses expensive per-acids, and produces large amount of effluents [139, 140]. Much effort has been made to develop the direct and selective epoxidation of olefins by use of molecular oxygen. However it is difficult to control the reaction because of over oxidation or side reactions under conventional severe reaction conditions, such as high pressure of oxygen or high reaction temperature. Therefore it is desirable to search for the heterogeneous catalyst and clean oxidant which survive the selective epoxidation under mild reaction conditions.

Oxidation of alkanes is an important industrial process for both economic and environmental reasons. Therefore, it is desirable to replace conventional processes that use stoichiometric oxidants with environmentally more benign ones using alkyl hydroperoxides and hydrogen peroxide, but the best of all would be processes that could selectively oxidize hydrocarbons using either dioxygen or air under mild conditions e.g. the aerobic oxidation of cyclohexane to mixture of cyclohexanol and cyclohexanone under mild conditions is of great industrial significance, since these two products are intermediates in the manufacture of nylon-6 and nylon-6,6.

### 1.8.1.1. Oxidation of alkenes/alkanes by tertiary butyl hydroperoxide (TBHP) and isobutyraldehyde/$O_2$

Metal phthalocyanines/salens are an important class of catalysts for the oxidation of alkenes as well as alkanes in the liquid phase. By suitable substitution on the aromatic ring, a variety of phthalocyanine/ salen derivatives have been prepared in an attempt to improve their catalytic performance. Metal phthalocyanines (MPCs) are comparatively cheap and effective selective oxidation catalysts [141]. In the solid state and in some solutions, the complexes are in an 'associative state' and are not very effective as catalysts. To achieve complete dispersion, many authors have encapsulated these complexes inside the cages of zeolites, such as X and Y. The major disadvantage of these encapsulated complexes is that the zeolite pores are narrow (pore diameter 7.4 Å) and little space is available inside the

cages for the substrates to undergo reaction. There is therefore, an obvious benefit in using large pore material to disperse the complex. Metallophthalocyanines of Fe, Mn and Co have been successfully anchored onto the surface of mesoporous silica and used as catalyst in liquid phase oxidation of alkenes [141]. A series of $Cu^{2+}$-perfluorophthalocyanines have been prepared inside the pores of MCM-41 using o-dicyanobenzene [139]. This heterogenized homogenous system gave higher product conversion as compared to neat metal complex due to large hydrophobic surface area of the mesoporous silica giving rise to dispersion of metal complex. Earlier workers reported that there is an enhanced catalytic activity for metal complex anchored catalyst as compared to encapsulated catalyst due to the presence of amine [142, 143]. The presence of catalytic amount of bases helps to increase the initial rate of epoxidation as well as epoxide selectivity due to the formation of higher oxo-intermediate for the oxidation of alkenes.

To cite few examples, Komia et al. [144] have discussed the role of different aldehydes in the oxidation of various alkenes and alkanes using copper salts, copper-crown ether complex and a mixture of copper salt and crown ether. Iron and Ruthenium catalyzed oxidation of alkanes with aerobic oxygen in the presence of aldehydes was studied by Murahashi et al. [145]. Per acids formed in the reaction further react with the metal species to offer the metal-oxo species. Sorokin et al. [146] have studied alkene epoxidation with molecular oxygen over iron phthalocyanine (FePc) -grafted silica in the presence of isobutyraldehyde. Styrene epoxidation reactions have also been studied by Diaz-Requejo et al. [147] using dihydridobispyrazolyborate and hydrotris (3,5-dimethylpyrazolyl) borate using Cu complexes as catalyst supported on silica gel. Mangemantin et al. [146] reported a styrene conversion above ~ 90% in the presence of isobutyraldehyde over iron phthalocyanine catalyst covalently bonded to silica. Transition metal complexes are well known to catalyze the decomposition of organic peroxides: (i) Lu et al. [148] have reported the reaction mechanism of styrene oxidation, resulting in three products (benzaldehyde, styrene epoxide, phenyl acetaldehyde) via the attack of tert. Butyl peroxo radical (t-BuOO$^{.}$) with styrene, followed by rearrangement. (ii) The formation of oxo-metal species may be taking place by the interaction of TBHP with metal, as suggested by Cramarossa et al. [149]. It appears that the yield of product differs as the isobutyraldehyde/$O_2$ system gives the higher product conversion as well as the higher epoxide selectivity as compared to yield using TBHP. The oxo-metal species formed in both the cases react directly with the alkene to give epoxide. But the catalytic decomposition of hydroperoxide into free radicals attack

the substrate molecules results in the formation of epoxide and benzaldehyde, which affect the total epoxide selectivity.

On the other hand, cooxidation is important from the practical view point; since it is possible to utilize the peroxidic intermediate for the additional oxidation e.g. the active oxygen of acyl peroxy radical and peracid are utilized for the epoxidation. This reaction gives a higher yield of epoxide as compared to oxidation using TBHP, since acyl peroxy radicals are more selective than alkyl peroxy redical i. e. favoring addition relative to abstraction. Alkanes are susceptible to homolytic attack in which free radicals are intermediates. The $^t$BuO$^.$ radical formed from homolytic decomposition of TBHP which is more favored than $^t$BuOO$^.$ [150], preferentially abstracts hydrogen to give the cyclohexyl radical. In the case of alkane oxidation this homolytic decomposition is more favored compared to the heterolytic decomposition of the O-O bond. Also alkyl peroxy radicals are more stable as compared to acyl peroxy radicals formed by isobutyraldehyde that are readily converted into per acids favoring a heterolytic mechanism. The above arguments may probably explain the larger alkane oxidation with TBHP compared to isobutyraldehyde/O$_2$**.**

**1.8.2. Hydroformylation of Olefins using carbon supported heterogeneous catalysts**

Hydroformylation or Oxo synthesis, as it is commonly known as, is one of the largest scale applications of homogeneous catalysis in industry with worldwide capacities of over $6.6 \times 10^6$ tonnes per annum [151]. This process involves a reaction of an olefin, carbon monoxide and hydrogen to produce linear or branched next higher aldehyde products (Figure 1.5). The process was discovered in 1938 by Otto Roelen at Ruhrchemie, where it was first commercialized [152]. The most important olefin starting material is propene, which is mainly converted to 1-butanol and 2-ethylhexanol via the initial product butyraldehyde. The original catalyst was [Co$_2$(CO)$_8$], which was modified with phosphines to increase the yield of the industrially more important linear aldehydes. A breakthrough was achieved in 1976 at Union Carbide with the introduction of rhodium catalysts such as HRh(CO)(PPh$_3$)$_3$. Almost all the commercial processes employ homogeneous cobalt or rhodium complex catalysts, of which the process using the Wilkinson's catalyst HRh(CO)(PPh$_3$)$_3$ has been considered as a major breakthrough because of its high activity and selectivity at mild operating conditions (at 100 °C and 10–25 bar pressure) [151]. While, HRh(CO)(PPh$_3$)$_3$ catalyst has been commercialized for hydroformylation of propylene, wherein, the product can be easily separated from the catalyst due to its high

volatility, its application for the higher olefinic substrates has been limited due to difficulties in catalyst – product separation [152, 153]. Therefore, several attempts have been made to heterogenize the homogeneous catalysts, so that the advantages of the homogeneous and heterogeneous catalysts can be combined. In previous work, polymer anchored [154], supported liquid phase (SLP) [155], supported aqueous phase (SAP) [156], biphasic catalysts using water-soluble metal complexes [157], using sulfonated [158] or fluorinated phosphines [159] as ligands, ionic liquids as new solvents [160, 161], as well as bimetallic catalysts [162] for hydroformylation have been proposed. Fig. 1.5 shows the representative hydroformylation of n-alkenes in to linear or branched chain aldehyde.
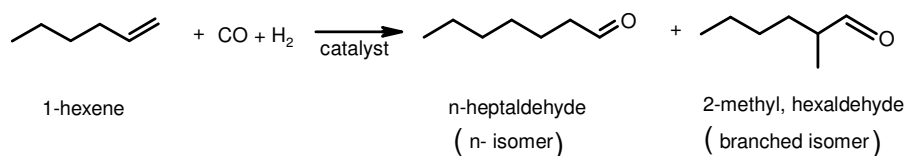


Fig. 1.5. Hydroformylation of straight chain olefins.

Earlier, heterogenized catalysts were reported using Rh complex dendrimers on silica [163], water soluble Calix[4]arene ligands [164] for biphasic hydroformylation of water-insoluble olefins, silica immobilized with tripodal polyphosphine rhodium catalysts [165] to name a few. But in majority of the cases, they suffer from lower selectivity and activity, low recyclability, use expensive ligands, unsuitable for commercial applications. The reports are available on rhodium(I) diphosphine complex anchored activated carbon support by means of covalent bond and hydroformylation of 1-octene [166]. Disser et.al [167] reported the hydroformylation of alkenes using carbonylhydrido-tris-(m-sulfo-triphenylphosphene)-rhodium complex immobilized on activated carbon.

## 1.9. SCOPE AND OBJECTIVES OF THE THESIS

This thesis is oriented around synthesis, characterization and applications of mesoporous materials. The presentation is in three sequential interrelated subparts.

The first part describes the synthesis of mesoporous silica MCM-41. Various factors, which affect the quality, kinetics and economics of the process are discussed. The chemically inert surface of this material requires modification before the main transition metal complex is grafted on this surface. The details of the process and its follow-up at

various stages using analytical tools are presented. Thus prepared catalyst is tested for catalyzing typical reactions viz. selective oxidation of alkenes and alkanes under mild reaction conditions and using different oxidants.

In the next part the casting of nanowires in the channels of MCM-41 is described. The workup and the characterization details are included.

The third subpart is related to casting mesoporous carbon. The essential precursor is mesoporous silica which is destroyed in the latter stages. An economic route is developed for mesoporous silica synthesis which determines the cost of the final product, mesoporous carbon. The applications of mesoporous carbon for grafting catalyst and its performance evaluation in typical reactions is described. This will be followed by an outline of the thesis.

## 1.10. OUTLINE OF THE THESIS

The present work has been sequentially placed under six chapters of this thesis entitled, "Synthesis, modification and catalytic evaluation of mesoporous molecular sieves" as follows:

**Chapter 1:** Introduction and literature review

This chapter presents a general introduction and literature survey about various physico-chemical aspects of mesoporous molecular sieve materials. Their synthesis and various controlling parameters, surface functionalization, characterization techniques and application as support for various catalytically active transition metal complexes using various oxidizing agents are discussed in brief. Next, the synthesis of nanowires in the porous channels of mesoporous materials and their characterization by various techniques is described. Finally the synthesis of mesoporous carbon materials from mesoporous silica templates having three dimensional interconnected channel arrangements is discussed. Scope and objectives of the present work are outlined at the end of this chapter.

**Chapter 2:** Synthesis, Characterization and Catalytic Evaluation of Co/Cu perchlorophthalocyanine immobilized Si-MCM-41

This chapter describes the hydrothermal synthesis of siliceous MCM-41, removal of templates and the modification of surface silanol groups with 3-aminopropyltriethoxysilane (3-APTES) to get surface modified MCM-41 (viz. $NH_2$-MCM-41). The catalysts were

prepared by immobilization of cobalt/ copper -perchlorophthalocyanine in the channels of MCM-41 by either direct impregnation [viz. Co/Cu-M(I)] or by anchoring through $NH_2$-MCM-41 [viz. Co/Cu-AM(PS)]. Further, catalyst characterization has been discussed using various techniques such as X-ray diffraction (XRD), $N_2$-adsorption-desorption, atomic absorption spectroscopy (AAS), microanalysis, transmission electron microscopy (TEM), solid state MAS NMR spectroscopy, UV-Vis. spectroscopy, FTIR spectroscopy, cyclic voltammeter. The catalytic evaluation has been done for liquid phase oxidation of hydrocarbons under mild reaction conditions using two different oxidants (TBHP and $O_2$/ aldehyde) and the performance is compared with that of neat metal complex. The product analysis has been done by gas chromatography (GC), gas chromatography/Infrared spectroscopy (GC/IR) and the results have been discussed in detail.

**Chapter 3:** Synthesis, Characterization and Catalytic Evaluation of Co/Cu-salen immobilized Si-MCM-41

This chapter describes synthesis and modification of MCM-41 using 3-APTES (viz. $NH_2$-MCM-41) followed by immobilization of cobalt/ copper -salen complexes in the channels of MCM-41. Immobilization have been done by direct impregnation [viz. Co/Cu-S-M(I)] or anchoring with organo-modified MCM-41 [viz. Co/Cu-S-AM(PS)]. The characterization is done using various physico-chemical and electroanalytical methods like XRD, $N_2$-sorption, AAS, microanalysis, solid state MAS NMR, UV-Vis., FTIP, X-ray photoelectron spectroscopy (XPS) and cyclic voltammeter. Further the catalysts were evaluated for oxidation of hydrocarbons under mild reaction conditions using TBHP and aldehyde/$O_2$ and the data is compared with that of neat metal salen. The product analysis have been done by gas chromatography, (GC), gas chromatography/infrared spectroscopy (GCIR).

**Chapter 4:** Synthesis, characterization and optical properties of Silver and Gold nanowires embedded in Si-MCM-41

This chapter describes the uniform synthesis of silver and gold nanowires inside MCM-41 matrix (i.e. Ag-MCM-41 and Au-MCM-41) by controlled reduction method. The presence of nanowires inside the host have been proved by X-ray diffraction (XRD), transmission electron microscopy (TEM), surface area measurement, absorption spectroscopy, emission spectroscopy etc. Non-linear optical properties (NLO)

25

corresponding to second harmonic generation (SHG) values were also recorded for self supported films of these heterostructured materials.

**Chapter 5:** Synthesis of mesoporous silica templated mesoporous carbon

This chapter describes the synthesis of three-dimensional interconnected mesoporous silica material using tetraethylorthosilicate (TEOS) and low cost non-surfactant templating agents (hydroxy-carboxylic acids). This chapter also describes the synthesis of mesoporous silica using sodium silicate as source of silica and elaborates the various synthesis parameters to optimize the method to prepare silica with high surface area and narrow pore size distribution. This mesoporous silica structure used as template to prepare mesoporous carbon material is described in details. The modification of surface silanol groups of mesoporous silica using 3-APTES and immobilization of cobalt salen for olefin oxidation have been studied. In the next part the impregnation of Rh- complex on the mesoporous carbon support is described along with their applications for hydroformylation of alkenes. Both the silica and carbon materials were characterized by FTIR, $N_2$-sorption, XRD, TEM, thermal analysis, XPS analysis and cyclic voltammetry for capacitance behavior is discussed.

**Chapter 6:** Summary and Conclusions

The last chapter elaborately presents the summary and conclusions of the thesis work.

## 1.11. REFERENCES

1.  (a) R. M. Barrer, *Hydrothermal Chemistry of Zeolites*, Academic Press, New York, 1982. (b) R. Szostak, *Molecular Sieves: Principles of Synthesis and Identification*, Van Nostrand Reinhold, New York, 1989. (c) M. E. Davis, *Acc. Chem. Res.,* 26 (1993) 111. (d) P. G. Schultz, *Angew. Chem. Int. Ed.,* 28 (1989) 1283. (e) A. Corma, *Chem. Rev.,* 95 (1995) 559.

2.  (a) S. M. Csicsery, *Zeolites,* 4 (1984) 202. (b) S. M. Csicsery, *Pure Appl. Chem.,* 58 (1986) 841. (c) P. Ratnasamy, R. Kumar, *Stud. Surf. Sci. Catal.,* 97 (1995) 367.

3.  (a) P. -S. E. Dai, *Catal. Today,* 26 (1995) 3. (b) R. A. Sheldon, *J. Mol. Catal. A: Chem.,* 107 (1996) 75. (c) J. H. Clark, D. J. Macquarrie, *Chem. Soc. Rev.,* 25 (1996)

303.

4.  K.S.W. Sing, D.H. Everett,  R.H.W.Haul, L. Moscou, R. A. Pierotti, J. Rouquerol, and T. Siemieniewska, *Pure Appl. Chem.*, 57 (1985) 603.

5.  R. K. Iler,  *The Chemistry of Silica*, J. Willy & Sons, Inc., 1979.

6.  K. Wefers and C. Misra, *Oxides and Hydroxides of Aluminium*, Alcoa Technical Paper No. 19, Revised, Alcoa Laboratories, 1987.

7.  T. J. Pinnavaia, *Science*, 220 (1983) 365.

8.  T. Yanagisawa, T. Schimizu, K. Kuroda and C. Kato, *Bull. Chem. Soc. Japan.*, 63 (1990) 988.

9.  (a) C. T. Kresge, M. E. Leonowicz, W. J. Roth, J. C. Vartuli and J. S. Beck, *Nature,* 359 (1992) 710. (b) J. S. Beck, J. C. Vartuli, W. J. Roth, M. E. Leonowicz, C. T. Kresge, K. D. Schmitt, C. T. -W. Chu, D. H. Olson, E. W. Sheppard, S. B. McCullen, J. B. Higgins and J. L. Schlenker, *J. Am. Chem. Soc.,* 114 (1992) 10834. (c) S. Inagaki, Y. Fukushima and K. Kuroda, *J. Chem. Soc., Chem. Commun.,* (1993) 680.

10.  J. S. Beck, J. C. Vartuli, G. J. Kennedy, C. T. Kresge, W. J. Roth and S. E. Schramm, *Chem. Mater.,* 6 (1994) 1816.

11.  C. F. Cheng, H. He, W. Zhou and J. Klinowski, *Chem. Phys. Lett.*, 244 (1995) 117.

12.  C.-Y. Chen, S. L. Burkett, H. Y. Li, and M. E. Davis, *Microporous Mater.*, 2 (1993) 27.

13.  A. Steel, S. W. Carr, and M. W. Anderson, *J. Chem. Soc. Chem. Commun.*, (1994) 1571.

14.  J. C. Vartuli, K. D. Schmitt, C. T. Kresge, W. J. Roth, M. E. Leonowicz, S. B. McCullen, S. D. Hellring, J. S. Beck, J. L. Schlenker, D. H. Olson and E. W. Sheppard, *Chem. Matter.*, 6 (1994) 2317.

15.  C. T. Kresge, M. E. Leonowicz, W. J. Roth and J. C. Vartuli, *U. S. Patent*, US 5,098,684 (1992).

16.  D. Khushalani, A. Kuperman, G. A. Ozin, K. Tanaka, J. Garces, M. M. Olken and N. Coombs, *Adv. Mater.*, 7 (1995) 842.

17.  S. X. Zhao, G. Q. (Max) Lu and G. J. Millar, *Ind. Eng. Chem. Res.*, 35 (1996) 2075

18.  X. Chen, L. Huang and Q. Li, *J. Phys. Chem. B*, 101 (1997) 8460.

19.  R. Schmidt, D. Akporiaye, M. Stocker and O. H. Ellestad, *J. Chem. Soc. Chem. Commun.*, (1994) 1493.

20.  G. D. Stucky, A. Monnier, F. Schuth, Q. Huo, D. I. Margolese, D. Kumar, M. Petroff,

P. Krishnamurthy, A. Firouzi, M. Janicke and B. F. Chmelka, *Mol. Cryst. Liq. Cryst.,* 240 (1996) 187.

21. K. A. Koyona and T. Tatsumi, *Chem. Commun*., (1996) 145.

22. N. Ulagappan, B. V. N. R. Neeraj, C. N. R. Rao, *Chem. Commun*., (1996) 2243.

23. D. Zhao and D. Goldfarb, *J. Chem. Soc., Chem. Commun.,* (1995) 875.

24. Q. Huo, D. I. Margolese, U. Ciesla, P. Feng, T. E. Gier, P. Sieger, R. Leon, P. M. Petroff, F. Schuth and G. D. Stucky, *Nature*, 368 (1994) 317.

25. Q. Huo, D. I. Margolese, U. Ciesla, D. G. Demuth, P. Feng, T. E. Gier, P. Sieger, A. Firouzi, B. F. Chmelka, F. Schuth and G. D. Stuky, *Chem. Mater*., 6 (1994) 1176.

26. P. T. Tanev and T. J. Pinnavaia, *Science*, 267 (1995) 865.

27. M. Hudlicky, *Oxidation in organic chemistry,* ACS Monograph, Washington, DC, 186 (1990).

28. W. Adam, W. A. Herrmann, J. Lin, C. R. Saha-Möller, R. W. Fisher and J. D. G. Correia, *Angew. Chem. Int. Ed. Engl.,* 33 (1994) 2475.

29. W. A. Herrmann, J. J. Haider and R. W. Fisher, *J. Mol. Catal. A: Chem.,* 138 (1999) 115.

30. R. Song, A. Sorokin, J. Bernadou, B. Meunier, *J. Org. Chem.,* 62 (1997) 673.

31. W. Kain and J. Rall, *Angew.Chem.Int. Ed. Engl,* 35 (1996) 43.

32. J. T. Groves, R. C. Haushalter, M. Nakamura, T. E. Nimo and B. J. Evans, *J. Am. Chem. Soc.,* 103 (1981) 2884.

33. R. H. Holm, *Chem. Rev.*, 87 (1987) 1401.

34. P. S. Dixit, K. Shrinivasan, *Inorg. Chem.,* 27 (1988) 4507.

35. S. Nakagaki, A. M. Machado, F. Wypych, S. M. Drechsel, *J. Colloid Interf. Sci.,* 254 (2002) 158.

36. F. Bedioui, *Coord. Chem. Rev.,* 144 (1995) 39.

37. L. Barloy, J. P. Lallier, P. Battioni, D. Mansuy, Y. Piffard, M. Tournous, J. B. Valim and W. Jones, *New J. Chem.*, 16 (1992) 71.

38. M. A. Schiavon, Y. Iamamoto, O. R. Nacsimento and M. D. Assis, *J. Mol. Catal. A: Chem.,* 174 (2001) 213.

39. P. M. Price, J. H. Clark and D. J. Macquarrie, *J. Chem. Soc., Dalton Trans.,* (2000)101.

40. K. Moller and T. Bein, *Stud. Surf. Sci. Catal.,* 117 (1998) 53.

41. J. H. Clark and D. J. Macquarrie, *Chem. Commun.,* (1998) 853.

42. J. J. Kirkland and J. J. DeStefano, *J. Chromatogr. Sci.*, 8 (1970) 309.

43. D. J. Macquarrie, D. B. Jackson, J. E. G. Mdoe and J. H. Clark, *New J. Chem.*, 23 (1999) 539.

44. D. J. Macquarrie, J. H. Clark, A. Lambert and J. E. G. Mdoe, *React. Func. Polym.*, 35 (1997) 153.

45. A. Butterworth, J. H. Clark, P. H. Walton and S. J. Barlow, *Chem. Commun.*, (1996) 1859.

46. J. H. Clark, D. J. Macquarrie, J. Chisem, I. Chisem and J. S. Rafelt *Chem. Commun.*, (1997) 2203.

47. I. C. Chisem, J. Rafelt, M. T. Shieh, J. Chisem, J. H. Clark, R. Jachuck, D. J. Macquarrie, C. Ramshaw and K. Scott, *Chem. Commun.*, (1998) 1949.

48. P. Sutra and D. Brunel, *Chem. Commun.,* (1996) 2485.

49. C. J. Liu, S. G. Li, W. Q. Pang and C.-M. Che, Chem. Commun., (1997) 65.

50. J. F. DÌaz, K. J. Balkus Jr., F. Bedioui, V. Kurshev and L. Kevan, *Chem. Mater.,* 9 (1997) 61.

51. P. Battioni, J. P. Lallier, L. Barloy and D. Mansuy, *J. Chem. Soc., Chem. Commun.*, (1989) 1149.

52. B. V. Romnovsky *Proc. 8th Int. Congr. Crystal.,* Verlag Chemie, Weinhein, 4 (1984) 657.

53. C. Bowers and P. K . Dutta*, J. Catal.,* 122 (1990) 271.

54. D. E. De Vos, E. J. P. Feijen, R. A. Schoonheydt and P. A. Jacobs, *J. Am. Chem. Soc.,* 116 (1994) 4746.

55. A. G. Gabrielov, K. J. Balkus, Jr. , S. L. Bell, F. Bedioui and J. Devynck, *Microporous Mater.,* 2 (1994) 119.

56. R. F. Parton, C. P. Benzoukhanova, J. Grobet, P. J. Grobet and P. A. Jacobs, *Stud. Surf. Sci. Catal.,* 83 (1994) 371.

57. S. Ernst, R. Glaser and M. Selle, *Stud. Surf. Sci. Catal.,* 105 B (1997) 1021.

58. A. T. Bell, *Science,* 299 (2003)1688.

59. G. Markovich, C. P. Collier, S. E. Henrichs, F. Remacle, R. D. Levine and J. R. Heath, *Acc. Chem. Res.,* 32 (1999) 415.

60. J. Kunther, R. Seshadri, G. Nelles, W. Assenmacher, H. -J. Butt, W. Mader and W. Tremel, *Chem. Mater.,* 11 ( 1999) 1317.

61. W. Baschong and N. G. Wrigley, *J. Electron Microsc. Technique,* 14 (1990) 313.

62. R. Elghanian, J. J. Storhoff, R. C. Mucic, R. L. Letsinger, C. A. Mirkin, *Science,* 277

(1997) 1078.

63. A. Bhattacharya, P. C. Chakraborti, S. Mukharjee, M. K. Mitra and G. C. Das, *Adv. Mater.,* 2 (2001) 449.

64. N. Arul Dhas and A. Gadanken*, J. Mater. Chem.,* 8 (1998) 445.

65. A. B. R. Mayer, *Sci. Eng.,* C6 (1998) 155.

66. Y. Ni, X. Ge, Z. Zhang and Q. Ye, *Mater. Lett.,* 55 (2002) 171.

67. Y.-P. Sun, H. W. Rollins and R. Guduru, *Chem. Mater.,* 11 (1999) 7.

68. J. Zhu, S. Liu, O. Palchik, Y. Koltypin and A. Gadanken, *Langmuir,* 16 (2002) 6396.

69. V. S-Maceira, M. A. Duarte, E. Duman and M. Farle, *J. Magnetism Magnet. Mater.,* 299 (2006) 467.

70. J. H. Fendler, *Chem. Mater.,* 8 (1996) 1616.

71. C. H. Ko and R. Ryoo, *Chem. Commun.,* (1996), 2467.

72. U. Junges, F.Schuth, G. Schmid, Y. Uchida and R. Schogl, *Ber. Bunsen-Ges. Phys. Chem., 101*(1997), 1631.

73. G.L. Hornyak, C.J. Patrissi and C.R. Martin, *J. Phys. Chem., B* 101 (1997) 1548.

74. R. Leon, D. Margolese, G. Stucky, and P.M. Petroff, *Phys. Rev., B.* 52 (1995) R2285.

75. V.I. Srdanov, I. Alxneit, G.D. Stucky, C.M. Reaves and  S.P. DenBaars, *J. Phys. Chem., B* 102 (1998) 3341.

76. F. Atsushi, H. Naonori, S. Yuzuru, I. Shinji, F. Yoshiaki and I. Masaru, *Microporous Mesoporous Materials,* 48 (2001) 171.

77. J. Cheon, K. Lee, H. Kang, S.J. Oh and  H.C. Ri, *Mater. Res. Soc. Symp.,* 635 (2000).

78. Y.J. Han, J. Kim and G.D. Stucky, *Chem. Mater.*, 12 (2000) 2068.

79. N. K. Raman, M. T. Anderson and C. J. Brinker, *Chem. Mater.*, 8 (1996) 1682.

80. P. T. Tanev and T. J. Pinnavaia, *Chem. Mater.,* 8 (1996) 2068.

81. P. T. Tanev and T. J. Pinnavaia, *Science,* 271 (1996) 1267.

82. Y. Wei, D. T. Ding, W. H. Shih, X. Liu, S. Z. D. Cheng, Q. Fu, *Adv. Mater.*, 3 (1998) 313.

83. J. B. Pang, K. Y. Qiu, Y. Wei, *J. Non-Cryst. Solids*, 283 (2001) 101.

84. J.Y. Ying, C.P. Mehnert and M.S.Wong, *Angew. Chem. Int. Ed,.* 38 (1999)57.

85. G.J.A.A. Soler-Illia, C. Sanchez, B. Lebeau and J. Patarin, *Chem. Rev.*,102 (2002) 4093.

86. M.E. Davis*, Nature* ,417 (2002) 813.

87. F. Chen, L. Huang and Q. Li, *Chem. Mater.,* 9 (1997) 2685.

88.  Y. Liu, A. Karkamkar, T.J. Pinnavaia, *Chem. Commun.*, (2001) 1822.

89.  B. Lindlar, A. Kogelbauer, P.J. Kooyman, R. Prins, *Microporous and Mesoporous Mater.,* 44–45 (2001) 89.

90.  L. Sierra and J.-L. Guth, *Microporous and Mesoporous Mater.*, 27 (1999)243.

91.  M. Kruk, M. Jaroniec, R. Ryoo and J.M. Kim, *Chem. Mater.,*11 (1999) 2568.

92.  J.M. Kim and G.D. Stucky, *Chem. Commun.,* (2000) 1159.

93.  M.-C. Chao, D.-S. Wang, H.-P. Lin and C.-Y. Mou, *J. Mater. Chem.,* 13 (2003) 2853.

94.  K. Kosuge, T. Sato, N. Kikukawa and M. Takemori, *Chem. Mater.*, 16 (2004) 899.

95.  C. Boissière, A. Larbot and E. Prouzet, *Chem. Mater.*, 12 (2000) 1937.

96.  S.-S. Kim, T.R. Pauly and T.J. Pinnavaia, *Chem. Commun.,* (2000) 835.

97.  S.-S. Kim, T.R. Pauly and  T.J. Pinnavaia, *Chem. Commun.,* (2000) 1661.

98.  S.-S. Kim, A. Karkamkar, T.J. Pinnavaia, M. Kruk and M. Jaroniec, *J. Phys. Chem., B* 105 (2001) 7663.

99.  J. B. Pang, C. M. Dong, K. Y. Qui and Y. Wei, Chinese J. Poly. Sci. 20 (2002) 361.

100. C. R. Bansal, J. B. Donnet, F. Stoeckli, Active Carbon, Marcel Dekker, New York, 1998.

101. A. B. Fuertes, F. Pico and J. M. Rojo, J. Power Sources, 133 (2004) 329.

102. R. Ryoo, S.H. Joo, S. Jun, J. Phys. Chem. B 103 (1999) 7743.

103. S. Jun, S. H. Joo, R. Ryoo, M. Kruk, M. Jaroniec, Z. Liu, T. Ohsuna, O. Terasaki, J. Am. Chem. Soc. 122 (2000) 10712.

104. Tae-Wan. Kim, R. Ryoo, K. P. Gierszal, M. Jaroniec, L. A. Solovyov, Y. Sakamoto, O. Terasaki, J. Mater. Chem. 15 (2005) 1560.

105. J. Lee, S. Yoon, S. M. Oh, C. H. Shin, T. Hyeon, Adv. Mater. 12 (2000) 359.

106. W. W. Lukens, G. D. Stucky, Chem. Mater. 14 (2002) 1665.

107. M. Sevilla, S. Alvarez, A. B. Fuertes, Micropor. Mesopor. Mater. 74 (2004) 49.

108. J. Lee, K. Sohn, T. Hyeon, Chem. Commun. (2002) 2674.

109. S. S. Kim, T. J. Pinnavai, Chem. Commun. (2001) 2418.

110. C. Niu, E. K. Sichel, R. Hoch, D. Moy, H. Tennent, Appl. Phys. Lett. 70 (1997) 1480.

111. D. Qu, H. Shi, J. Power Sources, 74 (1998) 99.

112. H. Shi, Electrochim. Acta. 41 (1999) 1633.

113. E. Frackowiak, F. Beguin, Carbon, 39 (2001) 937.

114. W. H. Bragg, W. L. Bragg, *The Crystalline State*, McMillan, New York, 1 (1949).

115. S. Biz, M. Occelli, *Catal. Rev. -Sci. Eng.,* 40 (1998) 329.

116. G. Bergeret, in: *Handbook of Heterogeneous Catalysis*, *Vol. 2*, Eds: G. Ertl, H. Knozinger, J. Weitkamp, Wiley-VCH, Weinheim, (1997) 464.

117. C. K. Jorgensen, *Absorption Spectra and Chemical Bonding in Complexes*, Pergamon, New York, (1962).

118. G. Kortum, *Reflectance Spectroscopy*, Springer, Berlin, (1969).

119. P. R. Griffiths, J. A. De Haseth, *Fourier Transform Infrared Spectrometry*, John Wiley and Sons Inc., New York, 1986.

120. J. C. Vartuli, K. D. Schmidt, C. T. Kresge, W. J. Roth, M. E. Leonowicz, S. B. McCullen, S. D. Hellring, J. S. Beck, J. L. Schlenker, D. H. Olson, E. W. Sheppard, Stud. Surf. Sci. Catal. 84 (1994) 53.

121. N. Topsoe, R. Pedersen and E.G. Derouane, *J. Catal.*, 70 (1984) 369.

122. P.A. Jacobs, and W.Y. Martier, *Zeolites*, 2 (1982) 226.

123. F. A. Rushworth, D. P. Tunstall, *Nuclear Magnetic Resonance*, Gordon and Breach Science Publishers Ltd., London, 1973.

124. M. Mehring, *High Resolution NMR Spectroscopy in Solids*, Springer-Verlag, Berlin, 1976.

125. G. Engelhardt, D. Michel, *High-Resolution Solid-State NMR of Silicates and Zeolites*, John Wiley and Sons Ltd., Chichester, (1987).

126. G. Engelhardt, in: *Handbook of Heterogeneous Catalysis*, *Vol. 2*, Eds: G. Ertl, H. Knozinger, J. Weitkamp, Wiley-VCH, Weinheim, (1997) 525.

127. C. S. Fadley, in: *Electron Spectroscopy: Theory, Techniques and Applications*, *Vol. 2*, Eds: C. R. Brundle, A. D. Baker, Academic Press, New York, (1978) 1.

128. W. N. Delgass, T. R. Hughes, C. S. Fadley, *Catal. Rev.,* 4 (1970) 179.

129. W. F. Egelhoff Jr., *Surf. Sci. Rep.,* 6 (1987) 253.

130. J. W. Robinson, *Atomic Absorption Spectroscopy*, Marcel Dekker, New York, 1975.

131. A. Corma, A. Martínez, V. Martínez-Soria and J.B. Monton, *J. Catal.*, 153 (1995) 25.

132. V. Alfredsson, M. Keung, A. Monnier, G.D. Stucky, K.K. Unger and F. Schüth, *J. Chem. Soc., Chem. Commun.*, (1994) 921.

133. G. Lawes, *Scanning Electron Microscopy And X-Ray Microanalysis*, John Wiley and Sons Ltd., Chichester, 1987.

134. C.F. Cheng, H. He, W. Zhou and Klinowski, J., *Chem. Phys. Lett.*, 244 (1995) 117.

135. A. Chenite, Y.L. Page and Sayari, *Chem. Mater.*, 7 (1995) 1015.

136. J. Manassen, in: *Catalysis, Progress in Research*, Eds: F. Basolo, R. E. Burwell Jr., Plenum Press, New York, (1973) 177.

137. D. E. De Vos, M. Dams, B. F. Sels and P. A. Jacobs, *Chem. Rev.*, 102 (2002) 3615.

138. J. H. Clark and D. J. Macquarrie, *Chem. Commun.,* (1998) 853.

139. G. A. Barf, R. A. Sheldon, *J. Mol. Catal. A*, 102 (1995) 23.

140. T. Mulkaiyamam, T. Yamada, *Bull. Chem. Soc. Jpn.,* 68 (1995) 17.

141. A. B. Sorokin and A. Tuel, *Catal. Today* 57 (2000) 45.

142. N. Safari and F. Bahadoran, *J. Mol. Catal. A: Chem.,* 171 (2001) 115.

143. J. Dongfeng, L. Xiaobing and He. Ren, *Appl. Catal. A: Gen.*, 203 (2000) 329.

144. N. Komiya, T. Naota, Y. Oda and S. Murahashi, *J. Mol. Catal A: Chem.,* 117 (1997) 21.

145. S. Murahashi, Y. Oda and T. Naota, *J. Am. Chem. Soc.*, 114 (1992) 7913.

146. S. Mangematin and A. B. Sorokin, *J. Porphyrins and Phthalocyanines*, 5 (2001) 674.

147. M. Mar. Diaz-Requejo, T. R. Belderrain and P. J. Perez, *Chem. Commun.*, 19 (2000) 1853.

148. Z.-R. Lu, Y. Q. Yin and D.-S. Jin, *J. Mol. Catal.,* 70 (1991) 391.

149. M. R. Cramarossa, L. Forti, M. A. Fedotov, L. G. Detusheva, V. A. Likholobov, L. I. Kuznetsova, G. L. Semin, F. Cavani and F. Trifiro, *J. Mol. Catal. A: Chem.,* 127 (1997) 85.

150. F. A. Chavez, C. V. Nguyen, M. M. Olmstead and P. K. Mascharak, *Inorg. Chem.,* 35 (1996) 6282.

151. B. Cornils and W. A. Hermann, Eds. *Applied Homogeneous Catalysis with Organometallic Compounds*, VCH, 1, 2 (1996).

152. B. Cornils, W. A. Hermann and C. W. Kohlpainter, *Nachr. Chem. Tech. Lab.,* 41 (1993) 544.

153. F. R. Hartley, *Supported Metal Complexes*, Reidel: Dordrecht, 1985.

154. C. U. Pittmann Jr. and L. R. Smith, *J. Am. Chem. Soc.,* 97 (1975) 1742.

155. P. R. Rony, *J. Catal.,* 14 (1969) 142.

156. J. P. Arhancet, M. E. Davis, J. S. Merola and B. E. Hanson, *Nature,* 339 (1989) 554.

157. W. A. Herrmann and B. Cornils, *Angew. Chem. Intl. Ed.,* 36 (1997) 1048.

158. W. A. Herrmann, G. P. Albanese, R. B. Manetsberger, P. Lappe and H. Bahrmann, *Angew. Chem. Intl. Ed. Engl.,* 34 (1995) 811.

159. I. T. Horvarth and J. Rabai, *Science,* 266 (1994) 72.

160. S. Kainz, A. Brinkman, W. Leitner, A. Pfaltz, *J. Am. Chem. Soc.,* 1211 (1999) 6421.

161. M. F. Sellin, P. B. Webb and D. J. Cole-Hamilton, *Chem. Commun.,* 781 (2001).

162. M. E. Broussard, B. Juma, S. G. Train, W-J. Peng, S. A. Laneman and G. G. Stanley, *Science,* 260 (1993) 1784.

163. S. C. Bourque and H. Alper, *J. Am. Chem. Soc.,* 122 (2000) 956.

164. S. Shimizu, S. Shirakawa, Y. Sasaki and C. Hirai, *Angew. Chem. Int. Ed. Engl.,* 39 (2000) 1256.

165. C. Bianchini, D. G. Burnaby, J. Evans, P. Frediani, A. Meli, W. Oberhauser, R. Psaro, L. Sordelli and F. Vizza, *J. Am. Chem. Soc.*, 121 (1999) 5961.

166. Z. Hao, L. Fen, G. Q. Lu, J. Liu, L. An and H. Wang, *Appl. Catal.,* 213 (2004) 177.

167. C. Disser, C. Muennich and G. Luft, *Appl. Catal.,* 296 (2005) 201.

# Chapter-2

# Synthesis, Characterization and Catalytic Evaluation of Co/Cu-perchlorophthalocyanine immobilized MCM-41

## 2.1. INTRODUCTION

MCM-41 (Mobil Crystalline Material-41) is a member of the M41S family first synthesized by researchers at Mobil Corporation [1-3]. It possesses a hexagonal array of unidimensional mesopores with pore diameter ranging between 15 to 100 Å, depending on the surfactant template used and synthesis conditions. Unlike other mesoporous materials such as intercalated clays, the pore size of MCM-41 molecular sieve is fairly uniform. Since the discovery of MCM-41, it has attracted considerable attention due to its large pore dimensions, uniform pore size distribution, high surface area ($> 800$ m$^2$/g) and distinct adsorption properties. Several synthesis methods have been proposed and successfully used to synthesize mesoporous MCM-41 molecular sives [4-8]. Kresge et al. [1, 2] first synthesized mesoporous silicates and aluminosilicates in alkaline conditions. Huo and co-workers [4, 9] reported the first synthesis of porous silicates in acidic conditions, while Yanagisawa et al. [10] pillared layered silica with surfactant cations and after calcination obtained a mesoporous silica with uniform distribution of pores.

Pure siliceous Si-MCM-41 mesoporous materials are electrically neutral, which limits their catalytic applications. In order to provide a specific catalytic activity to the chemically inert silicate framework, researchers have incorporated metal complexes into the walls of nanostructures either by direct synthesis, ion exchange, impregnation or grafting method. In recent years, surface modification of M41S type mesoporous silicates by reactive organic functional groups have been investigated extensively [11]. This surface modification allows tailoring of the surface properties for quite a lot of potential applications, *viz.*, catalysis, immobilization of catalytically reactive species, chemical sensing, fabrication of nanomaterials, to mention just a few [12, 13]. Organo-functionalization of the surfaces of mesoporous silica materials can be achieved either by covalent grafting or by incorporating functionalities directly during the synthesis [11, 12]. The grafting process has been widely applied to anchor desired organic functional groups *via* condensation with surface silanol groups of the mesoporous silica materials.

Oxidation of alkenes yields epoxides, which are important intermediates in the synthesis of fine chemicals. For the epoxidation of alkenes generally expensive per acids are used and produce large amounts of effluents [14, 15]. It is highly desirable to replace the conventional process with an environmentally more benign procedure. Cu and Fe are predominantly contained in metalloenzymes that play an important role in biological

dioxygen metabolism [16]. Metallophthalocyanines having structural similarity to reactive enzymes are an important class of catalysts for the liquid phase oxidation of hydrocarbons. Phthalocyanine complexes are especially attractive as potential oxidation catalysts because of their rather cheap and facile large scale preparation and their chemical and thermal stability [17]. By suitable substitution on the aromatic ring, a variety of phthalocyanine derivatives have been prepared in an attempt to improve their catalytic performance. The heterogenization of transition metal phthalocyanines onto robust inorganic supports are especially attractive due to combining the advantages of homogeneous (activity and selectivity) and heterogeneous (facile recovering and recycling of catalyst) catalyses [17-19]. Metallophthalocyanines of iron, manganese and cobalt have been successfully anchored onto the surface of mesoporous and amorphous silicas and have been used as catalysts in the liquid phase oxidation of aromatic compounds [17].

Covalent grafting of metallophthalocyanines onto silica presents another possible approach [20-22]. Sorokin et.al. [17, 19] reported controlled covalent anchoring of phthalocyanine complexes onto silicas in dimeric or monomeric form, gave selective heterogeneous catalysts for the oxidation of aromatic compounds to quinones. The immobilization of cobalt chelate complexes onto MCM-41 was performed through methoxysilyl coupling agents and showed some reactivity towards the formation of oxygen adduct [23].

Komia et al. [24] have discussed the role of different aldehydes in the oxidation of various alkenes and alkanes using copper salts, copper-crown ether complex and a mixture of copper salt and crown ether. Iron and Ruthenium catalyzed oxidation of alkanes with aerobic oxygen in the presence of aldehydes was studied by Murahashi et al. [25].

In the present study, we have carried out the immobilization of Co/Cu-Cl$_{16}$Pc in presence of 3-aminopropyltriethoxysilane (3-APTES) in the channels of MCM-41 by post synthesis i.e. [Co/Cu-AM(PS)] and impregnation of Co/Cu-Cl$_{16}$Pc in the channels of MCM-41 i.e. [Co/Cu-M(I)]. Amino-modified SiO$_2$ immobilized with Co/Cu-Cl$_{16}$Pc i.e. Co/Cu-ASiO$_2$ is also compared for catalytic study. The resulting samples have been characterized by X-ray diffraction (XRD), transmission electron microscopy (TEM), nitrogen adsorption-desorption (N$_2$-sorption), atomic absorption spectroscopy (AAS), microanalysis, magic angle spinning nuclear magnetic resonance spectroscopy (MAS NMR), ultra-violet, visible spectroscopy (UV-Vis.), infrared spectroscopy (IR) and cyclic voltammetry (CV). Catalytic

activity has been investigated for the oxidation of alkenes and alkanes using TBHP and aldehyde/$O_2$ as oxidants under mild reaction conditions (298 and 323 K).

Table 2.1. Specifications of Chemicals used:

| Reagent (Source) | Chemical composition/formula | Purity (%) |
|---|---|---|
| Fumed silica (Sigma) | $SiO_2$ | 99 |
| Tetramethyl ammonium silicate -TMA silicate (SACHEM Inc.,USA), | $(CH_3)_4NOH.2SiO_2$ | 10 wt.% silica solution, $TMA/SiO_2 = 0.5$ |
| Cetyltrimethylammonium bromide - CTMABr (Aldrich) | $C_{16}H_{33}N(CH_3)_3Br$ | 98 |
| Ammonium hydroxide – NH$_4$OH (S.D. Fine Chemicals) | $NH_4OH$ | 25 % solution in water |
| Tetramethyl ammonium hydroxide – TMAOH (Aldrich) | $(CH_3)_4NOH$ | 99 |
| 3-Aminopropyltriethoxysilane- 3-APTES (Aldrich) | $(C_2H_5O)_3Si(CH_2)3NH_2$ | 99 |
| Toluene (Loba Chem.Pvt. Ltd.) | $C_6H_5CH_3$ | 99 |
| Acetone (Loba Chem.Pvt. Ltd.) | $(CH_3)_2O$ | 99 |
| Co/Cu-perchlorophthalocyanine (Aldrich) | $Co/CuCl_{16}Pc$ | 99 |
| tert-Butyl hydroperoxide (TBHP) (Aldrich) | $(CH_3)_3COOH$ | 5.0 M solution in decane |
| Acetonitrile (Loba Chem.Pvt. Ltd.) | $CH_3CN$ | 99 |

| | | |
|---|---|---|
| Isobutyraldehyde (Loba Chem.Pvt. Ltd.) | $CH(CH_3)_2CHO$ | 98 |
| Benzaldehyde (Loba Chem.Pvt. Ltd.) | $C_6H_5CHO$ | 98 |
| Styrene (Loba Chem.Pvt. Ltd.) | $C_6H_5CHCH_2$ | 99 |
| Cyclohexene (Loba Chem.Pvt. Ltd.) | $C_6H_{10}$ | 99 |
| 1-Decene (Loba Chem.Pvt. Ltd.) | $C_{10}H_{20}$ | 99 |
| Cyclohexane (Loba Chem.Pvt. Ltd.) | $C_6H_{12}$ | 99 |
| Decane (Loba Chem.Pvt. Ltd.) | $C_{10}H_{22}$ | 99 |

## 2.2. EXPERIMENTAL

### 2.2.1. Synthesis of Si-MCM-41

Si-MCM-41 was synthesized according to the published procedure [26]. The molar composition of the synthesis gel in terms of oxides was as follows:

$$SiO_2 : 0.086 \ (NH_4)_2O : 0.089 \ (CTMA)_2O : 0.155 \ (TMA)_2O : 40 \ H_2O$$

Ammonium hydroxide (3.6 g; 25 % solution) diluted with water (25.0g) was added to cetyltrimethylammonium bromide (CTMABr) (9.6g) with stirring. To this mixture, 4.08 g tetramethylammonium hydroxide (TMAOH) dissolved in 25.0 g water was added, followed by the addition of 27.2 g tetramethylammonium silicate (TMA silicate). The mixture was stirred for 20 minutes. Fumed silica (6.2 g) was added slowly to the above gel under stirring which was continued for one hour. The pH of the final gel was 11.5. The gel was then transferred to stirred autoclave at 110°C up to 72 h for crystallization. The product thus obtained was filtered, dried at $110^{\circ}$C and finally calcined at 550° C for one hour in nitrogen and then for six hours in air; it is designated as Si-MCM-41.

### 2.2.2. Catalyst preparation

The preparation of catalyst has been done by immobilization of transition metal complexes in the channels of Si-MCM-41 support through (i) grafting and (ii) impregnation method as follows:

### 2.2.2.1. Grafting of Co/Cu-perchlorophthalocyanine (Co/Cu-Cl$_{16}$Pc) over Si-MCM-41
#### *2.2.2.1.1. Modification of Si-MCM-41 with 3-aminopropyltriethoxysilane (3-APTES)*

In a typical experiment, Si-MCM-41 (0.5g), prepared as above (section 2.2.1.) was dried by refluxing with dry toluene (8-10 h). The material was then filtered, washed with acetone and dried at room temperature under inert condition. Si-MCM-41 was then mixed with the solution of 3-APTES in toluene (70.0 ml:0.22g) and stirred. This NH$_2$-MCM-41 was filtered and washed with acetone / dichloromethane and vacuum dried.

#### *2.2.2.1.2. Anchoring of Co/Cu-perchlorophthalocyanine (Co/Cu-Cl$_{16}$Pc)*

A solution of 0.022g of Co/CuCl$_{16}$Pc in 20 ml of toluene was stirred and slowly added to a suspension of 0.5 g of NH$_2$-MCM-41 in toluene (as prepared in section 2.2.2.1.1.). The mixture was refluxed for 12 h. A green material was separated by filtration, washed with acetone, dried under inert atmosphere at the temperature of 80$^{\text{o}}$ C and designated as Co/CuCl$_{16}$Pc-NH$_2$-MCM-41 (PS) [or Co/Cu-AM(PS)]. Fig. 2.1 shows the schematic presentation of representative catalyst preparation by grafting method using CoCl$_{16}$Pc complex.
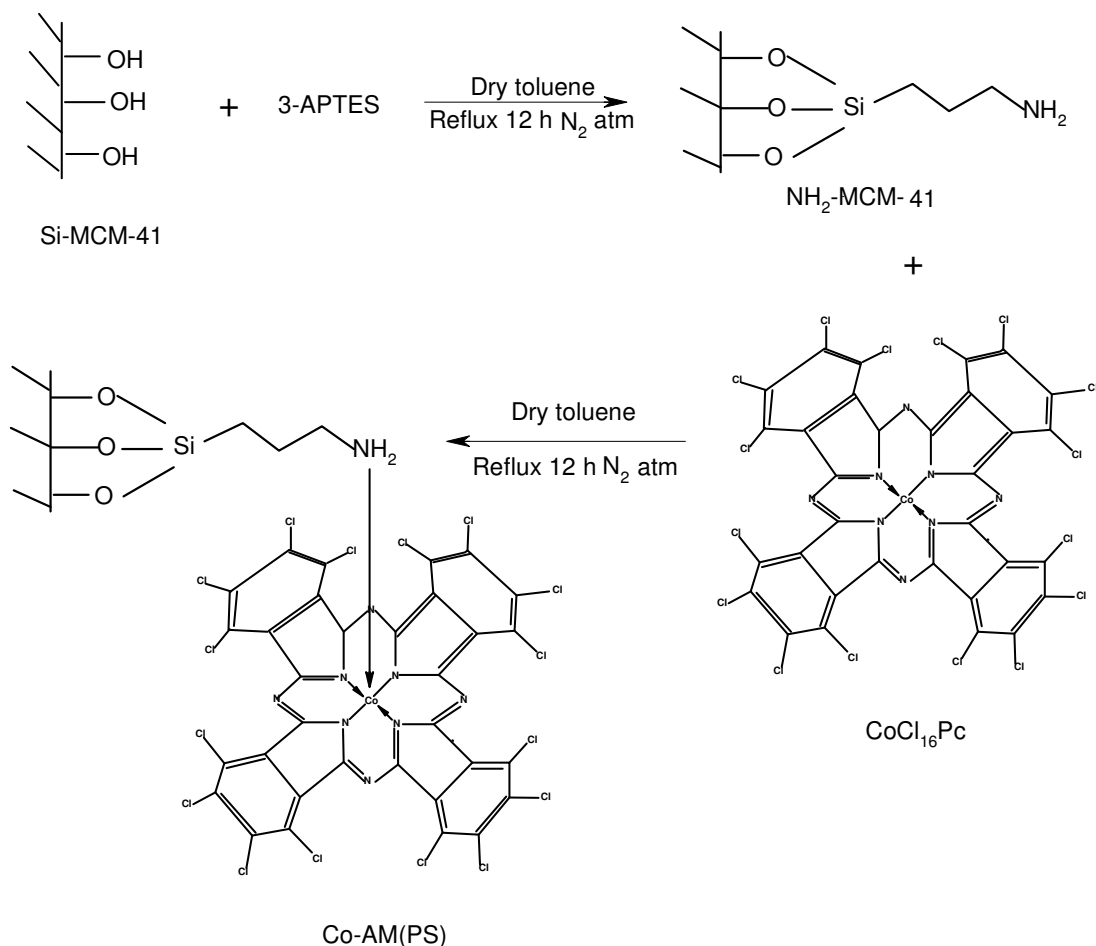
Fig. 2.1. Schematic presentation of grafted catalyst Co-AM(PS).

## 2.2.2.2. Impregnation of Co/Cu-Cl$_{16}$Pc

A solution of 0.022g of Co/Cu-Cl$_{16}$Pc in 20.0 ml of toluene was stirred and slowly added to a suspension of 0.5 g of Si-MCM-41 in toluene. It was refluxed for 12 h. A green material was separated by filtration, washed with acetone, dried under inert atmosphere at the temperature of 80$^o$ C and designated as Co/CuCl$_{16}$Pc-Si-MCM-41(I) [or Co/Cu-M(I)].

## 2.2.2.3. Grafting of Co/Cu-Cl$_{16}$Pc over SiO$_2$

### 2.2.2.3.1. Modification of SiO$_2$ with 3-aminopropyltriethoxysilane (3-APTES)

SiO$_2$ (0.5g), was dried by refluxing with dry toluene (8-10 h). The material was then filtered, washed with acetone and dried at room temperature under inert condition. SiO$_2$ was then mixed with the solution of 3-APTES in toluene (70.0 ml:0.22g) and stirred for a 12 h. This NH$_2$-SiO$_2$ was filtered and washed with acetone / dichloromethane and vacuum dried.

### 2.2.2.3.2. Anchoring of Co/Cu-Cl$_{16}$Pc

A solution of 0.022g of Co/Cu-Cl$_{16}$Pc in 20 ml of toluene was stirred and slowly added to a suspension of 0.5 g of NH$_2$- SiO$_2$ in toluene (as prepared in section 2.2.2.3.1.). The mixture was refluxed for 12 h. A green material was separated by filtration, washed with acetone, dried under inert atmosphere at the temperature of 80$^o$ C and designated as Co/CuCl$_{16}$Pc-NH$_2$-SiO$_2$ [or Co/Cu-A- SiO$_2$].

### 2.2.3. Catalytic reactions

Styrene (99 %), cyclohexene (99 %), 1-decene (99 %), cyclohexane (99 %), n-decane (99 %), acetonitrile (99 %) TBHP in decane (5.5 M), TBHP in ethylene dichloride (EDC 30 % solution), isobutyraldehyde (98 %) and benzaldehyde (98 %) were used as reactants without further purification. Catalytic reactions were carried out according to the following procedure. Substrate, solvent and catalyst were first introduced into a round-bottom flask. After the addition of oxidant, the reaction was started by immersing the flask in to the oil bath kept at the reaction temperature of 298 K and also 323 K. The reaction was carried out with vigorous stirring. All the products were quantified at different intervals by gas chromatography: Chrompack CP900 (Carbowax 20M): 50m X 0.32 mm capillary column using toluene as an internal standard.

### 2.3. CHARACTERIZATION

Crystalline phase identification of as synthesized, calcined and modified samples were carried out by XRD (Rigaku; Miniflex) using Nickel filtered CuK$\alpha$ radiation. Transmission electron images of Si-MCM-41 were obtained from a JEOL 1200 EX microscope operated at 100 kV. The sample was prepared by dispersing the powder in isopropanol. Depositing few drops of suspension on a carbon coated 400 mesh Cu grid enabled imaging. The chemical compositions of the samples were determined by a combination of wet chemical methods, atomic absorption  spectroscopy (AAS Hitachi, Model 2800) and elemental analysis  (Carlo Erba; EA1108). The surface area and pore volume were determined from N$_2$ adsorption-desorption isotherms using a Coulter (Omnisorb, 100 CX) instrument. The solid state magic-angle spinning MAS NMR spectroscopy studies were carried out on a Bruker MSL-500 FT-NMR spectrometer. The UV- Vis. spectra were recorded using a nujol mull on a SHIMADZU, UV-2101 PC

spectrometer. Fourier transform infrared (FT-IR) spectra were recorded with a Shimadzu FT-IR spectrometer (Model 8300). Electrochemical characterization (cyclic voltammetry) was carried out using a sample-coated Pt electrode (500 μm radius) and 0.1 M $KNO_3$ in DMSO with SCE as the reference electrode. The experiments were performed on a PAR 173 potentiostat coupled with a PAR 173 function generator. The data were recorded on a model RE0091 X-Y recorder. The solutions were purged with pure argon for 30 min. prior to the analysis.

## 2.3.1. Powder X-ray Diffraction

Since mesoporous molecular sieves lack strict crystallographic order on an atomic level, their wall structure cannot be determined from crystallographic data. Fig. 2.2. show X-ray diffraction pattern of (a) as synthesized MCM-41 and (b) calcined Si-MCM-41. As synthesized MCM-41 shows a typical four peak pattern [3], with a very strong (100) reflection at low angle ($2\theta = 2.1^{o}$) and three weaker (110), (200) and (210) reflections at the angle of $2\theta = 3.7^{o}$, $4.3^{o}$ and $5.6^{o}$ respectively from the quasi-regular arrangement of mesopores with hexagonal symmetry.
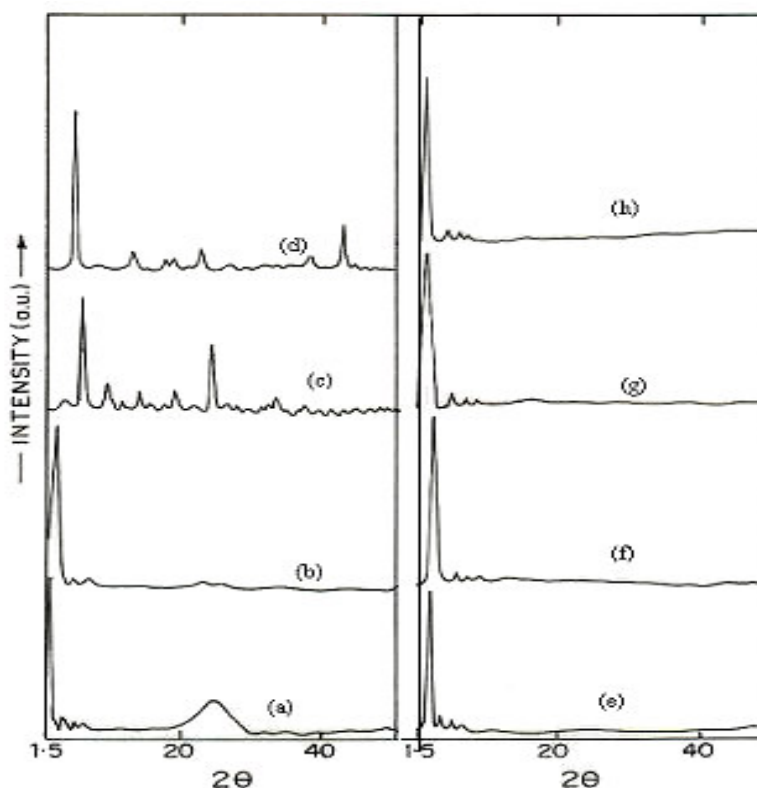
Fig. 2.2. XRD pattern of (a) as synthesized MCM-41, (b) calcined Si-MCM-41, (c) CuCl$_{16}$Pc, (d) CoCl$_{16}$Pc, (e) Cu-M(I), (f) Cu-AM(PS), (g) Co-M(I) and (h) Co-AM(PS).

On comparing the spectra of as-synthesized MCM-41 and calcined Si-MCM-41, it is observed that the most intense peak with (100) reflection is shifted to lower d$_{100}$ value with the other peaks showing marginal shift in the case of calcined sample, as calcination causes condensation of internal Si-OH groups giving rise to a contraction of the unit cell [3, 27, 28]. Si-MCM-41 shows intense peak at 2θ = 2.4$^o$ (100 reflection) with d$_{100}$ spacing value of ~ 42 Å. A significant increase in the intensity of this peak in calcined samples indicates that an atomic reorganization occurs during the removal of surfactant molecules in the calcination process [29]. XRD pattern of (c) CuCl$_{16}$Pc and (d) CoCl$_{16}$Pc shows characteristic peaks in the region of 2θ = 1.5 –50$^o$. The XRD pattern of CuCl$_{16}$Pc immobilized samples i.e. (e) Cu-M(I), (f) Cu-AM(PS) and CoCl$_{16}$Pc immobilized samples (g) Co-M(I), (h) Co-AM(PS) is similar to the host Si-MCM-41 i.e. sample (b). This indicates that the structure of Si-MCM-41 is retained even after grafting/impregnation of the metal complex with uniform dispersion of the complex in the pore of Si-MCM-41.

44

### 2.3.2. Transmission electron microscopy (TEM)

Transmission electron microscopy (TEM) has been used to obtain topographic information about the mesoporous matrices at near atomic resolution. Figure 2.3 shows the TEM images of Si-MCM-41 sample; (A) front view and (B) side view. TEM micrographs of the Si-MCM-41 samples seen along the pore direction, revealed regular hexagonal array of uniform channels as reported earlier [1-3].



|        (A)        |        (B)        |
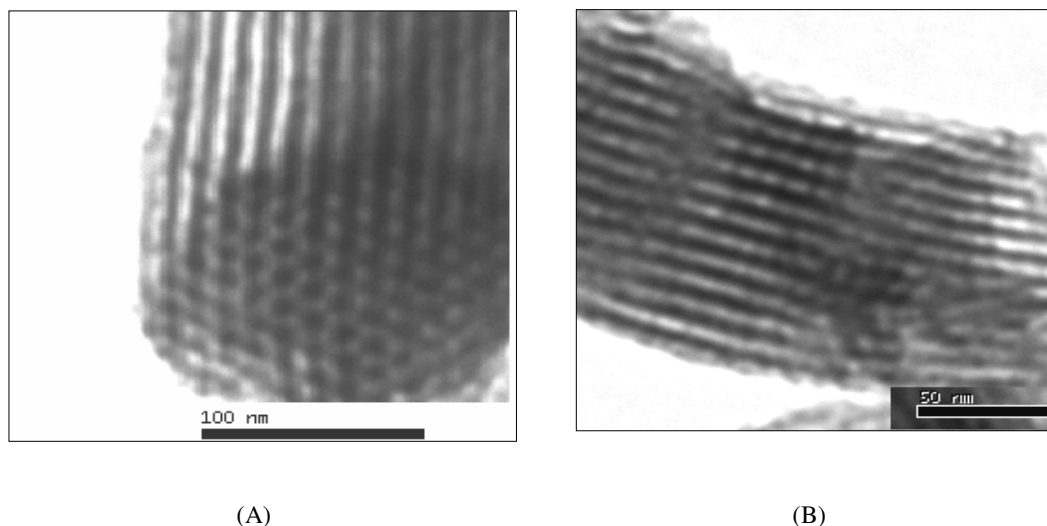
Fig. 2.3. TEM images of Si-MCM-41.

### 2.3.3. Physico-chemical analysis

Fig. 2.4 shows the representative $N_2$ adsorption-desorption isotherms for the samples (A) Si-MCM-41, (B) $NH_2$-MCM-41 and (C) Co-AM(PS). All the samples show type IV isotherms in the IUPAC classification [30] having a sharp capillary condensation step at $P/P_0 = 0.3–0.45$ region, which is characteristic of M41S type ordered mesoporous materials [31]. The insets of Fig. 2.4 represent the corresponding pore size distribution curves, computed from the BJH model. The surface area, pore volume and pore diameter of Si-MCM-41 and all the other catalysts are summarized in Table 2.2. The surface area of Si-MCM-41 decreases substantially on modification of 3-APTES. Further decrease in the surface area due to anchoring of the metal complex for [Co/Cu-AM(PS] is relatively smaller. A large surface area loss is also observed when Co/Cu-$Cl_{16}$Pc is loaded by impregnation. The decrease in the surface area during the grafting and impregnation of the metal complex may be attributed to channel occupation by the molecules.

(A)



(B)



(C)
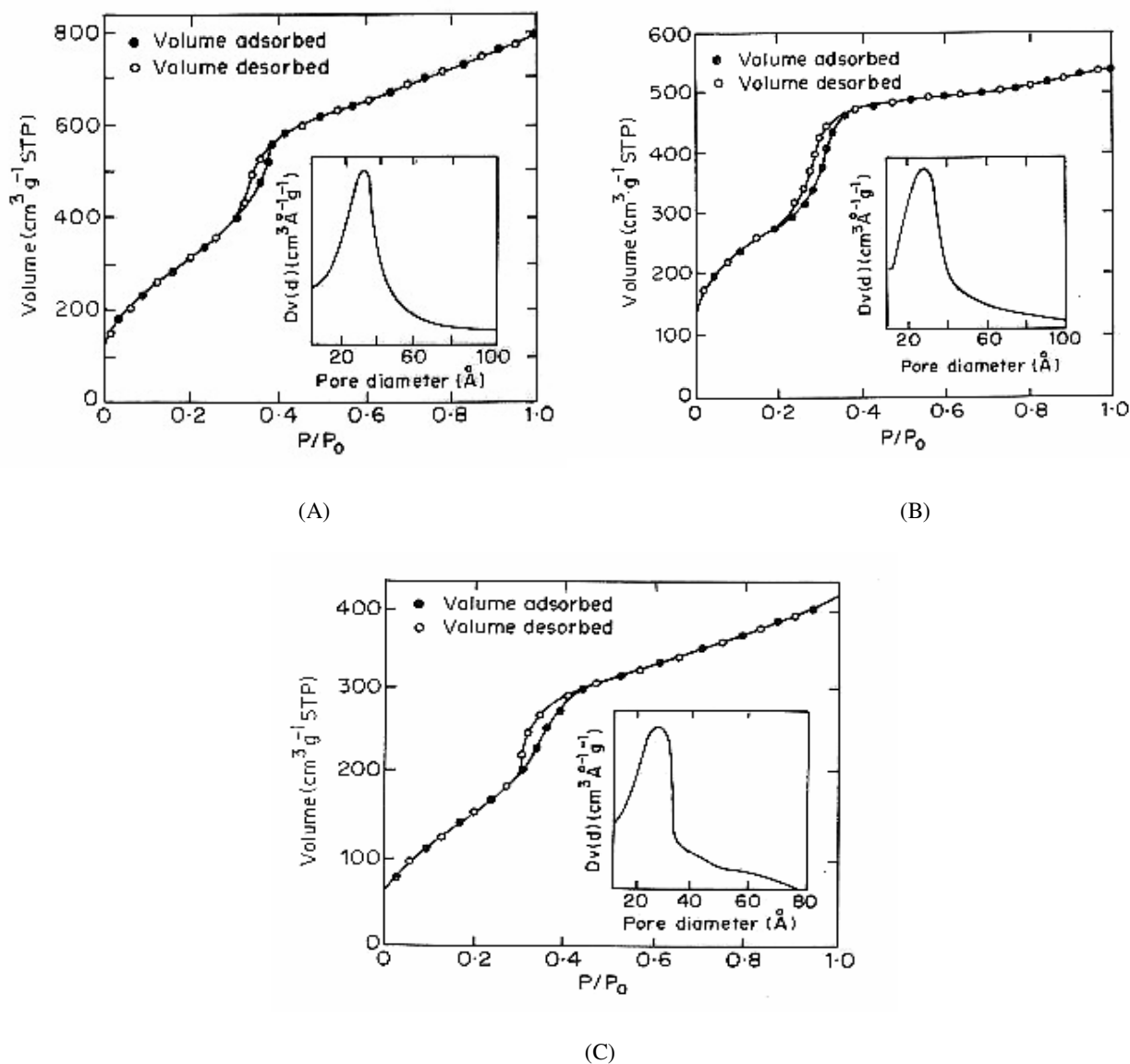
Fig. 2.4. $N_2$ adsorption-desorption isotherms of the samples (A) Si-MCM-41, (B) $NH_2$-MCM-41 and (C) Co-AM(PS). Inset shows pore size distribution of respective samples.

The carbon and nitrogen contents in the sample are presented in Table 2.2. The experimentally observed C/N (wt) ratio of 3.0 for the $NH_2$-MCM-41 sample is close to the expected value of 2.6. Assuming that all the carbon found in the 3-APTES treated samples comes from the amino-propyl group; calculations suggest that about one amino-propyl group is present for every 15 Si. Similarly, if we assume that the additional carbon present in the Co-Pc loaded sample [Co-AM(PS)] comes from the $CoCl_{16}Pc$ molecules, then the number of phthalocyanine molecules present are approximately one for about 500 Si. The

ratio of MPc/ amino group is nearly 46. Additionally, calculations reveal that for monolayer coverage of $CoCl_{16}Pc$ molecules on the surface of $NH_2$-MCM-41, the cobalt percentage should be ~ 3 wt %. This is about 15 times larger than the cobalt content (0.2 wt %) of Co-AM(PS) suggesting that only about 6 % of the surface is actually covered by phthalocyanine molecules. Similar calculations are also valid for Cu-AM(PS). The calculations suggest that $Co/Cu$-$Cl_{16}Pc$ molecules are well dispersed in the channels of MCM-41.

Table 2.2. Physicochemical properties of the samples.

| Sample | C/N analysis(wt %) | | $S_{BET}$ | Pore volume | Pore dia. |
|---|---|---|---|---|---|
| | C | N | $(m^2/g)$ | (cc/g) | (Å) |
| $CoC_{16}Pc$ | 34.00 | 9.00 | 54 | ----- | ----- |
| Si-MCM-41 | ---- | ---- | 1115 | 0.65 | 38 |
| $NH_2$-MCM-41 | 4.17 | 1.39 | 769 | 0.24 | 26 |
| Co-M(I); Co-0.2 % | 1.43 | 0.33 | 650 | 0.34 | 30 |
| Co-AM(PS); Co-0.2 % | 6.05 | 1.43 | 512 | 0.24 | 26 |
| $CuCl_{16}Pc$ | 33.86 | 9.94 | 57 | ---- | ---- |
| Cu-M(I); Cu-0.2 % | 1.43 | 0.33 | 621 | 0.32 | 29 |
| Cu-AM(PS); Cu-0.2 % | 6.00 | 1.42 | 584 | 0.22 | 25 |

### 2.3.4. Solid state MAS-NMR spectroscopy

The modification of Si-MCM-41 by 3-APTES was confirmed by the decrease of the silanol signals $Q_2$ (-91.6 ppm) and $Q_3$ (-101.5 ppm) and the appearance of a signal characteristic of $(SiO)_3Si-CH_3$ group (-68.22 ppm ) in the ^{29}Si MAS NMR spectrum (Figure 2.5.).
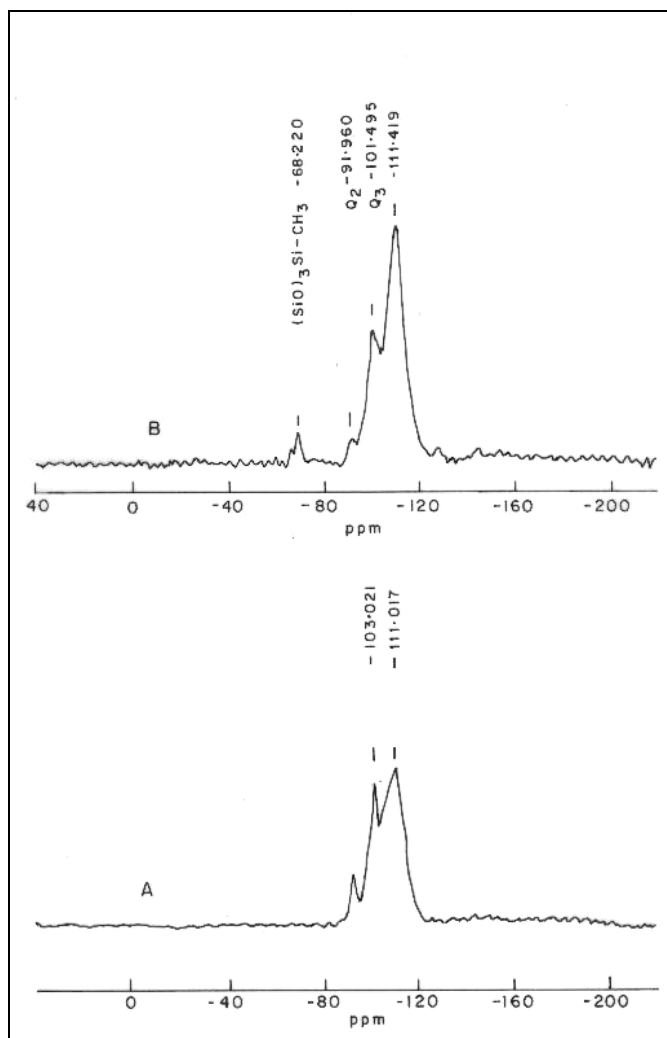


Fig. 2.5. ^{29}Si MASNMR spectrum of A) Si-MCM-41 and B) NH$_2$-MCM-41.

CP MASNMR of NH$_2$ - MCM-41 shows aminopropyl carbon signals at 6.4, 18.1 and 39.2 ppm, as seen in Figure 2.6. This indicates that 3-APTES has reacted with the hydroxyl groups on the walls of Si-MCM-41 [17].
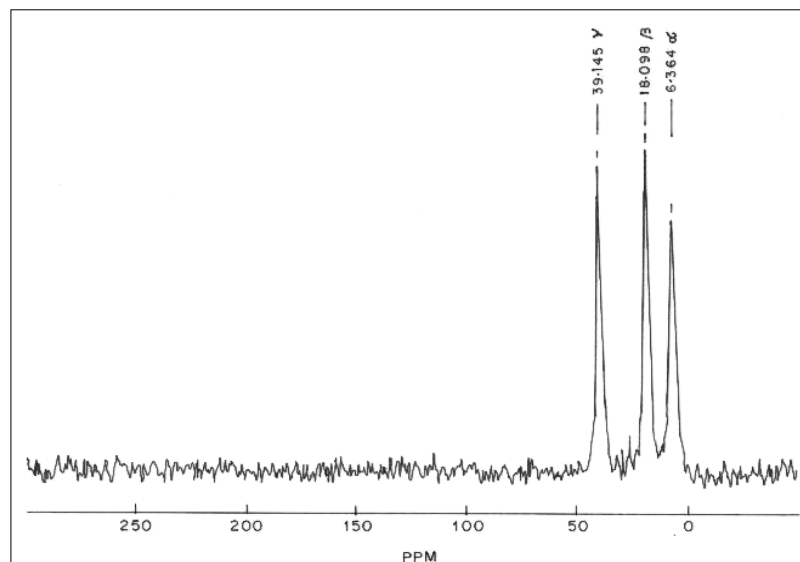
Fig. 2.6. CP MASNMR spectra of NH$_2$-MCM-41.

## 2.3.5. UV-Vis. spectroscopy

The UV-Vis. spectra of Co/Cu-Cl$_{16}$Pc, Co/Cu-M(I), NH$_2$-MCM-41 and Co/Cu-AM(PS) were recorded using nujol mull [Fig. 2.7. (A) and (B)]. The UV-Vis. spectra of NH$_2$-MCM-41 do not have any absorption band in the region 250-800 nm. Co/Cu-AM(PS), Co/Cu-M(I) and Co/Cu-Cl$_{16}$Pc [Fig. 2.7. (A) and (B),  curves 1, 2 and 3 respectively] exhibit strong absorption bands with a maximum at $\sim$ 300 nm and in the region of 550-800 nm due to ligand $\pi$-$\pi^*$ electronic transitions. The maximum position of the broad band of CoCl$_{16}$Pc is shifted from 652 to 637 nm on anchoring the complex with the 3-APTES modified MCM-41, [Co-AM(PS)]. Similarly the band maximum of CuCl$_{16}$Pc is also shifted from 654 to  633 nm for Cu-AM(PS). This blue shift is indicative of an increased $\pi$ overlap on grafting/impregnation of the complex molecule. In contrast to this, Balkus et al. [32] observed a red shift on encapsulation of   Co/Cu-F$_{16}$Pc in NaX zeolites and attributed it to a distortion of the phthalocyanine ligands in zeolite cages.

49
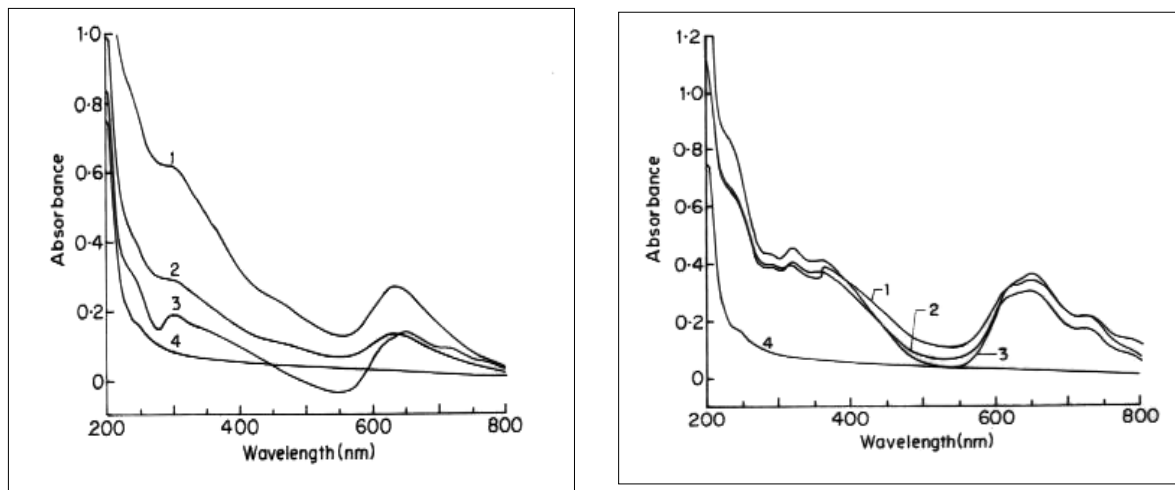
(A)                                                                      (B)

Fig. 2.7. UV-Vis. spectra of (A) 1. Co-AM(PS), 2. Co-M(I), 3. CoCl$_{16}$Pc, 4. NH$_2$-MCM-41 and
(B) 1. Cu-AM(PS), 2. Cu-M(I), 3. CuCl$_{16}$Pc, 4. NH$_2$-MCM-41.

## 2.3.6. Infra-red spectroscopy

The mid-infrared region from 1300-400 cm$^{-1}$ (recorded using nujol mull) contains vibrations due to the framework structure of zeolite [33]. The IR spectra due to lattice vibrations of as synthesized and calcined Si-MCM-41 molecular sieves revealed series of bands characteristic of SiO$_4$ tetrahedral unit assigned to asymmetric and symmetric stretching and deformation mode [34, 35] [ Fig. 2.8. (A) inset]. The IR spectra (2000-1300 cm$^{-1}$) of the original and grafted/impregnated samples of Si-MCM-41 were recorded using flurolube mull [Fig. 2.8. (A)]. The presence of metal phthalocyanine complex in the grafted samples was revealed by a band at ~ 1390 cm$^{-1}$. However, the intensity of the band was small compared to neat complex due to the low concentration of the Co/Cu-Cl$_{16}$Pc complex in the Co/Cu-AM(PS) samples (compare spectrum 2 with 3 for copper and spectrum 4 with 5 for cobalt containing samples). The negligible shift of the band position is indicative of the undisturbed planarity of the Co/Cu-Cl$_{16}$Pc complex on immobilization in Si-MCM-41 (effective pore diameter ~ 26 Å).
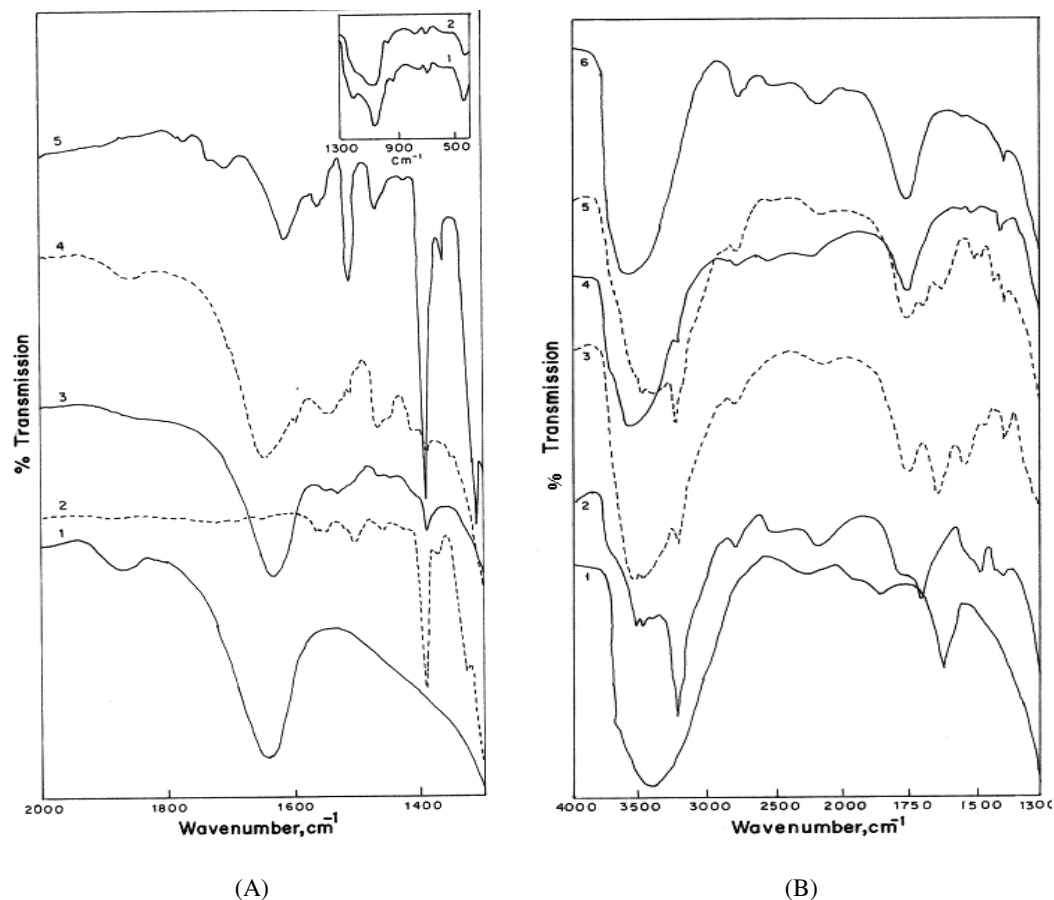
Fig. 2.8. (A) FTIR spectra of: 1. Si-MCM-41, 2. $CuCl_{16}Pc$ 3. Cu-AM(PS), 4. Co-AM(PS) 5. $CoCl_{16}Pc$

(Inset: 1. as synthesized Si-MCM-41, 2. calcined Si-MCM-41).

(B) FTIR spectra of: 1. Si-MCM-41, 2. $NH_2$-MCM-41, 3. Cu-AM(PS), 4. Cu-M(I), 5. Co-AM(PS),

6. Co-M(I).

The IR spectra (recorded using fluorolube) of Si-MCM-41, $NH_2$-MCM-41 and Co/Cu-AM(PS) in the 4000-1300 $cm^{-1}$ region are presented in Fig 2.8. (B). A broad band centered at ~ 3400 $cm^{-1}$ observed in the case of Si-MCM-41 (spectrum 1) is due to stretching vibrations of adsorbed water and silanol hydroxyl groups. The band at 1630 $cm^{-1}$ is assigned to the deformation vibrations of water.

The spectra of $NH_2$-MCM-41 and Co/Cu-AM(PS) (spectra 2, 3 and 5) exhibit bands at ~3365 and ~3285 $cm^{-1}$ superimposed on a broad band that can be assigned to asymmetric and symmetric stretching vibrations of amino group. Based on the FTIR spectra of the samples, it is not possible to confirm the interaction of the –$NH_2$ group of $NH_2$-MCM-41 with the central metal atom of Co/Cu-$Cl_{16}Pc$. However, this band is not observed very

51

clearly in the Co/Cu-AM(PS) samples due to strong absorption by water molecules in that region. Besides, in view of the large number of uncoordinated -NH$_2$ groups on the surface, it is unlikely that any shift in the –NH$_2$ frequency will be easily observed. Therefore, in view of the fact that metal phthalocyanine complex form adducts with amines and based on earlier reports that -NH$_2$ frequencies were not altered on coordination with Cu-schiff base complexes [36], it is concluded that interaction between the –NH$_2$ group of NH$_2$-MCM-41 and Co/Cu exists in the samples.

### 2.3.7. Cyclic Voltammetry

The electrochemical behavior of the samples was studied by cyclic voltammetry using 0.1 M KNO$_3$ in DMSO (dimethylsulphoxide) solution in the potential range of +0.5 to –2.0 V [37]. The sample coated Pt wire (500 μm diameter) was the working electrode and a Pt wire was used as the counter electrode. Standard calomel electrode (SCE) was used as the supporting electrode. The electrolyte solution was purged with argon prior to the analysis.

Fig. 2.9. show the cyclic voltammogram of the different catalysts of (A) CoCl$_{16}$Pc and (B) CuCl$_{16}$Pc. CoCl$_{16}$Pc reveal an initial central metal redox process followed by ring reduction process, whereas in the case of CuCl$_{16}$Pc, the central metal redox process is not observed until the phthalocyanine ring undergoes a redox cycle [38]. When cyclic voltammograms of different catalysts i.e. Co-ASiO$_2$, Co-M(I) and Co-AM(PS) along with neat metal complex, CoCl$_{16}$Pc were recorded, we observed the two redox processes, process I for the metal based electron transfer, Co(II)/Co(I) followed by process II for phthalocyanine ring reduction, [Co(I)Cl$_{16}$Pc(-2)]$^-$/ [Co(I)Cl$_{16}$Pc(-3)]$^{-2}$ (Table 2.3). It is observed that for the neat metal complex, Co(II)/Co(I) redox process is not well defined as a result of slow electron transfer kinetics which encourages the spontaneous aggregation of the complex. These redox processes are in agreement with those reported for the CoF$_{16}$Pc complex by Balkus et al. [32]. In the case of CoF$_{16}$Pc, the E$_{1/2}$ value shifted to a more positive potential compared to CoCl$_{16}$Pc due to the higher electronegativity of substituted fluorine atoms than the chlorine atoms in our case.

In the case of the CoCl$_{16}$Pc impregnated complexes [Co-M(I)] and the post synthesized catalysts [Co-AM(PS)] {Fig. 2.9. (A) c and d respectively} the Co(II)/Co(I) redox processes are well defined. This may be attributed to site isolation of the metal complex in the channels of Si-MCM-41 that makes the redox process well defined. For Co-

AM(PS), the redox process for the metal shifts to positive potential ($E_{1/2}$ = -0.220 V) which is higher by +0.04 V as compared to the impregnated catalyst; Co-M(I) ( i.e. $E_{1/2}$ = -0.260 V). This could be due to the interaction of the amino group with the four-coordinated $CoCl_{16}Pc$. The axial interaction of the fifth ligand causes the relative destabilization of Co(II) and stabilization of Co(I) state, thereby shifting the redox potential towards the positive side as compared to the four coordinated complex in the impregnated catalyst [39]. No significant change is observed for the redox process II (phthalocyanine ring reduction) in any of the above catalysts.



(A)                                                    (B)
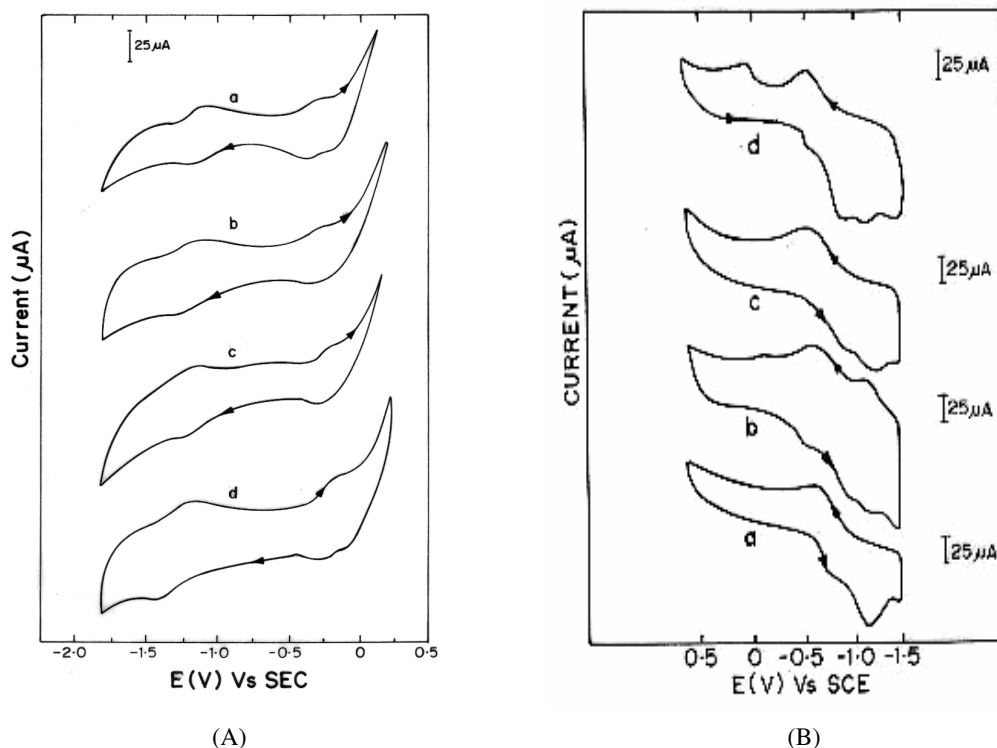
Fig. 2.9. Cyclic voltammogram of different catalysts of (A) $CoCl_{16}Pc$ i.e. (a) $CoCl_{16}Pc$ (b) Co-ASiO$_2$, (c) Co-M(I) and (d) Co-AM(PS).

and of (B) $CuCl_{16}Pc$ i.e. (a) $CuCl_{16}Pc$ (b) Cu-ASiO$_2$, (c) Cu-M(I) and (d) Cu-AM(PS).

In the case of $CuCl_{16}Pc$, {Fig. 2.9. (B) a} we did not get a redox peak for the metal as reported by Balkus et al. for $CuF_{16}Pc$ [32]. The last two redox waves in all cyclic voltammograms are attributed to ligand reduction process (Table 2.3). For the different $CuCl_{16}Pc$ catalysts we could observe the redox process for the metal due to the molecular distribution of complex avoiding the aggregation of the metal. Similar to cobalt catalysts, we observe a shift in the redox process I (redox process for the metal) for Cu-AM(PS) by +

0.087 V ($E_{1/2}$ = -0.25 V) as compared to the impregnated catalyst, Cu-M(I); ($E_{1/2}$ = -0.337 V).

Table 2.3. Summery of $E_{eq}$ (V/SCE) potential values of redox process.

| Catalyst | Process I (V) | Process II (V) | Process III (V) |
|---|---|---|---|
| CoCl$_{16}$Pc | -0.267 | -1.105 | --- |
| Co-M(I) | -0.260 | -1.160 | --- |
| Co- AM(PS) | -0.220 | -1.155 | --- |
| CuCl$_{16}$Pc | ---- | -0.750 | -1.280 |
| Cu-M(I) | -0.337 | -0.813 | -1.225 |
| Cu -AM(PS) | -0.250 | -0.785 | -1.275 |

The analogous processes for CuCl$_{16}$Pc can be represented as:

I.   $Cu^{II}$ [Cl$_{16}$Pc(−2)] / $Cu^{I}$ [Cl$_{16}$Pc(−2)]$^{-}$

II.   $Cu^{I}$ [Cl$_{16}$Pc(−2)]$^{-}$ / $Cu^{I}$ [Cl$_{16}$Pc(−3)]$^{2-}$

III. $Cu^{I}$ [Cl$_{16}$Pc(−3)]$^{2-}$ / $Cu^{I}$[Cl$_{16}$Pc(−4)]$^{3-}$

## 2.4. RESULTS AND DISCUSSION

### 2.4.1. Oxidation of alkenes

Epoxides are very useful and versatile synthetic compounds, constituting convenient building blocks for the synthesis of many commodity and fine chemicals. They are one of the most useful synthetic intermediates for the preparation of oxygen containing natural products or the production of epoxy resins etc. Selective epoxidation of alkenes using heterogeneous catalysts and clean oxidants under mild conditions is still a challenge [40, 41]. The direct epoxidation of alkenes generally uses expensive per-acids and produces large amount of effluents [14, 15]. It is highly desirable to replace conventional processes that use stoichiometric oxidants with environmentally more benign one using alkyl hydroperoxide and hydrogen peroxide. Much effort has been made to develop the direct and selective epoxidation of alkenes by use of molecular oxygen. However it is difficult to control the reaction because of over oxidations or side reactions under conventional severe reaction conditions, such as high pressure of oxygen or high reaction temperature. Therefore it is desirable to search milder reaction conditions using either dioxygen or air for development of an efficient epoxidation method.

Hence comparative study of oxidation of alkenes under mild reaction conditions using alkyl hydroperoxide and aldehyde/$O_2$ as oxidants is investigated.

### 2.4.1.1. Catalytic epoxidation using CoCl$_{16}$Pc immobilized catalysts

Table 2.4. show the results of oxidation of alkenes i.e. styrene, cyclohexene and 1-decene using two different oxidizing agents i.e. A- TBHP and B- isobutyraldehyde/$O_2$ and various catalysts of $CoCl_{16}Pc$ under mild reaction conditions (323 K). When the reaction is performed without the catalyst, it shows negligible product formation for both the oxidants i.e. A and B where as conversion is slightly improved when Si-MCM-41 is used as catalyst. This is due to the large hydrophobic surface area of MCM-41 adsorbing alkenes. For neat metal complex $CoCl_{16}Pc$, all the alkenes show higher conversion as compared to Si-MCM-41 as catalyst because the metal complex gives rise to highly active metal center due to the electron withdrawing effect of the substituted chlorine atoms.

Table 2.4 Comparison of two oxidizing agents for oxidation of olefins for various catalysts of $CoCl_{16}Pc$ (7 h data).

| Catalyst | Substrate | conversion (mole %) | | epoxide selectivity (mole %) | | TON | |
|---|---|---|---|---|---|---|---|
| | | A | B | A | B | A | B |
| Blank | Styrene | 3.0 | 7.9 | 1.2 | 3.3 | --- | --- |
| | Cyclohexene | 1.2 | 3.8 | 0.2 | 3.0 | --- | --- |
| | 1-decene | --- | --- | --- | --- | --- | --- |
| Si-MCM-41 | Styrene | 20.0 | 25.2 | 12.6 | 20.1 | --- | --- |
| (0.05g) | Cyclohexene | 9.6 | 14.2 | 1.6 | 13.0 | --- | --- |
| | 1-decene | 3.5 | 6.0 | 2.0 | 4.5 | --- | --- |
| $CoCl_{16}Pc$ | Styrene | 27.8 | 38.8 | 15.8 | 28.4 | 712 | 994 |
| (0.002g) | Cyclohexene | 16.2 | 27.4 | 3.5 | 23.6 | 415 | 702 |
| | 1-decene | 7.4 | 10.0 | 4.5 | 7.2 | 189 | 256 |
| Co-ASiO$_2$[a] | Styrene | 34.0 | 52.2 | 20.5 | 38.6 | 1075 | 1651 |
| (0.05g) | Cyclohexene | 23.0 | 36.0 | 3.5 | 28.2 | 727 | 1140 |
| | 1-decene | 10.0 | 17.6 | 6.0 | 11.4 | 316 | 556 |
| Co-M(I)[a] | Styrene | 45.6 | 80.6 | 27.6 | 62.2 | 1443 | 2548 |
| (0.05g) | Cyclohexene | 32.0 | 54.8 | 5.6 | 48.8 | 1012 | 1734 |
| | 1-decene | 20.0 | 38.7 | 12.8 | 30.1 | 632 | 1224 |
| Co-AM(PS)[a] | Styrene | 49.4 | 100 | 34.6 | 81.4 | 1563 | 3164 |
| (0.05g) | Cyclohexene | 36.2 | 77.8 | 7.0 | 70.0 | 1145 | 2462 |
| | 1-decene | 27.6 | 45.3 | 16.2 | 35.7 | 873 | 1433 |

[a] Co = 0.2 %, A- TBHP; B –isobutyraldehyde/ $O_2$

Conditions: substrate- 5 mmoles, solvent- acetonitrile, TBHP (in decane) -5 mmoles, isobutyraldehyde- 15 mmoles, molecular oxygen at atmospheric pressure, temperature 323 K.

The enhanced activity of Co-AM(PS) and Co-M(I) compared to the activity of the neat metal complex for both the oxidants i.e. A and B may be attributed to the larger hydrophobic surface area of mesoporous material favoring adsorption of alkenes and dispersion of metal complex resulting in increase the number of active sites. The fact that the performance of Co-AM(PS) is better than that of Co-M(I) may be due to the presence of

a lone pair of electrons of the amino group that originated from the aminopropyl group grafted on the silica wall. Earlier workers also reported an enhancement of catalytic activity in the presence of amines [42, 43]. The presence of a catalytic amount of bases helps to increase the initial rate of epoxidation; however, it also increases the yield of epoxides due to the base catalytic activity of the ligands, which facilitate O-O bond cleavage, and formation of high oxo intermediates [42].

## 2.4.1.2. Oxidation of styrene

Co-AM(PS) catalyst is found to be the most active one with 49.4 % conversion and 34.6 % epoxide selectivity for styrene when TBHP is used as the oxidant. Transition metal complexes are well known to catalyze the decomposition of organic peroxides. (i) Lu et al. [44] reported the reaction mechanism of styrene oxidation, resulting in three products (benzaldehyde, styrene epoxide, phenyl acetaldehyde) via the attack of t-BuOO$^{.}$ on styrene, followed by rearrangement. (ii) The formation of oxo-metal species may be taking place by the interaction of TBHP with metal, as suggested by Cramarossa et al. [45]. The oxo-metal species thus reacts directly with olefin to give epoxide.

It is observed that all the alkenes show 1.5 to 2 times higher product conversion (Fig. 2.10.) and higher epoxide yield [Fig. 2.11. for Co-AM(PS) catalyst] when isobutyraldehyde is used as oxidant as compared to TBHP. The oxo-metal species formed in both cases react directly with the alkene to give epoxide. But the catalytic decomposition of hydroperoxide into free radicals, attacking substrate molecules results in the formation of epoxide and benzaldehyde, which affect the total epoxide selectivity in the case of TBHP. On the other hand when isobutyraldehyde/$O_2$ is used as oxidant, it is possible to utilize the peroxidic intermediate for the additional oxidation e.g. the active oxygen of acyl peroxy radical and peracid are utilized for the epoxidation. This reaction gives a higher yield of epoxide as compared to oxidation using TBHP, since acyl peroxy radicals are more selective than alkyl peroxy redical i. e. favoring addition relative to abstraction [46].
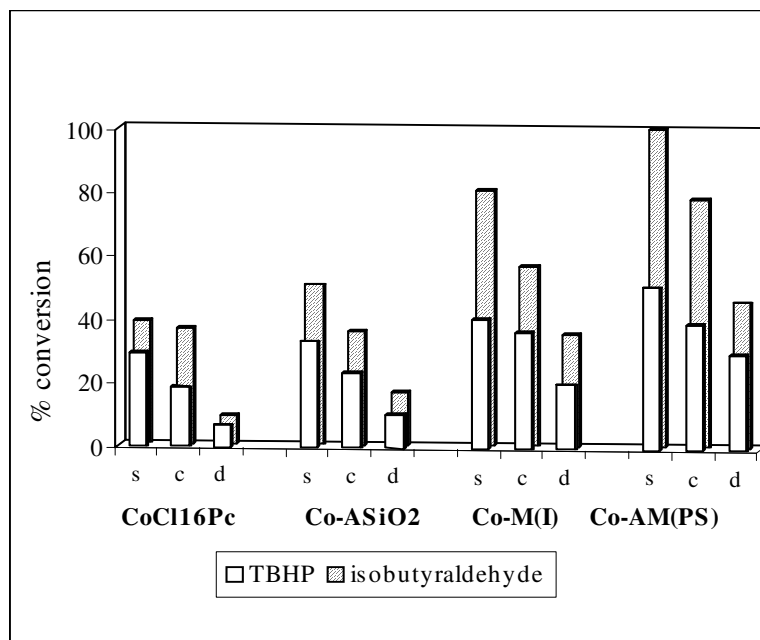
Fig. 2.10. Comparison of TBHP and isobutyraldehyde/$O_2$ for epoxidation of olefins using different catalysts of $CoCl_{16}Pc$ (s-styrene; c-cyclohexene; d-1-decene).
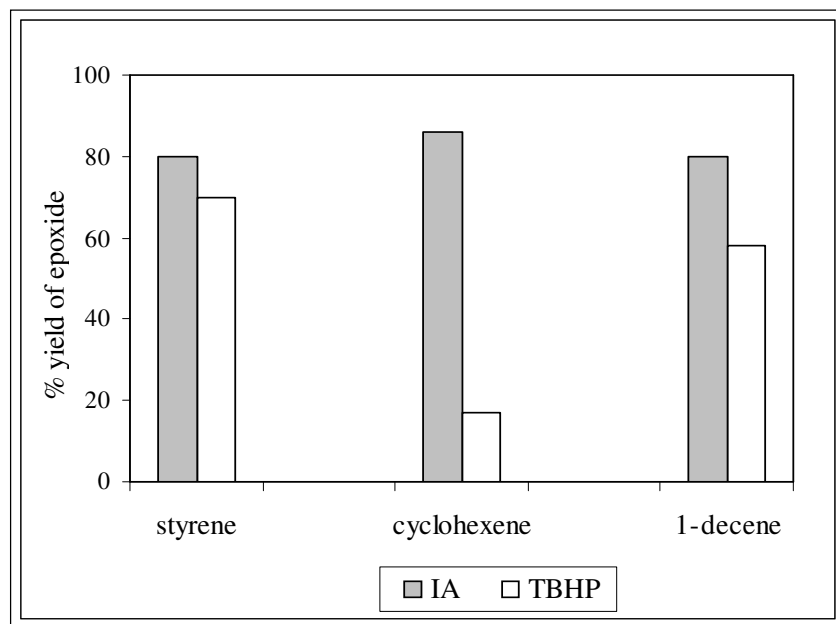


Fig. 2.11. Comparative study of two different oxidising agents for epoxide yield using Co-AM(PS) as catalyst (IA- isobutyraldehyde/$O_2$).

Conditions: substrate- 5 mmoles, solvent- acetonitrile, TBHP (in decane) -5 mmoles, isobutyraldehyde- 15 mmoles, molecular oxygen at atmospheric pressure, temperature 323 K.

The highly active catalyst Co-AM(PS) shows ~ 100 % conversion (81.4 % epoxide yield) for styrene when aldehyde is used as oxidant which is two times higher than for TBHP as oxidant. Mangemantin et al. [47] reported a styrene conversion above ~ 90% in presence of isobutyraldehyde over iron phthalocyanine catalyst covalently bonded to silica. But the ratio of catalyst : styrene used by them was ~ ten times more than ours, giving a TON ~ 250 as compared to TON ~ 3164 observed in the present work (Table 2.4.).

Typical conversion plots for the oxidation of styrene and isobutyraldehyde/$O_2$ show that relative rates of oxidation are in the ratio of 1:2 using Co-AM(PS) as 5 mmoles of styrene and 11 mmoles of isobutyraldehyde are converted after 7 h (Fig. 2.12.).
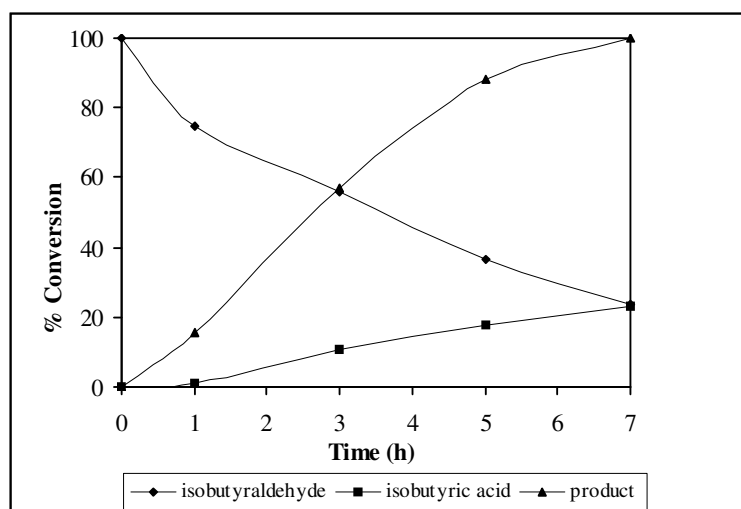


Fig. 2.12. Relative rates of oxidation of styrene and isobutyraldehyde over Co-AM(PS).

### 2.4.1.3. Oxidation of other olefins

As mentioned earlier, Co-M(I) and Co-AM(PS) appear to be the best catalysts for epoxidation of cyclohexene and 1-decene for both the oxidants i.e. A and B (Table 2.4). It is also observed that, when the reaction is carried out by using B as an oxidant, ~1.5 to 2 times higher conversion is obtained. When the oxidation of cyclohexene is carried out using Co-AM(PS) catalyst and TBHP as oxidant, cyclohexenone is the predominant product with 54 % yield. This is due to the presence of allylic hydrogen atom, which is more reactive as compared to double bond. Typically allylic oxidation products are found when hydrogen abstraction is the dominant reaction involving free radical mechanism (as in the case of TBHP as oxidant). But when the reaction is carried out using isobutyraldehyde/$O_2$ as an

oxidant, higher yield for cyclohexyl epoxide is observed i.e. 89.9 % (Table 2.4.). This is because in the case of B, predominant formation of metal oxo-species gives rise to electrophilic attack at the double bond resulting in higher epoxide formation or ring cleavage (Fig. 2.11) [48]. As the metal content in the catalyst is very low (0.2 % by AAS analysis), the TON for immobilized catalysts is larger compared to reported values [47]. In the case of $CoCl_{16}Pc$ immobilized catalysts TON is ~ 2 times higher in the presence of B (isobutyraldehyde/$O_2$) as compared to A (TBHP) as an oxidant.

When the reaction is carried out using copper perchlorophthalocyanine immobilized catalyst, a similar trend of product formation for A and B is observed (Table 2.5). Cu-AM(PS) is seen to be the best catalyst for both the oxidants and for the oxidation of styrene, 44.8 %  conversion for A and 90.6 % conversion for B is observed. Seelan et al. [49] have reported 95 % conversion of styrene and 23.8 % epoxide selectivity (after 24 h) on encapsulation of CuPc in zeolite Y. TBHP was used as oxidant and the TON observed was 10 times less than what we observed for above reactions over Cu-AM(PS) catalyst (Table 2.5.). Valente et al. [50] explain that, due to steric hindrance, the reactant molecules cannot approach the active metal site of encaged complexes and they react only with the radicals generated in the supercages of zeolite Y in the vicinity of the metallophthalocyanines, whereas in the case of Co/$CuCl_{16}Pc$ grafted on Si-MCM-41, because of the larger pore diameter, the approach of reactant molecules to oxo-metal species is not inhibited, resulting in higher epoxide selectivity.

Table 2.5. Comparison of two oxidizing agents for oxidation of olefins for various catalysts of $CuCl_{16}Pc$ (7 h. data).

| Catalyst | substrate | conversion (mole %) | | epoxide selectivity (mole %) | | TON | |
|---|---|---|---|---|---|---|---|
| | | A | B | A | B | A | B |
| $CuCl_{16}Pc$ | Styrene | 24.6 | 36.7 | 14.8 | 24.6 | 615 | 917 |
| (0.002g) | Cyclohexene | 14.3 | 24.0 | 3.6 | 21.8 | 366 | 615 |
| | 1-decene | 5.8 | 8.0 | 3.2 | 6.0 | 148 | 214 |
| $Cu-ASiO_2$[a] | Styrene | 28.8 | 48.5 | 17.8 | 31.5 | 900 | 1515 |
| (0.05g) | Cyclohexene | 18.7 | 32.6 | 3.7 | 24.5 | 489 | 857 |
| | 1-decene | 8.6 | 14.8 | 4.1 | 9.7 | 226 | 389 |
| $Cu-M(I)$[a] | Styrene | 35.5 | 75.8 | 23.8 | 65.4 | 1109 | 2368 |
| (0.05g) | Cyclohexene | 28.4 | 48.0 | 5.3 | 44.0 | 887 | 1600 |
| | 1-decene | 16.2 | 30.1 | 10.3 | 27.0 | 506 | 962 |
| $Cu-AM(PS)$[a] | Styrene | 44.8 | 90.6 | 30.5 | 70.0 | 1400 | 2831 |
| (0.05g) | Cyclohexene | 34.5 | 75.6 | 6.8 | 70.5 | 1090 | 2500 |
| | 1-decene | 25.7 | 40.0 | 14.7 | 35.4 | 813 | 1400 |

[a] $Cu = 0.2$ %, A- TBHP; B –isobutyraldehyde/$O_2$

Conditions: substrate- 5 mmoles, solvent- acetonitrile, TBHP (in decane) -5 mmoles, isobutyraldehyde- 15 mmoles, molecular oxygen at atmospheric pressure, temperature 323 K.

Here $CoCl_{16}Pc$ immobilized catalysts are seen to show slightly higher conversion for all the olefins and both the oxidants as compared to $CuCl_{16}Pc$ immobilized catalysts (see Table 2.4. and 2.5.). This is due to the higher oxidation potential of cobalt as compared to copper.

**2.4.2. Oxidation of alkanes**

Oxidation of alkanes is an important industrial process for both economic and environmental reasons. Therefore, it is desirable to replace conventional processes that use stoichiometric oxidants with environmentally more benign ones using alkyl hydroperoxides and hydrogen peroxide, but the best of all would be a process that could selectively oxidize hydrocarbons using either dioxygen or air under mild conditions. The previous section

(section 2.4.1.) presented a comparative study of oxidants i.e. TBHP and isobutyraldehyde/$O_2$ for alkene oxidation using various catalysts of Co/Cu-Cl$_{16}$Pc; the oxidation of alkanes (i.e. cyclohexane and decane) using the above oxidants and catalysts under mild reaction conditions is discussed next.

## 2.4.2.1. Oxidation of cyclohexane using Co/Cu-Cl$_{16}$Pc immobilized catalysts

Cyclohexane oxidation was carried out over Co/Cu-Cl$_{16}$Pc immobilized Si-MCM-41 catalysts using TBHP and isobutyraldehyde/$O_2$ as oxidizing agents at two different temperatures, 298 and 323 K (Table 2.6). It was observed that Co-AM(PS) showed the highest conversion of 5.1 % and 4.4 % for TBHP and isobutyraldehyde/$O_2$ respectively, at 298 K in 24 h. Similarly, Cu-AM(PS) showed a maximum of 3.7 % cyclohexane conversion when TBHP was used as the oxidant and 3.0 % conversion when isobutyraldehyde/$O_2$ was used as the oxidant at 298 K.

The kinetic studies at 323 K for both the oxidants (TBHP and isobutyraldehyde/$O_2$) show that cyclohexane conversion is in the order, Co/Cu-Cl$_{16}$Pc < Co/Cu-ASiO$_2$ < Co/Cu-M(I) < Co/Cu-AM(PS) [Fig. 2.13 (a) and 2.14 (a)]. The high activity of the supported complexes is due to the large hydrophobic surface area of MCM-41 and the molecular dispersion of the metal complexes within the pores. Further, the higher conversion of Co/Cu-AM(PS) compared to Co/Cu-M(I) may be due to the anchoring of the metal complex via the amino group to MCM-41, which could enhance the catalytic activity through easy reduction of the metal species [42, 43]. The kinetic plots also show a steady increase in the yields of cyclohexanol and cyclohexanone even at 24 h, specifically in the case of the grafted catalyst. This is due to the inherent stability of the chloro-substituted phthalocyanines, the neutral silica support and the mild conditions of the experiment. Kinetic plots reported earlier for cyclohexane oxidation at an oxygen pressure of 800 psi, using phthlocyanine anchored catalysts revealed that the conversion was nearly constant after ~5-8 h [51]. A similar behavior has been observed by Guo et al. [52] for iron/cobalt /manganese tetraphenyl porphyrins immobilized on chitosan at a relatively mild pressure of oxygen 0.6 MPa.

Table 2.6. Comparative study of oxidation of cyclohexane using (A) TBHP and (B) isobutyraldehyde/$O_2$ as oxidants at different temperatures and different catalysts of Co/Cu-$Cl_{16}Pc$ (24 h data).

| Catalyst | Oxidant | $T^a$ (K) | cyclohexane conversion mole % | % Yield -ol [b] | -one[c] | TON |
|---|---|---|---|---|---|---|
| $CoCl_{16}Pc$ (0.002 g) | A | 298 | - | - | - | - |
| | | 323 | 4.4 | 64 | 36 | 124 |
| | B | 298 | - | - | - | - |
| | | 323 | 2.2 | 59 | 41 | 62 |
| $Co-ASiO_2^*$ (0.05 g) | A | 298 | 2.0 | 69 | 30 | 63 |
| | | 323 | 5.2 | 67 | 33 | 164 |
| | B | 298 | 1.1 | 62 | 38 | 34 |
| | | 323 | 3.4 | 58 | 42 | 107 |
| $Co-M(I)^*$ (0.05 g) | A | 298 | 3.7 | 76 | 24 | 104 |
| | | 323 | 7.8 | 58 | 42 | 246 |
| | B | 298 | 2.3 | 39 | 60 | 67 |
| | | 323 | 4.2 | 41 | 59 | 123 |
| Co-AM(PS)$^*$ (0.05 g) | A | 298 | 5.1 | 64 | 35 | 161 |
| | | 323 | 13.4 | 56 | 43 | 424 |
| | B | 298 | 4.4 | 38 | 61 | 129 |
| | | 323 | 6.4 | 40 | 60 | 188 |
| $CuCl_{16}Pc$ (0.002 g) | A | 298 | - | - | - | - |
| | | 323 | 2.0 | ~100 | 0.0 | 57 |

| | | | | | | |
|---|---|---|---|---|---|---|
| | B | 298 | - | - | - | - |
| | | 323 | 1.6 | 62 | 37 | 47 |
| Cu-ASiO$_2$[*] (0.05 g) | A | 298 | - | - | - | - |
| | | 323 | 2.4 | 83 | 17 | 85 |
| | B | 298 | - | - | - | - |
| | | 323 | 2.2 | 63 | 36 | 70 |
| Cu-M(I)[*] (0.05 g) | A | 298 | 2.2 | 80 | 20 | 70 |
| | | 323 | 6.2 | 62 | 38 | 196 |
| | B | 298 | ~1.0 | 59 | 40 | 31 |
| | | 323 | 3.8 | 44 | 56 | 120 |
| Cu-AM(PS)[*] (0.05 g) | A | 298 | 3.7 | 66 | 34 | 117 |
| | | 323 | 10.4 | 58 | 42 | 330 |
| | B | 298 | 3.4 | 49 | 50 | 107 |
| | | 323 | 6.2 | 40 | 60 | 196 |

[*] Metal 0.2 % [a] temperature, [b] respective alcohol, [c] respective ketone.

Conditions: substrate 5 mmoles, TBHP 5 mmoles, aldehyde 15 mmoles, solvent acetonitrile, molecular oxygen 1 atm.

On comparing the performance of the two oxidizing agents, it is observed that TBHP is nearly two times more active compared to isobutyraldehyde/O$_2$ for cyclohexane oxidation at 323 K [Fig. 2.13. (b) and 2.14. (b)]. The conversion is 13.4% and 10.4 % for Co-AM(PS) and Cu-AM(PS) respectively, for TBHP, whereas it is 6.4 % and 6.2 % for isobutyraldehyde/O$_2$ at 24 h. These results are contradictory to the previous observation of alkene oxidation (section 2.4.1.) in which exclusive formation of oxo-metal species and heterolytic decomposition were shown to play an important role in enhanced conversion of alkenes when isobutyraldehyde/O$_2$ was used as the oxidant as compared to TBHP.

TON value for Co-AM(PS) being the largest compared to other catalysts for both TBHP (TON = 424) and isobutyraldehyde/ $O_2$ (TON = 188) [Fig. 2.14.(c)]. For copper containing catalysts we observed the similar trend of TON values and Cu-AM(PS) shows TON of 330 for TBHP and 196 for isobutyraldehyde/$O_2$ as oxidant [Fig. 2.13. (c)].

Alkanes are susceptible to homolytic attack in which free radicals are intermediates. The tBuO$^.$ radical formed from homolytic decomposition of TBHP which is more favored than to tBuOO$^.$ [53], preferentially abstracts hydrogen to give the cyclohexyl radical. In the case of alkane oxidation this homolytic decomposition is more favored compared to the heterolytic decomposition of the O-O bond. Also alkyl peroxy radicals are more stable as compared to acyl peroxy radicals formed by isobutyraldehyde that are readily converted into per acids favoring a heterolytic mechanism [46]. The above arguments may probably explain the larger alkane oxidation with TBHP compared to isobutyraldehyde/$O_2$.
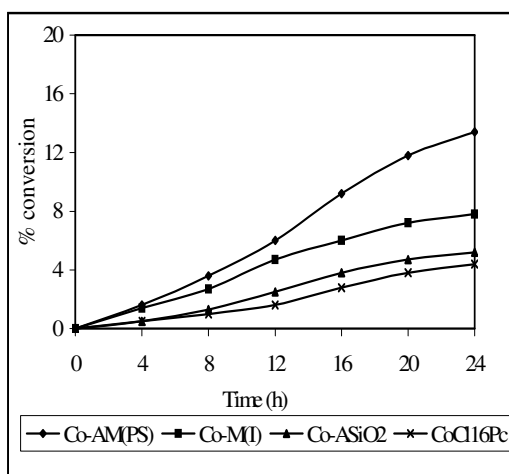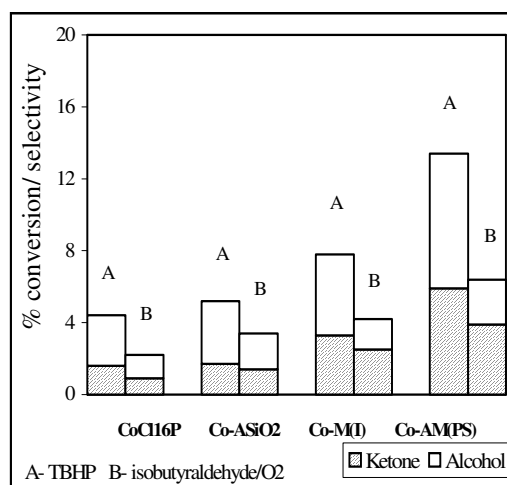


(a)                                                                 (b)
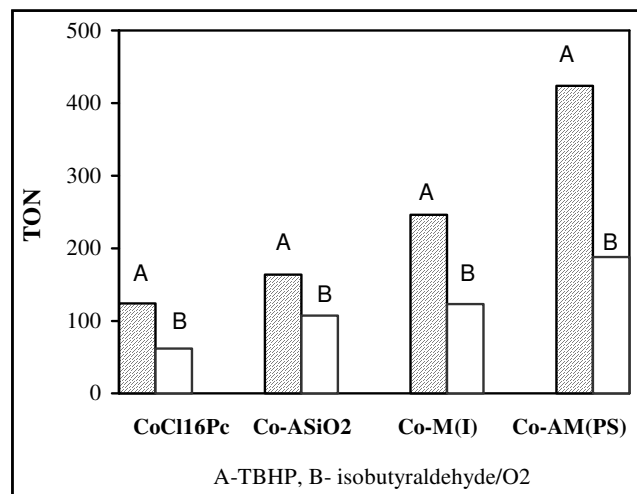
(c)

Fig. 2.13. (a) Kinetic study of cyclohexane oxidation using different $CoCl_{16}Pc$ catalysts using TBHP as oxidant at 323 K.

(b) Comparison of TBHP and isobutyraldehyde/$O_2$ for cyclohexane oxidation using different $CoCl_{16}Pc$ catalysts at 323K.

(c) Comparison of TON values for the different $CoCl_{16}Pc$ catalysts: (A) TBHP and (B) isobutyraldehyde/$O_2$.

TON = mole of product formation/ mole of metal present in the catalyst/ 24 h.



(a)



(b)

66
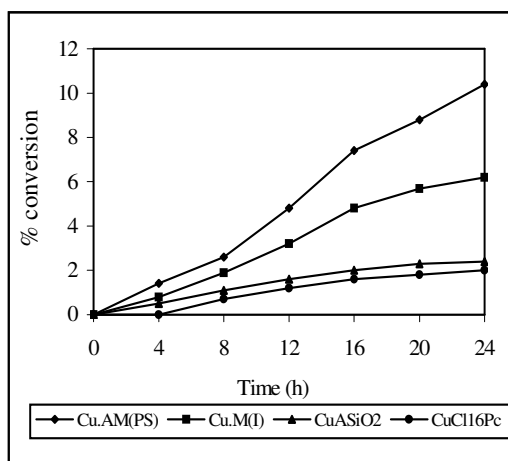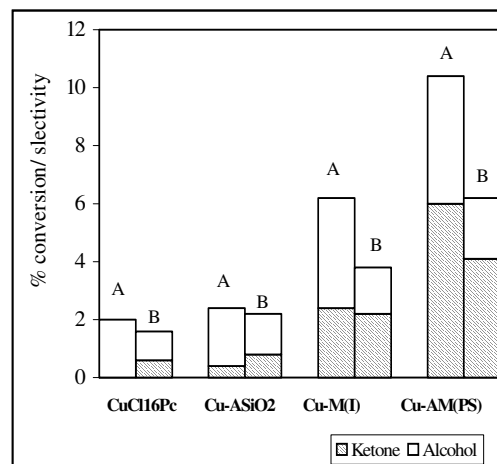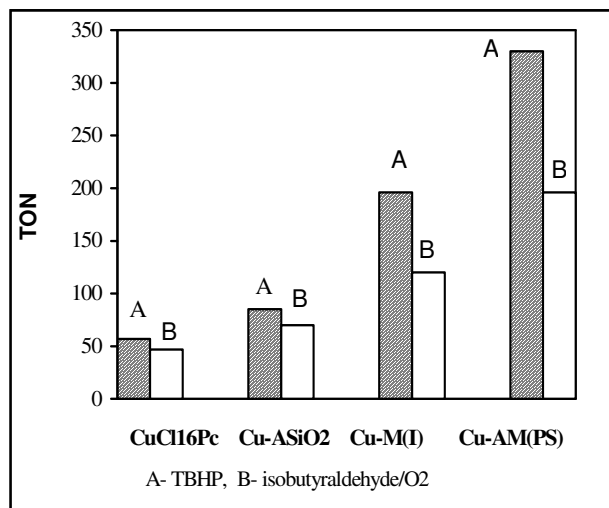
(c)

Fig. 2.14. (a) Kinetic study of cyclohexane oxidation over different $CuCl_{16}Pc$ catalysts using TBHP as oxidant at 323 K.

(b) Comparison of (A) TBHP and (B) isobutyraldehyde/$O_2$ for cyclohexane oxidation using different $CuCl_{16}Pc$ catalysts at 323K.

(c) Comparison of TON values for the different $CuCl_{16}Pc$ catalysts: (A) TBHP and (B) isobutyraldehyde/$O_2$.

TON = mole of product formed/ mole of metal present in the catalyst/ 24 h.

Conditions: substrate 5 mmoles, TBHP 5 mmoles, aldehyde 15 mmoles, solvent acetonitrile, molecular oxygen 1 atm.

The selectivity for cyclohexanone is higher for isobutyraldehyde/$O_2$ than for TBHP and the ratio of cyclohexanol : cyclohexanone being 1.0:1.5 for the grafted catalysts of cobalt and copper i.e. for Co/Cu-AM(PS) in spite of the low conversions [Fig. 2.13. (b) and 2.14 (b)]. The interaction of isobutyraldehyde with $M^{2+}$ (where M = Co or Cu) gives an acyl peroxy $M^{2+}$ complex followed by heterolytic O-O bond cleavage to give an oxo-metal species [24]. This species abstracts hydrogen to give a cyclohexane radical which reacts with $O_2$ to produce the cyclohexyl peroxy radical and thus leads to a 1.0:1.0 ratio of cyclohexanol and cyclohexanone according to a Russell type termination reaction [54]. Cyclohexanol is further oxidized simultaneously to give cyclohexanone which increases the overall ketone yield.

On the contrary, in the case of TBHP, the overall ratio of cyclohexanol : cyclohexanone is 1.5:1.0. The homolysis of the O-O bond in $M^{2+}$-O-O-tBu produces tBuO˙ which abstracts a hydrogen atom from cyclohexane to give the corresponding radical species. This species further reacts to give cyclohexanol as the primary product. Fig. 2.15.

67

presents a comparison of percentage yield of cyclohexanone using TBHP and isobutyraldehyde/$O_2$ over Co/Cu-AM(PS) catalysts.
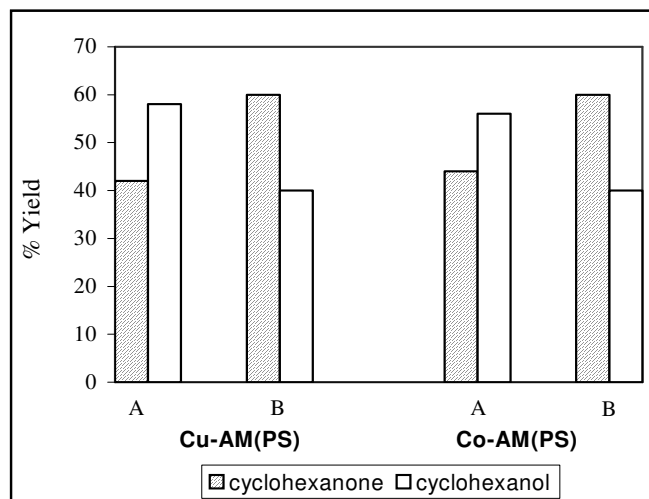


Fig. 2.15. Comparison of cyclohexanone yield for (A) TBHP and (B) isobutyraldehyde/$O_2$ over Cu-AM(PS) and Co-AM(PS) at 323 K.

## 2.4.2.2. Oxidation of n-decane using Co/Cu-Cl$_{16}$Pc immobilized catalysts

The oxidation of n-decane over different Co/Cu-Cl$_{16}$Pc catalysts was studied at 298 and 323 K using TBHP and isobutyraldehyde/$O_2$ as oxidizing agents (Table 2.7.). Decane conversion was low for all the Co/Cu-Cl$_{16}$Pc immobilized MCM-41 catalysts for both the oxidizing agents when the reactions were carried out at room temperature (298 K). It was observed that Co-AM(PS) showed a maximum conversion of 6.4 % and 4.6 % for TBHP and isobutyraldehyde/$O_2$ respectively, the conversions being 5.6 % for TBHP and 4.0 %, for isobutyraldehyde/$O_2$ over Cu-AM(PS) at 298 K.

As mentioned earlier, Co/Cu-M(I) and Co/Cu-AM(PS) are the most active catalysts for both the oxidizing agents [Fig. 2.16. (a) and 2.17. (a)]. When the two oxidizing agents are compared, the conversion of decane using TBHP is nearly double as compared to using isobutyraldehyde/$O_2$ for all the catalysts at 323 K with the higher selectivity for decanone [Fig. 2.16. (b) and 2.17. (b)]. Co-AM(PS) shows 16.4 % decane conversion for TBHP and 9.0 % for isobutyraldehyde/$O_2$ at 323 K. Similarly, Cu-AM(PS) shows 21.2 % conversion of decane for TBHP and 9.2 % for isobutyraldehyde/$O_2$ at the same temperature. For both the oxidizing agents and both Co/Cu-Cl$_{16}$Pc complexes a large yield of decanone ~ 95 to 97 % (mixture of 2, 3, 4-decanones) with a small selectivity for decanol is observed, whereas for the complex grafted catalysts, ~ 100 % yield of decanone is observed (Table 2.7). The

TON value for Co-AM(PS) is more than the other catalysts of $CoCl_{16}Pc$ which is 525 when TBHP is used and 284 when isobutyraldehyde/$O_2$ is used as oxidizing agent [Fig. 2.16 (c)]. For copper containing catalysts, we observed TON values for Cu-AM(PS) being more than the other catalysts for both TBHP (TON = 671) and isobutyraldehyde/$O_2$ (TON = 291) [Fig. 2.17. (c)].

It is noticed that the conversion of n-decane is more than cyclohexane over both the metal catalysts for both the oxidants. A similar behavior was observed in the case of titanium containing siliceous catalysts used for the oxidation of alkanes [55]. This may be due to the differences in adsorption of n-alkane and cyclohexane over siliceous supports like MCM-41 [56].

Table 2.7. Comparative study of oxidation of n-decane using (A) TBHP and (B) isobutyraldehyde/$O_2$ as oxidants at different temperatures and different catalysts of Co/Cu-Cl$_{16}$Pc (24 h data).

| Catalyst | Oxidant | $T^a$ (K) | n-decane conversio mole % | % Yield -ol [b] | % Yield -one[c] | TON |
|---|---|---|---|---|---|---|
| CoCl$_{16}$Pc (0.002 g) | A | 298 | 1.4 | trace | 97 | 62 |
| | | 323 | 4.8 | trace | 96 | 138 |
| | B | 298 | ~1.0 | trace | 97 | 28 |
| | | 323 | 2.0 | trace | 98 | 56 |
| Co-ASiO$_2$[*] (0.05 g) | A | 298 | 3.2 | 0 | ~100 | 101 |
| | | 323 | 7.6 | 0 | ~100 | 240 |
| | B | 298 | 2.2 | 0 | ~100 | 70 |
| | | 323 | 3.4 | 0 | ~100 | 107 |
| Co-M(I)[*] (0.05 g) | A | 298 | 4.7 | 0 | ~100 | 138 |
| | | 323 | 11.2 | 0 | ~100 | 354 |
| | B | 298 | 3.1 | 0 | ~100 | 91 |
| | | 323 | 5.4 | 0 | ~100 | 158 |
| Co-AM(PS)[*] (0.05 g) | A | 298 | 6.4 | 0 | ~100 | 202 |
| | | 323 | 16.4 | 0 | ~100 | 525 |
| | B | 298 | 4.6 | 0 | ~100 | 145 |
| | | 323 | 9.0 | 0 | ~100 | 284 |
| CuCl$_{16}$Pc (0.002 g) | A | 298 | 1.3 | trace | 97 | 36 |
| | | 323 | 4.1 | trace | 96 | 116 |

| | | | | | | |
|---|---|---|---|---|---|---|
| | B | 298 | ~1.0 | trace | 97 | 29 |
| | | 323 | 2.0 | trace | 98 | 59 |
| Cu-ASiO$_2$[*] (0.05 g) | A | 298 | 2.0 | 0 | ~100 | 63 |
| | | 323 | 7.4 | 0 | ~100 | 234 |
| | B | 298 | 1.2 | 0 | ~100 | 38 |
| | | 323 | 3.2 | 0 | ~100 | 101 |
| Cu-M(I)[*] (0.05 g) | A | 298 | 3.1 | 0 | ~100 | 98 |
| | | 323 | 10.8 | 0 | ~100 | 341 |
| | B | 298 | 2.0 | 0 | ~100 | 63 |
| | | 323 | 5.4 | 0 | ~100 | 170 |
| Cu-AM(PS)[*] (0.05 g) | A | 298 | 5.6 | 0 | ~100 | 177 |
| | | 323 | 21.2 | 0 | ~100 | 671 |
| | B | 298 | 4.0 | 0 | ~100 | 126 |
| | | 323 | 9.2 | 0 | ~100 | 291 |

[*] Metal 0.2 %, [a] temperature, [b] respective alcohol, [c] respective ketone.

Conditions: substrate 5 mmoles, TBHP 5 mmoles, aldehyde 15 mmoles, solvent acetonitrile, molecular oxygen 1 atm.
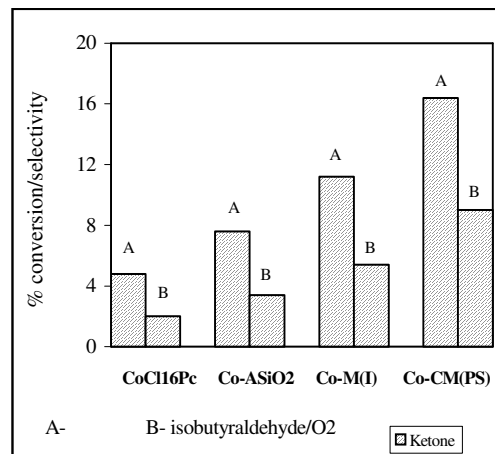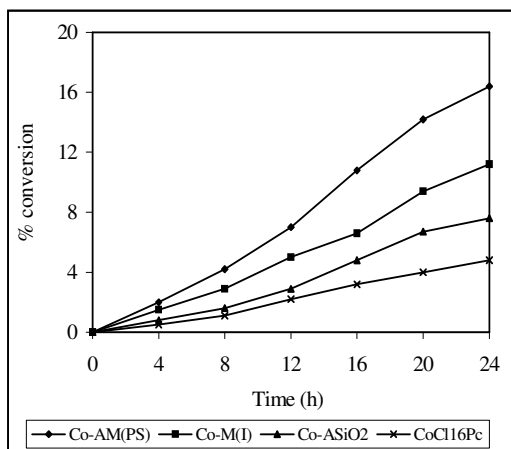
(a)



(b)
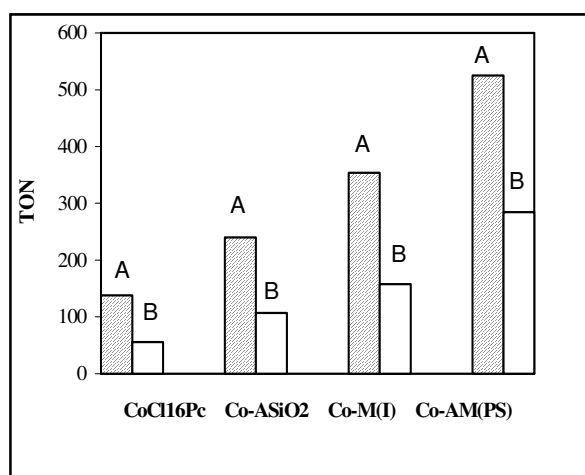


(c)

Fig. 2.16. (a) Kinetic study of n-decane oxidation using different $CoCl_{16}Pc$ catalysts using TBHP as oxidant at 323 K.

(b) Comparison of TBHP and isobutyraldehyde/$O_2$ for n-decane oxidation using different $CoCl_{16}Pc$ catalysts at 323 K.

(c) Comparison of TON values for the different $CoCl_{16}Pc$ catalysts: (A) TBHP and (B) isobutyraldehyde/$O_2$

TON = mole of product formed/ mole of metal present in the catalyst/ 24 h.
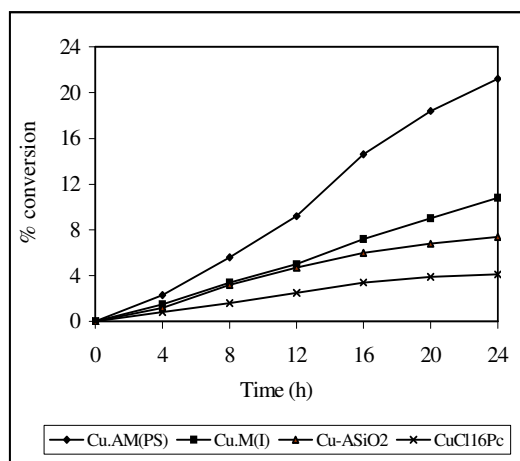
(a)
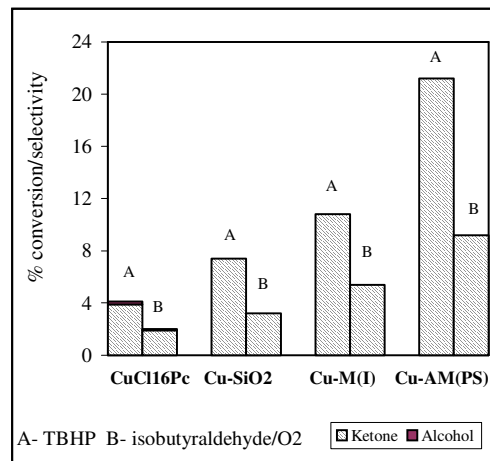


(b)
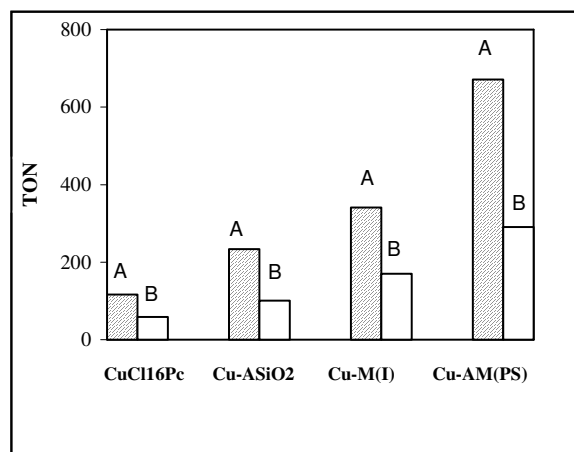


(c)

Fig. 2.17. (a) Kinetic study of n-decane oxidation using different CuCl$_{16}$Pc catalysts using TBHP as oxidant at 323 K.

(b) Comparison of TBHP and isobutyraldehyde/O$_2$ for n-decane oxidation using different CuCl$_{16}$Pc catalysts at 323K.

(c) Comparison of TON values for the different CuCl$_{16}$Pc catalysts (A) TBHP and (B) isobutyraldehyde/O$_2$.

TON = mole of product formed/ mole of metal present in the catalyst/ 24 h.

Conditions: substrate 5 mmoles, TBHP 5 mmoles, aldehyde 15 mmoles, solvent acetonitrile, molecular oxygen 1 atm.

73

### 2.4.2.3. Oxidation of alkanes using two different cooxidising agents

Table 2.8. presents a comparative study of isobutyraldehyde/$O_2$ with benzaldehyde/$O_2$ as co-oxidants for the oxidation of alkanes under mild reaction conditions (323 K). It is observed that for both the oxidants, Co/Cu-AM(PS) is a better catalyst compared to the neat metal complex, Co/Cu-ASiO$_2$, and Co/Cu-M(I) (Fig. 2.18. and 2.19.).

For the different catalysts of Co/Cu-Cl$_{16}$Pc, results of cyclohexane oxidation show that benzaldehyde/$O_2$ gives ~ 1.5 times higher TON values compared to isobutyraldehyde/$O_2$ (Table 2.8.). This may be due to the higher resonance stability of the intermediate aromatic acyl peroxy radical in the case of benzaldehyde compared to isobutyraldehyde. Co-AM(PS) gives 12.4 % conversion of cyclohexane for benzaldehyde/$O_2$ and 6.4 % for isobutyraldehyde/$O_2$ at 323 K [Fig. 2.18. (a)]. Cu-AM(PS) gives 9.4 % cyclohexane conversion for benzaldehyde/$O_2$ and 6.2 % for isobutyraldehyde/$O_2$ at 323 K [Fig. 2.19. (a)]. The selectivity of cyclohexanone is also higher in the case of benzaldehyde/$O_2$ as the oxidant; cyclohexanol : cyclohexanone ratio is 1.0:2.0 compared to 1.0:1.5 for isobutyraldehyde/$O_2$.



(a)                                                        (b)
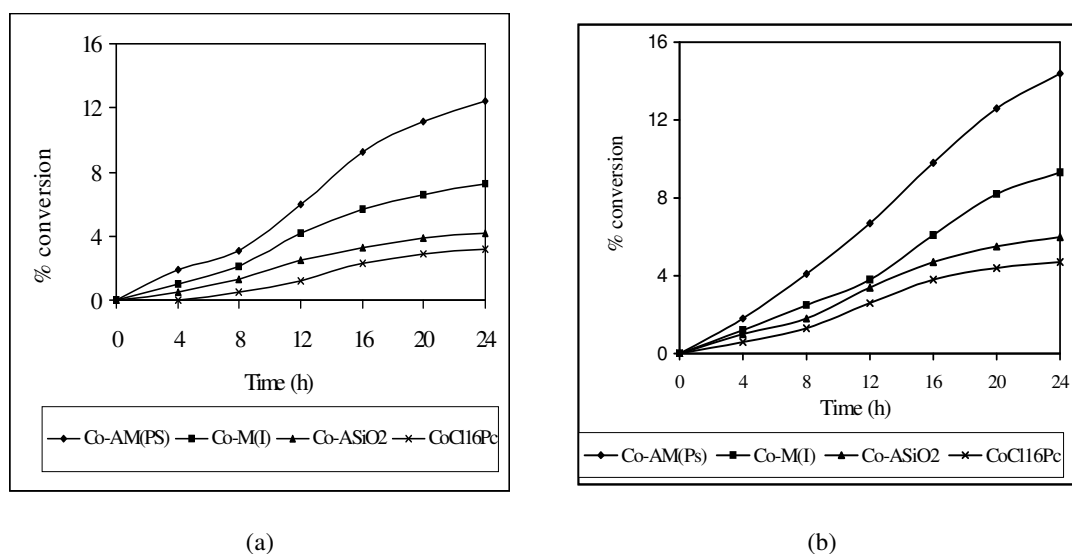
Fig. 2.18. (a) Kinetics study of cyclohexane oxidation using different catalysts of CoCl$_{16}$Pc using benzaldehyde/$O_2$; (b) Kinetics study of decane oxidation using different catalysts of CoCl$_{16}$Pc using benzaldehyde/$O_2$.

(a)                                                        (b)
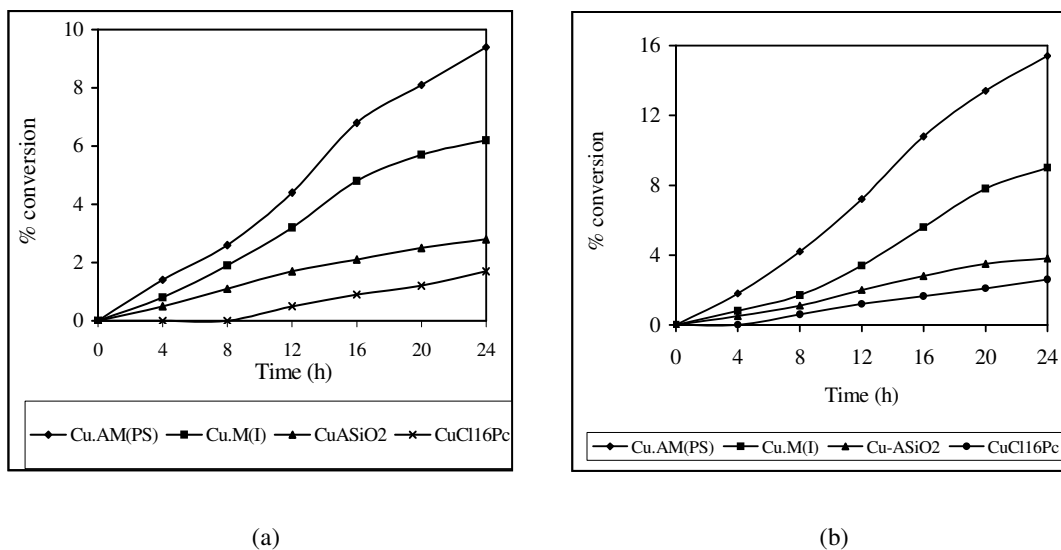
Fig. 2.19. (a) Kinetics study of cyclohexane oxidation using different catalysts of $CuCl_{16}Pc$ using benzaldehyde/$O_2$.; (b) Kinetics study of decane oxidation using different catalysts of $CuCl_{16}Pc$ using benzaldehyde/$O_2$.

Conditions: substrate= 5 mmoles, cooxidant= 15 mmoles; (1:3), solvent= acetonitrile, 10 g., molecular oxygen, 1 atm, temp. 323 K.

Table 2.8. also presents the data for the oxidation of decane over both the metal catalysts. It is again observed that Co/Cu-AM(PS) is the most active catalyst for the oxidation of decane for both the oxidants at 323 K [Fig. 2.18. (b) 2.19. (b)]. Benzaldehyde/$O_2$ gave more than 1.5 times higher decane conversion than isobutyraldehyde/$O_2$. For both the oxidants, and all the catalysts the selectivity for decanone (2, 3 and 4-decanone) is large (percentage yield more than 96 %).

Table 2.8. Oxidation of alkanes using (B) isobutyraldehyde/$O_2$ and (C) benzaldehyde/$O_2$ as co-oxidants over different catalysts of Co/Cu-Cl$_{16}$Pc.

| Catalyst | oxidant | cyclohexane | | | 1-decane | | |
|---|---|---|---|---|---|---|---|
| | | conv. (%) | TON[a] | % yield[b] (mole %) | conv. (%) | TON[a] | % yield[b] (mole %) |
| CoCl$_{16}$Pc | B | 2.2 | 62 | 41 | 2.0 | 56 | 98 |
| (0.002 g) | C | 3.2 | 89 | 77 | 4.7 | 138 | 96 |
| Co-ASiO$_2$ | B | 3.4 | 107 | 42 | 3.4 | 107 | ~ 100 |
| (0.05 g) | C | 4.2 | 132 | 67 | 6.0 | 190 | ~ 100 |
| Co-M(I) | B | 4.2 | 123 | 59 | 5.4 | 158 | ~ 100 |
| (0.05 g) | C | 7.3 | 214 | 66 | 9.3 | 273 | ~ 100 |
| Co-AM(PS) | B | 6.4 | 188 | 60 | 9.0 | 284 | ~ 100 |
| (0.05 g) | C | 12.4 | 364 | 68 | 14.4 | 423 | ~ 100 |
| CuCl$_{16}$Pc | B | 1.6 | 47 | 37 | 2.0 | 59 | 98 |
| (0.002 g) | C | 1.7 | 50 | 77 | 2.6 | 76 | 96 |
| Cu-ASiO$_2$ | B | 2.2 | 70 | 36 | 3.2 | 101 | ~ 100 |
| (0.05 g) | C | 2.8 | 88 | 66 | 3.8 | 120 | ~ 100 |
| Cu-M(I) | B | 3.8 | 120 | 56 | 5.4 | 170 | ~ 100 |
| (0.05 g) | C | 6.2 | 196 | 70 | 9.0 | 184 | ~ 100 |
| Cu-AM(PS) | B | 6.2 | 196 | 60 | 9.2 | 291 | ~ 100 |
| (0.05 g) | C | 9.4 | 297 | 68 | 15.4 | 487 | ~ 100 |

[a] TON = mole of product formed/ mole of metal present in the catalyst/ 24 h; [b] % yield for respective ketone

Conditions: substrate= 5 mmoles, cooxidant= 15 mmoles; (1:3), solvent= acetonitrile, 10 g., molecular oxygen, 1 atm, temp. 323 K.

## 2.5. CONCLUSIONS

The immobilization of cobalt/copper-chlorophthalocyanine (Co/Cu-Cl$_{16}$Pc) complex in the channels of Si-MCM-41 molecular sieves with the walls modified by 3-aminopropyl silane group has been achieved by post synthesis method [Co/Cu-AM(PS)]. This sample is compared with the sample prepared by impregnation method [Co/Cu-M(I)] in the absence of 3-APTES. Co/Cu-AM(PS) is found to be superior over Co/Cu-M(I). Different characterization techniques such as UV-Vis., IR and cyclic voltammetry reveal that the complex is monomolecularly distributed in the channels of MCM-41, presumably through interaction of the grafted -NH$_2$ group with the metal in the case of the most active Co/Cu-AM(PS) sample. It is observed that planar complexes of cobalt and copper immobilized on a hydrophobic silica surface inside appropriately wide channels (as in MCM-41) are good catalysts for the oxidation of hydrocarbons under mild conditions using oxidants such as TBHP and aldehyde/O$_2$. The molecular dispersion of the complex with sufficient void space and the hydrophobic surface are appropriate for activation of hydrocarbons, as evidenced by higher TON number on immobilization compared to the reported values.

Co-oxidation with the aldehyde gives a higher rate of epoxidation as compared to oxidation using TBHP, as the acyl peroxy radicals are more selective than alkyl peroxy radicals preferentially attack on the double bond. On the contrary studies on the oxidation of cyclohexane and 1-decane with TBHP and aldehyde/O$_2$ as oxidants suggest that the difference in the conversions and product selectivity observed with the two oxidants may be attributed to mechanistic differences associated with the ease of formation of the free radical (alkyl/acyl species). Benzaldehyde/O$_2$ leads to a higher conversion of alkane compared to isobutyraldehyde/O$_2$. This is attributed to the higher resonance stability of the intermediate aromatic acyl peroxy radical in the case of benzaldehyde compared to isobutyraldehyde. Also both TBHP and benzaldehyde/O$_2$ possess comparable activity in oxidation of alkanes.

## 2.6. REFERENCES

1. C. T. Kresge, M. E. Leonowicz, W. J. Roth, and J. C. Vartuli, *U.S. Patent*, 5,098,684 (1992).

2. C. T. Kresge, M. E. Leonowicz, , W. J. Roth, J. C. Vartuli and J. S. Beck, *Nature*, 359 (1992) 710.

3. J. S. Beck, J. C. Vartuli, W. J. Roth, M. E. Leonowicz, C. T. Kresge, K. D. Schmitt, C.T-W. Chu, D. H. Olson, E. W. Sheppard, S. B. McCullen, J. B. Higgins and J. L. Schlenker, *J. Am. Chem. Soc.*, 114 (1992) 10834.

4. Q. Huo, D. I. Margolese, U. Ciesla, , D. G.Demuth, , P. Feng, , T. E.Gier, P. Sieger, A. Firouzi, B. F. Chmelka, F. Schüth and G. D. Stucky, *Chem. Mater.*, 6 (1994) 1176.

5. G. D. Stucky, A. Monnier, F. Schüth, Q. Huo, D. I.Margolese, D. Kumar, M. Krishnamurthy, P. Petroff, A. Firouzi, M. Janicke and B. F. Chmelka, *Mol. Cryst. Liq. Cryst.,* 240 (1994) 187.

6. R. Schimdt, , D. Akporiaye, M. Stöcker and O. H. Ellestad, *J. Chem., Soc., Chem. Commun.*, (1994) 1493.

7. D. Zhao and D. Goldfarb, *J. Chem. Soc., Chem. Commun.* (1995) 875.

8. K. A. Koyoano and T. Tatsumi, *Chem. Commun.* (1996) 145.

9. Q. Huo, D. I. Margolese, U. Ciesla, P. Feng, T. E. Gier, P. Sieger, R. Leon, P. M. Petroff, F. Schüth and G. D. Stucky, *Nature*, 368 (1994) 317.

10. T. Yanagisawa, T. Schimizu, K. Kuroda and C. Kato, *Bull. Chem. Soc. Japan.*, 63 (1990) 988.

11. A. Stein, B. J. Melde and R. C. Schroden, *Adv. Mater.,* 12 (2000) 1403.

12. A. P. Wight and M. E. Davis, *Chem. Rev.*, 102 (2002) 3589.

13. K. Moller and T. Bein, *Chem. Mater.,* 10 *(*1998) 2950.

14. G. A. Barf and R. A. Sheldon, *J. Mol. Catal. A: General,* 102 (1995) 23.

15. T. Mulkaiyamam and T. Yamada, *Bull. Chem. Soc. Jpn.,* 68 (1995) 17.

16. W. Kain and J. Rall, *Angew. Chem.Int. Ed. Engl.,* 35 (1996) 43.

17. A. B. Sorokin and A. Tuel, *Catal. Today,* 57 (2000) 45.

18. D. Brunel, N. Bellocq, P. Sutra, A. Cauvel, M. Lasperas, P. Moreau, F. Di Renzo, A. Galarneau and F. Fajula, *Coord. Chem. Rev.,* 178 (1998) 1085.

19. A. B. Sorokin and A. Tuel, *New J. Chem.,* 23 (1999) 473.

20. A. Hirth, A. K. Sobbi and D. W. Wohrle, *J. Porphyrins Phthalocyanines*, 1 (1997) 275.

21. G. Schneider, D. Hohrle and W. Spiller, *Photochem. Photobiol.,* 60 (1994) 333.

22. C. C. Leznoff, C. R. McArthur and Y. Qin, *Can. J. Chem.,* 71 (1993) 1319.

23. Y. Yuan, W. Cao and W. Weng, *J. Catal.,* 228 (2004) 311.

24. N. Komiya, T. Naota, Y. Oda and S. Murahashi, *J. Mol. Catal. A: Chem.,* 117 (1997) 21.

25. S. Murahashi, Y. Oda and T. Naota, *J. Am. Chem. Soc.,* 114 (1992) 7913.

26. K. Choudhari, T. K. Das, P. R. Rajmohanan, K. Lazar, S. Sivasanker and A. J. Chandwadkar, *J. Catal.,* 183 (1999) 281.

27. C.-Y. Chen, S. L. Burkett, H.-X. Li and M.E. Davis, *Microporous Mater.,* 2 (1993) 27.

28. R. Ryoo, J. M. Kim and C. H. Ko, *Stud. Surf. Sci. Catal.*, 117 (1998) 151.

29. Z. Chang, Z. Zhu, and L. Kevan,  *J.Phys. Chem. B*, 103 (1999) 9442.

30. S. J. Gregg and K. S. W. Sing, *Adsorption, Surface Area and Porosity*, Academic Press, London, (1967) 121.

31. C. -Y. Chen, H. -X. Li and M. E. Davis, *Microporous Mater.,* 2 (1993) 17.

32. K. J. Balkus Jr., A. G. Gabrielov, S. L.Bell, F. Bedioui, L. Roue and J. Devynck, *Inorg. Che*m., 33 (1994) 67.

33. J. C. Vartuli, K. D. Schmidt, C. T. Kresge, W. J. Roth, M. E. Leonowicz, S. B. McCullen, S. D. Hellring, J. S. Beck, J. L. Schlenker, D. H. Olson and E. W. Sheppard, *Stud. Surf. Sci. Catal.,* 84 (1994) 53.

34. B. P. Feuston and  J. B. Higgins, *J. Phys. Chem.*, 98 (1994) 4459.

35. R. Szostak, *"Molecular Sieves: Principles of Synthesis and Identification",* Van Nostrand Reinhold, New York (1989).

36. H. Keypour, S. Salehzadeh, R. G. Pritchard and R. V. Parish, *Inorg. Chem.*, 39 (2000) 5787.

37. M. P. Vinod, T. Kr. Das, A. J. Chandwadkar, K. Vijayamohanan and  J. G. Chandwadkar, *Materials Chemistry and Physics*, 58 (1999) 37.

38. A. Wolberg and J. Manassen, *J. Am. Chem. Soc.* 92 (1970) 2982.

39. E. V. Rybak-Akimova, A. Y. Nazarenko, L. Chen, P. W. Krieger, A. M. Herrera, V. V. Tarasov and P. Robinson, *Inorg. Chim. Acta,* 324 (2001) 1.

40. J. M. Fraile, J. Garcia, J. I. Mayoral and E. Vispe, *J. Catal.,* 189 (2000) 40.

41. D. E. Vos De and P. A. Jacobs, *Catal. Today*, 57 (2000) 105.

42. N. Safari and F. Bahadoran, *J. Mol. Catal. A: Chem.*, 171 (2001) 115.

43. J. Dongfeng, L. Xiaobing and He. Ren, *Appl. Catal. A: Gen.,* 203 (2000) 329.

44. Zheng-Rong Lu, Yuan-Qi Yin and Dao-Sen Jin, *J. Mol. Catal.,* 70 (1991) 391.

45. M. R. Cramarossa, L. Forti, M. A. Fedotov, L. G. Detusheva, V. A. Likholobov, L. I. Kuznetsova, G. L. Semin, F. Cavani and F. Trifiro, *J. Mol. Catal. A: Chem.,* 127 (1997) 85.

46. R. A. Sheldon and J. K. Kochi, *Metal Complex Catalyzed Oxidation of Organic Compounds,* Academic Press New York, 1981.

47. S. Mangematin and A. B. Sorokin, *J. Porphyrins and Phthalocyanines,* 5 (2001) 674.

48. K. Kaneda, S. Haruna, T. Imanaka and K. Kawamoto, *J. Chem. Soc., Chem. Commun.,* (1990) 1467.

49. S. Seelan, A. K. Sinha, D. Srinivas and S. Sivasanker, *J. Mol. Catal. A: Chem.,* 157 (2000) 163.

50. A. A. Valente and J. Vital, *J. Mol. Catal. A: Chem.,* 156 (2000) 163.

51. R. Raja and P. Ratnasamy, *Catal. Lett.*, 48 (1997) 1.

52. C-C. Guo, M-F. Chu, Q. Liu, D-C. Guo and X-Q. Liu, *Appl. Catal. A: Gen.,* 246 (2003) 303.

53. F. A. Chavez, C. V. Nguyen, M. M. Olmstead and P. K. Mascharak, *Inorg. Chem.* 35 (1996) 6282.

54. G. Russell, *J. Am. Chem. Soc.,* 79 (1957) 3871.

55. R. Poladi and C. C. Landry, *Microporous Mesoporous Mater.* 52 (2002) 11.

56. Y. Long, T. Xu, Y. Sun and W. Dong, *Langmuir*, 14 (1998) 6173.

# Chapter-3

# Synthesis, Characterization and Catalytic Evaluation of Co/Cu-salen immobilized MCM-41

## 3.1. INTRODUCTION

The development of environment friendly technologies has promoted much research in heterogeneous catalysis and in particular the heterogenization of known active homogeneous catalysts for oxidation reactions [1]. Several model complexes containing porphyrin and shiff base ligands have been synthesized and studied for their oxygen uptake and oxidative catalysis [2-4]. Flexibility of the ethylenediamine backbone in salen as observed in a number of transition metal complexes with bidentate oxygen ligands is responsible for the complex to mimic the biological activity of enzymes [5].

In the last decade, salen ligand [salen = 1,6-bis(2- hydroxyphenyl)-2,5-diazahexa-1,5-diene] and its derivatives have received more attention, mainly because of their extensive applications in the fields of synthesis and catalysis [6-11]. This attention is still growing and considerable research efforts are devoted to the synthesis of modified and supported reagents for catalysis and materials chemistry [12-15]. Due to the structural rigidity combined with the ease of preparation and derivatization of salen ligand, it is an attractive scaffold for the development of bifunctional complexes [15, 16]. Salen ligands bind metal ions through four atoms; two nitrogen and two oxygen atoms. This tetradentate-binding motif is reminiscent of the porphyrin framework in the heme-based oxidative enzymes [17-19]. Nonetheless, salen derivatives are more easily synthesized than porphyrins and their structures are more easily manipulated to create an asymmetric environment around the active metal site. A breakthrough has been the introduction of chiral manganese–salen catalyst by the groups of Jacobsen and Katsuki, particularly, for the epoxidation of alkenes [6, 7, 20-23].

From the sustainable and green chemistry point of view, heterogeneous catalysts would be attractive since they offer the advantages of easy catalyst separation, possible catalyst recycle and sometimes high activity and selectivity. In this respect encapsulation of transition metal complex in zeolites gained much interest in the previous research [24-26], since heterogenization can give rise to the materials with both homogeneous-catalysis and heterogeneous catalysis characters. In addition, degradation of the organic ligands and dimerization of the transition metal complexes could occur during homogeneous catalysis reactions, resulting in reduced activity, and even irreversible deactivation. In contrast, upon encapsulation in zeolites and molecular sives, transition metal complex molecules are encaged and site-isolated, making these complexes stable, highly active and selective for the

oxidation of alkenes, alkanes, alcohols and so on. Manganese complexes based on Schiff's base are known to be active homogeneous catalysts in the oxidation reactions in the presence of a variety of oxidants [27-29], and their immobilization on solid supports combines easy product separation with the good selectivity of the catalytic reaction. Therefore, a variety of supports have been studied, such as clays [30], silicas [31, 32] and zeolites [33-35]. The immobilization of Mn-salen complexes on polymeric supports has also received considerable attention [36, 37].

Komia et al. [38] have discussed the role of different aldehydes in the oxidation of various alkenes and alkanes using copper salts, copper-crown ether complex and a mixture of copper salt and crown ether. Iron and Ruthenium catalyzed oxidation of alkanes with aerobic oxygen in the presence of aldehydes was studied by Murahashi et al. [39].

In the present work, the preparation of MCM-41, surface modification and covalent attachment of metal-salen complexes are presented along with the directly impregnated complex. The detailed characterization of the support material and all the catalysts is presented using different techniques such as X-ray diffraction, nitrogen sorption, atomic absorption spectroscopy (AAS), microanalysis, MAS NMR, UV-Vis., FTIR, EPR, thermal analysis and X-ray photo electron spectroscopy (XPS). Catalytic activity has been investigated for the oxidation of alkenes and alkanes using TBHP and aldehyde/$O_2$ as oxidants under mild reaction condition.

## 3.2. EXPERIMENTAL

The materials and chemicals used for the synthesis, catalysts preparation and reactions are same as mentioned in Chapter II (Table 2.1.). Cobalt and copper salen complexes are prepared and used for catalyst preparation.

### 3.2.1. Synthesis of Si-MCM-41
Si-MCM-41 have been synthesized according to the procedure reported in the Chapter II; section 2.2.1.

### 3.2.2. Synthesis of Co/Cu-salen complex
The Schiff's base ligand salen was prepared and purified according to established procedure [40]. Salicylaldehyde (12.2g, 0.1 mol) was diluted with ethyl alcohol (100 ml)

and mixed drop wise with a solution of ethylenediamine (3g, 0.05 mol) in ethyl alcohol (50 ml) to get salen ligand as yellow flakes. The slurry was then refluxed for one hour to complete the reaction. The solid product was filtered, washed with cold ethyl alcohol and dried under vacuum.

Co-salen was synthesized by dissolving schiff's base salen (7.34g, 0.03 mol) in ethyl alcohol (200 ml) and warming in $N_2$ atmosphere. An ethanolic solution of $Co(CH_3COO)_2.4H_2O$ (6.4g, 0.03 mol in 100 ml ethanol) was boiled until all the crystalline solid had gone into solution. Both the solutions (equimolar quantities) were mixed and refluxed for 4 hour under $N_2$, cooled to obtain a wine red precipitate which was filtered, washed, recrystallized and dried under vacuum.

Cu-salen was synthesized by mixing equi molar solutions of $Cu(CH_3COO)_2.4H_2O$ (0.39g, 0.002 mol) and the Schiff's base ligand (0.53g, 0.002 mol) in 200 ml ethyl alcohol. The solution was refluxed for 4 hour in $N_2$ atmosphere, cooled to obtained greenish precipitate which was filtered, washed recrystallized and dried under vacuum. The purity of both the metal complexes was determined by elemental analysis and FT-IR technique.

### 3.2.3. Catalyst preparation

The catalyst preparation has been done by immobilization of transition metal complexes in the channels of MCM-41 support through (i) grafting and (ii) impregnation method as follows:

### 3.2.3.1.  Grafting of Co/Cu-salen complex over Si-MCM-41

#### *3.2.3.1.1.  Modification of Si-MCM-41 with 3-aminopropyltriethoxysilane (3-APTES)*

In a typical experiment, Si-MCM-41 (0.5g), prepared as above (section 3.2.1.) was dried by refluxing with dry toluene (8-10 hours). The material was then filtered washed with acetone and dried at room temperature under inert condition. This dried Si-MCM-41 was then mixed with the solution of 3-APTES in toluene (70.0 ml:0.22g) and stirred for 12 h. This $NH_2$-MCM-41 was then filtered, washed with acetone / dichloromethane and dried under vacuum.

#### *3.2.3.1.2. Anchoring of Co/Cu-salen*

A solution of 0.236 g of Co-salen [for Cu-salen; 0.240 g] in 20ml of toluene was stirred and slowly added to a suspension of 0.5 g of $NH_2$-MCM-41 in toluene (above prepared in 3.2.3.1.1.). It was refluxed over night. Brown colored material [green material

when Cu-salen complex is used] was separated by filtration, washed with acetone, dried under vacuum and designated as Co-salen-$NH_2$-MCM-41(PS) or Co-S-AM(PS) [For Cu-salen; Cu-S-AM(PS)]. Fig. 3.1 shows schematic presentation of grafting of metal salen with amino-modified MCM-41.
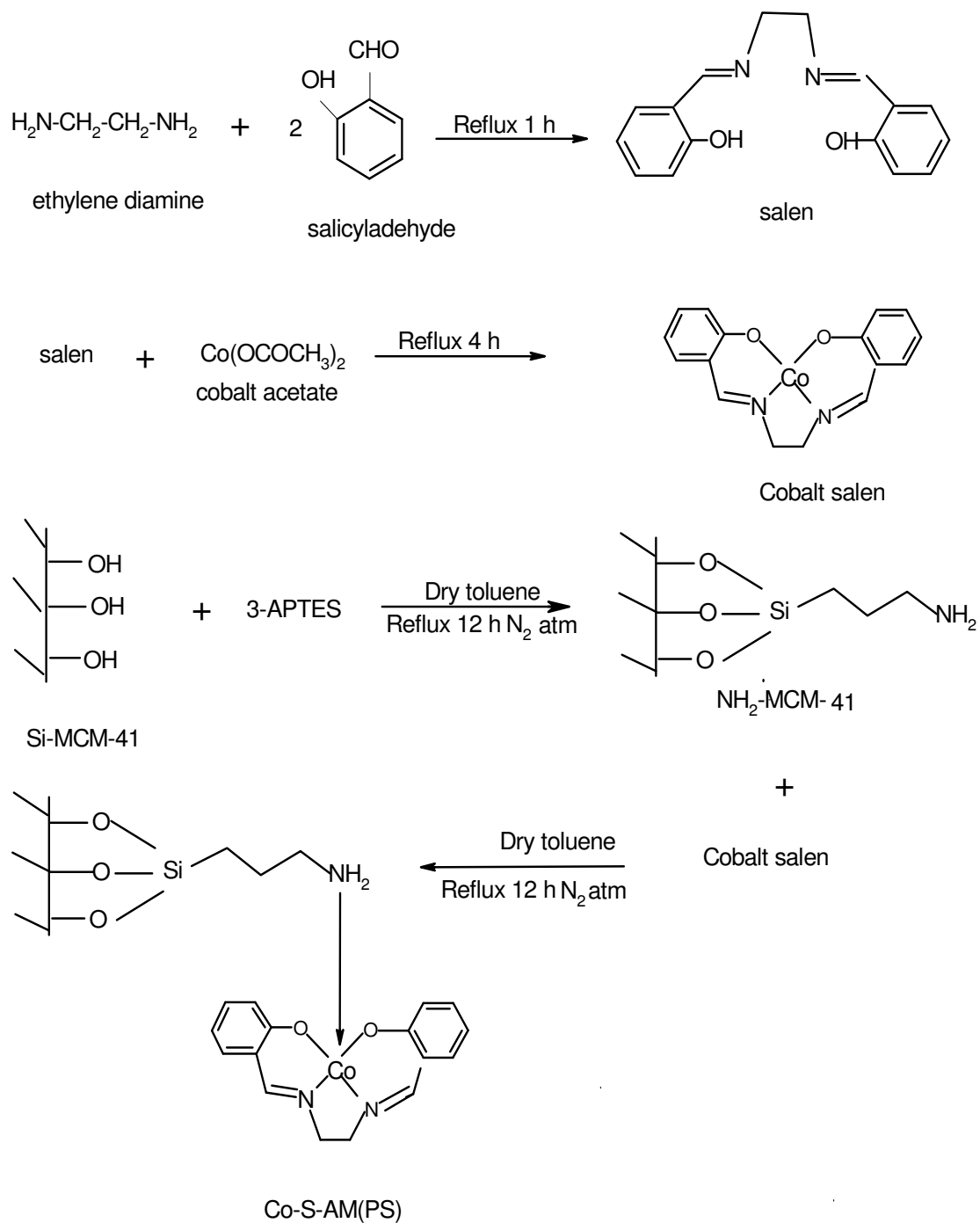


Fig. 3.1 Schematic presentation of grafting of cobalt salen with amino-modified MCM-41.

### 3.2.3.2. Impregnation of Co/Cu-salen

A solution of 0.236 g of Co-salen [for Cu-salen; 0.240 g] in 20.0 ml of toluene was stirred and slowly added to a suspension of 0.5 g of Si-MCM-41 in toluene (prepared as in 3.2.1. above). It was refluxed for 12 h. A brown material [green material when Cu-salen complex is used] was separated by filtration, washed with acetone, dried at ambient temperature under vacuum and designated as Co-salen-MCM-41(I) or Co-S-M(I) [For Cu-salen; Cu-S-M(I)].

### 3.2.3.3. Grafting of Co/Cu-salen over SiO$_2$

#### 3.2.3.3.1. Modification of SiO$_2$ with 3-aminopropyltriethoxysilane (3-APTES)

SiO$_2$ (0.5g), was dried by refluxing with dry toluene (8-10 hours). The material was then filtered washed with acetone and dried at room temperature under inert condition. This dry SiO$_2$ was then mixed with the solution of 3-APTES in toluene (70.0 ml:0.22g) and stirred for 12 h. This NH$_2$-SiO$_2$ was filtered, washed with acetone / dichloromethane and dried under vacuum.

#### 3.2.3.3.2. Anchoring of Co/Cu-salen

A solution of 0.236 g of Co-salen [for Cu-salen; 0.240g] in 20ml of toluene was stirred and slowly added to a suspension of 0.5 g of  NH$_2$-SiO$_2$ in toluene (above prepared in 3.2.3.3.1.) and the solution refluxed for 12 h. A brown material [green material for Cu-salen anchored catalyst] was separated by filtration, washed with acetone, dried at ambient temperature under vacuum and designated as Co-salen-NH$_2$-SiO$_2$  or Co-S- ASiO$_2$ [For Cu-salen; Cu-S- ASiO$_2$]. This catalyst is used for comparison in the catalytic reactions.

### 3.2.3.4. Catalytic reactions

Catalytic reactions were carried out at 323 K in a round bottom flask fitted with a condenser. Alkenes, alkanes, acetonotrile, TBHP in decane, TBHP in ethylene dichloride and isobutyraldehyde were used without further purification. Hydrocarbons (5 mmol), TBHP as oxidant (5 mmol), isobutyraldehyde (15 mmoles), acetonitrile as solvent (10 g) and catalyst (0.05 g) along with toluene as internal standard were introduced into a round bottom flask. The reactions were carried out with vigorous stirring. All the products were quantified at different intervals by gas chromatography: Chrompack CP900 (Carbowax 20M): 50m X 0.32 mm capillary column.

### 3.3. CHARACTERIZATION

Crystalline phase identification of as synthesized, calcined and modified samples was carried out by XRD (Rigaku; Miniflex) using Nickel filtered Cu Kα radiation. The surface area and pore volume were determined from $N_2$ sorption isotherms using a Coulter (Omnisorb, 100 CX) instrument. The chemical compositions of the samples were determined by a combination of wet chemical methods, atomic absorption spectroscopy (AAS Hitachi, Model 2800) and elemental analysis (Carlo Erba; EA1108). The solid state magic-angle spinning MAS NMR spectroscopy studies were carried out on a Bruker MSL-500 FT-NMR spectrometer. The UV- Vis. spectra were recorded using a nujol mull on a SHIMADZU, UV-2101 PC spectrometer. Fourier transform infrared (FT-IR) spectra were recorded with a Shimadzu FT-IR spectrometer (Model 8300). EPR spectra were recorded on a Bruker EMX X band spectrometer (microwave frequency 9.45 GHz) with 100 kHz-field modulation. DPPH was used as a field marker (g = 2.0036). Experiments at 77 K were carried out using a quartz inserting Dewar. The elemental composition of the samples were determined by X-ray photoelectron spectroscopy (XPS) using ESCA 3000 electron spectrometer (VG Scientific, UK with MgKα and AlKα twin anode).

### 3.3.1. Powder X-ray Diffraction

Since mesoporous molecular sieves lack strict crystallographic order on an atomic level, their wall structure cannot be determined from crystallographic data. However, the X-ray diffraction pattern of Si-MCM-41 shows a typical four peak pattern [41] with a very strong (100) reflection at a low angle and three weaker (110), (200) and (210) reflections, from the quasi- regular arrangement of mesopores with hexagonal symmetry as shown in Fig. 3.2. spectra 1. Along with this spectra, the XRD patterns of 2. calcined Si-MCM-41, 3. Co-salen, 4. Cu-salen, 5. Co-S-AM(PS) and 6. Cu-S-AM(PS) samples are presented in Fig. 3.2. On comparing the spectra of as- synthesized MCM-41 and calcined Si-MCM-41, a marginal decrease in "d" value is observed which is due to the removal of the template on calcination. The XRD pattern of 3. Co-salen and 4. Cu-salen show several peaks in the range of $2\theta = 1.5$ to $50^o$. The XRD pattern of 5. Co-S-AM(PS) and 6. Cu-S-AM(PS), prepared by grafting method are similar to the original Si-MCM-41 (XRD pattern 2). This indicates that there is no damage to the structure of Si-MCM-41 even after immobilization of transition metal complexes. We did not observe any peak of metal salen in these spectra.

This is an indication of the grafting/impregnation with uniform dispersion of the complex in the channels of Si-MCM-41.
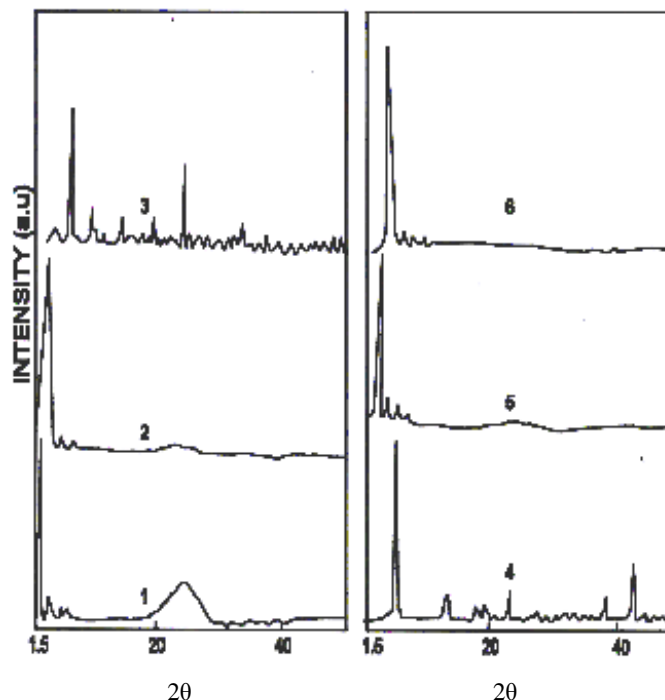


Fig. 3.2. XRD of 1. as synthesized MCM-41, 2. Si-MCM-41, 3. Co-salen 4 .Cu-salen, 5. Co-S-AM(PS), and 6. Cu-S-AM(PS).

### 3.3.2. Physico-chemical analysis

The surface area, pore volume and pore diameters of calcined Si-MCM-41, modified $NH_2$-MCM-41 and catalyst samples are given in Table.3.1. All the samples showed isotherms of type IV in the IUPAC classification [42] having a sharp capillary condensation step at $P/P0 = 0.3$–$0.45$ region, which is characteristic of M41S type ordered mesoporous materials ( Figure not shown) [43]. Surface modified sample ($NH_2$-MCM-41) shows decrease in surface area from 1115 (for Si-MCM-41) to 769 $m^2$/g, pore diameter from 38 to 32 Å and pore volume from 0.65 to 0.38 cc/g. Further decrease in the surface area, pore diameter and pore volume for impregnated and grafted catalysts [Co/Cu-S-M(I) and Co/Cu-S-AM(PS) see Table 3.1.] indicate the pores of Si-MCM-41 are occupied by Co/Cu-salen complex.

Atomic absorption spectroscopy shows ~ 4.4 % loading for cobalt and ~ 4.0 % for copper. Theoretical value of carbon content in $NH_2$-MCM-41 is 5.5 % and nitrogen 1.8 %.

Practically, we observed ~ 4.99 % carbon (0.5 % less) with 1.39 % (0.4 % less) nitrogen present in the sample. It is assumed that one mole of nitrogen will anchor with one mole of metal. The actual amount of 3-APTES loaded on the Si-MCM-41 gives rise to 1.8 % nitrogen corresponding to 6 % of metal loading. But in practice we observe 1.39 % nitrogen present in the sample which corresponds to ~ 4.5 % metal loading which is very near to observed value for both the Co/Cu grafted catalysts. This leads to explain the amount of nitrogen present equivalent to the metal in the channels of MCM-41.

Table.3.1. Physicochemical properties of samples.

| Sample | C/N analysis (Wt.%) | | $S_{BET}$ ($m^2$/g) | Pore Volume (ml/g) | Pore dia. (Å) |
|--------|------|------|------|------|------|
| | C | N | | | |
| Si-MCM-41 | ---- | ---- | 1115 | 0.65 | 38 |
| NH$_2$-MCM-41 | 4.99 | 1.39 | 769 | 0.38 | 32 |
| Co-salen | 58.81 | 8.62 | ---- | ---- | ---- |
| Co-S-M(I)[a] | 14.30 | 2.10 | 678 | 0.33 | 32 |
| Co-S-AM(PS)[a] | 18.60 | 3.30 | 580 | 0.23 | 26 |
| Cu-salen | 58.20 | 8.78 | ---- | ---- | ---- |
| Cu-S-M(I)[b] | 12.30 | 1.80 | 660 | 0.34 | 30 |
| Cu-S-AM(PS)[b] | 16.50 | 3.10 | 573 | 0.21 | 27 |

[a] Co ~ 4.4 % and [b] Cu ~ 4.0 % by AAS.

### 3.3.3. UV-Vis. spectroscopy

The UV-Vis. spectra of all the Co/Cu-salen complex grafted catalysts, Co/Cu-salen-hexylamine adduct as well as neat metal complexes were recorded using nujol mull. Table 3.2 shows the electronic spectral data of all the above samples.

UV-Vis. spectra for Co-salen show the typical absorption at ~ 253 ($\lambda_1$) and 354 nm ($\lambda_2$) attributable to ligand n → $\pi^*$ and π→ $\pi^*$ charge transfer bands. Further the additional broad band in the higher wavelength range i.e. 450 to 530 nm (470 nm; $\lambda_3$) ascribed to ligand to metal charge transfer similar to the related metal complex described in the literature [44]. For Co-S-AM(PS) and Co-salen-hexylamine we observed blue shift in the

position of these ligand to metal charge transfer bands. Co-S-AM(PS) show band at 435 nm ($\lambda_3$) and Co-salen-hexylamine show band at 445 nm ($\lambda_3$). The shift in the band position can be attributed to change in the environment of metal species due to coordination through apical nitrogen. Zangina et al. [45] have assigned the band at 375 nm and 421 nm to charge transfer from axial ligand to macrocycle and charge transfer from metal to axial ligand, respectively, in the spectra of iron (II) phthalocyanine complexes with phosphine or phosphite.

Table 3.2. Electronic spectral data for the different environments of Co/Cu-salen complex.

| Sample | Absorption bands ($\lambda_{max}$ nm) | | |
| --- | --- | --- | --- |
| | $\lambda_1$ | $\lambda_2$ | $\lambda_3$ |
| Co-salen | 253 | 354 | 470 |
| Co-S-AM(PS) | 250 | 349 | 435 |
| Co-salen-hexylamine | 251 | 353 | 445 |
| Cu-salen | 253 | 326 | 414 |
| Cu-S-AM(PS) | 248 | 323 | 368 |
| Cu-salen-hexylamine | 249 | 325 | 386 |

In the UV-vis electronic spectra of Cu-salen, typical absorptions at ~253 ($\lambda_1$) and ~326 nm ($\lambda_2$) attributable to ligand n$\rightarrow \pi^*$ and $\pi \rightarrow \pi^*$ charge transfer bands (Table 3.2.). Cu-salen exhibits a broad band centered around ~414 nm ($\lambda_3$) ascribed to ligand to metal charge transfer band similar to related metal-salen compounds described in the literature [46, 47]. After immobilization, the sample Cu-S-AM(PS) shows a narrow band centered at 368 nm ($\lambda_3$) overlapping the broad band at 326 nm and the adduct of Cu-salen-hexylamine shows the band at 386 nm ($\lambda_3$). By comparison of the spectra, it may be concluded that the blue shift in the spectra of Cu-S-AM(PS) and Cu-salen-hexylamine, respectively, is associated with axial lone pair coordination to the metal.

### 3.3.4. FTIR spectroscopy

The FTIR spectra (recorded using fluorolube mull) of 1. Si-MCM-41, 2. $NH_2$-MCM-41 3. Cu-salen, 4. Cu-S-AM(PS) 5. Cu-salen-hexylamine  6. Co-salen, 7. Co-S-AM(PS) and 8. Co-salen-hexylamine in the range of 4000-1300 $cm^{-1}$ are presented in Fig.3.3. The IR spectrum of $NH_2$-MCM-41 (spectrum 2) shows band in the region of 3000-2800 $cm^{-1}$ assigned to $>CH_2$ groups indicative of the modification of the wall of mesoporous silica material by aminoporopyl group. The bands at 3365 and 3392 $cm^{-1}$ superimposed on the broad band in the region 3600 to 2800 $cm^{-1}$ can be assigned to amino asymmetric and symmetric stretching frequencies. However the broad nature of the band may be due to hydroxyl group on the silica walls, hydrogen bonded to amino group and adsorbed moisture. From the presence of these bands it can be inferred that the wall of Si-MCM-41 is modified by aminopropyl groups successfully after the reaction between 3-APTES and the silanol groups in MCM-41 (Fig. 3.3.). The presence of Co-salen (spectrum 6) is clearly noticeable in the IR spectrum of Co-S-AM(PS) (spectrum 7). This indicates the incorporation of Co-salen in MCM-41. The absorption due to the amino group is not observed in the spectrum of Co-S-AM(PS), instead a broad band centered at ~ 3300 $cm^{-1}$ is observed. In order to study the origin of this band, the spectrum of Co-salen-hexylamine adduct was compared (spectrum 8). Both the spectra (spectra 7 and 8) show the broad band centered around 3300 $cm^{-1}$ without any significant change in the bands of salen complex. Therefore, the broad band at 3300 $cm^{-1}$ is assigned to $>NH_2^+$ stretching, confirming the axial coordination between the amino group and the metal. This supports and gives direct evidence of immobilization of the complex through coordinate bonding as reported earlier by Xiang-Ge Zhou *et al.* [48]. Also, their observation that metal salen complexes can not get immobilized on the walls of MCM-41 by mere adhesion is supported by the failure in immobilization of copper and cobalt salen complexes on Si-MCM-41 in the present work. The bands in the region 1670 to 1300 $cm^{-1}$ observed in the spectra of the complex containing samples are ascribed to C–C, C–O stretching modes in quasi-aromatic chelates in metal salens. The invariance in the frequencies of Co-salen is due to the coordinate bond being at right angles to the plane of the complex not affecting the structure of the complex in any significant manner. The adduct formation of copper salen with the amino group was also inferred from the similar nature of Cu-S-AM(PS) (spectrum 4 with spectrum 5).
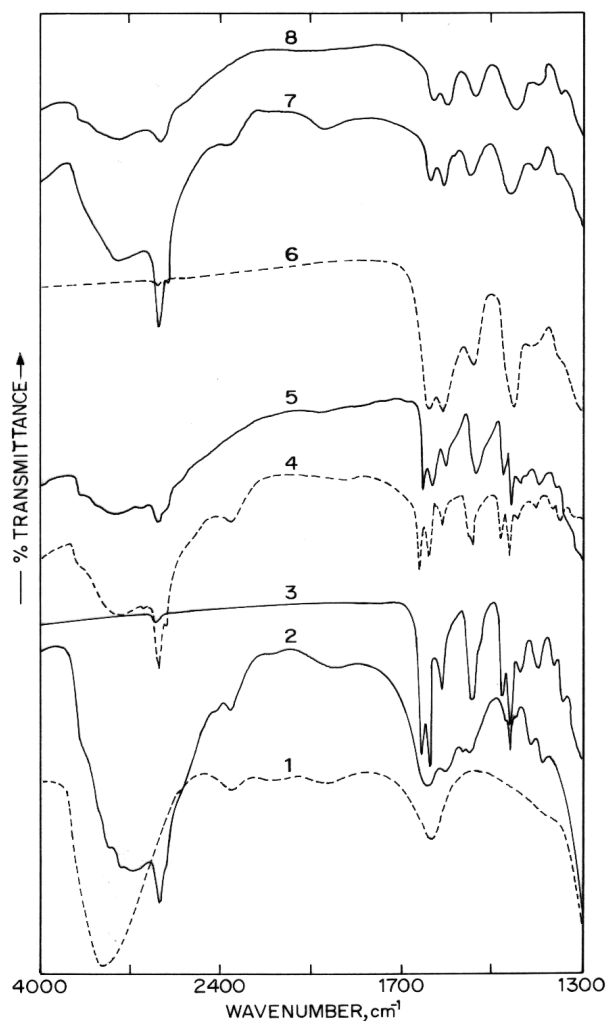
Fig. 3.3. FTIR spectra of 1. Si-MCM-41 2. NH$_2$-MCM-41, 3. Cu(salen), 4. Cu-S-AM(PS) 5. Cu(salen)-hexylamine 6. Co-salen, 7. Co-S-AM(PS) and 8. Co-salen-hexylamine.

### 3.3.5. EPR spectroscopy

EPR spectra of neat and immobilized Co-salen and Cu-salen complexes were recorded at 298 K and 77 K. The spectra were typical of axial symmetry with $g_{II}$ = 2.183 and $g_\perp$ = 2.084. Hyperfine features due to Cu was not resolved due to inter molecular interactions. Single crystal X-ray structure of Cu-salen revealed that the complex molecules form dimers with Cu-Cu separation of about 3.45Å. This molecular association was reported to lead to the broadening of the EPR signals and the absence of metal hyperfine features [49]. The spectrum of the immobilized complex is similar to that of the neat complex. This similarity might arise from the oxygen-metal interaction observed in the dimer and the nitrogen lone pair coordination with the metal as well as the retention of planarity in the immobilized complex. When the complexes are heterogenized by

92

encapsulation in Zeolite-Y, molecular isolation along with molecular distortion was observed. Metal hyperfine features were resolved and the spectrum was similar to that of frozen solutions. However, such a resolution is not observed in the immobilized complexe Cu-S-AM(PS), studied in this work. These observations confirm that immobilization of MCM-41 does not result in the distortion of the salen complex as pore dimensions are wide enough to accommodate the complex molecule. Co-salen complexes did not exhibit ESR spectra due to short spin lattice relaxation times.

### 3.3.6. XPS analysis for surface study

### 3.3.6.1. XPS nitrogen and oxygen

In the case of cobalt salen complex, the nitrogen $1S_{1/2}$ binding energy is 399.0 eV which shifted to a higher value of 399.8 eV (higher by 0.8 eV) (Table 3.3.) in the impregnated catalyst [i.e. Co-S-M(I)]. This shift may be due to the interaction of metal complex with the matrix of Si-O-Si framework [50, 51]. For the metal complex grafted catalyst, Co-S-AM(PS) two types of nitrogen environments are observed, (i) nitrogen from salen ligand and (ii) nitrogen from amino group of $NH_2$-MCM-41. Here the shift in the binding energy of ligand nitrogen is not observed as the metal complex is away from the silica wall when anchored with $NH_2$-MCM-41. The other nitrogen from $NH_2$-MCM-41 shows shift to higher binding energy value of 401.0 eV as compared to the neat $NH_2$-MCM-41 sample (B.E. 399.6 eV) due to the electron donation effect. This indicates the coordinative interaction of nitrogen with copper [52].

In the case of Cu-salen complex, $1S_{1/2}$ binding energy for nitrogen is 398.5 eV (Table 3.3.). For complex impregnated MCM-41 catalyst, this binding energy is shifted to a higher value of 399.5 eV (higher by 1.0 eV) due to the interaction between framework silica matrix and nitrogen from the salen ligand.  In the case of Cu-salen grafted catalyst, Cu-S-AM(PS), we observed broad band with two types of nitrogen signals, one from nitrogen of salen ligand and another from amino-modified MCM-41. For nitrogen of salen ligand, there is no increase in the binding energy and the peak is observed at 398.6 eV (N $1S_{1/2}$). This may be due to the fact that, in the case of grafted catalyst the metal complex is away from the wall of the silica matrix due to the anchoring with the organic moiety. Here, the nitrogen of $NH_2$-MCM-41 shows higher binding energy of 400.8 eV as compared to the neat $NH_2$-MCM-41 which shows the binding energy of 399.6 eV for nitrogen $1S_{1/2}$ level. This shift in

the binding energy arises from the donation of electron from nitrogen of amino-group to central metal of complex.

It is observed that, XPS of oxygen shows broad band with two types of oxygen in the case of Co/Cu-salen complexes. For Co-salen complex along with intense spectra at 532.0 eV for oxygen of salen ligand, [52] a small band at 529.2 eV (Table 3.3.) which may be due to the presence of small amount of CoO species in the sample. In the case of impregnated catalyst Co-S-M(I) the oxygen 1 $S_{1/2}$ binding energy is 532.9 eV which is higher by + 0.9 eV as compared to neat metal complex may be due to the surrounding silica matrix. Here we did not observe the small signal for the oxygen of CoO due to the small percentage of metal present in the catalyst (~ 4.4 %). For Co-salen anchored catalyst Co-S-AM(PS) oxygen $1S_{1/2}$ binding energy is 532.1 eV which is nearly equal to the neat metal complex. For copper complex immobilized catalysts we observed the similar trend in the XPS of oxygen.

Table 3.3. Nitrogen and Oxygen core electron binding energies in Co/Cu-salen immobilized catalysts.

| Sample | N $1S_{1/2}$ from salen (eV) | N $1S_{1/2}$ from NH$_2$-MCM-41 (eV) | O $1S_{1/2}$ from salen (eV) |
|---|---|---|---|
| NH$_2$-MCM-41 | --- | 399.6 | --- |
| Co-salen | 399.0 | --- | 532.0, (529.2 for CoO) |
| Co-S-M(I) | 399.8 (+0.8) | --- | 532.9 (+ 0.9) |
| Co-S-AM(PS) | 399.0 | 401.0 | 532.1 |
| Cu-salen | 398.5 | --- | 532.0, (529.2 for CuO) |
| Cu-S-M(I) | 399.5 (+1.0) | --- | 532.6 (+0.6) |
| Cu-S-AM(PS) | 398.6 | 400.8 | 532.2 |

### 3.3.6.2. XPS Co and Cu

XPS analysis of different catalysts of Co-salen viz. Co-S-M(I) and Co-S-AM(PS) has been done to investigate the effect of encapsulation on the central metal atom [Fig. 3.4. (A)]. In the case of Co-salen complex it is observed that Co$^{2+}$ 2P XPS show two intense

peaks at 780.6 eV (Co$^{2+}$ 2P$_{3/2}$ level) and 795.9 eV (Co$^{2+}$ 2P$_{1/2}$ level). For Co-S-M(I) it is observed that there is a shift in the binding energy of central metal atom for Co$^{2+}$ 2P$_{3/2}$ level by + 0.6 eV (i.e. 781.2 eV for) with nearly the same binding energy for Co$^{2+}$ 2P$_{1/2}$ level i.e. 796.0 eV. In this case we observed satellite signal for Co$^{2+}$ 2P$_{3/2}$ level at 786.1 eV and Co$^{2+}$ 2P$_{1/2}$ level at 802 eV. This may be due to the interaction of central metal with the surrounding silica matrix which pulls the electron density of the metal [53].

In the case of Co-salen anchored catalyst i.e. Co-S-AM(PS), we observed the binding energy for Co$^{2+}$ 2P$_{3/2}$ is 780.8 eV and for Co$^{2+}$ 2P$_{1/2}$ is 795.9 eV which is nearly the same as that of Co-salen complex. It is expected that the binding energy will decrease due to the interaction of the amino group. The apparent contradiction can be explained by the fact that in case of Co-S-AM(PS) the pentadentate metal complex is high spin complex where as Co-salen is low spin complex. Because of the metal ligand electron repulsion, the nucleus of metal is more shielded in the case of high spin form than the low spin form. Consequently the positive charge on the metal ion is not reduced as much as it would be if the complex were low spin and the binding energies for the metal core electrons are higher. [52].

Cu-salen exhibit two intense peaks at 933.9 eV and 953.0 eV assignable to Cu$^{2+}$ 2 P$_{3/2}$ and 2 P$_{1/2}$ along with Cu$^{2+}$satallite peaks at 939-943 Ev [Fig. 3.4 (B)]. After impregnation of the complex viz. Cu-S-M(I), it is observed that there is shift in the binding energy of central metal i.e. binding energy corresponding to Cu$^{2+}$ 2P$_{3/2}$ level is 934.8 eV (+0.9 eV) and Cu$^{2+}$ 2P$_{1/2}$ level is 954.1 eV (+1.1 eV). The increase in the binding energy may be due to the interaction of metal complex with the surrounding silica framework [54]. In case of anchored catalyst i.e. Cu-S-AM(PS) the metal complex will be away from the wall of Si-MCM-41. Hence the interaction with the framework will not be observed as in the case of Cu-S-M(I). Instead we observed shift towards lower binding energy. This might be due to the interaction of amino group (electron donating) with central metal atom. The observed peak levels are 933.1 eV corresponding to Cu$^{2+}$ 2P$_{3/2}$ and 952.7 eV corresponding to Cu$^{2+}$ 2P$_{1/2}$.
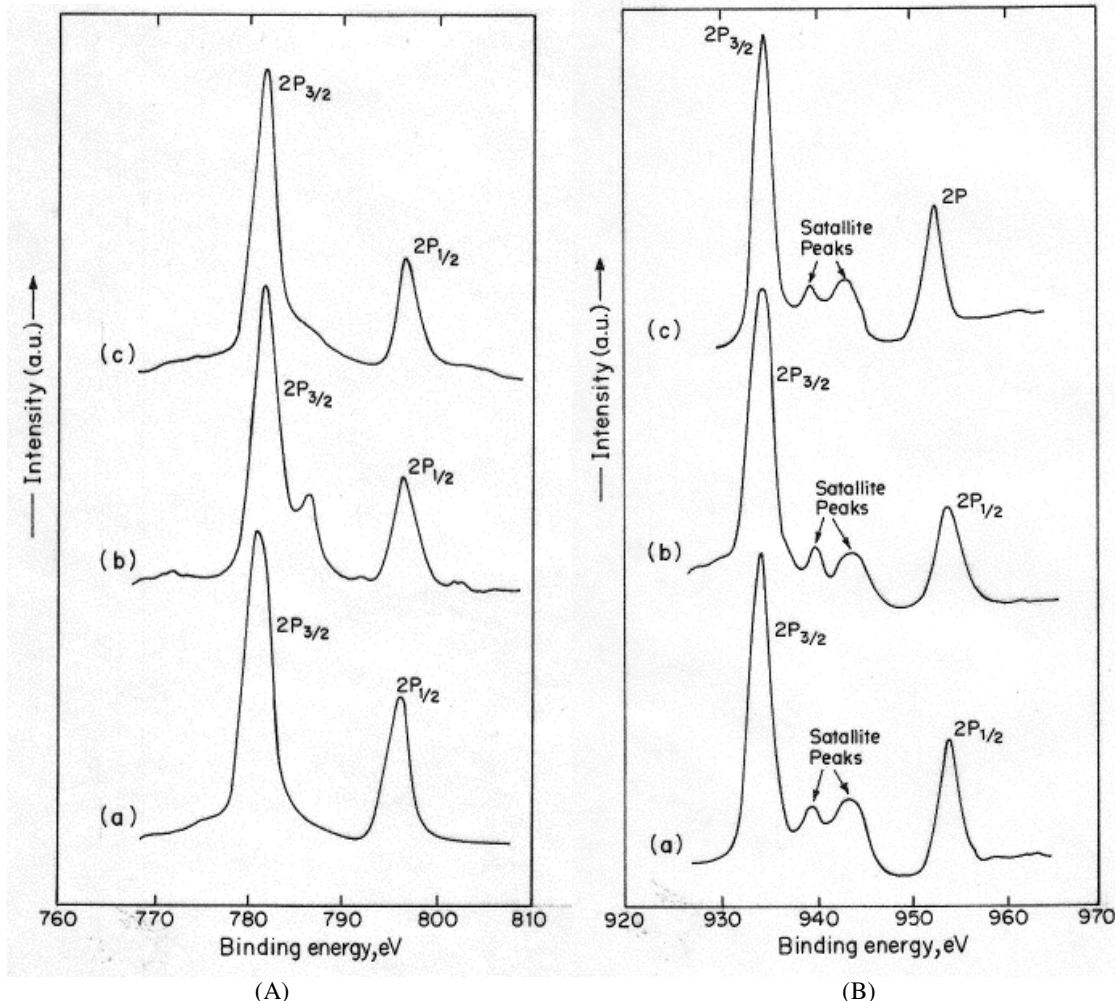
Fig. 3.4. XPS of (A) cobalt salen catalysts i.e. (a) Co-salen, (b) Co-S-M(I), (c) Co-S-AM(PS) and (B) copper salen catalysts i.e. (a) Cu-salen, (b) Cu-S-M(I), (c) Cu-S-AM(PS).

## 3.4. RESULTS AND DISCUSSION

### 3.4.1. Oxidation of alkenes using TBHP as an oxidant

The oxidation reactions of styrene, cyclohexene and 1-decene were carried out using various catalysts of Co/Cu-salen and TBHP as oxidant under mild reaction condition (i.e. 323 K). It is observed that Co/Cu-S-M(I) and Co/Cu-S-AM(PS) show 1.5 to 2 times higher conversion for all the olefins as compared to the neat complex and Co/Cu -S-ASiO$_2$ (Table 3.4.). This may be attributed to the larger hydrophobic surface area of mesoporous material, favoring hydrocarbon adsorption and increased activity of metal complex due to the dispersion in the case of MCM-41 supported catalysts. It is also noticed that the conversion

rate decreases after 8 h for the neat complex and Co/Cu-S-ASiO$_2$, while the conversion proceeds to near completion on the immobilized catalyst with time [Fig. 3.5. (A) and (B) for styrene]. The performance of Co/Cu-S-AM(PS) is better than that of Co/Cu-S-M(I) which may also be due to the presence of a lone pair of the amino group that originated from the aminopropyl group grafted on the silica wall. The presence of a catalytic amount of bases helps to increase the initial rate of epoxidation; however, it also increases the yield of epoxides due to the base catalytic activity of the ligands which facilitate O-O bond cleavage and formation of high oxo intermediates [55].

Fig. 3.5. (C) and (D) show the comparative study of conversion of alkenes using Co/Cu-S-AM(PS) catalysts and it is observed that styrene conversion is higher as compared to other olefins (Table 3.4). For cyclohexene oxidation, the allylic hydrogen is more reactive than the C=C double bond towards the t-butyl peroxy radical and the reaction mainly gives the allylic oxidation product i.e. cyclohexenone [56], whereas in the case of styrene, the t-butyl peroxy radical attacks the double bond to give the epoxide as a major product. In the case of 1-decene, the allylic hydrogen is not that predominantly active. So both the products i.e. epoxide and decenone are mainly observed. Fig. 3.5. (E) and (F) shows the comparison of product yield for Co/Cu-S-AM(PS) as catalysts

Table 3.4. Olefin oxidation using metal-salen catalysts and TBHP as oxidant (12 h data).

| Catalyst | Amount (gms) | Substrate | Conversion (mole %) | Product distribution (mole %) | | | TOF ($h^{-1}$) |
|---|---|---|---|---|---|---|---|
| | | | | -EPO[c] | -ONE[d] | Others | |
| Co-salen | 0.02 | Styrene | 40.4 | 26.2 | 2.1 | 12.1 | 3.0 |
| | | Cyclohexene | 38.4 | 1.8 | 29.8 | 6.8 | 2.5 |
| | | 1-decene | 19.5 | 11.3 | 6.1 | 2.1 | 1.2 |
| Co-S-ASiO$_2$[a] | 0.05 | Styrene | 48.4 | 33.8 | 1.5 | 13.1 | 3.5 |
| | | Cyclohexene | 38.4 | 2.3 | 26.4 | 9.7 | 2.5 |
| | | 1-decene | 24.8 | 13.1 | 9.2 | 2.5 | 1.5 |
| Co-S-M(I)[a] | 0.05 | Styrene | 60.4 | 44.3 | 2.5 | 13.6 | 4.0 |
| | | Cyclohexene | 52.3 | 2.4 | 40.6 | 10.3 | 3.5 |
| | | 1-decene | 36.4 | 21.4 | 10.2 | 4.8 | 2.5 |
| Co-S-AM(PS) [a] | 0.05 | Styrene | 76.3 | 57.6 | 2.2 | 16.5 | 5.5 |
| | | Cyclohexene | 61.3 | 3.2 | 48.4 | 9.7 | 4.0 |
| | | 1-decene | 46.8 | 27.2 | 15.2 | 4.4 | 3.5 |
| Cu-salen | 0.02 | Styrene | 30.7 | 20.5 | 1.1 | 9.1 | 2.5 |
| | | Cyclohexene | 29.7 | 1.4 | 21.5 | 6.8 | 2.0 |
| | | 1-decene | 15.7 | 9.5 | 4.1 | 2.1 | 1.0 |
| Cu-S-ASiO$_2$ [b] | 0.05 | Styrene | 36.2 | 28.8 | 2.9 | 10.9 | 2.5 |
| | | Cyclohexene | 32.4 | 1.3 | 22.4 | 8.7 | 2.0 |
| | | 1-decene | 22.5 | 12.1 | 8.2 | 2.2 | 1.5 |
| Cu-S-M(I)[b] | 0.05 | Styrene | 55.4 | 41.3 | 2.5 | 11.6 | 3.5 |
| | | Cyclohexene | 46.3 | 2.0 | 36.0 | 8.3 | 3.0 |
| | | 1-decene | 29.4 | 17.4 | 8.2 | 3.8 | 1.5 |
| Cu-S-AM(PS)[b] | 0.05 | Styrene | 68.5 | 52.5 | 1.8 | 14.2 | 5.0 |
| | | Cyclohexene | 57.4 | 2.9 | 42.9 | 8.58 | 4.0 |
| | | 1-decene | 38.8 | 22.2 | 12.4 | 3.4 | 3.5 |

Conditions:  Olefins 5 mmoles,   TBHP 5 mmoles,   acetonitrile 10 g., catalyst 0.05 g temp. 323 K.
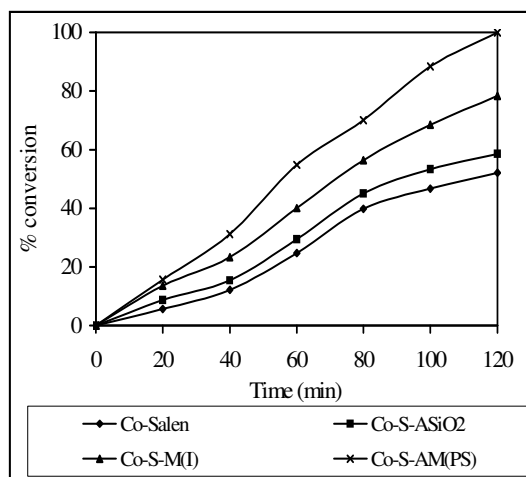


(A)
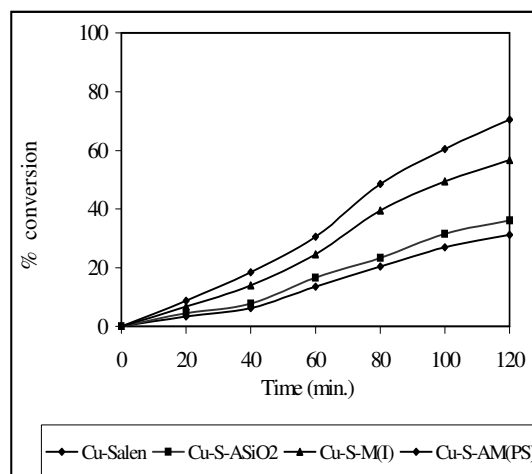


(B)
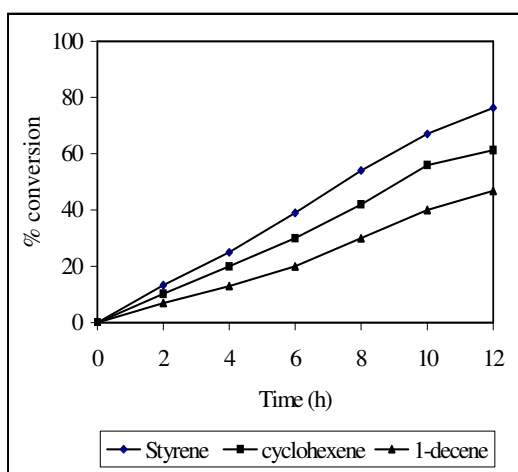


(C)
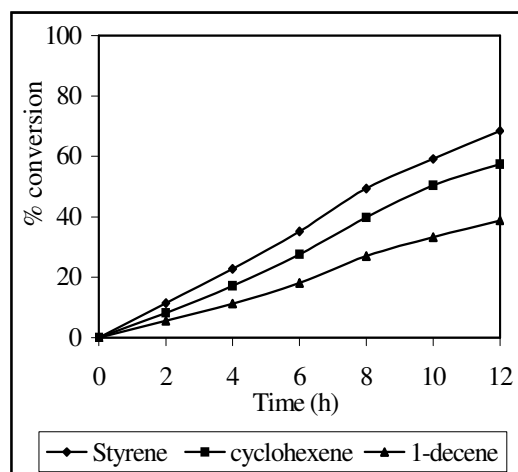


(D)
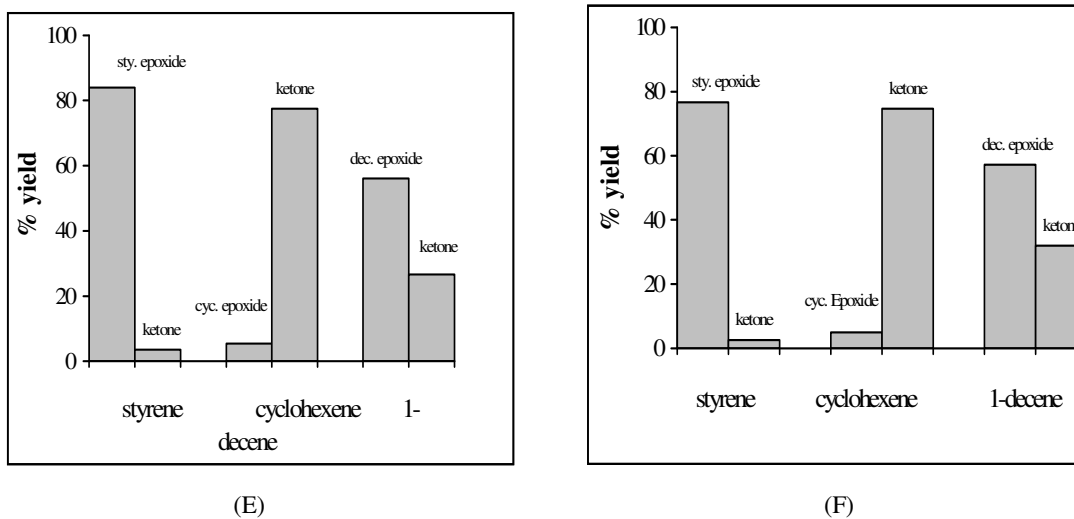
Fig. 3.5.  (A) and (B), Styrene epoxidation on different catalysts of Co-Salen and Cu-Salen  respectively

(C) and (D), Olefin oxidation using Co-S-AM(PS) and Cu-S-AM(PS) respectively

(E) and (F), % yield for Co-S-AM(PS) and Cu-S-AM(PS) respectively for olefin oxidation.

### 3.4.2. Oxidation of alkenes using isobutyraldehyde/O$_2$ as an oxidant

The oxidation of styrene, cyclohexene and decene was also carried out using isobutyraldehyde/O$_2$ as oxidant under mild reaction condition (323 K).  Here also we observed the similar trend of the product formation for the different catalysts of Co/Cu-salen complexes (Table 3.5.). Co/Cu-S-M(I) and Co/Cu-S-AM(PS) show 1.5 to 2 times higher conversion for all the olefins as compared to the neat complex and Co/Cu-S-ASiO$_2$ due to the larger hydrophobic surface area of mesoporous material, favoring hydrocarbon adsorption. Also the superior performance of Co/Cu-S-AM(PS) as compared to Co/Cu-S-M(I) may be due to the presence of a lone pair of the amino group that originated from the aminopropyl group grafted on the silica wall (Fig. 3.6.).

Here the reaction is carried out for 2 hours and Co-S-AM(PS) shows ~ 100 % and Cu-S-AM(PS) shows 70.0 % conversion for styrene. When the reactions were carried out using TBHP as oxidant, we observed 76.3 % conversion for Co-S-AM(PS) and 68.5 % for Cu-S-AM(PS) catalysts for 12 h (section 3.4.1. Table 3.4.). The yield of styrene epoxide observed was ~ 80 % as compared to the 75 % when TBHP is used as oxidant for Co-S-AM(PS) as catalyst. The oxo-metal species formed in both oxidants react directly with the alkene to give epoxide. But when TBHP is used, the catalytic decomposition of hydroperoxide into free radicals when attacking substrate molecules, results in the formation of epoxide and benzaldehyde, which affects the total epoxide selectivity. On the

other hand, in the case of isobutyraldehyde/$O_2$, cooxidation is important from the practical view point; since it is possible to utilize the peroxidic intermediate for the additional oxidation e.g. the active oxygen of acyl peroxy radical and peracid are utilized for the epoxidation. This reaction gives a higher yield of epoxide as compared to oxidation using TBHP, since acyl peroxy radicals are more selective than alkyl peroxy redical i. e. favoring addition relative to abstraction [57].

As mentioned earlier, Co/Cu-S-M(I) and Co/Cu-S-AM(PS) are observed to be the best catalysts for epoxidation of cyclohexene and 1-decene (Table 3.5.). When cyclohexene oxidation was carried out using Co/Cu-salen catalysts and TBHP as an oxidant (section 3.4.1. Table 3.4.) cyclohexenone was found to be predominant product and epoxide yield was observed to be in the range of 4-6 %. This is due to presence of allylic hydrogen atom, which is more reactive as compared to double bond. Typically allylic oxidation products are found when hydrogen abstraction is the dominant reaction involving free radical mechanism. But when the reaction is carried out using isobutyraldehyde/$O_2$ as an oxidant we observed higher yield for cyclohexyl epoxide [84.78 % for Co-S-AM(PS) and 78.70 % for Cu-S-AM(PS)]. This is because the predominant formation of metal oxo-species gives rise to electrophilic attack at the double bond which results in higher epoxide formation or ring cleavage [58]. The results of different oxidation systems are directly affecting turn over frequency TOF ($h^{-1}$) and for isobutyraldehyde/$O_2$ as an oxidant we observed ~ 8 times higher TOF as compared to when TBHP is used as an oxidant (Table 3.4. and 3.5.).

Table 3.5. Olefin oxidation using metal-salen catalysts and isobutyraldehyde/$O_2$ as oxidant (2 h data).

| Catalyst | Amount (gms) | Substrate | Conversion (mole %) | Product distribution (mole %) | | | TOF ($h^{-1}$) |
|---|---|---|---|---|---|---|---|
| | | | | -EPO[c] | -ONE[d] | Others | |
| Co-salen | 0.02 | Styrene | 52.2 | 31.0 | 1.3 | 19.9 | 21 |
| | | Cyclohexene | 45.6 | 28.0 | 4.5 | 13.1 | 18 |
| | | 1-decene | 34.6 | 15.6 | 10.2 | 8.8 | 14 |
| Co-S-ASiO$_2$[a] | 0.05 | Styrene | 58.6 | 34.2 | 2.1 | 22.9 | 39 |
| | | Cyclohexene | 48.0 | 30.6 | 5.6 | 11.8 | 32 |
| | | 1-decene | 38.6 | 20.1 | 6.0 | 12.5 | 25 |
| Co-S-M(I)[a] | 0.05 | Styrene | 78.4 | 65.2 | 2.3 | 10.9 | 52 |
| | | Cyclohexene | 70.1 | 59.2 | 7.2 | 3.7 | 46 |
| | | 1-decene | 62.0 | 38.2 | 13.0 | 10.8 | 41 |
| Co-S-AM(PS)[a] | 0.05 | Styrene | ~100.0 | 80.0 | 3.4 | 16.6 | 67 |
| | | Cyclohexene | 92.5 | 78.0 | 6.8 | 7.7 | 62 |
| | | 1-decene | 78.2 | 45.0 | 14.4 | 18.8 | 52 |
| Cu-salen | 0.02 | Styrene | 31.4 | 20.0 | 2.3 | 9.1 | 13 |
| | | Cyclohexene | 26.4 | 17.9 | 3.0 | 5.5 | 11 |
| | | 1-decene | 21.0 | 13.4 | 4.0 | 3.6 | 9 |
| Cu-S-AMSiO$_2$[b] | 0.05 | Styrene | 36.5 | 22.0 | 2.2 | 12.7 | 28 |
| | | Cyclohexene | 32.0 | 20.0 | 4.0 | 8.0 | 25 |
| | | 1-decene | 24.4 | 14.0 | 3.2 | 7.2 | 19 |
| Cu-S-M(I)[b] | 0.05 | Styrene | 56.7 | 34.0 | 2.0 | 20.7 | 45 |
| | | Cyclohexene | 50.5 | 31.2 | 4.3 | 15.0 | 40 |
| | | 1-decene | 42.3 | 23.6 | 9.0 | 9.7 | 33 |

| Cu-S-AM(PS)[b] | 0.05 | Styrene | 70.0 | 58.3 | 2.0 | 9.7 | 55 |
|---|---|---|---|---|---|---|---|
| | | Cyclohexene | 65.8 | 51.0 | 5.0 | 9.8 | 51 |
| | | 1-decene | 56.0 | 34.4 | 10.5 | 11.1 | 44 |

[a] Co= 4.4 %, [b] Cu= 4.0 %, [c] epoxide [d] ketone

Conditions: substrate- 5 mmoles, solvent- acetonitrile, isobutyraldehyde- 15 mmoles, molecular oxygen at atmospheric pressure, temperature 323 K.

Here we observed, Co-salen immobilized catalysts show slightly higher conversion for all the olefins and both the oxidants as compared to Cu-salen immobilized catalysts. This is due to the higher oxidation potential of cobalt as compared to copper.



(A)                 (B)
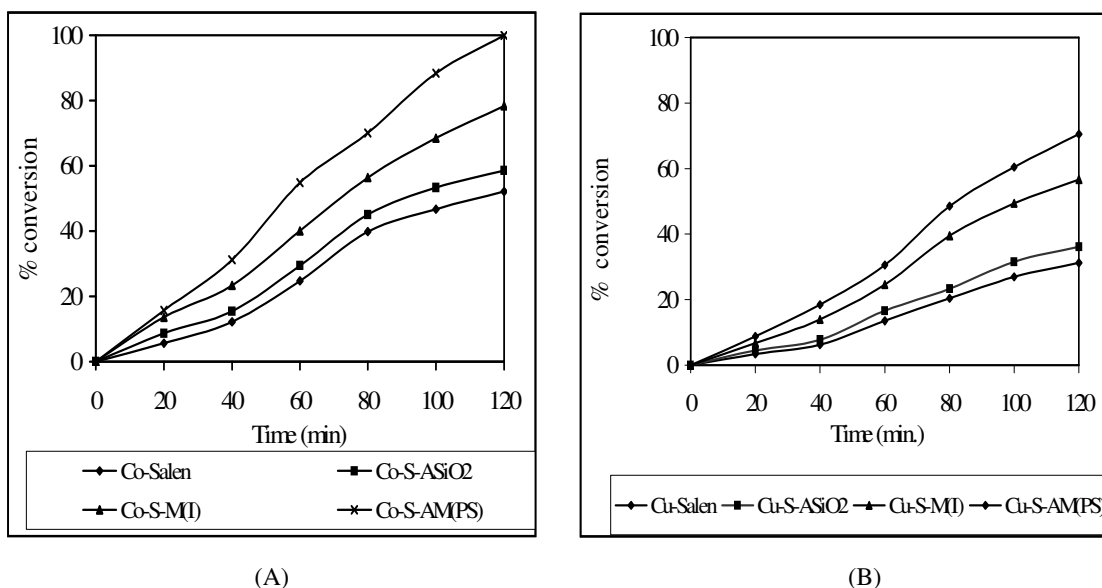
Fig. 3.6. Kinetic study of oxidation of styrene using (A) Co-salen catalysts and (B) Cu-salen catalysts.

### 3.4.3. Oxidation of alkane using TBHP

The study of alkane oxidation (cyclohexane and decane) at 323 K using TBHP as an oxidants show that cyclohexane conversion is in the order, Co/Cu-salen < Co/Cu-S-SiO$_2$ < Co/Cu-S-M(I) < Co/Cu-S-AM(PS) (Table 3.6.). The high activity of the supported complexes [i.e. Co/Cu-S-M(I) and Co/Cu-S-AM(PS)] are due to the large hydrophobic surface area of MCM-41 and the molecular dispersion of the metal complexes within the pores. Further, the higher conversion of Co/Cu-S-AM(PS) compared to Co/Cu-S-M(I) may be due to the anchoring of the metal complex via the amino group to MCM-41, which could enhance the catalytic activity [55].

Table 3.6. Oxidation of alkanes using Co/Cu-salen supported catalysts.

| Catalyst | Amount (gms) | substrate | Conver. (mole %) | product distribution -ol[a] | -one[b] | TON |
|---|---|---|---|---|---|---|
| Co-salen | 0.02 | cyclohexane | 5.5 | 4.4 | 1.1 | 4.5 |
|  |  | decane | 3.1 | --- | 3.1 | 2.5 |
| Co-S-ASiO$_2$ (Co- 4.4 %) | 0.05 | cyclohexane | 8.2 | 6.3 | 1.9 | 13.2 |
|  |  | decane | 5.0 | 0.5 | 4.5 | 8.0 |
| Co-S-M(I) (Co- 4.4 %) | 0.05 | cyclohexane | 13.8 | 10.8 | 3.8 | 22.2 |
|  |  | decane | 8.2 | 0.8 | 7.4 | 13.2 |
| Co-S-AM(PS) (Co- 4.4 %) | 0.05 | cyclohexane | 23.4 | 15.8 | 7.6 | 37.7 |
|  |  | decane | 13.4 | 1.5 | 11.9 | 21.6 |
| Cu-salen | 0.017 | cyclohexane | 4.6 | 3.5 | 1.1 | 3.8 |
|  |  | decane | 2.8 | --- | 2.8 | 2.3 |
| Cu-S-ASiO$_2$ (Cu- 4 %) | 0.05 | cyclohexane | 7.2 | 5.4 | 1.8 | 8.5 |
|  |  | decane | 4.2 | 0.6 | 3.6 | 6.6 |
| Cu-S-M(I) (Cu- 4 %) | 0.05 | cyclohexane | 11.2 | 8.0 | 3.2 | 12.6 |
|  |  | decane | 7.2 | 1.0 | 6.2 | 11.3 |
| Cu-S-AM(PS) (Cu- 4 %) | 0.05 | cyclohexane | 18.4 | 13.2 | 5.2 | 29.0 |
|  |  | decane | 11.4 | 1.2 | 10.2 | 18.0 |

[a] alcohol, [b] Ketone

Fig.3.7 shows that selectivity towards the formation of alcohols is more than ketones for the oxidation of cyclohexane whereas more ketones are formed for decane oxidation. As expected Co-S-AM(PS) is more active and selective than Cu-S-AM(PS).
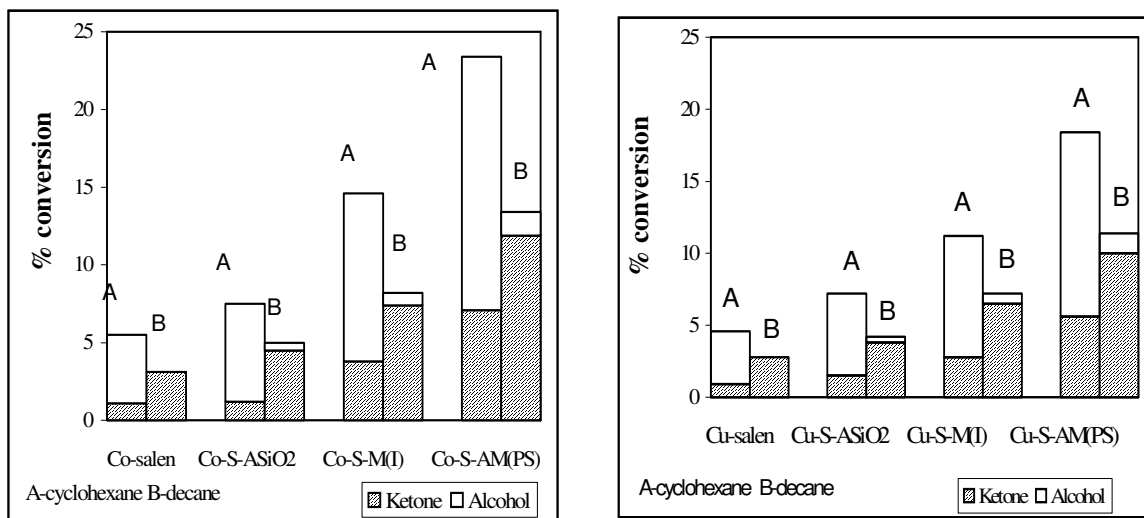


Fig. 3. 7. Comparison of various catalysts of Cu/Co-salen for oxidation of alkanes.

## 3.5. CONCLUSIONS

The immobilization of Co and Cu-salen complexes in the channels of Si-MCM-41 molecular sieves with the walls modified by 3-APTES has been achieved by a post synthesis method. Different characterization techniques such as XRD, FT-IR, EPR, UV-vis. and TG reveal that the complex is monomolecularly attached to the walls of MCM-41. NMR, FT-IR and UV-vis. spectra show the modification of the walls of MCM-41 with propylamine group. FT-IR and UV-Vis. spectra show evidence for adduct formation of the amino group through the axial coordination with the metal which enhances the catalytic activity. The molecular dispersion of the complex with sufficient void space and the hydrophobic surface are appropriate for activation of hydrocarbons as evidenced by higher TON's on immobilization. Co-oxidation with the aldehyde gives a higher rate of epoxidation as compared to oxidation using TBHP, as the acyl peroxy radicals are more selective than alkyl peroxy radicals. Where as oxidation of alkanes using TBHP shows batter results for Co/Cu-S-AM(PS) catalysts.

## 3.6. REFERENCES

1. E. F. Murphy, T. Mallat and A. Baiker, *Catal. Today,* 57 (2000) 115.

2. (a) J. T. Groves, R. C. Haushalter, M. Nakamura, T. E. Nimo and B. J. Evans, *J. Am. Chem. Soc.,* 103 (1981) 2884; (b) R. H. Felton, G. S. Owens, D. Dolphin and J. Fajer, *J. Am. Chem. Soc.,* 93 (1971) 6332.

3. R. H. Holm, *Chem. Rev.*, 87 (1987) 1401.

4. P. S. Dixit and K. Shrinivasan, *Inorg. Chem.,* 27 (1988) 4507.

5. F. Lloret, M. Julve, M. Mollar, I. Castro, J. Latorre, J. Faus, X. Solans and I. Morgenstern-Badaran, *J. Chem. Soc., Dalton Trans.,* (1989) 729.

6. (a) E. N. Jacobsen, in: I. Ojima (Ed.), *Catalytic Asymmetric Synthesis,* VCH, Weinheim, (1993) Chapter 4.2; (b) E. N. Jacobsen, in: G. Wilkinson, F.G.A. Stone, E.W. Abel, L. S. Hegedus (Eds.), *Comprehensive Organometallic Chemistry II,* Pergamon Press, New York, 12 (1995) Chapter 11.1; (c) T. P. Yoon and E. N. Jacobsen, *Science,* 299 (2003) 1691.

7. (a) T. Katsuki, *Coord. Chem. Rev.*, 140 (1995) 189; (b) T. Katsuki, *J. Mol. Catal. A: Chem.,* 113 (1996) 87.

8. C. T. Dalton, K. M. Ryan, V. M. Wall, C. Bousquet and D. G. Gilheany, *Top. Catal.,* 5 (1998) 75.

9. L. Canalai and D. C. Sherrington, *Chem. Soc. Rev.,* 72 (1999) 603.

10. E. N. Jacobsen, A. Pfaltz and H. Yamamato (Eds.), *Comprehensive Asymmetric Catalysis,* Springer, New York, 1-3 (1999).

11. I. Ojima (Ed.), *Catalytic Asymmetric Synthesis,* second ed., Wiley–VCH, New York, (2000).

12. M. Bandini, P. G. Cozzi and A. Umani-Ronchi, *J. Chem. Soc., Chem. Commun.*, (2002) 919.

13. H.-V. Blaser, J. Chem. Soc., Chem. Commun. (2003) 293.

14. (a) B. S. Lane, K. Burgess, *Chem. Rev.,* 103 (2003) 2457; (b) N. E. Leadbeater, M. Marco, *Chem. Rev.,* 102 (2002) 3217; (c) C. E. Song, S. Lee, *Chem. Rev.,* 102 (2002) 2495.

15. M. Costas, M. P. Mehn, M. P. Jensen and L. Que Jr., *Chem. Rev.,* 104 (2004) 939.

16. E. F. Di Mauro, A. Mamai and M. C. Kozlowski, *Organometallics,* 22 (2003) 850.

17. P.R. Ortiz de Montellano (Ed.), *Cytochrome P-450: Structure, Mechanism and*

*Biochemistry,* II$^{nd}$ edn  Plenum Press, New York, (1995).

18.    (a) J. P. Collman, X. Zhang, V. J. Lee, E. S. Uffelman and J. I. Brauman, *Science*, 261 (1993) 1404; (b) M. Sono, M. P. Roach, E. D. Coulter, J. H. Dawson, *Chem. Rev.,* 96 (1996) 2841; (c) K. M. Kadish, K. M. Smith and R. Guilard (Eds.), *The Porphyrin Handbook,* Academic Press, New York, 4 (2000).

19.    H. Fujii, *Coord. Chem. Rev.,* 226 (2002) 51.

20.    (a) E. G. Samsel, K. Srinivasan and J. K. Kochi, *J. Am. Chem. Soc.,* 107 (1985) 7606; (b) K. Srinivasan and J. K. Kochi, *Inorg. Chem.*, 24 (1985) 4671.

21.    (a) K. Srinivasan, P. Michand and J. K. Kochi, *J. Am. Chem. Soc.,* 108 (1986) 2309; (b) K. Srinivasan, S. Perrier and J. K. Kochi, *J. Mol. Catal.,* 36 (1986) 297.

22.    (a) T. Katsuki, *Adv. Synth. Catal.,* 344 (2002) 131; (b) T. Katsuki, *Curr. Chem. Org.,* (2001) 63.

23.    M. Palucki, N. S. Finney, P. J. Pospisil, M. L. Guler, T. Ishida and E. N. Jacobsen, *J. Am. Chem. Soc.,*120 (1998) 948, and references cited.

24.    F. Farzaneh, M. Majidian, M. Ghandi, *J. Mol. Catal. A,*  148 (1999) 227.

25.    E. L. Pires, J. C. Magalhaes, U. Schuchardt, *Appl. Catal. A,* 203 (2000) 231.

26.    C. R. Jacob, S. P. Varkey, P. Ratnasamy, *Microporous Mesoporous Mater.,* 22 (1998) 465.

27.    N. S. Finney, P. J. Pospisil, S. Chang, M. Palucki, R. G. Konsler, K. B. Hansen and E. N. Jacobsen, *Angew. Chem. Int. Ed. Engl.,* 36 (1997) 1720.

28.    M. Palucki, G. J. McCormick and E. N. Jacobsen, *Tetrahedron Lett.,* 36 (1995) 5457.

29.    E. N. Jacobsen, W. Zhang and M. L. Gu¨ler, *J. Am. Chem. Soc.*,113 (1991) 6703.

30.    L. Barloy, P. Battioni and D. Mansuy, *J. Chem. Soc., Chem. Commun.,* (1990) 1365.

31.    D. Pini, A. Mandoli, S. Orlandi and P. Salvadori, *Tetrahedron: Asym.,* 10 (1999) 3883.

32.    E. F. Murphy, L. Schmid, T. Bu¨rgi, M. Maciejewski, A. Baiker, D. Gunther and M. Schneider, *Chem. Mater.,* 13 (2001) 1296.

33.    M. J. Sabater, A. Corma, A. Dome´nech, V. Fornes and H. Garcia, *J. Chem. Soc., Chem. Commun.*, (1997) 1285.

34.    S. B. Ogunwumi and T. Bein, *Chem. Commun.,* (1997) 901.

35.    G. J. Kim and J. H. Shin, *Catal. Lett.*, 63 (1999) 205.

36.    D. Disalvo, D. B. Dellinger and J. W. Gohdes, *React. Funct. Polym.,* 53 (2002) 103.

37.    L. Canali, E. Cowan, H. Deleuze, C. L. Gibson and D. C. Sherrington, *J. Chem. Soc.*

*Perkin Trans.,* I (2000) 2055.

38.  N. Komiya, T. Naota, Y. Oda and S. Murahashi, *J. Mol. Catal. A: Chem.,* 117 (1997) 21.

39.  S. Murahashi, Y. Oda and T. Naota, *J. Am. Chem. Soc.* 114 (1992) 7913.

40.  A. Bottcher, H. Elian, E-G. Jager, H. Langfelderova, M. Mazur, L. Muller, H. Paulus, P. Pelikan, M. Rudolph and M. Valko, *Inorg. Chem.* 32 (1993) 4131.

41.  J. S. Beck, J. C. Vartuli, W. J. Roth, M. E. Leonowicz, C. T. Kresge, K. D. Schmidt, C. T-W. Chu, D. H. Olson, E. W. Sheppard, S. B. McCullen, J. B. Higgins and J. L. Schlenker, *J. Am. Chem. Soc.,* 114 (1992) 10834.

42.  S. J. Gregg and K. S. W. Sing, *Adsorption, Surface Area and Porosity*, Academic Press, London, (1967) 121.

43.  C. -Y. Chen, H. -X. Li and M. E. Davis, *Microporous Mater.,* 2 (1993) 17.

44.  T. Joseph, C. S. Sajanikumari, S. S. Deshpande and S. Gopinathan, *Indian J. Chem.,* 38 (A) (1999) 792.

45.  A. Zangina, M. Byo-Bangoura, K. Bayo and G. V. Quedrago, *Bull. Chem. Soc. Ethiopia,* 16 (1) (2002) 73.

46.  I. E. Kingma, M. Wiersma, J. L. Van der Baan, S. Balt, F. Bickelheanpt, M. W. G. de. Bolster, G. W. Klumpp and A. L. Spek, *J. Chem. Soc., Chem. Commun.,* (1993) 832.

47.  A. Bigotto, E. Reisenhofer and R. Giordani, *Spectrochem. Acta,* 40A (1984) 203.

48.  Xiang-Ge Zhou, Xiao-Qi Yu, Jie-Sheng Huang, Shou-Gui Li, Lian-Sheng Li and Chi-Ming Che, *Chem. Commun.,* (1999) 1789.

49.  S. Seelan, A. K. Sinha, D. Srinivas and S. Sivasanker, *J. Mol. Catal. A: Chemical,* 157 (2000) 163.

50.  R. Guimaraes, F. C. Stedile and Joao H. Z. dos Santos, *J. Mol. Catal. A: Chemical,* 206 (2003) 353.

51.  M. C. Haag, C. Krug, J. Dupont, G. B. Galland, J. H. Z. dos Santos, T. Uozumi and T. Sano, *J. Mol. Catal. A: Chem.,* 169 (2001) 275.

52.  J. H. Burness, J. G. Dillard and L. T. Taylor, *J. Am. Chem. Soc.*, 97 (1975) 6080.

53.  T. Joseph, D. P. Sawant, C. S. Gopinath and S. B. Halligudi, *J. Mol. Catal. A: Chem.,* 184 (2002) 289.

54.  Q. Tang, Q. Zhang, H. Wu and Ye Wang, *J. Catal.,* 230 (2005) 384.

55.  N. Safari and F. Bahadoran, *J. Mol. Catal. A: Chem.*, 171 (2001) 115.

56.  E. F. Murphy, T. Mallat and A. Baiker, *Catalysis Today,* 57 (2000) 115.

57. R. A. Sheldon, J. K. Kochi, *Metal Complex Catalyzed Oxidation of Organic Compounds,* Academic Press, New York, (1981).

58. K. Kaneda, S. Haruna, T. Imanaka and K. Kawamoto, *J. Chem. Soc., Chem. Commun.,* (1990) 1467.

# Chapter-4

# Synthesis Characterization and optical properties of Silver and Gold nanowires embedded in MCM-41

## 4.1. INTRODUCTION

In recent years, interest in the preparation and characterization of nanostructured materials has grown constantly due to their potential applications in the fields of catalysis, optoelectronics, microelectronics etc. [1-7]. Accordingly, considerable effort has been focused on the development of nanostructures via synthetic techniques. Many studies on the methods for their preparation to achieve controlled size and shape have been reported, such as controlled chemical reduction [8, 9], photochemical or radiochemical reduction [10, 11], and gas evaporation [12]. The template method provides a convenient route for preparing nanorods of metals and other nanoparticles. The diameters of these nanorods can be varied by using template membranes with different pore diameters. Advantage of the template method is that it provides a good control over the size and shape of the nanowires and can be used to prepare the nanomaterial with desired aspect ratio [13]. Uniform Ag nanowires have been synthesized within the nanoscale channels of mesoporous silica SBA-15 using the template method by impregnation of $AgNO_3$ followed by thermal decomposition [14]. Reports on the reduction of $H_2PtCl_{16}$ in FSM-16 lead to template synthesis of platinum nanowires inside mesoporous silica FSM-16 host are available [15]. Nanonecklaces of platinum and gold with high aspect ratio are synthesized in mesoporous organosilica templates by hydrogen reduction [16]. Cobalt hexacyanoferrate nanowires were prepared by electrodeposotion using carbon nanotube as template [17]. Regularly spherical or elliptical ZnO nanoparticles have been prepared using gel-template combustion method and studied for photoluminescence properties [18].

Spectroscopic studies of semiconductor nanoclusters fabricated in zeolite matrix are reported by Tel'biz et al. [20]. There are also various reports on quantum wires of semiconductors prepared inside MCM-41 silica matrix and optical properties of these materials are well studied e.g. Ge, GaAs, InP etc. inside MCM-41 host [21-23]. These quantum wires are well ordered and separated by silica walls of MCM-41 [24]. Due to optical transparency of host material, such inclusion of metal or semiconductor in zeolite matrix can produce good material for optoelectronic devices. The optical properties of Ag and Au nanowires grating were studied by optical excitation spectroscopy [25]. Similar to these reports, nanocomposite made of metal nanowires embedded in a dielectric matrix can be one of the future candidates to produce non-linear optical devices due to their fast

response and strong non-linear absorption [26, 27]. A novel photoluminescence was reported for small metal nanocrystals in the near infra-red region by Bigioni et.al. [28].

Nanoscale metal particles exhibit optical properties of great aesthetic, technological and intellectual value. These properties are conveniently elucidated through conventional optical spectroscopic methods [19]. At a fundamental level, optical absorption spectra provide information on the electronic structure of small metallic particles. The absorption spectra of many metallic nanoparticles are characterized by a strong broad absorption band that is absent in the bulk spectra. Furthermore, many studies have been made on series of materials with different dielectric constants; presenting typical non-linear optical properties contributed due to typical metal nanoclusters of Au, Ag, Cu, Rh etc. [29, 30]. These metal clusters exhibit characteristic surface plasmon resonance that influences the linear and non-linear optical properties of the sample when it is irradiated by a light source. Non-linear response depends on metal concentration and on the average particle size inside the matrix [31, 32]. Second harmonic generation (SHG) is a non-linear optical process that results in the conversion of an input coherent optical wave into an output coherent wave of twice the input frequency having the same pulse width as that of input wave and optical intensity is proportional to the square of the input intensity [33].

Reports on the 'second harmonic generation' (SHG) of small noble metal colloidal particles are rather scarce. Galletto et al. [34] reported SH signal from gold particles supported at air /liquid interface and hyper-raleigh scattering signal of gold colloidal solution in presence of pyridene. There are also reports of SHG studies for gold nanoparticles supported on silica surface [35] polymer materials [36] and liquid dispersion of gold nanoparticles [37, 38].

Here, we discussed the synthesis of silver and gold nanowires using template method inside MCM-41 matrix. Formation of nanowires inside MCM-41 was confirmed by XRD and TEM. These heterostructures were found to exhibit interesting luminescence properties as observed for direct band gap semiconductor heterostructures. These heterostructures were also used to study non-linear optical properties (NLO) corresponding to second harmonic generation (SHG).

## 4.2 EXPERIMENTAL

### 4.2.1. Synthesis of Si-MCM-41

Si-MCM-41 have been synthesized according to the procedure reported in the Chapter II; section 2.2.1.

### 4.2.2. Preparation of Ag/Au nanowires

Ag nanowires were prepared inside Si-MCM-41 by controlled reduction of $AgNO_3$ with sodium borohydrate ($NaBH_4$) [1]. In detail, 1 g Si-MCM-41 powder (as prepared in section 4.2.1.) was suspended in 100 ml aqueous solution of $10^{-4}$ M $AgNO_3$ and stirred at room temperature for 2 h. Controlled reduction of $AgNO_3$ by drop wise addition of $NaBH_4$ solution leads to the formation of yellow colored product. The reaction mixture was then subjected to stirring for 24 h at room temperature. After 24 h the yellowish colored powder was filtered, washed several times with water and dried in air. This product is designated as Ag-MCM-41.

Au nanowires were prepared inside Si-MCM-41 using the procedure similar to the preparation of Ag-MCM-41 by controlled reduction of chloroauric acid with sodium borohydrate ($NaBH_4$) [1]. 1 g Si-MCM-41 powder (as prepared in section 4.2.1.) was suspended in 100 ml aqueous solution of $10^{-4}$ M $HAuCl_4$ and stirred at room temperature for 2 h. Controlled reduction of $HAuCl_4$ by drop wise addition of $NaBH_4$ solution leads to the formation of purple colored solution. The reaction mixture was then subjected to stirring for 24 h at room temperature. After 24 h the pale purple colored powder was filtered, washed several times with water and dried in air. This product is designated as Au-MCM-41.

## 4.3. RESULTS AND DISCUSSION

The material was characterized by various techniques like XRD, nitrogen sorption studies, TEM, UV-Vis. spectrophotometer, photoluminescence and second harmonic generation studies (SHG). Powder X-ray diffraction patterns were recorded on a Philips, Holland (for high angle) and Rigaku Miniflex diffractometer, Japan instrument (for low angle) using nickel-filtered Cu Kα radiations (λ = 1.5406 Å). The surface area and pore volume were determined from $N_2$ adsorption isotherms using a Coulter (Omnisorb, 100 CX)

instrument. Transmission electron imaging was performed on a JEOL 1200 EX microscope operated at 100 kV. The samples were prepared by dispersing the powders in methanol. Imaging was enabled by depositing few drops of suspension on carbon coated 400 mesh Cu grid. The solvent was allowed to evaporate before imaging.

Optical spectra were taken on an UV-Visible Hitachi spectrophotometer model U-3210. Spectra were recorded in the solution formed by suspending small amount of powder in aqueous medium. Room temperature photoluminescence experiments were performed on Perkin-Elmer (LS-50) photoluminescence spectrophotometer in back scattering geometry. The emission spectrum was collected in the range between 300 to 800 nm using 250 nm excitation and 290 nm filter. For second harmonic generation (SHG) studies aqueous suspension of samples were illuminated with Q-switched Nd-YAG laser (wavelength 1064 nm, pulse width 40 ns and 1 pps) beam. The generated SHG signal at 532 nm was separated from the fundamental wave by using filters. Urea used as a standard reference sample. SHG signal was measured as a function of input laser energy.

### 4.3.1 X-ray diffraction

The reduction of metal ions by sodium borohydride leads to the agglomeration of nanoparticles inside the channels of Si-MCM-41. Figure 4.1. (A) shows low angle X-ray diffraction patterns of calcined Si-MCM-41, Ag-MCM-41 and Au-MCM-41. The four peak appearing at low angle corresponds to (100), (110), (200) and (210) planes of Si-MCM-41 indicating ordered pore structure of Si-MCM-41, which can be attributed to quasi two dimensional hexagonal lattice of Si-MCM-41 {Fig. 4.1 (A) a} [39]. Further, loss in the intensity is observed for most intense peak at ($2\theta = 2.6^0$) due to the formation of metallic nanowire inside the channels of Si-MCM-41 which is also confirmed by high angle X-ray diffraction data ($2\theta = 30\text{-}60^0$), Fig. 4.1. (B). Diffraction pattern of Ag-MCM-41 show peaks at ($2\theta = 36.4^0$) and ($2\theta = 44.6^0$) corresponding to (111) and (200) planes of silver lattice. Similarly, Au-MCM-41 shows peaks at ($2\theta = 38.34^0$) and ($2\theta = 44.66^0$) corresponding to (111) and (200) planes of gold lattice. Peaks corresponding to the (200) and (311) planes of cubic Au crystal being very weak are not observed.
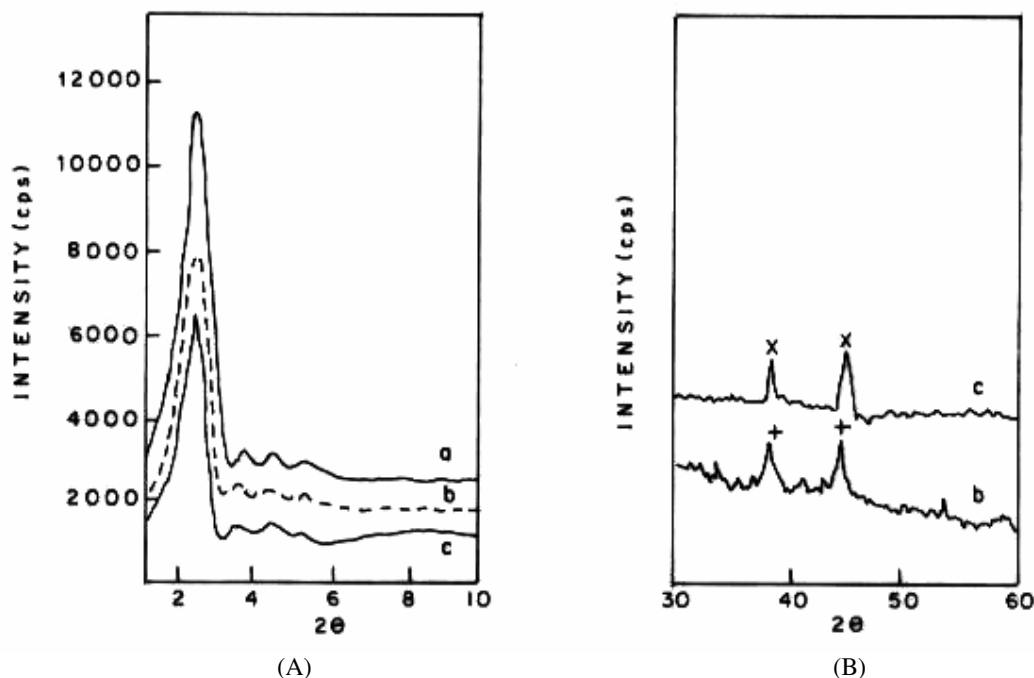
Fig. 4.1. (A) Low angle X-ray diffraction pattern of (a) Si-MCM-41, (b) Ag-MCM-41 and (c) Au-MCM-41

(B) High angle X-ray diffraction pattern of (b) Ag-MCM-41 and (c) Au-MCM-41.

### 4.3.2 Transmission electron microscopy

The formation of Ag/Au nanowires inside Si-MCM-41 channels is further confirmed by the Transmission Electron microscopy. The formation of nanowires may be due to low nucleation rate, unidirectional diffusion of Ag/Au atoms along pore channels and the size confinement of pore channels. Dark lines within the channels indicate nanowire formation due to agglomeration of metal clusters. Fig. 4.2. (b) and (c) (corresponding to Ag-MCM-41 and Au-MCM-41 respectively) revealed the average diameter of nanowires about ~ 2.8 nm which is coincident with pore diameter of Si-MCM-41 host [Fig. 4.2. (a)]. Some of the nanowires in Au-MCM-41 are curved with branches, although some are straight with uniform diameter. Along with TEM images of Ag/Au-MCM-41, the presence of some smaller Ag/Au particles, removed from the silica host by ultrasonic vibration during preparation of TEM specimen and few silica aggregates outside the channels cannot be neglected.

115
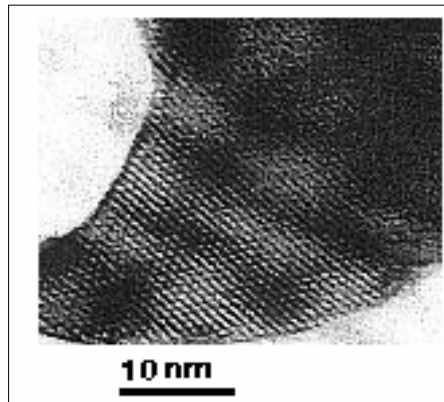
(a)
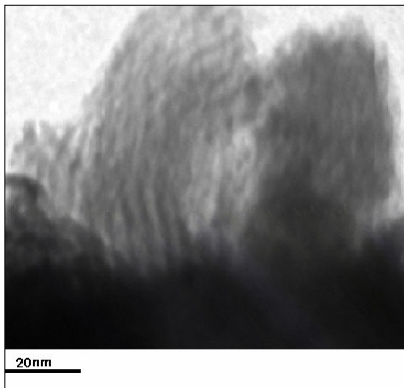


(b)
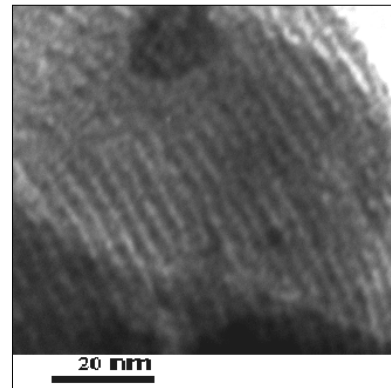


(c)

Fig. 4.2 TEM images of (a) MCM-41, (b) Ag-MCM-41 and (c) Au-MCM-41.

### 4.3.3. $N_2$- sorption studies

Pore characteristics of all the mesoporous samples were studied by using $N_2$-sorption technique. Fig. 4.3 shows the $N_2$-adsorption-desorption isotherms and the corresponding pore size distributions (inset) of (a) Si-MCM-41, (b) Ag-MCM-41 and (c) Au-MCM-41. All the samples show type IV isotherm with the presence of two hysteresis loops. One at low relative pressure ~ 0.2-0.45 $P/P_0$ indicate framework confined mesoporosity and other one at $P/P_0 > 0.7$ correspond to capillary condensation within interparticle pores. This indicates the pore filling of the nanowires without damaging the mesoporosity. The values of specific surface area pore volume and pore diameter are summarized in Table 4.1. It is observed that on embedding Ag and Au nanowires inside the

mesoporous Si-MCM-41 there is a decrease in the surface area by 20 % for Ag-MCM-41 and 23 % for Au-MCM-41 indicative of pore occupancy of the host by Ag/Au nanowires. Pore diameter and pore volume of these samples also decrease as shown in Table 4.1
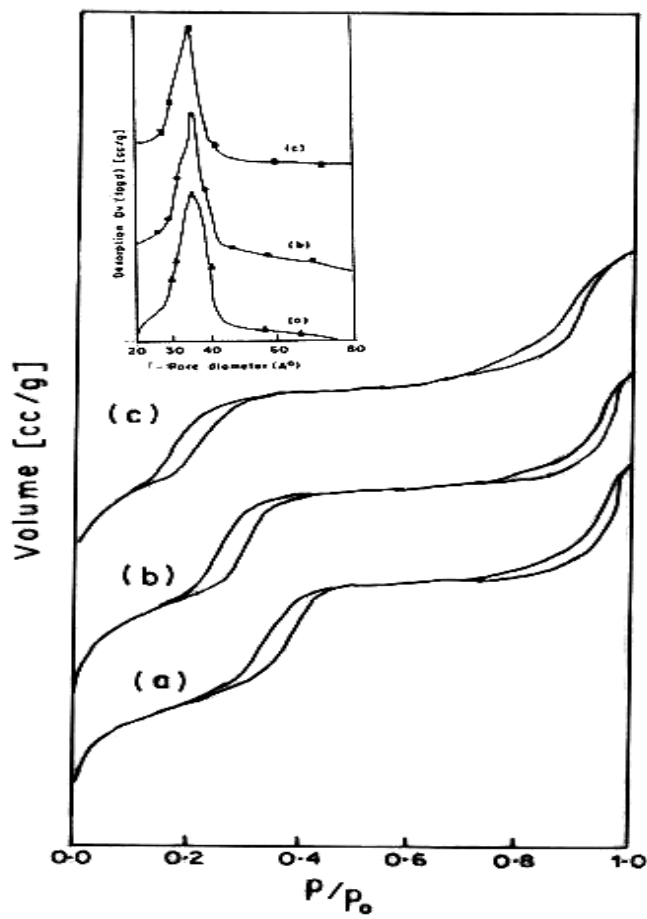


Fig. 4.3. $N_2$-adsorption-desorption isotherms of (a) Si-MCM-41, (b) Ag-MCM-41 and (c) Au-MCM-41 with the pore size distributions (inset) of the respective sample.

Table 4.1. Sorption data for Si-MCM-41 embedded with Ag and Au nanowires.

| Samples | $S_{BET}$ (m$^2$/g) | Pore diameter (Å) | Pore volume cc/g |
|---|---|---|---|
| Si-MCM-41 | 1115 | 38 | 0.65 |
| Ag-MCM-41 | 892 | 33 | 0.44 |
| Au-MCM-41 | 859 | 30 | 0.40 |

## 4.3.4 Absorption spectroscopy

The optical properties of the noble metal nanoparticles are substantially different from that of planar metal surfaces. This difference is due to the curved geometry of the particles that allows direct coupling of light to resonant collecting electron plasma oscillations [19, 40]. Such plasmon modes can also be sustained by metal structures of cylinder like geometry with cross section dimensions small compared to the wavelength of the exciting light and a quasi-infinite extension along the symmetry axis. The shape and position of the plasmon band is known to depend on the matrix in which the nanorods are dispersed, the stabilizing polymers in colloid, the particle size and the aspect ratio [13, 41]. The intensity of this absorption band depends on the aspect ratio and diameter of the nanorods and on the quantity of the metal suspended. Fig. 4.4. (a) and (b) represents the optical absorption spectrum of Ag-MCM-41 and Au-MCM-41. It was usually seen that the color of Ag-MCM-41 sample was pale yellow, while that of Au/MCM-41 was pale purple, and were quite transparent for optical measurements. The optical absorption spectra show a broad peak at 410 nm for Ag-MCM-41 [Fig. 4.4 (a)] and at 515 nm for Au-MCM-41 [Fig. 4.4. (b)] .These characteristic peaks are due to the oscillation of conduction band electrons of silver and gold (also known as surface plasmon resonance) [42]. The broadening in the peak as seen from the figure is due to the smaller diameter (~2.8 nm) of the nanowires formed. In the case of Ag-MCM-41, the observed peak position is red shifted as compared with bare silver nanoparticles, which exhibit a sharp absorption peak at 390 nm [43]. The nature of Au-MCM-41 absorption spectrum is also similar to that of Au-SiO$_2$ mesoporous composite reported elsewhere [44]. In present work, the shift in the $\lambda_{max}$ with the tailing of absorption to the longer wavelength can be attributed to the high dielectric constant of water ($\varepsilon = 80$), particle size, aspect ratio and diameter of nanowires also plays important role in deciding the position of plasmon absorption band [45].
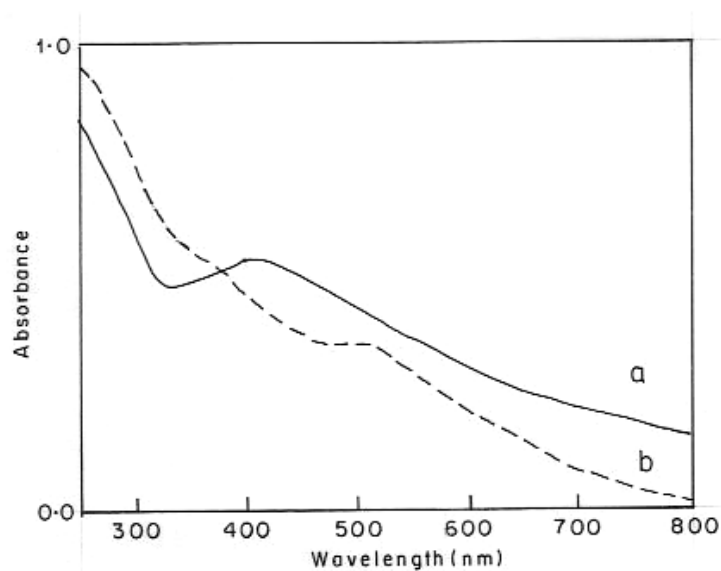
Fig. 4. 4. Optical absorption spectrum of (a) Ag-MCM-41 and (b) Au-MCM-41.

### 4.3.5 Emission spectroscopy

Luminescence from metal surface has received only limited amount of attention [46, 47] because metals do not have a band gap. If the energy gap is present among the higher lying states one could expect to see an appreciable amount of photoluminescence from the metal. Photoluminescence studies have been conducted on nanometers size gold clusters in the visible region of the spectrum [48] where chromatographically separated gold clusters < 5 nanometers in diameter were shown to be luminescent. The inclusion of silver and gold inside MCM-41 provides a three-dimensional heterostructure. Fig. 4.5. (a) and (b) show the room temperature emission spectrum of Ag-MCM-41 and Au-MCM-41. Due to quantum confinement effect of metals inside the matrix, such a heterostructure shows optical properties as observed for direct band gap semiconductors. The nanowires within the channels of Si-MCM-41, which are separated by silica walls, represent conventional quantum well structure. The electronic charge distribution is delocalized along the direction normal to the well layer. Silica wall barrier thickness is 16 Å (calculated from XRD) [49], which is sufficiently small to allow the coupling of electrons between adjacent well that gives rise to new broadening and delocalized quantized state called minibands [43]. Transition of electrons in these minibands gives rise to two emission peaks at 325 and 625 nm for Ag-MCM-41 and at 375 and 675 nm for Au-MCM-41, respectively.

119
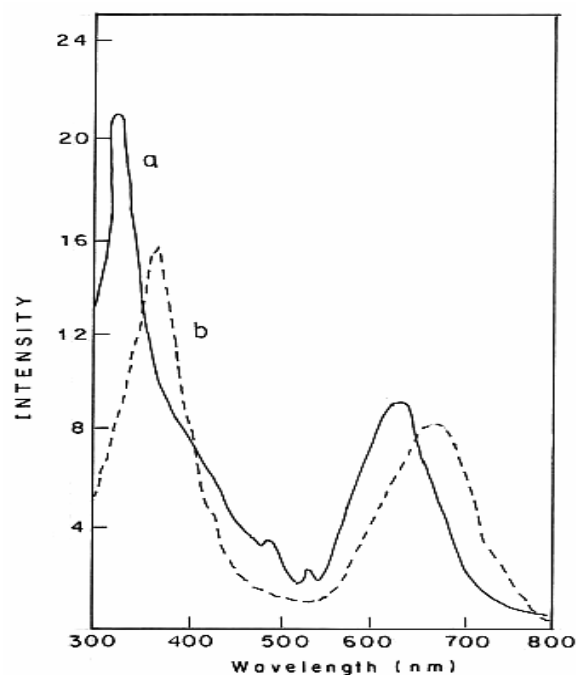
Fig. 4.5 Room temperature emission spectrum of (a) Ag/MCM-41 and (b) Au/MCM-41 using 250 nm excitation and 290 nm filter.

### 4.3.6 Second harmonic generation studies

The SHG intensity versus laser input energy of Ag-MCM-41 and Au-MCM-41 is shown in Fig. 4.6. (a) and (b) respectively. To study the second harmonic generation of Ag and Au nanowires, self supported films were prepared by dissolving polymethyl methacrylate (PMMA) in chloroform followed by addition of Ag-MCM-41, Au-MCM-41 samples and films were prepared by spin coating technique. Poling was done to align the nanowires by applying a DC of 30 V. Films were poled at near the glass transition temperature (Tg) of the polymer ($\sim 90^0$ C). The frequency doubling was observed using Nd:YAG laser with $\lambda = 1064$ nm with pulse width of 20 ns and repetition rate one pulse per second. Powder urea was used as the reference sample. The SHG intensity varies as the square of the input intensity, the pulse width of fundamental beam and 2 $\omega$ beam was found to be the same confirming the second harmonic generation (measured on FND-100 with appropriate filters). The coherence SHG was confirmed by using polarizer.

Metal nanoparticles such as Ag and Au show characteristic surface plasmon absorption in the visible near infrared wavelength region, known to cause a highly localized

120

electric field at the interface between the metal surface and surrounding medium [50]. Enhanced optical non-linearity arises from the enhancement of local field near the surface plasmon resonance. Fig. 4.6. (a) and (b) shows the SHG of self supported films of Ag-MCM-41 and Au-MCM-41 without and with poling respectively. SHG enhanced with poling as shown in Fig. 4.6. (b). It is mainly due to near Tg the molecular segment along with the dopant reaches to an anisotropic state due to induced order of orientation and hence the non-linearity arises. The orientation order is retained without relaxation by reducing the temperature to ambient with electric field on where the aligned dopants are active and the polymer segmental motion is retarded. Thus poling helps to enhance the SHG. Without poling less SHG is observed as shown in Fig. 4.6 (a). It is well known that inhomogenities present in the guest host system scatter  the SHG light. This results in less SHG intensity.



(a)                                                          (b)
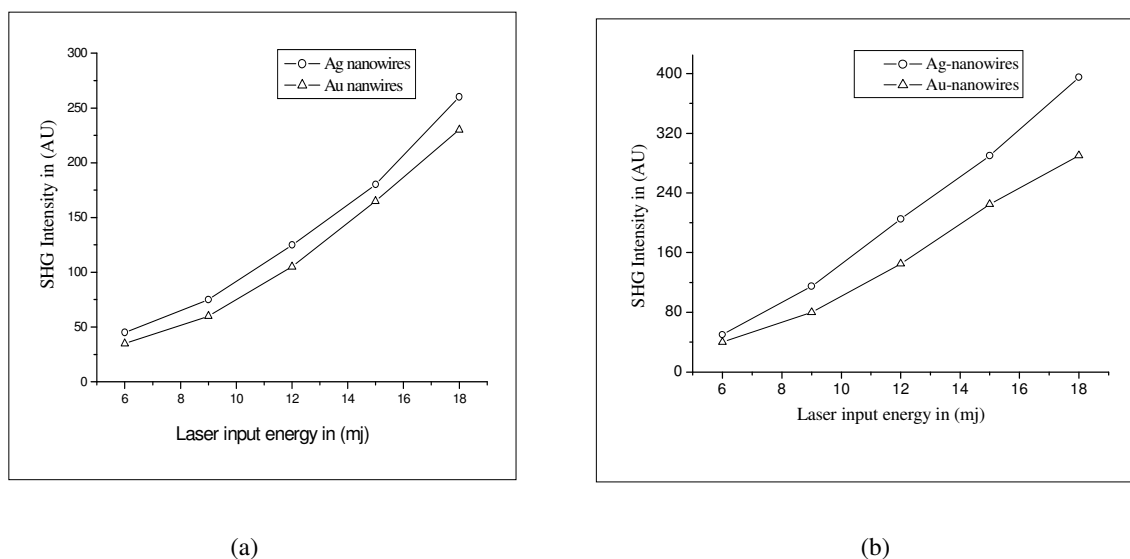
Fig. 4.6. Second harmonic generation (a) without poling and (b) with poling.

## 4.4. CONCLUSIONS

Here the nanowires of silver and gold were formed inside the channels of Si-MCM-41 host. Controlled reduction of respective metal salts with sodium borohydrate leads to agglomeration of nanoparticles inside the channels of host materials which resulted in to nanowires formation. By utilizing the template method Ag/Au nanowires of ~2.8 nm coincident with channel diameter of Si-MCM-41 were confirmed by TEM. This may be due to unidirectional diffusion of Ag/Au atoms along pore channels indicated by dark lines [Fig. 4.2 (a) and (b)]. These heterostructured materials exhibit interesting luminescence

properties as observed for direct band gap semiconductors. The optical characterization of these heterostructure materials show second harmonic generation with more SHG intensity after poling than the unpoled samples.

## 4.5. REFERENCES

1. G. Schmid: Clusters and Colloids: From Theory to Applications, VCH, New York, Weinhein, 1994.
2. A. P. Alivisatos, *J. Phys. Chem.,* 100 (1996) 13226.
3. P. Yang, G. Wirnsberger, H. C. Huang, S. R. Cordero, M. D. McGehee, B. Scott, T. Deng, G. M. Whitesides, B. F. Chemelka, S. K. Buratto and G. D. Stucky, *Science,* 287 (2000)65.
4. W. Z. Wang, Y. Geng, Y. T. Qiam, M. G. Ji and X. M. Liu**,** *Adv. Mater.*, 10 (1998) 1479.
5. R. P. Andres, J. D. Dielefeld, J. I. Hendersom, D. B. Janes, V. R. Kolagunta, C. P. Kubiak, W. J. Mahaney and R. J. Osifehin, *Science*, 273 (1996). 1690.
6. M. Moffit and A. Eisenderg, *Chem. Mater.* 7 (1995) 1178.
7. S. Forster and M. Antonietti, *Adv. Mater.,* 10 (1998) 195.
8. L. Bronstein, E. Kramer, B. Berton, C. Burger, S. Forster and M. Antoniethi, *Chem. Mater.,* 11 (1999) 1402.
9. S. Sato, K. Toda and S. Oniki, *J. Colloid. Interface Sci.,* 218 (1999) 504.
10. K. Fukumi, A. Chayahara, K. Kadono, T. Sakaguchi, Y. Horino, M. Miya, J. Hayakawa and M. Satou, *Jpn. J. Appl. Phys.,* 30 (1991) 742.
11. K. Kurihara, J. Kizling, P. Stenius and J. H. Fendler, *J. Am. Chem. Soc.,* 105 (1983) 2579.
12. N. Satoh and K. Kimura, *Bull. Chem. Soc. Jpn.,* 62 (1989) 1758.
13. G. L. Hornyak, C. J. Patrissi and C. R. Martin**,** *J. Phy. Chem. B,* 101 (1997) 1548.
14. M. H. Huang, A. Choudrey and P. Yang, *Chem. Commun.,* (2000) 1063.
15. A. Fukuoka, N. Higashimoto, M. Sasaki, M. Harada, S. Inagaki, Y. Fukushima and M. Ichikawa, *Stud. Surf. Sci. Catal.,* 130 (2000) 3041.
16. A. Fukuoka, T. Higuchi, T. Ohtake, T. Oshio, J.-i. Kimura, Y. Sakamoto, N. Shimomura, S. Inagaki and M. Ichikawa, *Chem. Mater.,* 18 (2006) 337.
17. L. Qian and X. Yang, *Talanta,* 69 (2006) 957.

18. J. Zhou, Y. Wang, F. Zhao, Y. Wang, Y. Zhang and L. Yang, *J. Luminescence,* 119 (2006) 248.

19. U. Kreibig, M. Vollmer, *Optical Properties of Metal Clusters,* Springer, Berlin, (1995).

20. G. Tel'biz, I. Blonskij, S. Shevel and V. Voznyi, *Stud. Surf. Sci. Catal.,* 105 (1997) 2101.

21. J. R. Agger, M. W. Anderson, M. E. Pemble, O. Terasaki and Y. Nozue**,** *J. Phys Chem. B*., 102 (1998) 3345.

22. V. I. Srdanov, I. Alxneit, G. D. Stucky, C. M. Reaves and S. P. DenBaars, *J. Phys. Chem. B.,*102 (1998)3341.

23. R. Leon, D. Margolese, G. Stucky and P. M. Petroff, *Phys. Rev. B.,* 52 (1995) 2285.

24. P. V. Adhyapak, P. Karandikar, K. Vijayamohanan, A. A. Athavale and A. J. Chandwadkar, *Mater. Lett.,* 58 (2004) 1168.

25. G. Schider, J. R. Krenn, W. Gotschy, B. Lamprecht, H. Ditlbacher, A. Leitner and F. R. Aussenegg, J. Appl. Physics, 90 (2001) 3825.

26. P. Mazzoldi, G. W. Arnold, G. Bataglin, I. Gonella and R. F. Haglund Jr., *J. Non-Linear Opt. Phys.,* 5 (1996) 285.

27. G. Yang, W. Wang, L. Yan, H. Lu, G. Yang and Z. Chen, *Opt. Commun.,* 209 (2002) 445.

28. T. P. Bigioni and R. L. Whetten, *J. Phy. Chem. B,* 104 (2000) 6983.

29. M. Ballesteros, R. Serna, J. Solic, C. N. Afonso, A. K. Petford Long, D. H. Osborne and R. F. Haglund Jr., *Appl. Phys. Lett.,* 71 (1997) 2445.

30. B. W. Wessels, *J. Cryst. Growth,* 195 (1998). 706.

31. G. Yang, W. Wang, Y. Zhou, H. Lu, G. Yang and Z. Chen, *Appl. Phys. Lett.,* 81 (2002) 3969.

32. R. A. Ganeev, A. I. Ryasnyansky, S. R. Kamalov, M. K. Kodirov and T. Usmanov, *J. Phys. D: Applied Phys*., 34 (2001). 1602.

33. R. Antoine, P. F. Brevet, H. H. Girault, D. Bethell and D. Schiffrin, *Chem.  Commun.,* (1997)  1901.

34. P. Galletto, P. F. Brevet, H. H. Girault, R. Antoine and M. Broyer,  *J. Phys. Chem. B,* 103 (1999) 8706.

35. K. Pedersen, T. B. Kristensen, T. G. Pedersen, T. Jensen, Per Morgen, Z. Li and S. V. Hoffmann, *Surface Science,* 523 (2003). 21.

36. I. Vargas-Baca, A. P. Brown, M. P. Andrews, T. Galstian, Y. Li, H. Vali and M. G. Kuzyk, *Can J. Chem.,* 80 (2002) 1625.

37. F. W. Vance, B. I. Lemon and J. T. Hupp, *J. Phys. Chem. B.,* 102 (1998) 10091.

38. P. Galletto, P. F. Brevet, H. H. Girault, R. Antoine and M. Broyer, *Chem. Commun.,* (1999) 581.

39. C. T. Kresge, M. E. Leomowicz, W. J. Roth, J. C. Vartuli and J. S. Beck, *Nature.* 359 (1992) 710.

40. C. F. Bohren and D. R. Huffman, *Absorption and Scattering of Light by Small Particles,* Wiley, New York, (1983).

41. C. R. Martin, *Science,* 266 (1994) 1961.

42. S. Kapoor, *Langmuir,* 14 (1998) 1021.

43. S. Pethkar, M. Islam, I. S. Mulla, P. Ganeshan and K. Vijaymohanan, *J. Mater. Chem.,* 11 (2001) 1710.

44. W. Chen, W. Cai, L. Zhang, G. Wang and L. Zhang, *J. Colloid Surf. Sci.,* 238 (2001) 291.

45. V. M. Cepak and C. R. Marten, *J. Phys. Chem. B.,* 102 (1998) 9985.

46. J. K. Gimzewski, J. K. Sass, R. R. Schlitter, J. Schott, *Europhys. Lett.,* 8 (1989) 435.

47. B. Reihl, J. H. Coombs and J. K. Gimzewski, *Surf. Sci.,* 211-212, (1989) 156.

48. J. P. Wilcoxon, J. E. Martin, F. Parsapour, B. Wiedenman and D. F. Kelley, *J. Chem. Phys.,* 108 (1998) 9137.

49. M. Krak, M. Jaroniec, Y. Sakamoto, O. Terasaki, R. Ryoo and C. H. Ko, *J. Phys. Chem. B,* 104 (2000) 292.

50. K. Murakoshi, H. Tanaka, Y. Sawai and Y. Nakato, *J. Phys. Chem. B,* 106 (2002). 3041.

# Chapter-5
# Synthesis of Mesoporous Silica Templated Mesoporous Carbon

## 5.1. INTRODUCTION

It is important to develop an inexpensive and environmentally benign route for fabrication of three dimensionally interconnected mesoporous silica/carbon materials. Carbon materials with high surface area, large pore volume and chemical inertness are useful in many material application areas including water and air purification, adsorption, as catalyst support, chromatographic column and capacitor for energy storage [1, 2]. Most of the activated carbons [3-5] are however microporous and these carbons have limited material applications as adsorbents for large molecules and as an electrode [6. 7]. Recently various porous carbon materials have been fabricated using different kinds of nanostructural silica materials as templates. The technique consists of: (i) impregnation of the inorganic porous structure (template) with a carbon precursor (generally a polymer or prepolymer), (ii) carbonization of the precursor inside the nanocomposite, and (iii) elimination of the template that gives rise to the pores.

Synthesis of mesoporous carbon materials using inorganic/organic templates is currently an active area of research. Mesoporous silica materials with diverse pore structures synthesized using various organic templates including neutral amine surfactants [8, 9], alkyl (PEO) surfactant [10] and triblock copolymers [11] with uniform pore sizes and high surface area are suitable to make mesoporous carbon materials. Ryoo et al. [12, 13] reported the first synthesis of new type of mesoscopically ordered carbon molecular sieve CMK-1 and CMK-3 (cubic and hexagonal, respectively) by carbonizing sucrose inside the pores of the cubic MCM-48 and hexagonal SBA-15 mesostructured silica materials. Whereas furfuryl alcohol was found to be suitable as carbon precursor to synthesize hollow or fully filled cage-like silica/carbon mesostructures from SBA-16 [14]. Wormhole [15], foam like [16] mesostructured carbons and mesoporous carbons with high textural porosity [17] were fabricated using mesoporous aluminosilicate, organic colloids and mesostructered HMS silica materials as templates, respectively. However the materials applications of MCM-48, SBA-15 etc. have been limited partly due to relatively high costs of the reagents.

One of the most important research areas in mesoporous materials is developing an inexpensive and environmentally benign route for the fabrication of three dimensionally interconnected mesoporous materials containing large amount of textural mesopores. However, the synthesis of mesoporous carbon involves sacrificing the mesoporous silica

templates, hence developing low cost mesoporous silica templates would open the door for relatively cheap production of mesoporous carbon [18, 19].

The synthesis of mesoporous silica materials using surfactants as templates has been studied extensively since 1992 [20, 21]. So far, surfactants (ionic [22, 23] or neutral [24, 25]) have been the most commonly used templates for directing the formation of mesopores. All the ionic pathways are based on charge matching between the ionic surfactants and ionic inorganic precursors through electrostatic interactions. For the neutral surfactants it was suggested that hydrogen bonding between the surfactants and the precursors directs the formation of mesostructures. The preparation of mesoporous silica by the neutral route has advantages over the electrostatic route because of the easy removal of the surfactants by solvent extraction and the tendency to produce materials with thicker walls and smaller particle size. The second advantage is that they are relatively inexpensive, environmentally compatible and biodegradable.

A general non-surfactant route for the preparation of mesoporous silica materials via a sol-gel route with a large surface area and pore volumes is reported by Wei et al. [26] and Pang et al. [27], where they use TEOS as the source of silica. Titanium containing mesoporous silica prepared using tartaric acid as template having wormlike three-dimensional pore structure was used for oxidation of olefins [28].

In the preparation of mesoporous silica by the neutral route, TEOS has usually been used as the silicon source; this is a rather expensive silica precursor. In view of the diversity of real and potential applications of these materials, the design of low cost successful synthetic strategies becomes a challenging task. Indeed, Chen and coworkers reported for the first time the use of low cost sodium silicate (as silica source) in the surfactant assisted procedure that yields a mesoporous silica displaying an interconnected channel system MCM-48 [29]. The use of sodium silicate as reagent has been described in a diversity of synthesis of mesoporous silicas, MCM-41 [30-32], MCM-48 [33], SBA-n [34-36], MSU-X [37, 38], MSU-H [39, 40] etc. These mesoporous silicas prepared by using inexpensive silica source can be used as templates to design the mesoporous carbon material of tunable porosity.

Porous carbon has been widely employed as electrode for energy storage in double layer capacitors [41-43]. The small pore size of activated carbon has imposed serious problems relating to the rate of molecular transport through the pores and thus limited the application of the carbon as electrodes in electrochemical systems such as electric double

layer capacitors [42, 43]. Therefore, high surface area carbon materials containing regularly interconnected mesopores (>2 nm) are highly desirable for electric double layer capacitors. In fact, some compromise must be found in the meso/micro ratio as the micropores determine the high surface area on which ions are adsorbed and mesopores are essential for ion transportation [44].

The hydroformylation of olefins is one of the most important industrial processes exclusively relying on homogeneous catalysis [45]. The recovery of the homogeneous catalysts from high boiling hydroformylation products is still an unsolved problem [46]. Attempts were made to heterogenize the homogeneous catalysts to overcome this difficulty by immobilization of the metal complexes on a variety of organic/inorganic solid supports using different methods i.e. anchoring [47], tethering [48], encapsulation [49], and impregnation of the solid support with a liquid medium containing the catalyst i.e. supported liquid phase catalyst (SLPC) [50] and supported aqueous phase catalyst (SAPC) [51].

Carbon materials are attractive supports in heterogeneous catalytic processes because of their high surface area, stability at high temperatures etc. Active carbon exhibits suitable characteristics in carbonylation; it has been found to promote strong or multiple adsorption of CO and to inhibit dissociative CO adsorption [52]. Zhang et al. [53] studied low pressure hydroformylation of 1-hexene over active carbon supported noble metal catalysts, whereas the hydroformylation of long chain alkenes with activated carbon supported rhodium complex catalyst was studied by Disser et al. [54].

Here we discussed the synthesis of mesoporous silica material by a low cost method using hydroxy carboxylic acids as templates/pore forming agents and tetraethylorthosilicate and sodium silicate as silica source. Anchoring of a Co-salen complex on the amino functionalized mesoporous silicas is next carried out and the resulting catalysts i.e. Co-A-SST and Co-A-MS-(0.6) are used for olefin oxidation employing TBHP as the oxidant. Mesoporous carbon replicas are obtained via infiltration of sucrose inside the mesoporous silica samples. The mesoporous silica/carbon materials are characterized by various physico-chemical, spectroscopic and electroanalytical techniques. The electrochemical performance of the prepared mesoporous carbon has been studied for electrochemical double layer capacitance application. The applications of the mesoporous carbon as a support for preparation of novel supported rhodium complexes [HRhCO(TPPTS)$_3$] and the

use of the prepared catalysts i.e. Rh-SCT and Rh-MC-(0.6) for the hydroformylation reaction of alkenes are investigated.

Table 5.1. Specifications of Chemicals used:

| Reagent (Source) | Chemical composition/formula | Purity (%) |
|---|---|---|
| Tetraethylorthosilicate (TEOS) (Aldrich) | $(C_2H_5O)_4Si$ | 98 % |
| Sodium silicate solution (Loba Chemie Pvt. Ltd.) | $Na_2SiO_3$ | ~9.03 % $Na_2O$, ~ 28 % $SiO_2$ |
| Tartaric acid, (Loba Chemie Pvt. Ltd.) | $HO_2CCH(OH)CH(OH)CO_2H$ | 99 % |
| Malic acid, (Loba Chemie Pvt. Ltd.) | $HO_2CCH_2CH(OH)CO_2H$ | 99 % |
| Citric acid, (Loba Chemie Pvt. Ltd.) | $HOC(CO_2H)(CH_2CO_2H)_2$ | 99 % |
| Sucrose (Loba Chemie Pvt. Ltd.) | $C_{12}H_{22}O_{11}$ | 99 % |
| Ethanol (absolute) (S.D.Fine Chem. Ltd. India) | $CH_3CH_2OH$ | 99 % |
| Hydrochloric acid (Loba Chemie Pvt. Ltd.) | HCl | 35.4 % (sp. gr. 1.18) |
| Sulphuric acid (Loba Chemie Pvt. Ltd.) | $H_2SO_4$ | 98 % |
| Cobalt salen (Loba Chem India) | $CuC_{16}N_2O_2H_{13}$ | 99 % |
| Barium nitrate (Loba Chem India) | $Ba(NO_3)$ | 99 % |

| | | |
|---|---|---|
| Tetrahydrofuran (THF, Aldrich) | $C_4H_8O$ | 99 % |
| 3-Aminopropyltriethoxysilane 3-APTES (Aldrich) | $(C_2H_5O)_3Si(CH_2)3NH_2$ | 99 % |
| Toluene (Loba Chem.Pvt. Ltd.) | $C_6H_5CH_3$ | 99 % |
| Acetone (Loba Chem.Pvt. Ltd.) | $(CH_3)_2O$ | 99 % |
| tert-Butyl hydroperoxide (Aldrich) (TBHP) | $(CH_3)_3COOH$ | 5.0 M solution in decane |
| Acetonitrile (Loba Chem.Pvt. Ltd.) | $CH_3CN$ | 99 % |
| Styrene (Loba Chem.Pvt. Ltd.) | $C_6H_5CHCH_2$ | 99 % |
| Cyclohexene (Loba Chem.Pvt. Ltd.) | $C_6H_{10}$ | 99 % |
| 1-Decene (Loba Chem.Pvt. Ltd.) | $C_{10}H_{20}$ | 99 % |
| Activated microporous carbon (Aldrich) | carbon | 99 % |
| Rhodium chloride (Arora Matthey) | $RhCl_3.3H_2O$ (Rh 40 %) | 99 % |
| Triphenylphosphene (S.D. Fine Chem.) | $P(Ph)_3$ | 99 % |
| 1-Hexene (Loba Chem.Pvt. Ltd.) | $C_6H_{12}$ | 99 % |

**Synthesis of mesoporous carbon from mesoporous silica template, prepared using tetraethylorthosilicate (TEOS) as silica source**

## 5.2. EXPERIMENTAL

### 5.2.1. Synthesis of mesoporous silica using hydroxy carboxylic acid templates.

Mesoporous silica was prepared on the basis of reported procedure [27] with some modification. The molar composition of the gel was:

$$1.0 \text{ [TEOS]} : 0.01 \text{ [HCl]} : 4.0 \text{ [H}_2\text{O]} : 3.0 \text{ [EtOH]}.$$

Tetraethylorthosilicate in absolute ethanol was hydrolyzed using hydrochloric acid as a catalyst in deionized water at room temperature in the presence of an aqueous solution of hydroxy-carboxylic acid (0.45 g/ml for 50 wt % ) as the template. The hydroxy-carboxylic acids used as template or pore forming agent may be tartaric acid (T), malic acid (M) or citric acid (C). Slow hydrolysis in the presence of templates might play a role for some regularity in the mesophase formation.

The final gel was kept at room temperature for one month. The transparent monolithic disk obtained may be due to the aggregation/self assembly formation of the template and their hydrogen bonding interactions with the inorganic precursor playing an important role in directing the mesostrcture formation [22, 55]. This transparent, monolithic mesoporous silica disk containing template was then grind into fine powder and the template was removed by two methods: (I) soxhlet extraction using deionized water and (II) calcination at 550º C (0.5º C/min. in air) for 5-6 hours. The soxhlet-extracted samples were designated as SSA (i.e., soxhlet extracted mesoporous silica of respective hydroxy-carboxylic acids). These are, SST (tartaric acid templated silica), SSM (malic acid templated silica) and SSC (citric acid templated silica). For the calcined samples, the abbreviations are CSA (i.e. calcined mesoporous silica of respective hydroxy-carboxylic acids) i.e. CST, CSM and CSC as above respectively.

### 5.2.1.1. Catalyst preparation by Grafting of Co-salen complex.

#### 5.2.1.1.1. *Modification of SST with 3-aminopropyltriethoxysilane (3-APTES)*

In a typical experiment, SST (0.5g), prepared as above (section 5.2.1.) was dried by refluxing with dry toluene (8-10 h). The material was then filtered, washed with acetone and dried at room temperature under inert condition. The SST was then mixed with the solution

of 3-APTES in toluene (70.0 ml:0.22g) and refluxed for 12 h. This $NH_2$-SST was filtered and washed with acetone / dichloromethane and dried under vacuum.

### 5.2.1.1.2. Anchoring of Co-salen complex

A solution of 0.236 g of Co-salen in 20ml of toluene was stirred and slowly added to a suspension of 0.5 g of $NH_2$-SST in toluene (above prepared in 5.2.1.1.1.). It was refluxed for 12 h. A brown material was separated by filtration, washed with acetone, dried at ambient temperature and designated as Co-salen-$NH_2$-SST or Co-A-SST.

## 5.2.2. Synthesis of mesoporous carbon using above prepared (section 5.2.1.) mesoporous silica as template

In order to get the mesoporous carbon material, the mesoporous silica sample was impregnated with the aqueous solution of sucrose containing sulfuric acid, as reported earlier [12, 13]. In brief, 1 g of mesoporous silica material (SSA or CSA) was added to the solution obtained by dissolving 1 g of sucrose and 0.12 g of $H_2SO_4$ in 5 ml of $H_2O$. The mixture was placed in a drying oven for 6 h at 100º C and subsequently the oven temperature was raised to 160º C and maintained for 6 h. The sample was cooled and the heat treatment was repeated after the addition of 0.6 g of sucrose and 0.09 g of $H_2SO_4$ in 5 ml of $H_2O$. The resulting brownish black sample was then carbonized under $N_2$ atmosphere at 900º C (heating rate 2º C/min) for 5 h. The silica template was subsequently removed by dissolving the carbon-silica composite in the 50 % ethanolic aqueous solution of 1 M sodium hydroxide The mesoporous carbon samples thus produced were designated as SCA (carbon: using silica as template obtained on removing the respective hydroxy-carboxylic acids by soxhlet extraction) and CCA (carbon: using silica as template obtained on removing respective hydroxy-carboxylic acids by calcinations method).

### 5.2.2.1. Electrode fabrication using above prepared mesoporous carbon

A homogeneous mixture was obtained by thorough mixing of 75% of activated mesoporous carbon (~ 10 mg.) with 20 % graphite, and 5 % ethyl cellulose binder for 30 minutes. The mixture was pasted on to a stainless steel (SS) mesh current collector with the help of tetrahydrofuran (THF) as the solvent. The electrode was pressed at room temperature and then at a temperature of $155^{o}$ C under a pressure of 1400 kPa for two

minutes to obtain the electrode of the required quality. The electrode was then vacuum dried at a temperature of 110°C for 12 hours to remove the adsorbed solvent.

### 5.2.2.2. Preparation of carbon supported catalysts

The dispersed heterogenized catalyst was synthesized from a water-soluble metal complex prepared by known methods [56] and then precipitating it as its barium salt on a porous support. In a typical case, an aqueous solution of 20% $Ba(NO_3)_2$ (0.060 g) was added to 0.3 g of carbon support. The mixture was refluxed for 4-5 hours and evaporated to dryness to get barium nitrate impregnated carbon.

The carbon supported barium salt of rhodium triphenylphosphene trisulphonate complex $[HRhCO(TPPTS)_3]$ was prepared by taking 0.3 g of above prepared $Ba(NO_3)_2$ impregnated carbon in a small two-neck round bottom flask. An aqueous solution of $HRhCO(TPPTS)_3$ [48 mg] and TPPTS [60 mg] was added under constant stirring in a positive flow of argon. The stirring was continued for 4-5 hours. The mixture was filtered, the solid was washed 2-3 times with cold and hot water respectively followed by water and toluene for 12 hours each employing a soxhlet apparatus, to remove the unreacted catalyst. The solid was dried under vacuum (yield= 0.33 g). Two catalysts thus prepared from activated microporous carbon (C-1) and mesoporous carbon (SCT) were designated as Rh-C-1 and Rh-SCT respectively.

### 5.2.3.  Catalytic reaction

### 5.2.3.1. Mesoporous silica supported Co-A-SST for olefin oxidation

Catalytic reactions were carried out at 333 K in a round bottom flask fitted with a condenser. Olefins, acetonotrile and TBHP in decane were used without further purification. Olefins (5 mmol), TBHP as oxidant (5 mmol), acetonitrile as solvent (10 g) and catalyst (0.05 g) along with toluene as internal standard were introduced into a round bottom flask. The reactions were carried out with vigorous stirring. All the products were quantified at different intervals by gas chromatography: Chrompack CP900 (Carbowax 20M): 50m X 0.32 mm capillary column.

### 5.2.3.2. Mesoporous carbon supported Rh-SCT for hydroformylation

The reactions were carried out in a 50 ml high pressure stainless steel reactor manufactured by Amar Instruments, India. This reactor was fitted with a transducer for

monitoring the pressure, a temperature controler with automatic heating and cooling, as well as magnetic stirrer with variable speed. A reservoir filled with syngas was connected to the reactor via a constant pressure regulator. This enabled continuous feeding of the syngas from the reservoir, as per the consumption in the rector, while maintaining constant pressure in the rector. The reaction was monitored by observing the pressure drop in the reservoir. During the course of the reaction, the reactants and catalyst were charged into the rector and the contents were flushed with nitrogen and syngas. Following this the reactor and contents were heated to the desired temperature under low stirring [200 rpm]. Once the temperature was attained, the syngas [ CO : $H_2$, 1:1] was pressurized into the reactor as and when required. The reaction was started by increasing the agitation speed to 1400 rpm. The gas consumed by the reaction was made up by a continuous addition from the reservoir, wherein the pressure was monitored with time. During the course of the reaction, samples were withdrawn periodically and analyzed by GC for reactant and products. At the end of the reaction, the autoclave was cooled and final samples were taken for GC analysis (Agilent 6890, HP-5 capillary column 30 m) and confirmation of the mass balance.

## 5.3. CHARACTERIZATION

The surface area and pore volume were determined from $N_2$ adsorption isotherms using a Coulter (Omnisorb, 100 CX) instrument. Metal content of the catalysts were analyzed by atomic absorption spectroscopy (AAS Hitachi, Model 2800) as well as inductively coupled plasma with atomic emission spectra (ICP-AES) performed using Perkin-Elmer 1200 instrument. Fourier transform infrared (FT-IR) spectra of mesoporous silica was recorded with a Shimadzu FT-IR spectrometer (Model 8300). Mesoporous silica and carbon samples were characterized using X-ray diffraction method (Regaku X-ray diffractometer; model Dmax 2500 with Cu K$\alpha$ radiations of $\lambda$ =0.154 nm). Transmission electron image was obtained from JEOL 1200 EX microscope operated at 100 kV. The sample was prepared by dispersing the powder in isopropanol. Imaging was enabled by depositing few drops of the suspension on a carbon coated 400 mesh Cu grid. Thermal stability of the mesoporous silica/carbon samples was investigated using a computer controlled thermal analyzer (Setaram, France, Model TG-DTA 92). ^{31}P CP-MAS NMR spectra was obtained on a Bruker DRX 500 FT-NMR spectrometer at 202.64 MHz and 11.7 Tesla using 3 mm CP-MAS probe. The elemental compositions of the carbon samples were

determined by X-ray photoelectron spectroscopy (XPS) using a ESCA 3000 electron spectrometer (VG Scientific, UK with MgKα and AlKα twin anode). Electrochemical measurements were performed with a computer controlled Potentiostat/Galvanostat (autostat PGSTAT 100 with GPES software) using a three-electrode assembly. Activated mesoporous carbon electrode was used as the working electrode, platinum foil as the counter electrode, and Hg│Hg$_2$SO$_4$ as the reference electrode in 1M H$_2$SO$_4$. Cyclic voltammetric measurements were carried out in the voltage range of –1.1V to –0.2V in 1M H$_2$SO$_4$ at scan rates of 1, 5, 10mV/s.

### 5.3.1. Adsorption studies

N$_2$ adsorption-desorption isotherms of all the silica/carbon samples exhibit type IV isotherm with type H2 hysteresis loop which can be attributed to capillary condensation taking place in the mesoporous silica /carbon samples [27]. The representative tartaric acid templated mesoporous silica samples obtained by soxhlet extraction method i.e. SST and calcination method i.e. CST [Fig. 5.1. (A) and 5.2. (A)] and their carbon replicas i.e. SCT and CCT respectively [Fig. 5.1. (B) and 5.2. (B)] show type IV isotherms. The corresponding Barret Joyner Halenda (BJH) pore size distribution plots determined from the desorption branch of N$_2$ isotherm are shown as inset in the figures. The initial part of type IV isotherm at lower relative pressure (P/P$_0$ < 0.4) is mainly attributed to the monolayer-multilayer adsorption of mesopores [55]

It is observed that surface area, pore volume and pore diameter of all mesoporous silica samples obtained by soxhlet extraction i.e. SST, SSM and SSC are higher than the respective samples obtained by calcination method i.e. CST, CSM and CSC (Table 5.2.). This behavior may be attributed to the rearrangement of the silica wall due to dehydroxylation and thermal decomposition of corresponding hydroxy carboxylic acid, during slow heating up to 550$^o$ C. The BET surface area (700 m$^2$/g) and total pore volume (0.85 cm$^3$/g) of SST samples are comparable to those of the mesoporous materials prepared using surfactants as templates [57].

Fig. 5.1. $N_2$ adsorption-desorption isotherm and corresponding pore size distribution plots (insert) determined from the desorption branch of $N_2$ isotherm for the soxhlet extracted mesoporous silica sample (A) SST and its carbon replica (B) SCT.

Fig. 5.2. $N_2$ adsorption-desorption isotherms and corresponding pore size distribution plots (insert) determined from the desorption branch of $N_2$ isotherm for the calcined mesoporous silica sample (A) CST and its carbon replica (B) CCT.

All the mesoporous silica templated carbon samples show higher surface area and pore volume than the respective silica templates (Table 5.2.). This may be due to

contribution from the microporosity within the carbon walls and the extra porosity due to the incomplete replication process. Mesoporous carbon replica SCT shows higher surface area of 1027 m$^2$/g and pore volume of 1.0 cm$^3$/g than the respective mesoporous silica template SST. The average pore diameter of mesoporous carbon material is smaller than the diameter of respective mesoporous silica sample in the case of soxhlet extracted silica samples. Mesoporous silica SST shows an average pore diameter of 46 Å where as carbon replica SCT shows a pore diameter of 39 Å. In the case of mesoporous silica samples obtained by calcination method, we observed a decrease in the pore diameter compared to mesoporous silica samples obtained by soxhlet extraction method due to the contraction of the pore at the temperature of calcination. Also, the pore diameter of the calcined sample is smaller than that of the respective carbon replica. Mesoporous silica sample (CST) shows a pore diameter of 40 Å whereas carbon replica shows pore diameter of 43 Å. SCT and CCT possess average pore diameters of ~ 39 Å and 43 Å respectively. This difference in pore diameters may be attributed to difference in the wall thickness of the silica materials i.e. SST shows ~ 34 Å and CST ~ 37 Å (The wall thickness has been calculated by subtracting the pore diameter of the respective sample obtained by N$_2$-sorption from the unit cell parameter a$_0$ calculated using XRD spectrum by employing standard method.). In general, it is observed that the pore diameters are in the order: SCA< SSA and CCA > CSA. The pore diameters observed for the above-prepared mesoporous carbons are comparable to the carbon materials derived from MCM-48 [13], SBA-15 and MSU-H [19]. From the t-plot analysis with Harkins-Jura Equation (Table-5.2), the measured surface areas and pore volumes in the pure silica powder (SiO$_2$ – gel) are predominantly contributed by micropores. We observed a large pore diameter for mesoporous carbon than the corresponding silica wall thickness, which may be due to the shrinkage of carbon wall as reported by Jun et al. [13].

Co-salen grafted mesoporous silica support i.e. Co-A-SST shows a decrease in the surface area from 700 to 450 m$^2$/g, pore diameter from 46 to 32 Å and pore volume of 0.85 to 0.40 cc/g indicating that the pores of silica are occupied by metal complex. Rhodium complex impregnated catalyst Rh-SCT shows decrease in the surface area, pore volume and pore diameter as compared to parent mesoporous carbon SCT as shown in Table 5.2. This

indicates that the pores of SCT are occupied by the metal complex. On the other hand the activated microporous carbon C-1 did not show much change in the surface area after impregnation of metal complex i.e. Rh-C-1 (Table 5.2.). This is due to the microporous nature of C-1 (pore diameter ~ 18 Å) which may not be sufficient to accommodate the bulky metal complex. Fig. 5.3. shows the $N_2$-sorption isotherms of Rh-SCT and Rh-C-1 with the pore size distribution (inset).
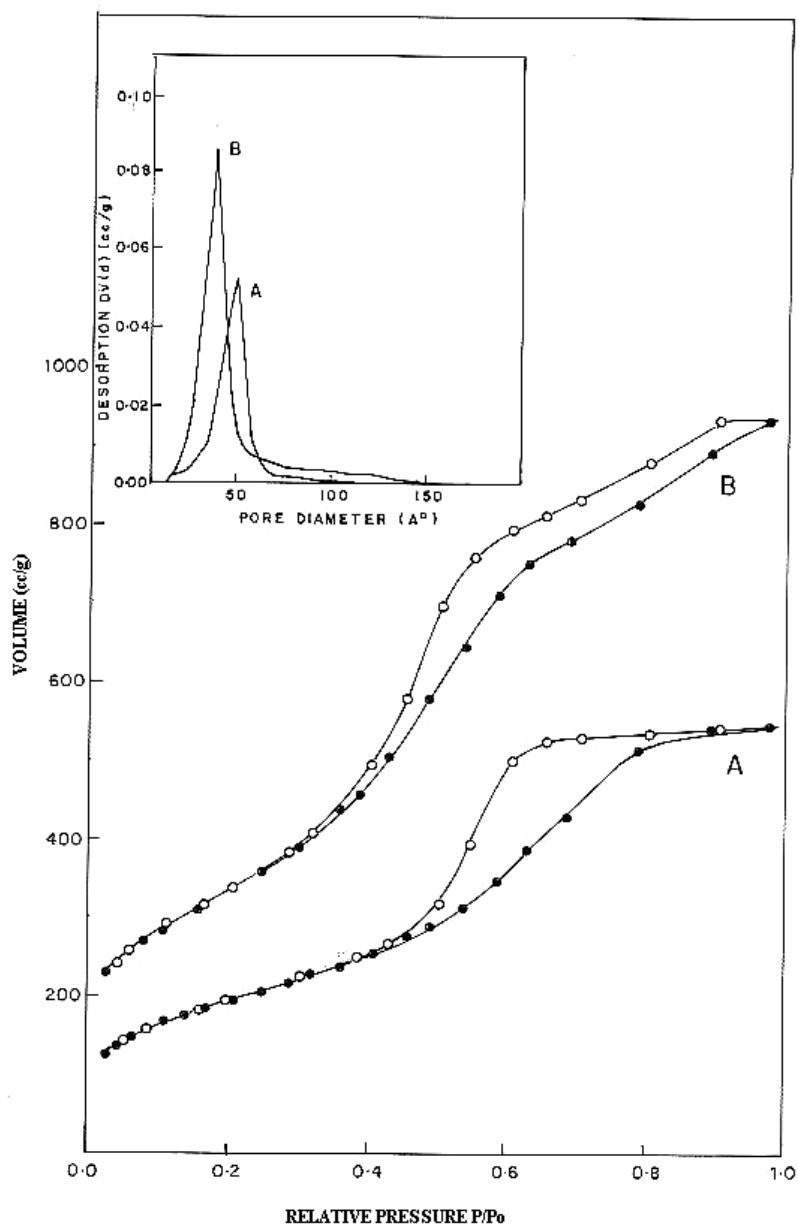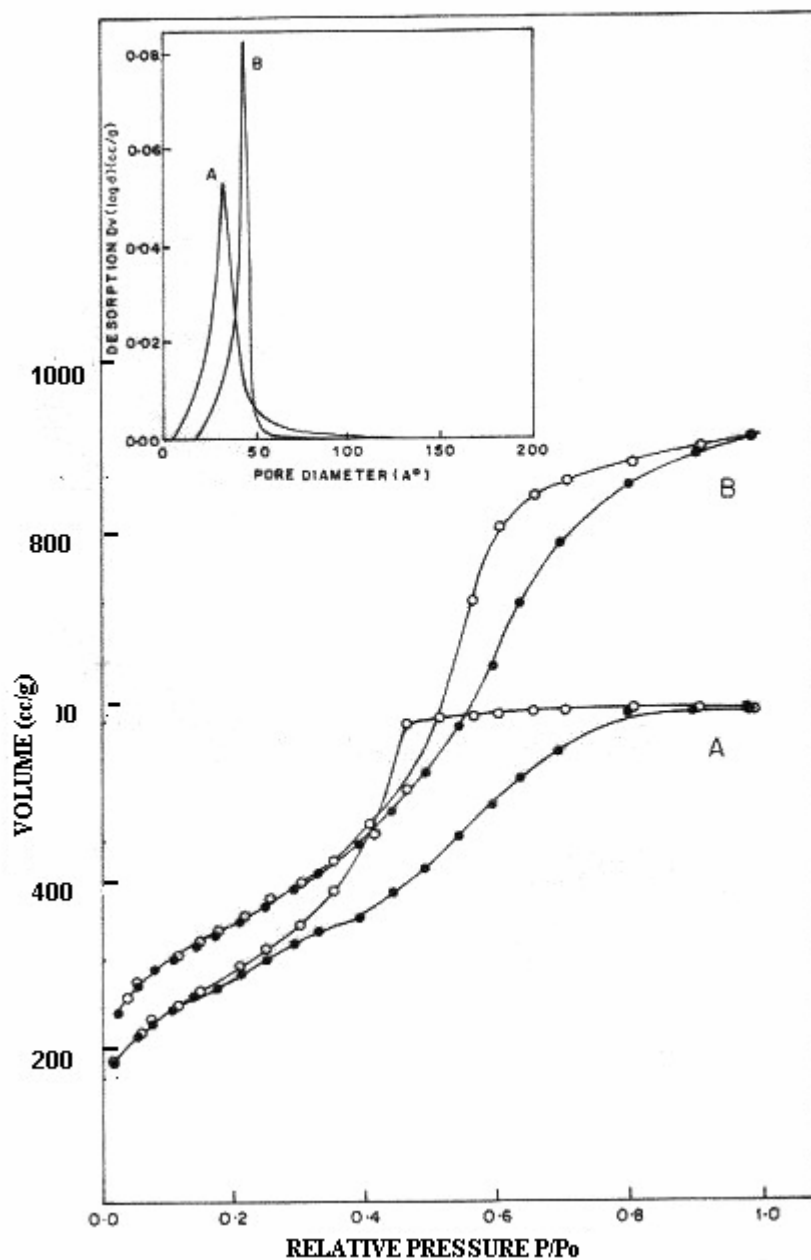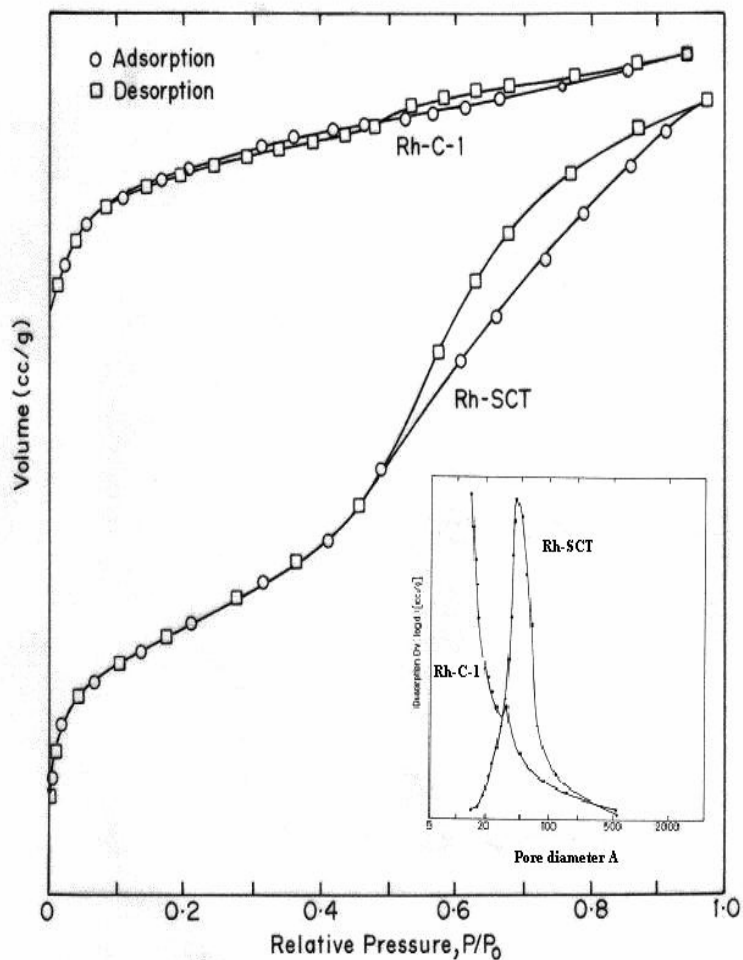


Fig. 5.3. $N_2$ adsorption-desorption isotherms and corresponding pore size distribution plots (insert) determined from the desorption branch of $N_2$ isotherm for Rh-SCT and Rh-C-1.

Table 5.2. Sorption properties of mesoporous silica templates, corresponding mesostructured carbon replicas, Co-salen immobilized SST and Rh-complex immobilized SCT catalysts.

| Sample[a] | Pore diameter BJH Å | $S_{BET}$ m$^2$/g | Total pore volume cm$^3$/g | micropore area m$^2$/g | Wall thickness Å |
|---|---|---|---|---|---|
| SiO$_2$-gel[b] | 28 | 325 | 0.16 | 285 | --- |
| SST | 46 | 700 | 0.85 | 24 | 34 |
| SSM | 40 | 879 | 0.84 | 22 | 32 |
| SSC | 50 | 727 | 0.93 | 56 | 35 |
| CST | 40 | 664 | 0.78 | 15 | 37 |
| CSM | 38 | 720 | 0.83 | 13 | 35 |
| CSC | 37 | 650 | 0.65 | 40 | 34 |
| SCT | 39 | 1027 | 1.00 | 125 | 33 |
| SCM | 35 | 1120 | 0.88 | 156 | 30 |
| SCC | 40 | 1068 | 1.19 | 134 | 34 |
| CCT | 43 | 1013 | 0.92 | 160 | 27 |
| CCM | 45 | 981 | 0.86 | 96 | 29 |
| CCC | 45 | 910 | 1.00 | 83 | 30 |
| Co-A-SST[c] | 32 | 450 | 0.40 | 21 | 34 |
| C-1[d] | 18 | 1142 | 0.54 | 1008 | --- |
| Rh-C-1[e] | 17 | 1124 | 0.51 | 994 | --- |
| Rh-SCT[e] | 32 | 390 | 0.80 | 33 | 33 |

[a] The first letter of the sample codes describes the template removing method, S- soxhlet extraction, C- calcination; the second letter denotes the materials S- mesoporous silica or C- mesoporous carbon; the third letter refers to the template used for building the unit, T- tartaric acid; M- malic acid; C- citric acid.

[b] Control sample: sol gel SiO$_2$ prepared without template. [c] Co-salen grafted on NH$_2$-SST i.e. A-SST; (microanalysis data: carbon – 16.7 %, nitrogen – 2.9 % and elemental analysis data; by AAS, Cobalt – 4.5 %,

[d] activated microporous carbon, [e] Rh-content is 0.37 % w/w by ICP analysis.

### 5.3.2. FTIR spectroscopy

Mesoporous silica materials have been prepared via sol-gel reactions of TEOS in the presence of tartaric, malic and citric acids as templates. Fig. 5.4. show the FTIR spectra of mesoporous silica samples prepared by (A) soxhlet extraction and (B) calcination method. All characteristic absorption bands due to asymmetric stretching mode (1088-1084 cm$^{-1}$) with shoulder at ~1200 cm$^{-1}$ and others at 960 cm$^{-1}$, 800 cm$^{-1}$, 730 cm$^{-1}$, 550 cm$^{-1}$ and 450 cm$^{-1}$ assigned to symmetric stretching and deformation mode are observed like other mesoporous silica materials [58]. On comparing the set of spectra (A) and (B) in Fig. 5.4., it has been observed that band intensity at 960 cm$^{-1}$ (due to coupled mode of Si-O stretching and O-H deformation) is lower for calcined samples than for the soxhlet extracted samples. This intensity reduction may be related to dehydroxylation and rearrangement of silica wall during calcination. All the mesoporous silica samples show the absence of strong absorption band at ~1700-1750 cm$^{-1}$ corresponding to the C=O stretching vibration of hydroxy-carboxylic acid indicate that all template molecules are completely removed (Fig. 5.5.) [27].



(A)
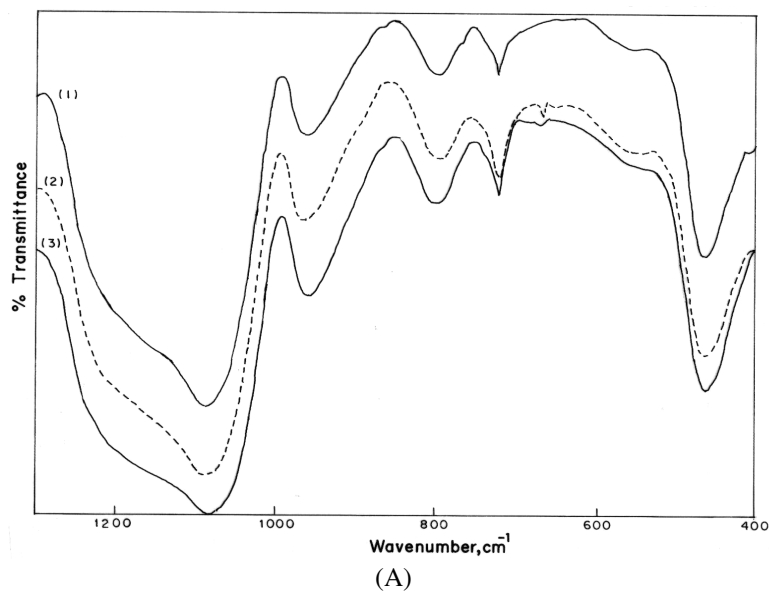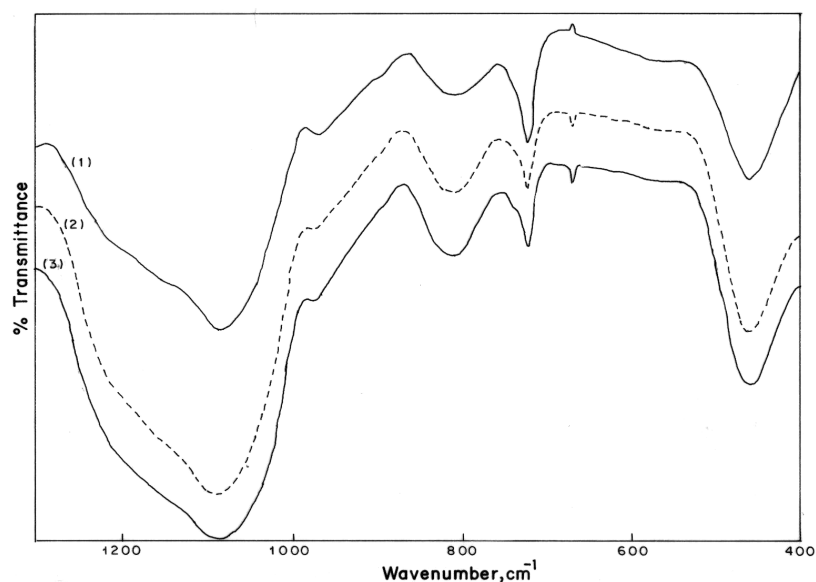
(B)

Fig. 5.4. FTIR spectra of (A) soxhlet extracted mesoporous silica materials; (1) SST, (2) SSM and (3) SSC, (B) calcined mesoporous silica; (1) CST, (2) CSM and (3) CSC.

The IR spectrum of NH$_2$-SST (recorded using fluorolube mull) in Fig. 5.5. shows bands in the region of 3000-2800 cm$^{-1}$ assigned to >CH$_2$ groups indicative of the modification of the wall of mesoporous silica material by aminoporopyl group. The bands at 3365 and 3392 cm$^{-1}$ superimposed on the broad band in the region 3600 to 2800 cm$^{-1}$ can be assigned to amino stretching frequencies. However, the broad nature of the band may be due to hydroxyl groups on the silica walls, hydrogen bonded to the amino group and adsorbed moisture. IR spectrum of Co-A-SST shows a broad band at ~ 3300 cm$^{-1}$ assigned to >NH$_2^+$ group due to co-ordination to the metal atom.
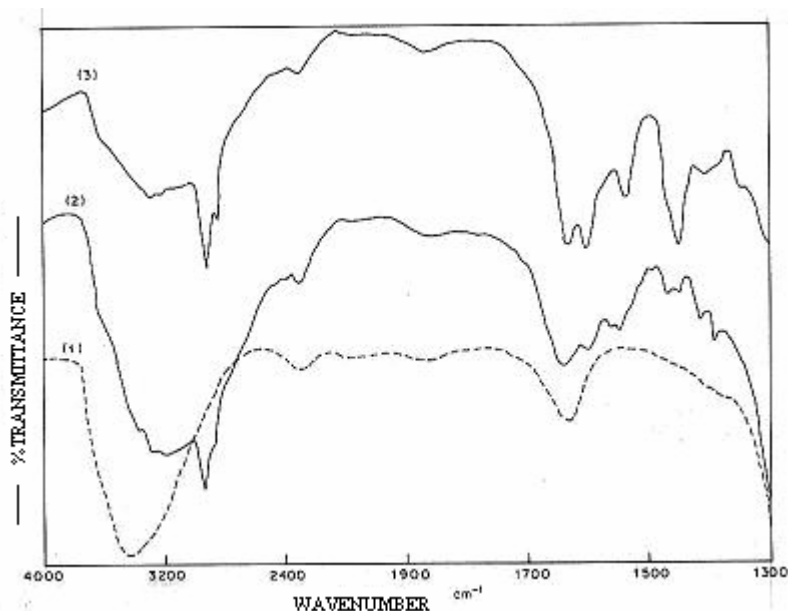
Fig. 5.5. FTIR spectra of (1) SST, (2) $NH_2$-SST and (3) Co-A-SST.

### 5.3.3. X-ray diffraction

The representative low angle XRD patterns of mesoporous silica prepared using soxhlet extraction method (a) SST and corresponding mesoporous carbon (b) SCT are shown in Fig.5.6. The XRD pattern of mesoporous silica SST, shows a broad diffraction peak (100 reflection) centered at $2\theta = 1.1^o$ suggesting a short range ordered mesoporosity corresponding to d spacing of 80 Å calculated from Bragg's equation. We observe a slight shift in the peak positions for the corresponding mesoporous carbon material and the prominent peak at 100 reflection is shifted to a higher $2\theta$ value of $1.2^o$ with a d-spacing of 73 Å. The small decrease in the d-spacing of mesoporous carbon samples is due to shrinkage of the carbon framework during carbonization and removal of silica template [12].

143
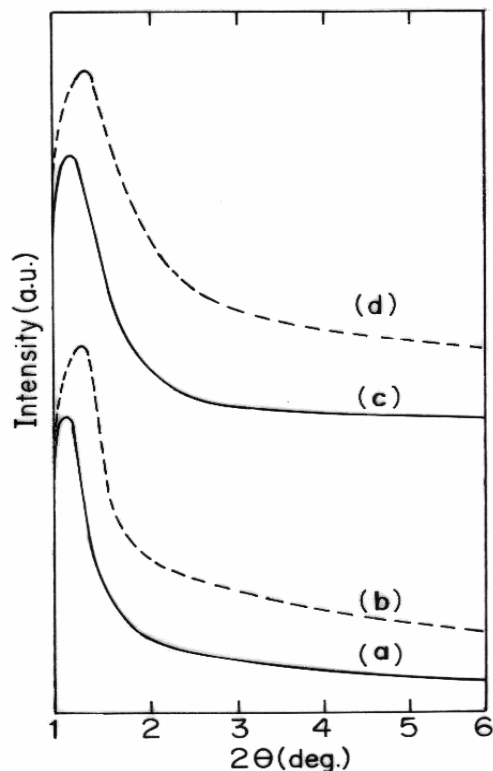
Fig. 5.6. XRD pattern of (a) SST, (b) SCT, (c) CST and (d) CCT.

Fig. 5.6 also shows the low angle XRD patterns of mesoporous silica prepared by calcination method (C) CST and the corresponding mesoporous carbon replica (D) CCT. Here also we observed the broad diffraction patterns for both the silica and carbon samples. CST shows the peak at $2\theta = 1.15^{o}$ (100 reflection) with the d-spacing of 76 Å. The mesoporous carbon sample shows slight shift in the peak position at $2\theta = 1.25^{o}$ with the d-spacing of 70 Å. The XRD pattern of mesoporous carbon SCT, in the high angle region (10-$90^{o}$) shows the absence of peaks characteristic of graphitized carbon ($2\theta = 26^{o}$ and $44^{o}$) assigned to (002) and (10) diffraction (Fig. 5.7.) [59, 68].

The XRD patterns of mesoporous silica supported Co-salen complex grafted catalyst Co-A-SST and mesoporous carbon supported HRhCO(TPPTS)$_3$ complex grafted catalyst Rh-SCT are similar to the parent mesoporous silica SST and mesoporous carbon SCT respectively at low angle. This indicates that the structure of SST and SCT is intact after immobilization of Co-salen and HRhCO(TPPTS)$_3$ complex. The XRD patterns at high angle

144

for both the catalysts show absence of peaks for cobalt-salen and rhodium, confirming the encapsulation of the metal complex in the channels (Fig. not shown).
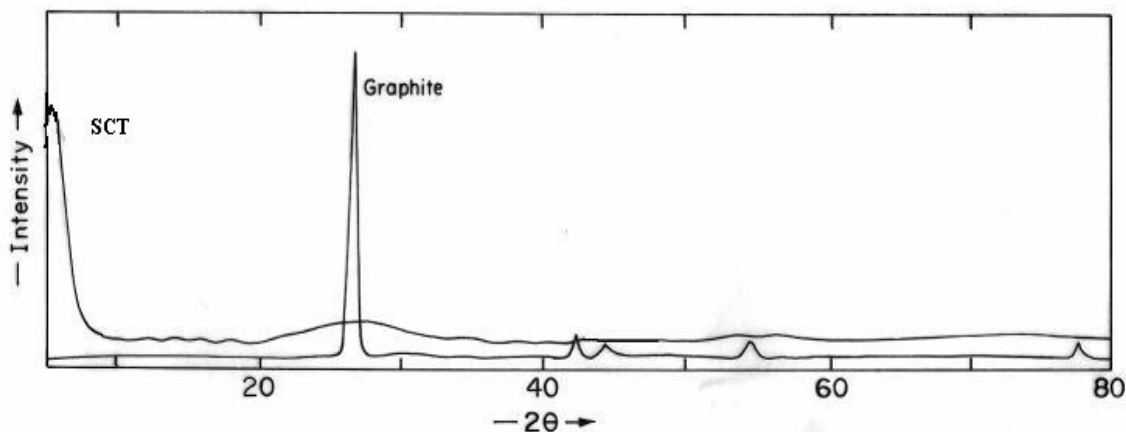


Fig. 5.7. XRD pattern of mesoporous carbon SCT and graphite.

## 5.3.4. Transmission electron microscopy

TEM images of mesoporous silica material obtained by (A) soxhlet extraction method (SST) and (B) calcination method (CST) and their respective carbon replicas (C) SCT and (D) CCT are shown in Fig. 5.8. Aggregation of the non-surfactant template molecules and the hydrogen bonding between the aggregated templates and the inorganic precursors in solution during the gelation may direct mesophase formation [60]. In the present study, these samples show wormhole like channel array together with regions of regular ordering of the pores in parallel arrangements to the channels as seen from TEM images similar to MSU-Si [61]. This may be due to the slow hydrolysis of TEOS at room temperature in the presence of templates. Whereas Pang et al. [27] reported the formation of mesoporous silica with only wormhole channels.

<div align="center">(A)</div>

<div align="center">(B)</div>

<div align="center">(C)</div>

<div align="center">(D)</div>
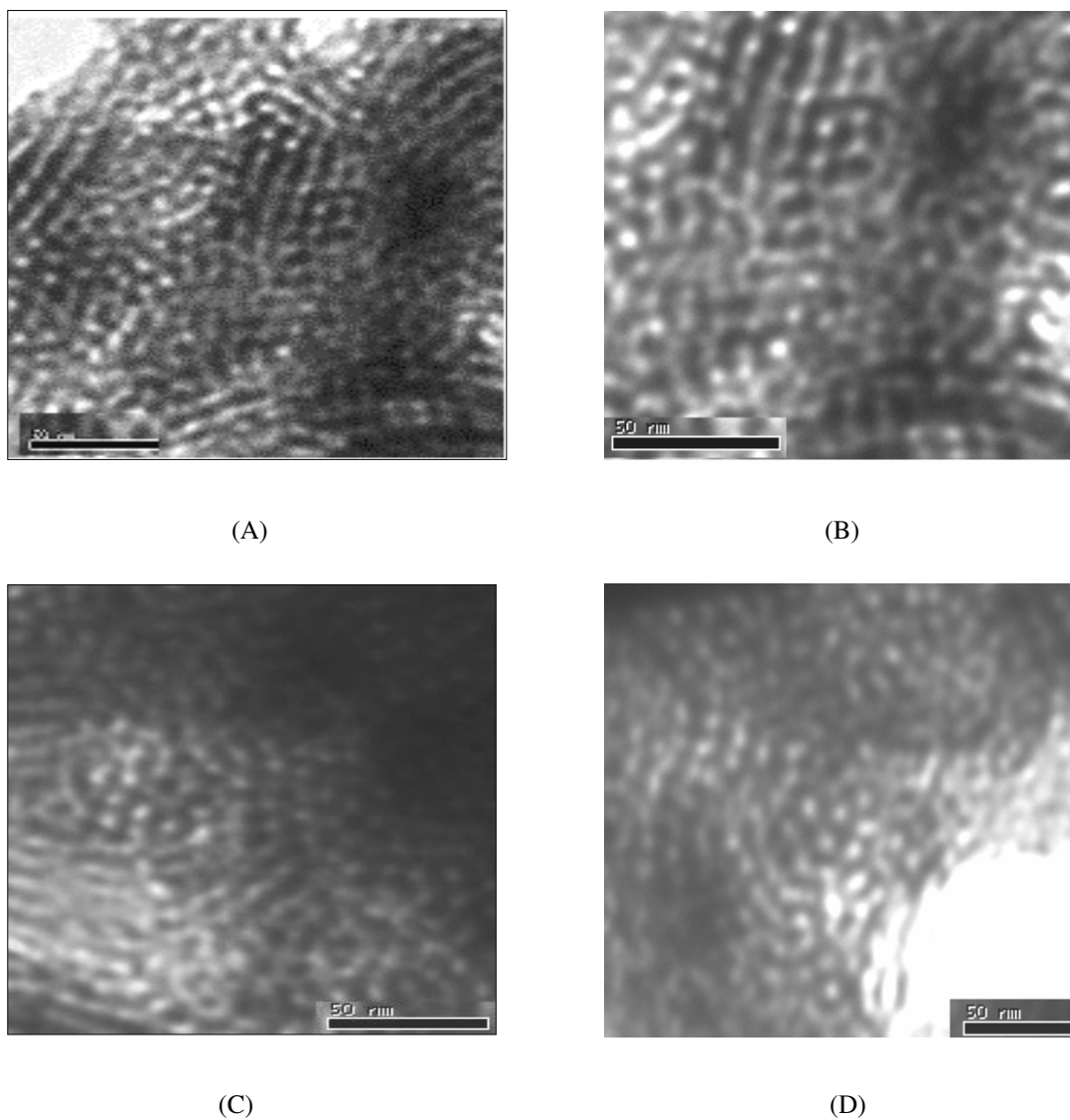
Fig. 5.8. TEM images of mesoporous silica samples (A) SST, (B) CST and respective mesoporous carbon samples (C) SCT, (D) CCT.

## 5.3.5. Thermal analysis

Table 5.3. shows the TGA data of various mesoporous silica/carbon samples. Mesoporous silica samples show weight loss in the temperature range of 700-850°C. All the silica samples of SSA series (soxhlet extracted silica prepared using respective hydroxy-carboxylic acid) show slightly lower stability (decomposition temperature ~ 700-750° C; weight loss up to 25 %) as compared to mesoporous silica samples obtained by calcination

method i.e. CSA series (calcined silica prepared using respective hydroxy-carboxylic acid) (decomposition temperature ~ 800-850$^o$ C; weight loss up to 23 %). This may be due to the difference in wall thickness of the samples (see Table 5.2.). The mesoporous carbon replicas show significant weight loss in the temperature range of 500 to 600$^o$ C (weight loss ~ 98 %) due to the combustion and decomposition of carbon to carbon dioxide. This temperature is much lower than the temperature reported for nanotubes and other graphitized carbons [59] which provides a confirmation of non-graphitized nature of all the mesoporous carbon samples prepared by us. The mesoporous carbon samples prepared by using calcined mesoporous silica as templates show stability between 500 to 550$^o$C which is lower as compared to the mesoporous carbon samples prepared by using soxhlet extracted mesoporous silica as templates. This is because mesoporous carbon samples of SCA series (mesoporous carbon prepared using soxhlet extracted mesoporous silica) are having higher wall thickness as compared to mesoporous carbons of CCA series ( mesoporous carbon prepared using calcined mesoporous silica; see Table 5.2.).

Table 5.3. Thermogravimetric data of mesoporous silica/carbon.

| mesoporous silica | $T_{max}$ $^o$C | mesoporous carbon | $T_{max}$ $^o$C |
|---|---|---|---|
| SST | ~700$^o$ C | SCT | ~550$^o$ C |
| SSM | ~ 750$^o$ C | SCM | ~600$^o$C |
| SSC | ~ 750$^o$ C | SCC | ~600$^O$C |
| CST | ~800$^o$ C | CCT | ~500$^o$C |
| CSM | ~850$^o$ C | CCM | ~500$^o$C |
| CSC | ~ 800$^o$ C | CCC | ~550$^o$C |

## 5.3.6. $^{31}$P CP-MAS NMR spectra of HRh(CO)[TPPTS]$_3$ along with Rh-SCT

$^{31}$P CP-MAS (cross polarized, magic angle spinning) NMR spectra of HRh(CO)[TPPTS]$_3$ complex and Rh impregnated catalyst were obtained on a Bruker DRX 500 FT-NMR spectrometer at 202.64 MHz and 11.7 Tesla using 3 mm CP-MAS probe. The chemical shifts were referred to H$_3$PO$_4$ at 0 ppm and the spectra were collected at a spectral width of 20 kHz, with a flip angle of 45$^\circ$, 6000 real data points and 5 second relaxation delay.
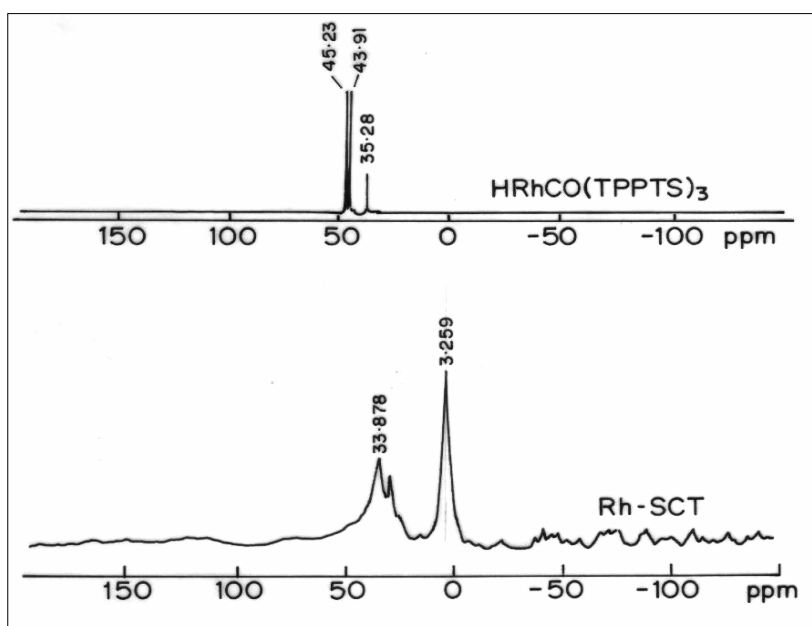


Fig. 5.9. $^{31}$P MAS NMR spectra of HRhCO(TPPTS)$_3$ and Rh-SCT.

Fig. 5.9. show solid state $^{31}$P MAS NMR spectra of HRh(CO)[TPPTS]$_3$ and Rh-SCT. Solid-state $^{31}$P NMR of Rh-SCT showed a signal at 3.26 δ and a multiplet at 33.87 δ. The signal at 3.26 δ $_{3/2}$ is due to free TPPTS-B as an excess of TPPTS is used in the preparation of the supported complex.The multiplet at 33.87 δ may arise from the mixing of the signals from the coordinated phosphine and phosphine oxide. The shift in the signals as compared to HRhCO(TPPTS)$_3$ could be a result of interaction of the catalyst with support.

**Synthesis of mesoporous carbon from mesoporous silica as template prepared using sodium silicate as silica source**

## 5.4. EXPERIMENTAL

### 5.4.1. Synthesis of mesoporous silica using hydroxy carboxylic acid templates

Mesoporous silica was prepared by using the inexpensive silica source, Na-silicate and tartaric acid as templating agent via sol-gel method [64] with the following molar composition:

$$[SiO_2] : 0.4\text{-}1.0 \ [TA] : 0.6 \ [HCl] : 36.0 \ [H_2O]$$

In one of the examples, an aqueous solution of 7.5 g tartaric acid was mixed with 6.14 g of HCl and kept stirring at room temperature. 21.43 g of Na-silicate was added slowly to the above mixture. On complete addition the mixture was allowed to stir vigorously for 2 h (pH of the solution was < 2) and then it was transferred to a stainless steel autoclave having teflon lining and heated at 110° C. The kinetics of mesophase formation was carried out at different time intervals (12, 24, 36 and 48 h). At the end the gel was filtered, washed with ethanol followed by deionized water until free from acid and then dried at 110$^{\text{o}}$ C.

In other examples, the material of the same composition was reacted at different temperatures i.e. 50, 110 and 150° C for 24 h. Here, we also carried out the preparation of mesoporous silica using different molar ratios of TA/SiO$_2$ keeping HCl/SiO$_2$ and H$_2$O/SiO$_2$ constant.

### 5.4.1.1. Catalyst preparation by Grafting of Co-salen complex

Surface modification of MS-(0.6) silica (Table 5.6) using 3-APTES [i.e. NH$_2$-MS-(0.6)] followed by anchoring of Co-salen complex with organic spacer has been done according to the procedure mentioned in section 5.2.1.1. The catalyst prepared is denoted as [Co-A-MS-(0.6)].

### 5.4.2. Synthesis of mesoporous carbon

Mesoporous carbon material was prepared by using the above prepared mesoporous silica material (section 5.4.1.) as template. The template was impregnated with the aqueous solution of sucrose containing catalytic amount of sulfuric acid as reported earlier [13, 19]. In brief, 1 g of mesoporous silica material was added to the solution of 1 g of sucrose and 0.12 g of $H_2SO_4$ in 5 ml of $H_2O$. The mixture was placed in a drying oven for 6 h at 100º C and subsequently the oven temperature was raised to 160º C and maintained for 6 h. The sample was cooled and the heat treatment was repeated after the addition of 0.6 g of sucrose and 0.09 g of $H_2SO_4$ in 5 ml of $H_2O$. The resulting brownish black sample was then carbonized under $N_2$ atmosphere at 900º C (heating rate 2º C/min) for 5 h. The silica template was subsequently removed by dissolving the carbon-silica composite in the 50 % ethanolic aqueous solution of 1 M sodium hydroxide.

### 5.4.2.1. Electrode fabrication

A homogeneous mixture was obtained by mixing 75% of activated mesoporous carbon (~ 8 mg) with 20% graphite, and 5% ethyl cellulose binder for 30 minutes. The mixture was pasted on to a stainless steel (SS) mesh current collector with the help of tetrahydrofuran as the solvent. The electrode was pressed at room temperature and then at a temperature of $155^o$ C under a pressure of 1400 kPa for two minutes to obtain the electrode of the required quality. The electrode was then dried under vacuum at a temperature of $110^o$ C for 12 h to remove the adsorbed solvent.

### 5.4.2.2. Preparation of carbon supported catalysts

The precipitation of barium salt $Ba(NO_3)_2$ on mesoporous carbon support MC-(0.6) (Table 5.7.) followed by impregnation of HRhCO[TPPTS]$_3$ complex was done according to the procedure mentioned earlier in section 5.2.2.2. The catalyst prepared is denoted as Rh-MC-(0.6).

### 5.4.3. Catalytic reactions

Oxidation of olefins using the mesoporous silica supported catalyst i.e. Co-A MS-(0.6) and hydroformylation of n-alkenes using the mesoporous carbon supported catalyst i.e. Rh-MC-(0.6) was done according to the procedure mentioned in the section 5.2.3. The reaction products were analyzed by gas chromatography.

### 5.5. CHARACTERIZATION

Surface area and pore volume were determined from $N_2$ adsorption isotherms using a Coulter (Omnisorb, 100 CX) instrument. Fourier transform infrared (FT-IR) spectra of mesoporous silica were recorded with a Shimadzu FT-IR spectrometer (Model 8300). Mesoporous silica samples and mesoporous carbon replicas were characterized using X-ray diffraction method (Rigaku X-ray diffractometer; model Dmax 2500 with CuKα radiations of λ =0.154 nm). Transmission electron images of silica and carbon were obtained from a JEOL 1200 EX microscope operated at 100 kV. The sample was prepared by dispersing the powder in isopropanol. Depositing few drops of suspension on a carbon coated 400 mesh Cu grid enabled imaging. The substrates to be deposited were first cleaned by organic solvents and then rinsed with double distilled water. Thermal stability of the mesoporous silica/carbon samples where carried out using computer controlled thermal analyzer (Setaram, France, Model TG-DTA 92). The elemental composition of the carbon samples was determined by X-ray photoelectron spectroscopy (XPS) using an ESCA 3000 electron spectrometer (VG Scientific, UK with MgKα and AlKα twin anode). Electrochemical measurements were performed with a computer controlled Potentiostat/Galvanostat (autostat PGSTAT 100 with GPES software) using a three-electrode assembly. Activated mesoporous carbon electrode was used as the working electrode, platinum foil as the counter electrode, and Hg│$Hg_2SO_4$ as the reference electrode in 1M $H_2SO_4$. Cyclic voltammetric measurements were carried out in the voltage range of –1.1V to –0.2V in 1M $H_2SO_4$ at scan rates of 1, 5, 10mV/s.

### 5.5.1. N$_2$-sorption study for mesoporous silica samples

### 5.5.1.1. Effect of synthesis time

Mesoporous silica materials were prepared hydrothermally at 110$^{\circ}$ C by varying reaction time i.e.12, 24, 36 and 48 h. The molar composition of the synthesis gel was:

$$[SiO_2] : 0.5 [TA] : 0.6 [HCl] : 36 [H_2O]$$
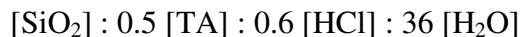
Fig. 5.10. A and B shows the N$_2$-adsorption-desorption isotherms and pore size distributions (from desorption branch using BJH method) respectively of samples prepared at different reaction times i.e. (a) MS-(12), (b) MS-(24), (c) MS-(36) and (d) MS-(48) wherein the values in the bracket indicate the period (in hour) of material synthesis.



(A)                                                                           (B)

Fig. 5.10. (A) N$_2$-adsorption-desorption isotherms and (B) pore size distributions of mesoporous silica samples prepared at the different time intervals (a) MS-(12), (b) MS-(24), (c) MS-(36) and (d) MS-(48).

The sample MS-(12) shows type II isotherm [Fig. 5.10. A (a)] with a surface area of 347 $m^2/g$ (micropore area ~ 300 $m^2/g$) and broad pore size distribution indicative of insufficient period for the phase formation (Table 5.4.) where as the sample prepared in 24 h [Fig. 5.10. A (b)], shows a type IV isotherm with well defined step in adsorption-desorption isotherm between the partial pressure of 0.2-0.4 $P/P_0$ due to the monolayer multilayer adsorption of mesopores. The type H2 hysteresis loop between the relative pressure of 0.45-0.80 $P/P_0$ likely to be due to the capillary condensation-taking place in mesopores [65]. This sample shows total surface area of 914 $m^2/g$ with very narrow pore size distribution and pore diameter ~ 56 Å. For the reaction time of 36 h, there is decrease in surface area and pore volume but an increase in pore diameter is observed as shown in Table 5.4. It is observed that the position of $P/P_0$ is shifted to higher relative pressure with broad pore size distribution as the reaction time increases [66]. On further increase in the reaction time up to 48 h [Fig. 5.10. A (d)], surface area of the sample decreases to 586 $m^2/g$ and shows broad pore size distribution. This is due to the formation of interparticle pores at higher reaction time. This observation confirms that, 24 h is the optimum time of product formation for the given conditions which gives material with a large surface area and narrow pore size distribution.

Table 5.4. Sorption study of mesoporous silica samples at different times of material synthesis.

| Sample | surface area (m²/g) | pore dia. (Å) | pore volume (cc/g) | micropore area (m²/g) |
|---|---|---|---|---|
| MS-(12) | 347 | 27.2 | 0.60 | 300 |
| MS-(24) | 914 | 56.0 | 1.00 | 84.5 |
| MS-(36) | 700 | 60.0 | 0.94 | 72.6 |
| MS-(48) | 586 | 68.0 | 0.85 | 56.0 |

### 5.5.1.2. Effect of temperature

Keeping the molar composition same as in 5.5.1.1. and synthesis time of 24 h, the reaction temperature is varied. The products are labeled as (a) MS-(50), (b) MS-(110) and (c) MS-(150) with the value in the bracket indicating the temperature of material formation in degree centigrade.
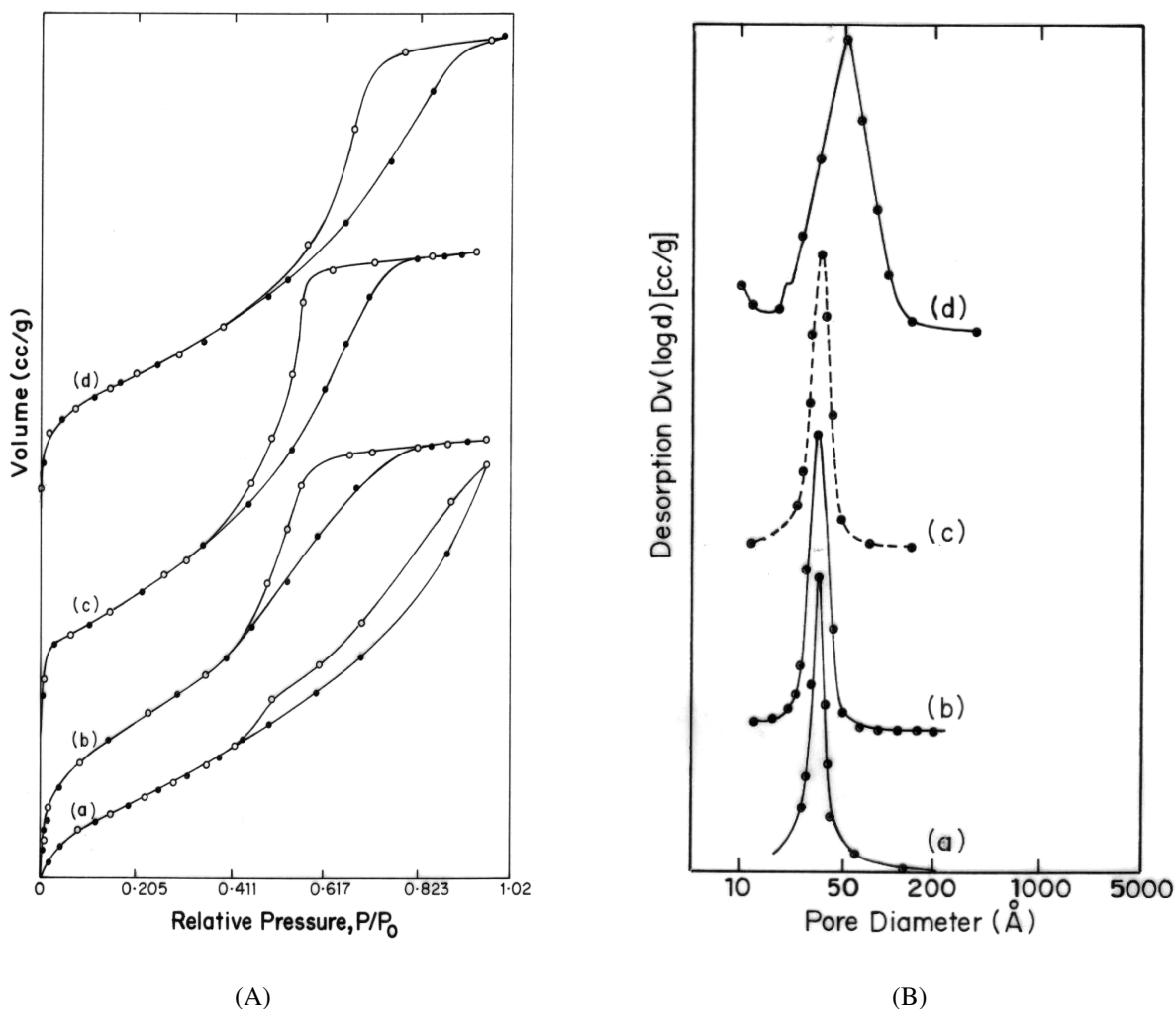


Fig. 5.11. (A) $N_2$-adsorption-desorption isotherms and (B) pore size distributions of mesoporous silica samples prepared at the different temperatures (a) MS-(50), (b) MS-(110) and (c) MS-(150).

The type IV isotherm of MS-(50) sample with broad hysteresis loop between 0.40-0.85 P/P$_0$ is indicative of disordered channel arrangement of the sample. This is reflected in

154

broad pore size distribution from micropore to mesopore range as shown in Fig. 5.11. B. (a). The sample possess a surface area of 587 $m^2$/g (micropore area 172 $m^2$/g) with the pore volume of 0.50 cc/g and pore diameter of 34 Å (Table 5.5.). The rate of condensation between silica and the template is very low at 50$^o$ C. With an increase in the temperature (110$^o$C), the rate of condensation increases and sample MS-(110) shows type IV isotherm with steep increase in the adsorption at low pressure followed by a well defined adsorption-desorption step in isotherm between 0.45 to 0.8 $P/P_0$ due to capillary condensation inside the mesopores [Fig. 5.11. A (b)]. This sample shows the surface area of 914 $m^2$/g with the pore volume of 1.0 cc/g and a pore diameter of 56 Å as shown in Table 5.4. for MS-(24). For the sample prepared at 150$^o$ C, i.e. MS-(150), position of $P/P_0$ shifted to higher relative pressure i.e. in the range of 0.55-0.80. Hence it is observed that at higher temperature, the rate of condensation increases and the polarity at the interface decreases which gives rise to the decrease in the hydrogen bonding interaction at the silica –surfactant interface. This increases the surfactant packing parameter which gives rise to decrease in micelle curvature, resulting in increase in pore size [67]. Thus total surface area decreased to 759 $m^2$/g with pore diameter of 65 Å and the pore volume 1.3 cc/g (Table 5.5.)

Table 5.5. Sorption study of mesoporous silica samples at different temperature of material synthesis.

| Sample | surface area ($m^2$/g) | pore dia. (Å) | pore volume (cc/g) | micropore area ($m^2$/g) |
|--------|------------|-----------|-------------|---------------|
| MS-(50) | 587 | 34 | 0.50 | 172 |
| MS-(110) | 914 | 56 | 1.00 | 84.5 |
| MS-(150) | 759 | 65 | 1.3 | 60.6 |

**5.5.1.3. Effect of template concentration**

A set of mesoporous silica samples were prepared at optimized temperature of $110^{o}$ C and reaction time of 24 h with different molar ratios of $TA/SiO_2$ keeping $HCl/SiO_2$ and $H_2O/SiO_2$ ratios constant. Fig. 5.12. A and B show nitrogen adsorption desorption isotherm and pore size distribution of these mesoporous silica samples having $TA/SiO_2$ ratios from 0.4-1.0 i.e. (a) MS-(0.4) to (d) MS-(1.0) wherein the value in the bracket indicates the molar ratio of $TA/SiO_2$. All samples exhibit type IV isotherm with steep increase in the adsorption desorption curve ($P/P_0 < 0.4$) due to monolayer, multilayer adsorption in the mesopores and type H2 hysteresis loop at higher pressure (0.45-0.85 $P/P_0$) corresponds to pore filling by capillary condensation.



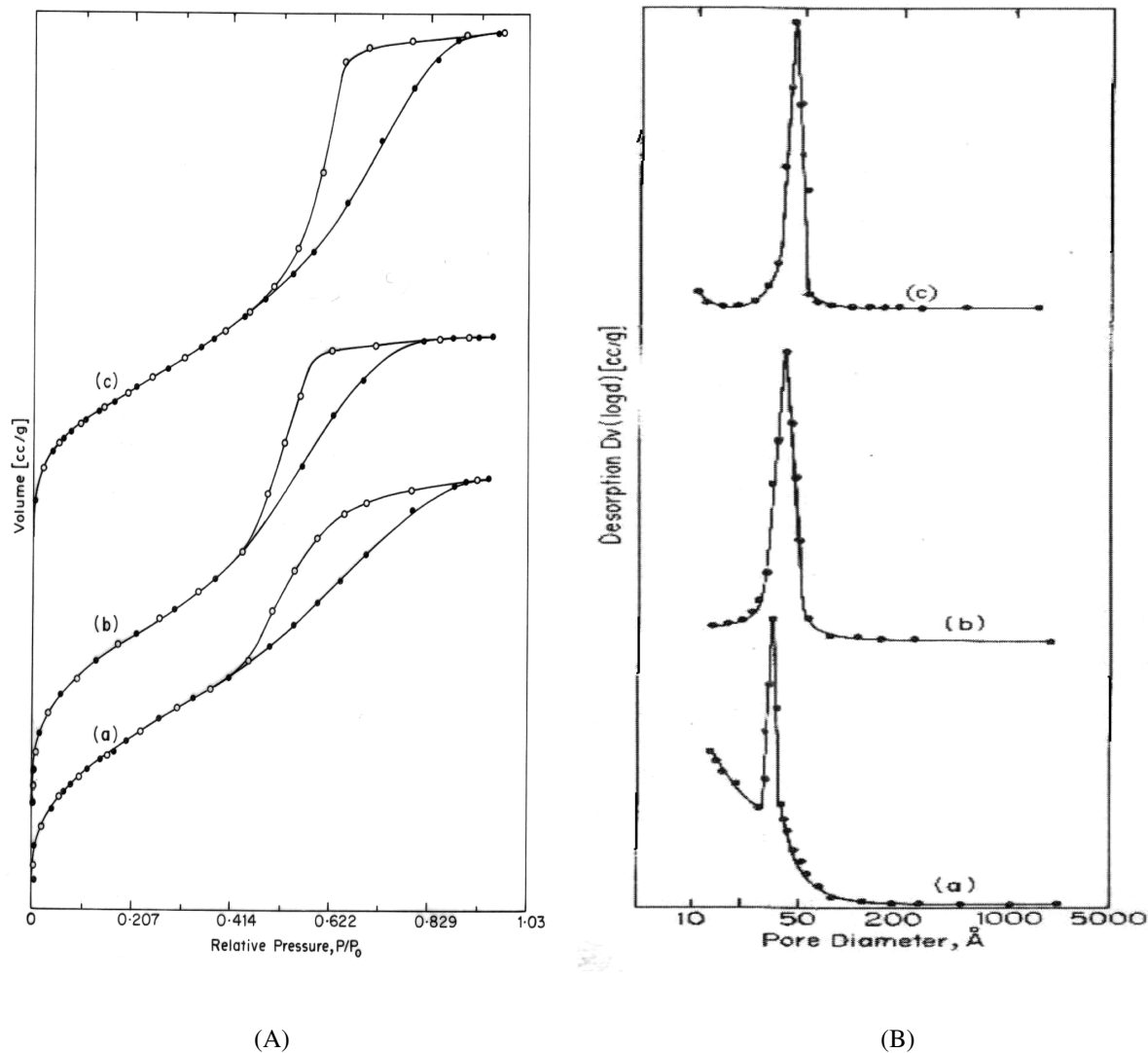(A)                                                                 (B)
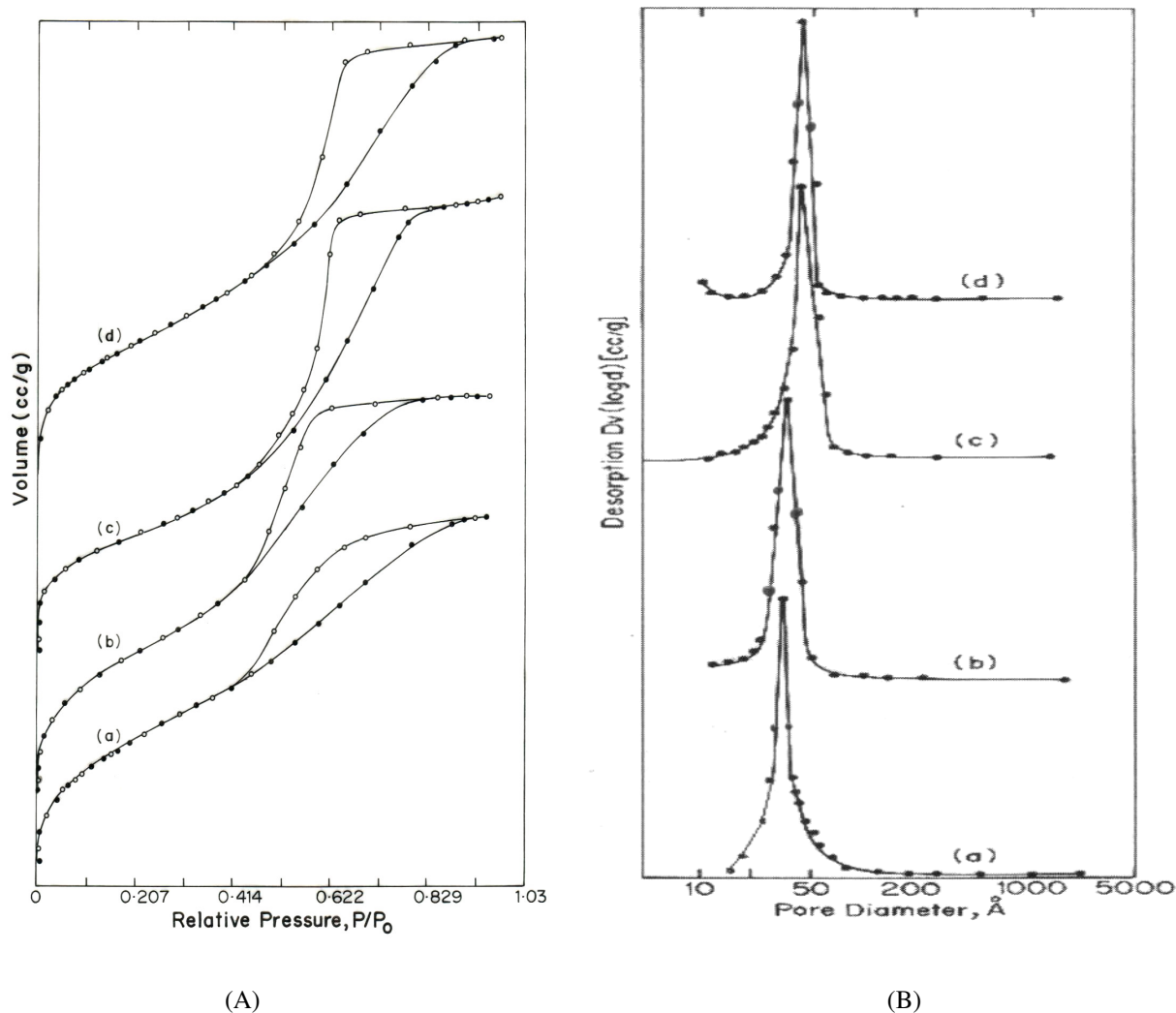
Fig. 5.12. (A) $N_2$-adsorption-desorption isotherms and (B) pore size distributions of mesoporous silica samples prepared at different molar ratios of $TA/SiO_2$ (a) MS-(0.4), (b) MS-(0.6), (c) MS-(0.8) and (d) MS-(1.0).

Presence of a hysteresis loop in the broad range of relative pressure (0.45 to 0.85 $P/P_0$) for MS-(0.4) sample suggests a broad pore size distribution [Fig. 5.12. A (a) and B (a)]. With the increase of $TA/SiO_2$ ratio from 0.4 to 1.0 (Table 5.6.), the micropore contribution shows decrease (expressed as micropore area) whiles the pore volume and pore diameter show increase. However, $S_{BET}$ shows maximum at $TA/SiO_2 = 0.6$. It is also observed that, there is shift to higher relative pressure for well-defined step in desorption branch of the isotherm as the template concentration increases from 0.4 to 1.0.

It is observed that for $TA/SiO_2$ molar ratio of 0.4, the molar ratio of $TA/H_2O$ also decreases (i.e. 0.01) and therefore in the very dilute system, the assembly formation takes longer time and hence the sample with higher percentage of micropore area is observed (~ 28.0 %). With the increase in the molar ratio of $TA/H_2O$ to 0.027, [i.e. MS-(1.0)] mesoporous silica with relatively higher pore diameter and less contribution from micropores (~ 4 %) is observed. It is well known that addition of inorganic salts can increase the aggregate number of the micelles which enhance the diameter of the micell [36]. In the present case, sodium silicate is believed to act as both a silica source and inorganic salt in the formation of mesoporous silica resulting in to large pore diameters. Hence in the above study, pore diameter of mesoporous silica using $Na_2SiO_3$ is higher than those of mesoporous silica using TEOS as silica source [27].

Co-salen grafted mesoporous silica support i.e. Co-A-MS-(0.6) shows a decrease in the surface area from 1014 to 605 $m^2$/g, pore diameter from 57.5 to 35 Å and pore volume of 1.1 to 0.6 cc/g (Table 5.6) indicating that the pores of silica are occupied by the metal complex.

Table 5.6. Sorption study of mesoporous silica samples using different mole ratios of TA/SiO$_2$.

| Sample | TA/SiO$_2$ (mole ratio) | S$_{BET}$ (m$^2$/g) | micropore area (m$^2$/g) | pore dia. (A°) | pore volume cm$^3$/g | Wall thickness (A°) |
|--------|-------------------------|---------------------|--------------------------|-----------------|----------------------|---------------------|
| MS-(0.4) | 0.4 | 756 | 211.7 | 51.2 | 0.7 | 44.1 |
| MS-(0.6) | 0.6 | 1014 | 58.0 | 57.5 | 1.1 | 42.0 |
| MS-(0.8) | 0.8 | 890 | 40.4 | 61.0 | 1.3 | 40.4 |
| MS-(1.0) | 1.0 | 818 | 32.7 | 65.0 | 1.4 | 36.7 |
| Co-A-MS-(0.6)[a] | 0.6 | 605 | 30.0 | 35.0 | 0.6 | 42.0 |

[a] Co-salen grafted on NH$_2$-MS-(0.6), (microanalysis data: carbon – 16.0 %, nitrogen – 2.7 % and elemental analysis data by AAS; Cobalt – 4.4 %).

### 5.5.1.4. N$_2$-sorption study of mesoporous carbon samples

Mesoporous silicas prepared at different mole ratios of TA/SiO$_2$ were used as template to prepare mesoporous carbon materials. The structure of templated carbon is obtained after the dissolution of silica framework using 50 % ethanoic solution of NaOH (1.0 M). Fig. 5.13. A. and B. show N$_2$ adsorption desorption isotherm and pore size distribution, respectively of mesoporous carbon samples prepared by infiltration of mesoporous silica using sucrose as source of carbon. The samples are labeled as MC-(0.4) to MC-(1.0) where the values in the bracket indicate the mole ratio of TA/SiO$_2$ of the respective mesoporous silica template.
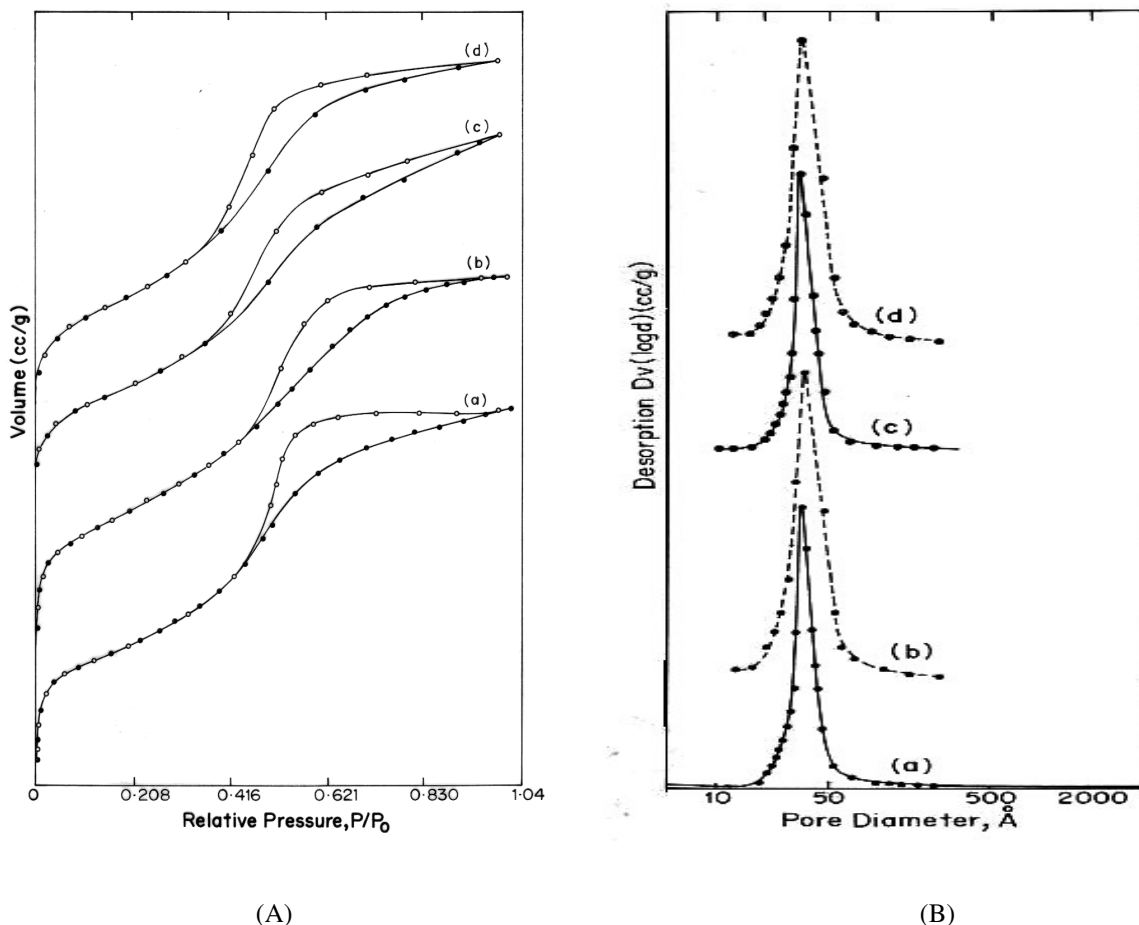
Fig. 5.13. (A) $N_2$-adsorption-desorption isotherms and (B) pore size distributions of mesoporous carbon samples prepared by using variable amount of mesoporous silica templates i.e. (a) MS-(0.4), (b) MS-(0.6), (c) MS-(0.8) and (d) MS-(1.0).

All the samples show type IV isotherm with the capillary condensation step becoming less steep as compared to respective mesoporous silica template, which indicate broadening of pore size distribution. The higher surface area and pore volume of the carbon samples than for the respective silica templates (Table 5.6.) may be due to contribution partly from the microporosity within the carbon walls and the extra porosity due to the incomplete replication process. The pore diameters observed for the prepared mesoporous carbons are comparable to the carbon materials derived from MCM-48 [13], SBA-15 and MSU-H [19]. It is observed that the mesoporous carbon material prepared here shows higher pore diameter than the corresponding silica wall thickness, which may be due to the

159

shrinkage of the carbon wall as reported by Jun et al. [13]. The wall thickness has been calculated by subtracting the pore diameter of the respective sample obtained by $N_2$-sorption from the unit cell parameter $a_0$ calculated using XRD spectrum by employing standard method (Table 5.7.).

Table 5.7. Sorption studies of mesoporous carbon replicas.

| Sample | $S_{BET}$ (m²/g) | micropore area (m²/g) | pore dia. (A°) | pore volume cm³/g | Wall thickness (A°) |
|--------|-----------------|------------------------|----------------|-------------------|---------------------|
| MC-(0.4) | 930 | 345.0 | 46.5 | 0.96 | 47.4 |
| MC-(0.6) | 1200 | 167.7 | 51.0 | 1.34 | 44.0 |
| MC-(0.8) | 1084 | 123.4 | 54.4 | 1.45 | 41.0 |
| MC-(1.0) | 1110 | 159.0 | 56.2 | 1.55 | 39.7 |
| Rh-MC-(0.6)[b] | 435 | 68 | 39.0 | 0.96 | 44.0 |

[b] Rh- content is 0.37 % w/w by ICP analysis.

## 5.5.2. FTIR spectroscopy

Mesoporous silica materials have been prepared via hydrothermal reactions of sodium silicate with tartaric acid as template. The templates were removed by washing the material with ethanol followed by deionized water. Fig. 5.14. shows IR spectra of mesoporous silica samples MS, prepared using different molar compositions of template (i.e. TA/SiO$_2$ ratio). All characteristic absorption bands due to asymmetric stretching mode (1089-1084 cm$^{-1}$) with a shoulder at ~1200 cm$^{-1}$ and others at 960 cm$^{-1}$, 800 cm$^{-1}$, 730 cm$^{-1}$, 550 cm$^{-1}$ and 450 cm$^{-1}$ assigned to symmetric stretching and deformation mode are observed like in other mesoporous silica materials [58]. Absence of a strong absorption band at ~1700-1750 cm$^{-1}$ corresponding to the C=O stretching vibration of the hydroxy-carboxylic acid indicates that all the template molecules are completely removed after washing the

silica material. IR spectra of Co-salen grafted MS-(0.6) is similar to Co-A-SST which is shown in the section 5.3.2. [Fig. 5.5. (3)]. IR spectrum of Co-A-MS-(0.6) shows a broad band at ~ 3300 cm$^{-1}$ assigned to >NH$_2^+$ group due to co-ordination to the metal atom (Fig. not shown).
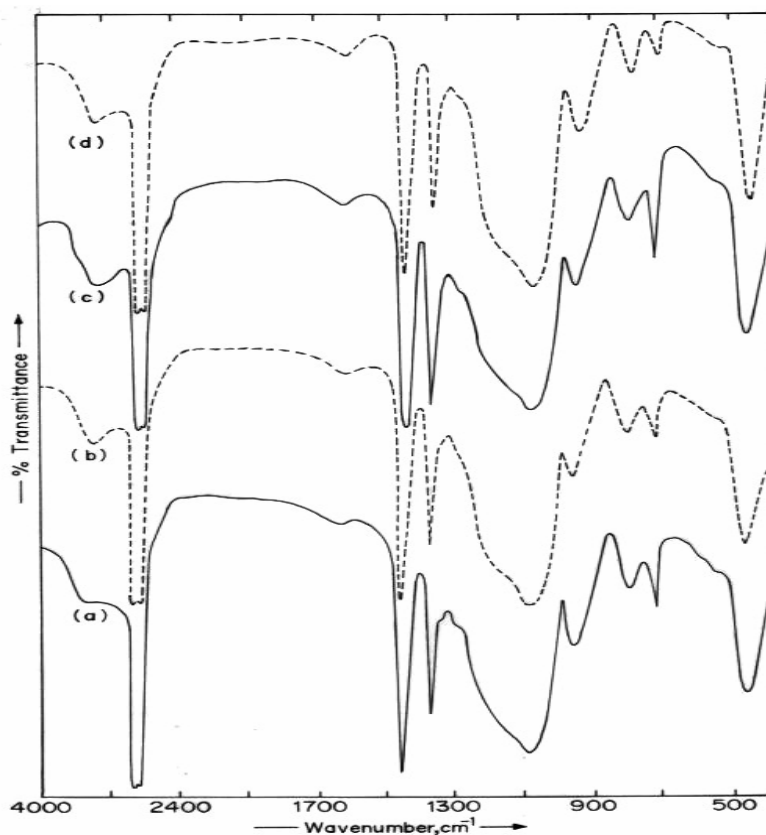


Fig. 5.14. FTIR spectra of (a) MS-(0.4), (b) MS-(0.6), (c) MS-(0.8) and (d) MS-(1.0).

### 5.5.3. X-ray diffraction

The representative XRD pattern of (A) mesoporous silica samples and corresponding mesoporous carbon samples (B) are shown in Fig. 5.15. All mesoporous silica samples having different mole ratios of TA/SiO$_2$ i.e. (a) MS-(0.4), (c) MS-(0.6), (e) MS-(0.8) and (g) MS-(1.0) show only one broad peak at low angle (110 reflection) indicative of the short range order of the mesoporous material. MS-(0.4) shows a relatively broader diffraction peak centered at $2\theta = 0.92^o$ with corresponding d-spacing of 95.4 Å calculated from Bragg's equation. TEM images of all the mesoporous silica samples show

161

worm-like pore structure due to which the d-spacing could be approximated as repeat distance of the materials [27]. A representative TEM image of MS-(0.6) sample is shown in Fig. 5.15. (A). The wall thickness of the above sample is 42.0 Å [Table 5.6.]. The wall thickness has been calculated by subtracting the pore diameter of the respective sample obtained by $N_2$-sorption from the unit cell parameter $a_0$ calculated using XRD spectrum by employing standard method. From the XRD patterns it is observed that d value of the mesoporous silica samples increase as the mole ratio of $TA/SiO_2$ increases. As a result, sample (g) i.e. MS-(1.0) shows a d-spacing of 101.7 Å ($2\theta = 0.87^o$) with the wall thickness of 36.7 Å [Table 5.6.].



Fig. 5.15. XRD pattern of mesoporous silica templates (a) MS-(0.4), (c) MS-(0.6), (e) MS-(0.8), (g) MS-(1.0) and respective mesoporous carbon replicas (b) MC-(0.4), (d) MC-(0.6), (f) MC-(0.8), (h) MC-(1.0).

XRD patterns of the respective mesoporous carbon samples [Fig. 5.15. (b), (d), (f) and (h)] reveal a similar XRD line at low angle indicating the presence of a short range

162

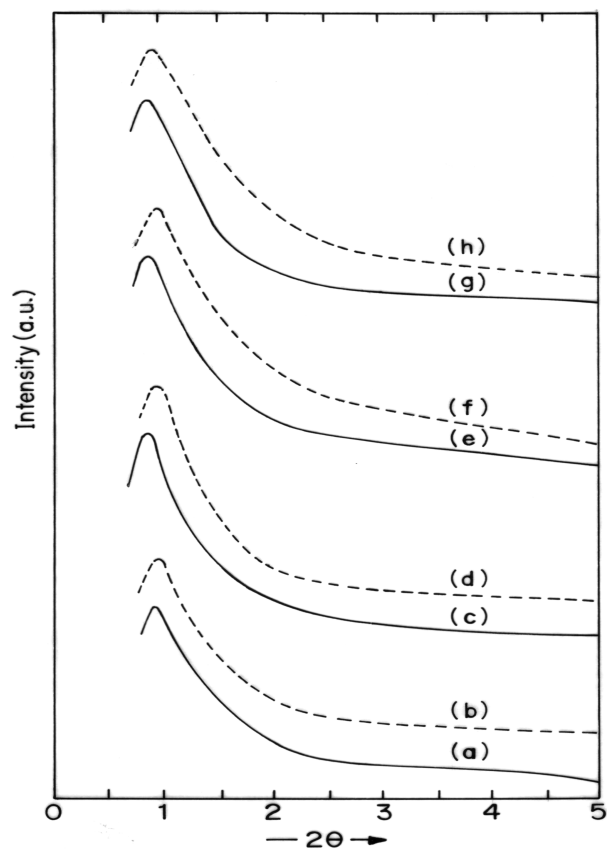ordered mesoporosity present in the samples. The small decrease in the d-spacing of the mesoporous carbon samples is due to shrinkage of the carbon framework during carbonization and removal of the silica template [12]. MC-(0.4) shows a broad peak at $2\theta$ = $0.94^o$ (110 reflection) with the d-spacing of 93.9 Å and wall thickness of 47.4 Å, while MC-(1.0) shows a d-spacing of 95.9 Å ($2\theta = 0.92^o$) and wall thickness of 39.7 Å [Table 5.7]. The XRD pattern of mesoporous carbon in the wide-angle region ($10-90^o$) shows the absence of peaks characteristic of graphitized carbon which observed at $2\theta = 26^o$ and $44^o$ assigned to (002) and (10) diffraction of the graphitic framework [59, 68].

The low angle XRD pattern of the mesoporous silica supported Co-salen complex grafted catalyst [Co-A-MS-(0.6)] and the mesoporous carbon supported $HRhCO(TPPTS)_3$ complex grafted catalyst [Rh-MC-(0.6)] are similar to the parent mesoporous silica MS-(0.6) ($2\theta = 0.89^o$) and mesoporous carbon MC-(0.6) ($2\theta = 0.93^o$), respectively. This indicates that the structures of MS-(0.6) and MC-(0.6) are intact after immobilization of Co-salen and $HRhCO(TPPTS)_3$ complexes respectively. The XRD pattern at high angle for both the catalysts show absence of peaks for cobalt-salen and rhodium, suggesting the encapsulation of the metal complex in the channels

## 5.5.4. Transmission electron microscopy

TEM image of mesoporous silica (A) MS-(0.6) and its replica mesoporous carbon (B) MC-(0.6) is shown in Fig. 5.16. Both samples show wormhole channels with three dimensional interconnected channel arrangement. Mesoporous silica sample exhibits a pore diameter of 57 Å with a wall thickness of 41 Å where as mesoporous carbon, MC-(0.6) exhibits a pore diameter of 50 Å and wall thickness of 44 Å. These observations are approximately in agreement with the results of wall thickness obtained by employing calculations as written above in the section 5.5.1.4.

<center>(A)                                                    (B)</center>
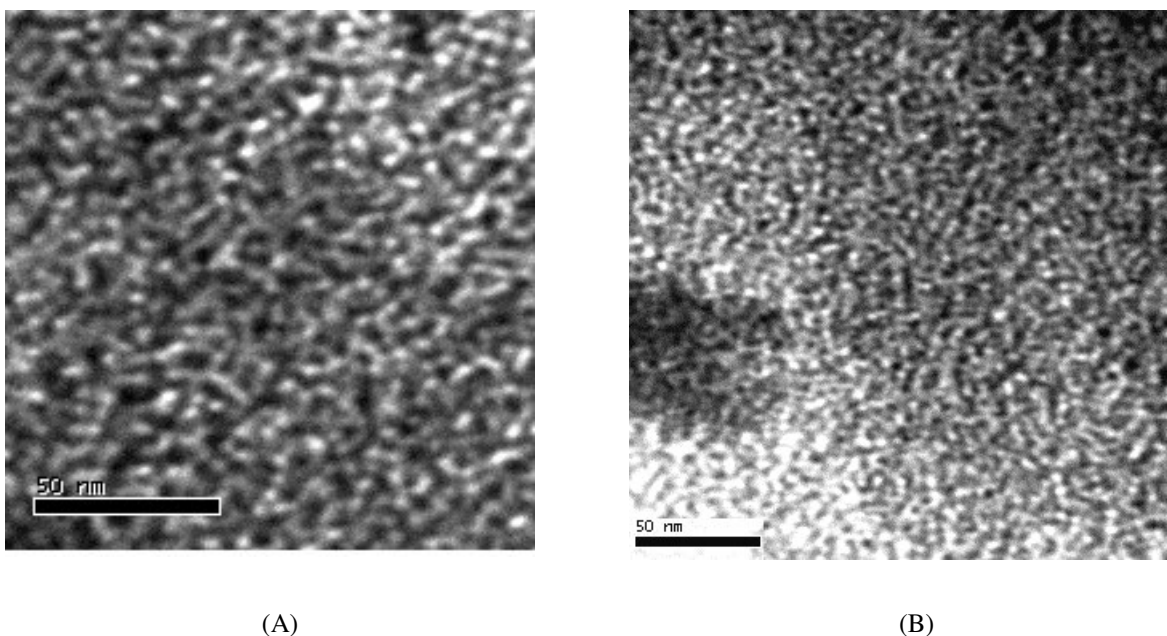
Fig. 5.16. TEM image of mesoporous silica (A) MS-(0.6) and respective mesoporous carbon (B) MC-(0.6).

## 5.5.5. Thermal analysis

TG/DTA profile of representative mesoporous carbon MC-(0.6) is shown in Fig. 5.17. Thermo gravimetric weight change recorded under air shows significant weight loss in narrow temperature range between $550^o$ to $660^o$ ($\sim 98$ %) due to the combustion and decomposition of carbon to $CO_2$. The decomposition temperature is much lower than the temperature of nanotubes and other graphitized carbons which confirms the non-graphitized nature of the sample. TG/DTA profiles of other carbon samples show stability up to the limit of $\sim 700^o$ C.

<center>164</center>
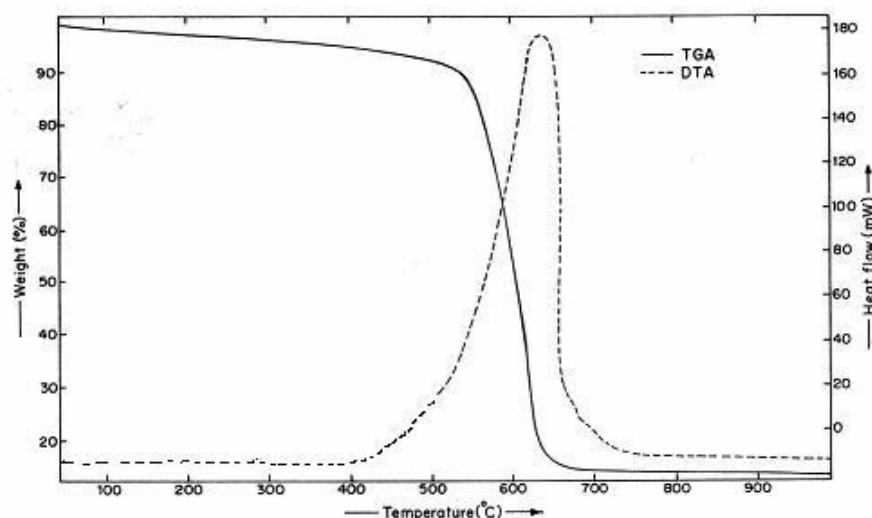
Fig. 5.17. TGA and DTA curves of mesoporous carbon MC-(0.6).

## 5.5.6. XPS analysis for surface studies

XPS analysis of different carbon samples were performed after carbonization at $900^o$ C followed by washing with 1 M ethanoic solution of NaOH (50 % alcohol). In addition to the prominent peak of carbon, all samples show the peak for oxygen with a small signal for silicon, but no peak for sodium was found. The most important element on the surface of the sample observed was carbon with the concentration range from 97.7-98.8 atom % along with a small amount of oxygen (~ 1.67 to 0.9 atom %) and silica (< 0.6 %) (Table 5.8).

Table 5.8 Elemental surface composition of different mesoporous carbon samples.

| Sample | Washing with NaOH solution, Elemental atom % | | |
| --- | --- | --- | --- |
| | C | O | Si |
| MC-(0.4) | 97.70 | 1.67 | 0.63 |
| MC-(0.6) | 97.70 | 1.78 | 0.52 |
| MC-(0.8) | 98.02 | 1.52 | 0.46 |
| MC-(1.0) | 98.80 | 0.90 | 0.30 |

### 5.5.6.1. XPS Carbon spectra

The survey spectrum of a representative sample MC-(0.6) is presented in Fig. 5.18. (A). The photoelectron peak for the above mesoporous carbon sample splits into four peaks as shown in Fig. 5.18. (B). These peaks correspond to: (C1); C-C or C-H bond at the binding energy of 285.1 eV [69-71], (C2 and C3); C-O, >C=O with the binding energy of 286.85 eV and 288.60 eV, respectively [69-71] and (C4); $\pi$-$\pi$* peak at the binding energy of 290.57 eV [72]. The nature of the spectra is typical for a carbonaceous sample with nanoporous polyaromatic surface such as carbon black [73] and carbon fibers [69-71]. The C1 peak is asymmetrical in shape while the other peaks are symmetrical.



(A)
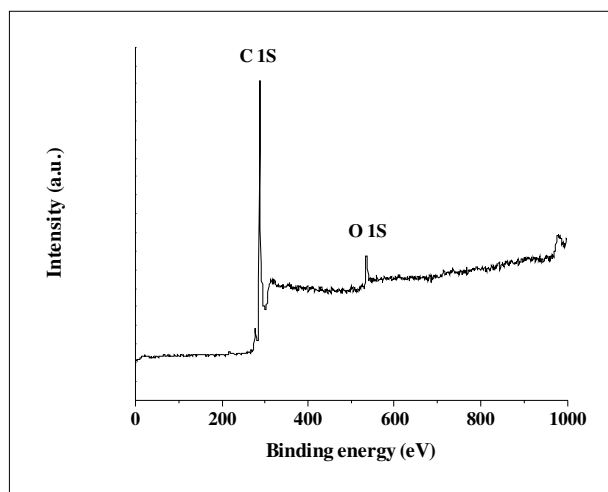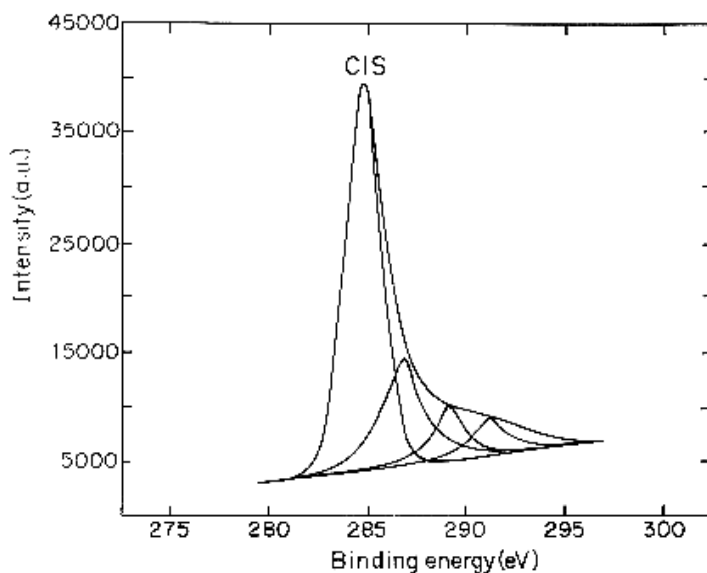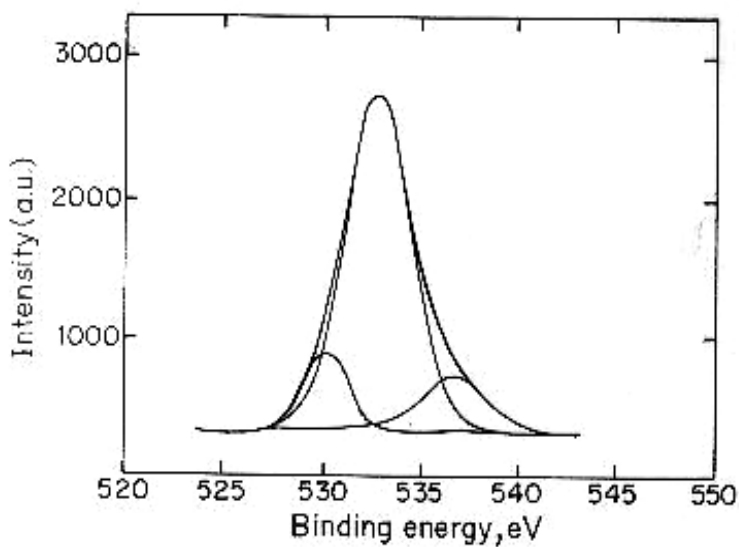
Fig. 5.18. XPS spectra of mesoporous carbon MC-(0.6); (A) Survey spectrum (B) carbon 1S (C) oxygen 1S.

### 5.5.6.2. XPS oxygen spectra

Fig. 5.18. (C) shows oxygen spectra of the representative sample MC-(0.6) with three peaks. One for oxygen atom with two bonds to carbon atom, O1 (C=O; B. E. =- 530.56 eV) a peak for oxygen atom with one bond to carbon atom, O2 ( C-OH; B. E. = 532.9 eV) and a peak at 535.6 eV for adsorbed oxygen [69, 70]. The contribution from

oxygen of silica (B.E. = 532.0 eV) is also added to the $O_2$ peak [71]. But this contribution will be very small as the silica percentage is very low (< 0.6 %).

The XPS spectra of mesoporous carbon reported in this section are similar to those reported earlier (section 5.2.2.).

## 5.6. RESULTS AND DISCUSSION

### 5.6.1. Electrochemical properties

The scan rate dependent voltammetric study of representative mesoporous carbon samples SCT and MC-(0.6) are presented in Table 5.9. The cyclic voltammogram study was performed in the potential range of –1.1 V to –0.2 V using 1 M $H_2SO_4$ as the supporting electrolyte. The voltammograms were recorded by keeping the reference electrode tip very near to the carbon working electrode using leggin capillary in order to minimize the solution resistance (Table 5.9.). Fig. 5.19. shows the representative cyclic voltammogram of MC-(0.6) sample performed at different scan rates, i.e. 1, 5 and 10 mV/s. The maximum capacitance of 88.0 F/g at 1 mV/s was observed for MC-(0.6) which could be attributed to the relatively higher mesoporosity of the sample. Further, the capacitances at the scan rate of 5 mV/s and 10 mV/s were found to be 56.8 F/g and 50.6 F/g, respectively.

Table 5.9. Specific capacitance of representative mesoporous carbon samples at different scan rates.

| Scan rate | Specific capacitance, F/g | |
|---|---|---|
| mV/s | SCT | MC-(0.6) |
| 1 | 65.0 | 88.0 |
| 5 | 40.0 | 56.8 |
| 10 | 36.0 | 50.6 |
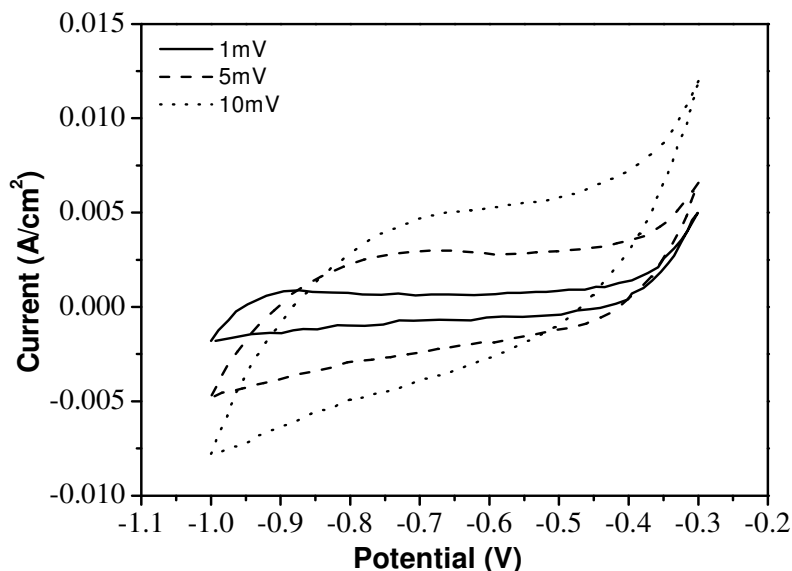
Fig. 5.19. Capacitance behavior of MC-(0.6) at different voltage scan rates.

A high surface area carbon material with regularly ordered three dimensional interconnected channels and compromised ratio of meso/micro pore structure is used as an electrode for supercapacitors [13, 15]. Improvement in the regularity of pore arrangement in the presently prepared carbon material along with appropriate ratio of meso/micro pore structure should lead to promising electrochemical material for super capacitor applications.

### 5.6.2. Catalytic reactions

### 5.6.2.1. Olefin oxidation using Co-salen grafted mesoporous silicas

Oxidation reactions were carried out using Co-salen, SST, Co-A-SST and Co-A-MS-(0.6) catalysts on styrene, cyclohexene and 1-decene with TBHP as oxidant. It is observed that Co-salen grafted catalysts i. e. Co-A-SST and Co-A-MS-(0,6) show ~ 2-2.5 times higher conversion as compared to neat Co-salen complex and SST (support) (Table 5.10.). This is because the large hydrophobic surface area of mesoporous silica supports and the dispersion of the metal complex gives rise to high reactivity of central metal atom. The performance of Co-A-SST and Co-A-MS-(0.6) being better than the neat metal complex may also be due to the presence of a lone pair of the amino group that originated from the

169

aminopropyl group grafted on the silica wall. Earlier workers also reported an enhancement of catalytic activity in the presence of amines [74, 75]. We also observed higher epoxide yield for styrene and 1-decene for both the grafted catalysts as compared to neat metal complex (Table 5.10.).

Table 5.10. Olefin oxidation using mesoporous silica supported Co-salen grafted catalysts (24 h data).

| Catalyst | Amount (g) | Substrate | % conversion (mole %) | % epoxide yield | TON |
|---|---|---|---|---|---|
| Co-salen | 0.02 | styrene | 30.7 | 50.5 | 25 |
| | | cyclohexene | 24.7 | 4.7 | 20 |
| | | 1-decene | 15.7 | 35.5 | 13 |
| SST | 0.05 | styrene | 22.8 | 45.3 | --- |
| | | cyclohexene | 10.3 | 3.8 | --- |
| | | 1-decene | 7.0 | 36.3 | ---- |
| Co-A-SST[a] | 0.05 | styrene | 80.0 | 82.0 | 65 |
| | | cyclohexene | 72.0 | 6.8 | 56 |
| | | 1-decene | 55.0 | 55.0 | 44 |
| Co-A-MS-(0.6)[a] | 0.05 | styrene | 78.8 | 75.0 | 63 |
| | | cyclohexene | 69.0 | 8.4 | 54 |
| | | 1-decene | 52.4 | 56.7 | 42 |

[a] Co = 4.4 %.

This observation is comparable to earlier reports on the oxidation of alkenes using Cu/Co-S-AM(PS) [75]. Fig. 5.20 (A), (B) and (C) shows the comparative study of rate of product conversion for Co-salen, SST and representative catalyst Co-A-SST for the oxidation of styrene, cyclohexene and 1-decene. Fig. 5.20. (D) shows the product distribution of olefin oxidation and it is observed that epoxide selectivity for styrene and 1-decene is ~ 82.0 % and 55.0 % respectively for Co-A-SST catalyst. This is due to the  attack

of the t-butyl peroxy radical on the double bond, while in the case of cyclohexene, 2-cyclohexene 1-one is the major product (selectivity ~ 68 %) as allylic hydrogen is more reactive than the C=C bond.



(A)                                                                (B)



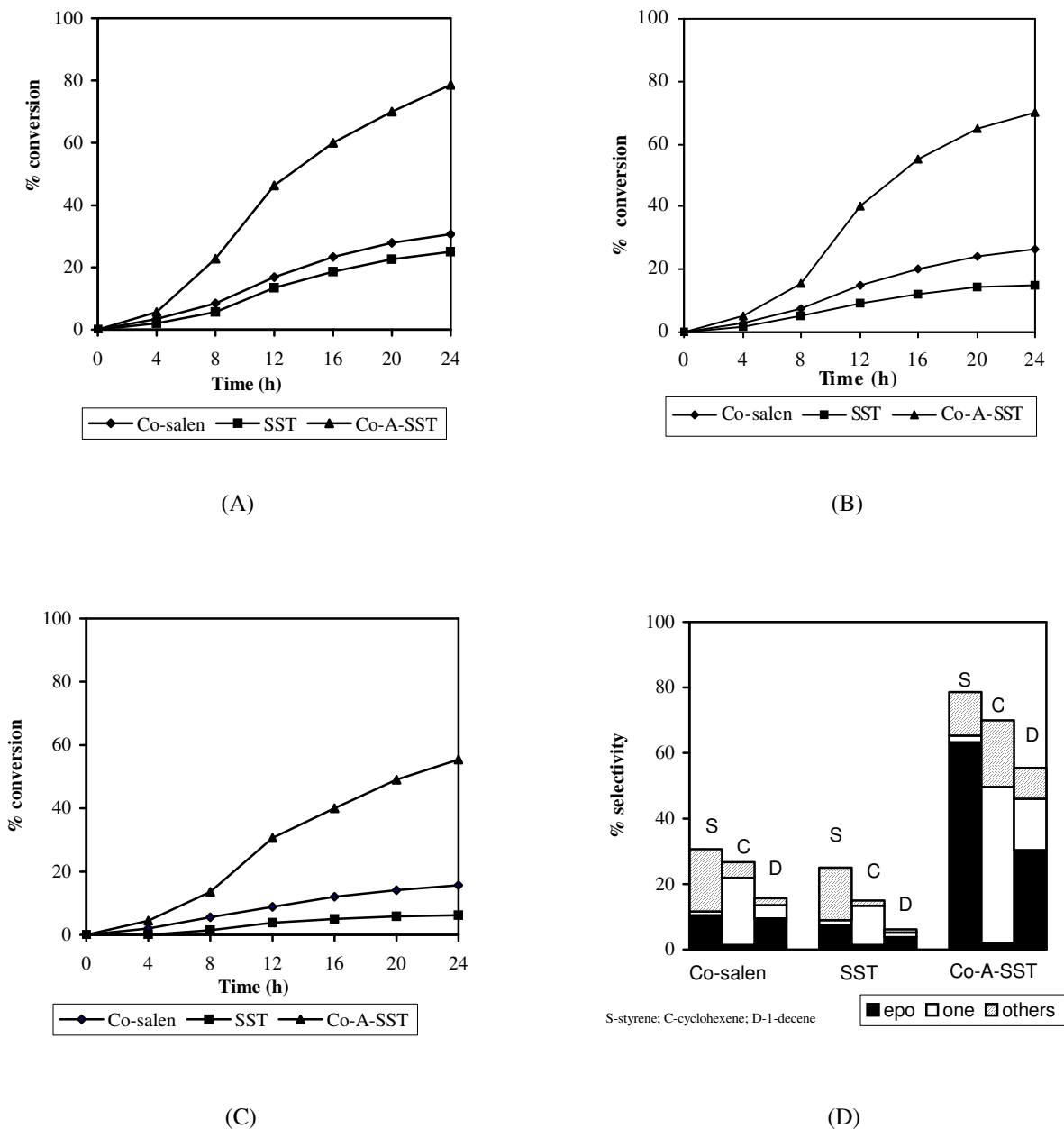(C)                                                                (D)

Fig.5.20. Kinetic study of oxidation of (A) styrene, (B) cyclohexene and (C) 1-decene using mesoporous SST as support (D) Comparison of product distribution of olefins oxidation using different catalysts.

The superior catalytic activity for the grafted catalysts Co-A-SST and Co-A-MS-(0.6) as compared to the earlier reported MCM-41 supported Co-salen catalysts [76] may be due to three dimensional pore structure and presence of interconnecting channels in the present samples (like in MCM-48) compared to the one dimensional channel in MCM-41 [77].

## 5.6.2.2. Hydroformylation of n-alkenes using Rh-complex impregnated mesoporous carbons

Hydroformylation reactions were carried out using both the mesoporous carbon supported catalysts Rh-SCT and Rh-MC-(0.6) and compared with activated carbon supported catalyst Rh-C-1. The substrates used were 1-hexene and 1-decene and the reaction was carried out at 373K. In all reactions a low n/i ratio was observed because of isomerisation of the olefins and hydroformylation of the internal olefins (Table 5.11).

It was observed that both the mesoporous carbon supported catalysts Rh-SCT and Rh-MC-(0.6) show ~ 1.5 to 2 times higher conversion as compared to Rh-C-1. This is due to the large pore diameters of mesoporous carbon supports SCT and MC-(0.6) which are sufficient to accommodate the bulky metal complex. This is evident from sorption study which shows a decrease in the surface areas after immobilization of the metal complex on these supports (Table 5.2. and Table 5.7.). Hence interaction of the olefins and diffusion of the product is easier in the case of Rh-SCT and Rh-MC-(0.6).

On the other hand, the activated microporous carbon C-1 with large surface area (1141 $m^2$/g ) and a micropore diameter of ~ 18 Å did not show major decrease in the surface area (> 2 % decrease) after impregnation of the metal complex i.e. for Rh-C-1. In this case the metal complex primarily occupies the external surface area of the support as the pore size is very small to accommodate the complex. This results in the less dispersed catalyst with a reduced surface area available for the reaction. This lowers the activity of the catalyst as compared to mesoporous carbon supported catalysts Rh-SCT and  Rh-MC-(0.6).

Table 5.11.Comparative study of hydroformylation reaction on Rh-C1, Rh-SST and Rh-MC-(0.6).

| catalyst | olefin | % conversion (4 h) | % aldehyde selectivity | % isomerization | n/i | TOF $(h^{-1})$ |
|---|---|---|---|---|---|---|
| Rh-C-1 | 1-hexene | 54.3 | 36.3 | 18.0 | 0.79 | 399 |
| | 1-decene | 48.6 | 32.3 | 16.3 | 0.73 | 357 |
| Rh-SCT | 1-hexene | 95.0 | 89.0 | 6.0 | 0.79 | 698 |
| | 1-decene | 92.3 | 81.4 | 10.9 | 0.75 | 678 |
| Rh-MC-(0.6) | 1-hexene | 95.6 | 86.5 | 9.1 | 0.80 | 700 |
| | 1-decene | 91.3 | 79.0 | 12.3 | 0.74 | 674 |

Conditions: Temperature 353 K, Stirring speed 1400 rpm, pCO+$H_2$ (1:1) 4.14 MPa, olefin: 0.391 kmol/m$^3$ Catalyst: 0.100g (Rh content 0.37 % w/w), Total charge 2.7 x10$^{-5}$ m$^3$, Solvent: toluene.

Fig. 5.21. (A) and (B) shows the concentration time profile for hydroformylation of 1-decene using representative Rh-SCT and compared with Rh-C-1. The product profiles were the same. In both the cases it was observed that syngas (CO+$H_2$) and 1- decene consumed were consistent with the amount of aldehyde formed. The time required for complete conversion of 1-decene to the product aldehyde is lesser for Rh-SCT catalyst compared to Rh-C-1 catalyst.
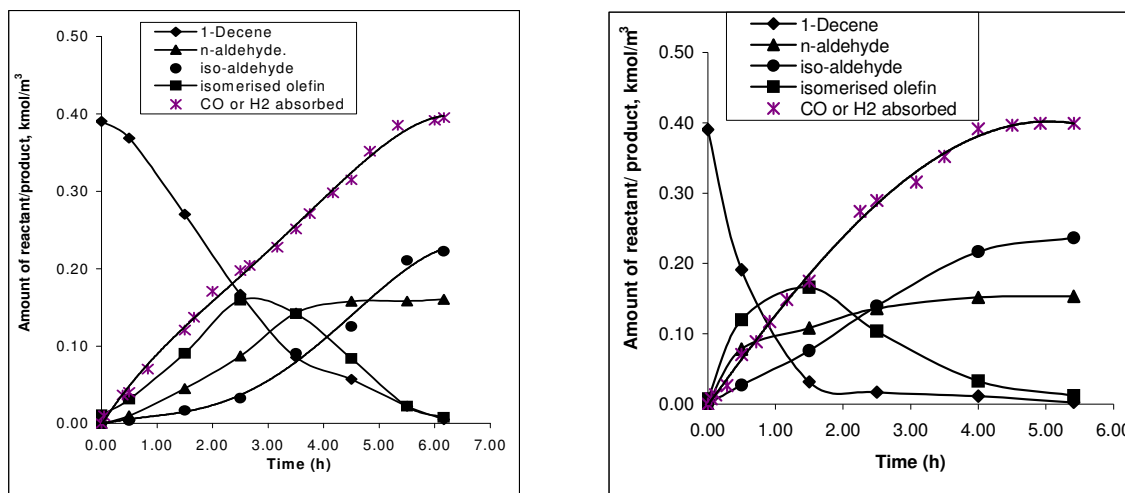
Fig. 5.21. C.T. Profile for hydroformylation of 1-decene using (A) Rh-C-1 and (B) Rh-SCT Catalyst.

## 5.7. CONCLUSIONS

Mesoporous silica materials with three dimensional interconnecting channel arrangements have been prepared using low cost hydroxy-carboxylic acids as templates/pore forming agents and tetraethyl orthosilicate (TEOS) as well as sodium silicate as source of silica. The resulting materials shows surface area in the range of 700 1000 $m^2$/g, pore diameter of 40-60 Å with narrow pore size distribution. Mesoporous silica supported Co-salen complex grafted catalyst show higher conversion and epoxide selectivity compared to conventional mesoporous silica (MCM-41) supported catalysts. These mesoporous silica materials were used as template to prepare mesoporous carbon materials with surface area ~ 1200 $m^2$/g and pore diameter in the range of 40-50 Å and pore volume above 1.0 cc/g. The mesoporous carbon samples show promising electrochemical double layer capacitance behavior with the specific capacitance of 88 F/g at the scan rate of 1 mV/s. Mesoporous carbon supported $HRh(CO)(TPPTS)_3$ impregnated catalyst showed ~ two times higher conversion over the catalyst made using conventional activated carbon support for hydroformylation of alkenes.

174

## 5.8. REFERENCES

1. C. R. Bansal, J. B. Donnet and F. Stoeckli, *Active Carbon,* Marcel Dekker, New York, 1998.

2. H. C. Foley, *J. Microporous Mater.*, 4 (1995) 407.

3. T. Kyotani, *Carbon,* 38 (2000) 269.

4. J. W. Patrick, *Porosity in carbon: characterization and applications,* Landon: Edward Arnold, 1995.

5. H. Marsh, *Introduction to carbon science,* Laodon: Butterworths, 1989.

6. S. Han, K. Sohn and T. Hyeon, *Chem Mater*., 12 (2000) 3337.

7. S. Yoon, J. Lee, T. Hyeon and SM Oha, *J. Electrochem. Soc.,* 147 (2000) 2507.

8. P. T. Tanev, M. Chibwe and T. J. Pinnavaia, *Nature*, 368 (1994) 321.

9. P. T. Tanev and T. J. Pinnavaia, *Science,* 267 (1995) 865.

10. S. A. Bagshaw, E. Prouzet and T. J. Pinnavaia, *Science,* 269 (1995) 1242.

11. D. Zhao, J. Feng, Q. Huo, N. Melosh, G. H. Fredrickson, B. F. Chmelka and G. D. Stucky, *Science,* 279 (1998) 548.

12. R. Ryoo, S.H. Joo and S. Jun, *J. Phys. Chem. B*, 103 (1999) 7743.

13. S. Jun, S. H. Joo, R. Ryoo, M. Kruk, M. Jaroniec, Z. Liu, T. Ohsuna and O. Terasaki, *J. Am. Chem. Soc.,* 122 (2000) 10712.

14. Tae-Wan. Kim, R. Ryoo, K. P. Gierszal, M. Jaroniec, L. A. Solovyov, Y. Sakamoto and O. Terasaki, *J. Mater. Chem.,* 15 (2005) 1560.

15. J. Lee, S. Yoon, S. M. Oh, C. H. Shin and T. Hyeon, *Adv. Mater.,* 12 (2000) 359.

16. W. W. Lukens and G. D. Stucky, *Chem. Mater.,* 14 (2002) 1665.

17. M. Sevilla, S. Alvarez and A. B. Fuertes, *Micropor. Mesopor. Mater.,* 74 (2004) 49.

18. J. Lee, K. Sohn and T. Hyeon, *Chem. Commun.*, (2002) 2674.

19. S. S. Kim and T. J. Pinnavaia, *Chem. Commun.,* (2001) 2418.

20. C. T. Kresge, M. E. Leonowicz, W. J. Roth J. C. Vertuli and J. S. Beck, *Nature,* 359 (1992) 710.

21. N. K. Raman, M. T. Anderson and C. J. Brinker, *Chem. Mater.,* 8 (1996) 1682.

22. J. S. Beck, J. C. Vartuli, W. J. Roth, M. E. Leonowicz, C. T. Kresge, K. D. Schmidt, C. T-W. Chu, D. H. Olson, E. W. Sheppard, S. B. McCullen, J. B. Higgins and J. L. Schlenker, *J. Am. Chem. Soc.,* 114 (1992) 10834.

23. Q. Huo, D. I. Margolese, U. Ciesla, P. Feng, T. E. Gier, P. Sieger, R. Leon, P. M. Petroff, F. Schuth and G. D. Stucky, *Nature,* 368 (1994) 317.

24. P. T. Tanev and T. J. Pinnavaia, *Chem. Mater.,* 8 (1996) 2068.

25. P. T. Tanev and T. J. Pinnavaia, *Science,* 271 (1996) 1267.

26. Y. Wei, D. T. Ding, W. H. Shih, X. Liu, S. Z. D. Cheng and Q. Fu, *Adv. Mater.,* 3 (1998) 313.

27. J. B. Pang, K. Y. Qiu and Y. Wei, *J. Non-Cryst. Solids,* 283 (2001) 101.

28. J. B. Pang, C. M. Dong, K. Y. Qui and Y. Wei, *Chinese J. Poly. Sci.,* 20 (2002) 361.

29. F. Chen, L. Huang and Q. Li, *Chem. Mater.,* 9 (1997) 2685.

30. Y. Liu, A. Karkamkar and T. J. Pinnavaia, *Chem. Commun.,* (2001) 1822.

31. B. Lindlar, A. Kogelbauer, P. J. Kooyman and R. Prins, *Micropor. Mesopor. Mater.,* 44–45 (2001) 89.

32. L. Sierra and J.-L. Guth, *Micropor. Mesopor. Mater.,* 27 (1999) 243.

33. M. Kruk, M. Jaroniec, R. Ryoo and J. M. Kim, *Chem. Mater.,* 11 (1999) 2568.

34. J. M. Kim and G. D. Stucky, *Chem. Commun.,* (2000) 1159.

35. M.-C. Chao, D.-S. Wang, H.-P. Lin and C.-Y. Mou, *J. Mater. Chem.,* 13 (2003) 2853.

36. K. Kosuge, T. Sato, N. Kikukawa and M. Takemori, *Chem. Mater.,* 16 (2004) 899.

37. C. Boissière, A. Larbot and E. Prouzet, *Chem. Mater.*, 12 (2000) 1937.

38. S.-S. Kim, T. R. Pauly and T. J. Pinnavaia, *Chem. Commun.,* (2000) 835.

39. S.-S. Kim, T. R. Pauly and T. J. Pinnavaia, *Chem. Commun.,* (2000) 1661.

40. S. S. Kim, A. Karkamkar, T. J. Pinnavaia, M. Kruk and M. Jaroniec, *J. Phys. Chem. B,* 105 (2001) 7663.

41. C. Niu, E. K. Sichel, R. Hoch, D. Moy and H. Tennent, *Appl. Phys. Lett.,* 70 (1997) 1480.

42. D. Qu and H. Shi, *J. Power Sources,* 74 (1998) 99.

43.	H. Shi, *Electrochim. Acta.,* 41 (1999) 1633.

44.	E. Frackowiak and F. Beguin, *Carbon,* 39 (2001) 937.

45.	H. Delmas and P. Purwanto, *Catal. Today,* 24 (1995) 135.

46.	U. Ritter, T. Borrmann and H.W. Roesky, *J. Mol. Catal. A: Chem.,*153 (2000) 31.

47.	R. R. Hartley, *Supported metal complexes,* Reidel, Dordrechiet, 1985.

48.	(a) R. Augustine, S. Tanielyan, S. Anderson and H. Yang, *Chem. Commun.,* (2001) 1257. (b) K. MuKhopadhyay and R.V. Chaudhari, *J. Catal.*, 213 (2003) 73.

49.	(a) A. A. Ostwald, L.L. Murrell and L. J. Boucher, *Petro. Chem. Am. Chem. Soc.,* (1974) 19, (b) K. Mukhopadhyay, A.B. Mandale and R.V. Chaudhari, *Chem. Mater.,*15 (2003) 1766.

50.	D. C. Bailey and J. H. Langer, *Chem. Rev.,* 81 (1981) 109.

51.	J. P. Arhancet, M.E. Davis, J. S. Merola and B. E. Hanson, *Nature,* 339 (1989) 454.

52.	K. Omata, K. Fujimoto, T. Shikada and H. Tominaga, *Ind. Eng. Chem. Res.,* 27 (1988) 2211.

53.	Y. Zhang, K. Nagasaka, X. Qiu and N. Tsubaki, *Appl. Catal. A: General,* 276 (2004) 103.

54.	C. Disser, C. Muennich and G. Luft, *Appl. Catal. A: General,* 296 (2005) 201.

55.	A. A. Zahidov, R. H. Banghman, Z. Jgbal, C. Lui, I. Khayrullin, S. O. Dantas, J. Marti and V. G. Rachenko, *Science,* 282 (1998) 897.

56.	P. Arhancet, M. E. Davis, J. S. Merola and B. E. Hanson, *J. Catal.*, 121 (1990) 327.

57.	K. Chaudhari, T. K. Das, P. R. Rajmohanan, K. Lazar, S. Sivasanker and A. J. Chandwadkar, *J. Catal.,* 183 (1999) 281.

58.	P. Karandikar, M. Agashe, K. Vijayamohanan and A. J. Chandwadkar, *Appl. Catal. A: Gen.,* 257 (2004) 133.

59.	P. V. Adhyapak, T. Maddanimath, S. Pethkar, A. J. Chandwadkar, Y. S. Negi and K. Vijayamohanan, *J. Power Sources,* 109 (2002) 105.

60.	G. Gottarelli, E. Mezzina, G. P. Spada, F. Carsughi, G. Di Nicola, P. Mariani, A. Sabatucci and S. Bonazzi, *Helv. Chemi. Acta*, 79 (1996) 220.

61.	A. Infantes-Molina, J. Merida-Robles, P. Maireles-Torres, E. Finocchio, G. Busca, E. Rodriguez-Castellon, J.L.G. Fierro and A. Jimenez-Lopez, *Micropor. Mesopor.*

*Mater.,* 75 (2004) 23.

62. K. Mukhopadhyay; B. R. Sarkar and R. V. Chaudhari, *J. Am. Chem. Soc.,* 124 (2002) 9692.

63. N. S. Pagar, R. M. Deshpande and R. V. Chaudhari, *Catalysis Letters*, 10 (2006) 129.

64. Indian Patent application no. 780/Del/2005.

65. K.S.W. Sing, D. H. Everett, R. A. W. Haul, L. Moscou, R. A. Pierotti, J. Rouquerol and T. Siemieniewska, *Pure Appl. Chem.,* 57 (1985) 603.

66. A-H. Lu, W-C Li, W. Schmidt and F. Schüth, *Micropor. Mesopor. Mater.,* 80 (2005) 117.

67. I. Park, Z. Wang and T. J. Pinnavaia, *Chem. Mater.*,17 (2005) 383

68. A. B. Fuertes and S. Alvarez, *Carbon,* 42 (2004) 3049.

69. Y. Xie and PMA. Sherwood, *Chem. Mater.,* 2 (1990) 293.

70. Y. Xie and PMA. Sherwood, *Appl. Spectrosc.*, 43 (1989) 1153.

71. E. Desimoni, GI. Casella, A. Morone and AM. Salvi, *Surf. Interface Anal.*, 15 (1990) 627.

72. JA. Gardella, SA. Ferguxson and RL. Chin, *Appl. Spectrosc.,* 40 (1986) 224.

73. H. Darmstadt, C. Roy and S. Kaliaguine, *Carbon,* 32 (1994) 1399.

74. N. Safari and F. Bahadoran, *J. Mol. Catal. A: Chem.,* 171 (2001) 115.

75. J. Dongfeng, L. Xiaobing and He. Ren, *Appl. Catal. A: Gen.,* 203 (2000) 329.

76. P. Karandikar, Dhanya K. C., S. Deshpande, A. J. Chandwadkar, S. Sivasanker and M. Agashe, *Catal. Commun.,* 5 (2004) 69.

77. P. Selvam and S. E. Dapurkar, *Catal. Today*, 96 (2004) 135.

# Chapter-6
# Summary and Conclusions

## 6.1. SUMMARY

The central theme of the thesis is to synthesize mesoporous materials and their applications in selected fields.

The first chapter of the thesis presents the necessary introduction and background material which drives the author to undertake the research work presented in the following chapters. The summary of the work, observations, experiments and conclusions are presented below:

**Chapter 2 and Chapter 3:**

Mesoporous silica, Si-MCM-41, prepared under stirred conditions results in rapid crystallization, saving energy and time in the process. The samples obtained are highly reproducible, show ordered hexagonal channel arrangement with very high surface area. The immobilization of Co/Cu-perchlorophthalocyanine and salen complexes (Co/Cu-$Cl_{16}Pc$/salen) in the channels of Si-MCM-41 molecular sieves with the walls modified by 3-aminopropyl silane group has been achieved by grafting [Co/Cu-AM(PS) and Co/Cu-S-AM(PS)]. The activity of these samples is compared with the samples prepared by impregnation method [Co/Cu-M(I) and Co/Cu-S-M(I)] for hydrocarbon oxidation.

X-ray diffraction patterns of impregnated and grafted catalysts are similar to the neat Si-MCM-41 and indicate that the structure of Si-MCM-41 remains intact after immobilization with a uniform distribution of the metal complex in the channels. Solid state MASNMR spectroscopy evidenced the modification of Si-MCM-41 by aminopropyl group, as silanol signals decrease ($Q_2$ and $Q_3$) and signals characteristic of $(SiO)_3Si-CH_3$ group appear. The adduct formation between amino group of $NH_2$-MCM-41 and central metal in the case of the grafted catalyst is evidenced by UV-Vis., FTIR and cyclic voltammetry. The immobilized catalysts show better performance for the oxidation of hydrocarbons with both the oxidants, TBHP and aldehyde/$O_2$. This is attributed to the molecular dispersion of the complex with sufficient void space and the hydrophobic surface area of the support being appropriate for the activation of hydrocarbons. The grafted catalysts show higher conversion as well as selectivity for hydrocarbons as compared to the impregnated ones due to the axial interaction of the amino group with the central metal of the complex. The presence of catalytic amount of base helps to increase the initial rate of epoxidation by facilitating O-O

bond cleavage and formation of high oxo-intermediate. The comparative study of the two different oxidants for the oxidation of alkenes shows that when isobutyraldehyde/$O_2$ is used as oxidant, a larger conversion and turn over number is observed compared to TBHP. This is because the active oxygen of the acyl peroxy radical and the per acid is utilized for the epoxidation. When isobutyraldehyde/$O_2$ is used as the oxidant for the oxidation of cyclohexene, heterolytic cleavage of oxygen favors electrophilic attack at the double bond leading to a higher epoxide conversion as compared to cyclohexenone, which is observed to be the major product when TBHP is used as the oxidant. A comparative study of the two different oxidants for the oxidation of alkanes shows a higher conversion with TBHP than with isobutyraldehyde/$O_2$ due to the mechanistic differences associated with the decomposition of O-O species and stability of the radical species. TBHP and benzaldehyde/$O_2$ possess comparable activity in oxidation of alkanes due to the similar stability of the intermediate radical species of the oxidant.

**Chapter 4:**

The embedding of silver and gold nanowires inside the channels of Si-MCM-41 host is achieved by the controlled reduction of respective metal salts with sodium borohydrate. Agglomeration of nanoparticles inside the channels of Si-MCM-41 results in the formation of nanowires with the diameter of ~2.8 nm, coincident with the channel diameter of the host material which is confirmed by TEM. XRD shows the presence of silver and gold at higher 2θ value for the (111) and (200) planes of silver and gold lattice. $N_2$ sorption shows a decrease in the surface area of Ag/Au-MCM-41 samples compared to neat Si-MCM-41 indicating the pore occupancy by the nanowires. The characteristic peaks for silver and gold in the absorption spectra of Ag/Au-MCM-41 are observed which are due to the oscillation of conducting band electrons of silver and gold. These heterostructured materials exhibit interesting luminescence properties as observed for direct band gap semiconductors. The optical characterization of these heterostructure materials shows second harmonic generation, with more SHG intensity after poling than the unpoled samples.

**Chapter 5:**

Mesoporous silica materials with three dimensional interconnecting channel arrangements are prepared using low cost hydroxy-carboxylic acids as templates/pore forming agents and tetraethyl orthosilicate (TEOS) /sodium silicate as source of silica. Mesoporous silica having wormhole channels along with some regions of regularly ordered channel arrangement are prepared at room temperature using tetraethyl orthosilicate as silica source. These exhibit surface areas in the range of 700-900 $m^2$/g with a narrow pore size distribution. Mesoporous silica prepared by an economical route using sodium silicate as the source of silica exhibit surface areas up to 1000 $m^2$/g and pore diameters larger than the materials prepared using TEOS, due to a synergetic effect of the sodium silicate. Oxidation of olefins, using Co-salen complex grafted mesoporous silica supported catalysts Co-A-SST and Co-A-MS-(0.6) reveal higher conversion and epoxide selectivity as compared to conventional mesoporous silica (Si-MCM-41) supported catalysts. This is because the three dimensional interconnected channel arrangement of SST and MS-(0.6) gives rise to a diffusion controlled reaction.

These mesoporous silica materials were used as templates to prepare mesoporous carbon materials with surface area ~ 1200 $m^2$/g and pore diameter in the range of 40-50 Å and pore volume above 1.0 cc/g. XPS of MC-(0.6) shows a prominent peak for carbon (~ 97 atom %) and the nature of the spectra is typical of a carbonaceous sample with nanoporous polyaromatic surface. The specific capacitance value of 88 F/g at the scan rate of 1 mV/s. for the mesoporous carbon MC-(0.6) shows that it may prove to be the promising material for double layer capacitance study.

Mesoporous carbon supported barium salt of $HRh(CO)(TPPTS)_3$ complex, Rh-SST and Rh-MC-(0.6) show better catalytic activity than the catalyst formed using conventional activated microporous carbon support for hydroformylation of alkenes and exhibit TOF value larger by a factor of about 2.

# LIST OF PUBLICATIONS

**(a) Papers Published**

1. "Aniline as a stabilizer for metal nanoparticles", Anjali A. Athawale, S. V. Bhagwat, Prachi P. Katre, Asha J. Chandwadkar and **P. Karandikar**, *Materials Letters,* 57 (2003) 3889.

2. "$Cu^{2+}$-perchlorophthalocyanine immobilized MCM-41: catalyst for oxidation of alkenes", **P. Karandikar**, M. Agashe, K. Vijayamohanan and A. J. Chandwadkar, *Applied Catalysis A: General,* 257 (2004) 133.

3. "Cu/Co-salen immobilized MCM-41: characterization and catalytic reactions" **P. Karandikar**, K. C. Dhanya, S. Deshpande, A. J. Chandwadkar, S. Sivasanker and M. Agashe, *Catalysis Communications,* 5 (2004) 69.

4. "Synthesis of silver nanowires inside mesoporous MCM-41 host", P. V. Adhyapak, **P. Karandikar,** K. Vijayamohanan, A. A. Athawale and A. J. Chandwadkar, *Materials Letters,* 58 (2004) 1168.

5. "A rapid hydrothermal synthesis route for nanocrystalline $SrZrO_3$ using reactive precursors", Anjali A. Athawale, Asha Chandwadkar, **P. Karandikar** and Malini Bapat, *Materials Science and Engineering B,* 119, (2005) 87.

6. "Liquid phase oxidation of alkanes using Cu/Co-perchlorophthalocyanine immobilized MCM-41 under mild reaction conditions," **P. Karandikar**, A.J. Chandwadkar, M. Agashe, N.S. Ramgir and S. Sivasanker, *Applied Catalysis A: General* 297 (2006) 220.

7. "Radiation Assisted Synthesis of Nanosized Barium Zirconate", Anjali A. Athawale, Asha J. Chandwadkar, **P. Karandikar**, Renu Pasricha and Malini S.Bapat *Radiation Physics and Chemistry,* 75 (2006) 755.

8. "Synthesis characterization and optical properties of silver and gold nanowires embedded in mesoporous MCM-41". Parag V. Adhyapak, **Prashant R. Karandikar** Jagdish W. Dadge, Rohini C. Aiyer, Asha J. Chandwadkar *Central Europian Journal of Chemistry,* 4 (2006) 317.

**b) Papers communicated and accepted**

1. "Synthesis and characterization of mesoporous carbon through inexpensive mesoporous silica as template".**P. Karandikar** , K. R. Patil, A. Mitra, B. Kakade and A. J. Chandwadkar accepted for publication to Microporous and Mesoporous materials (2006).

2. "Synthesis, characterization and catalytic study of mesoporous carbon materials prepared via mesoporous silica using non-surfactant templating agents", A.  J. Chandwadkar, **P. Karandikar**, M. S. Agashe, N. E. Jacob, R. K . Jha, R.  Kumar, N. S. Pagar, R. M. Deshpande and R. V. Chaudhari communicated to Applied Catalysis A: General (2006).


**c) Papers presented in Conference**

1.  "Role of Non-conventional energy for sustainable development"
   Subhada Naik Nimbalkar, P. Karandikar, A. J. Chandwadkar presented in **"VIII National Conference of Women in Science by IWSA Pune",** at ARI Pune during 12-14 sep. 2001 at ARI Pune

2. "Cu$^{2+}$-perchlorophthalocyanine immobilized MCM-41 as  heterogeneous catalyst for the oxidation of styrene", (Poster presentation) A. J. Chandwadkar , **P. Karandikar,** M. Agashe and S. Sivasanker presented in the **"National workshop on Catalysis, CATWORK 2002, Gauhati University"** during 8-10 March 2002.

3.  "Effect of synthetic zaeolites on invertase production of thermotolerant strain of Kluyveromyces marxianus" (Poster presentation) Sulbha Karandikar, Snehal Pradhan, Rahela Khan, **Prashant Karandikar**, Asha Chandwadkar, Asmita Prabhune; presented in **"10$^{th}$ International FAOBMB symposium"** at I.I.Sc. Banglore in 2003.

4. "Olefin oxidation with dioxygen and isobutyraldehyde catalyzed by Cu$^{2+}$-perchlorophthalocyanine immobilized MCM-41" (Poster Presentation) **P. Karandikar**, M. Agashe, K. Vijayamohanan and A. J. Chandwadkar,  presented in **"16$^{th}$ National Symposium and 1$^{st}$ Indo-German Conference on Catalysis, IICT Hyderabad"** during 6-8 Feb. 2003.

5. "Influence of oxidising agents on product selectivity for  oxidation of alkenes using

$Co^{2+}$-perchlorophthalocyanine immobilized MCM-41". (Oral Presentation) **P. Karandikar,** A. J. Chandwadkar, M. Agashe, N. Ramgir, B. Kokate and S. Sivasanker at "**17th National Symposium on Catalysis, CSMCRI, Bhavnagar"** during 18-20 Jan. 2005.

6      "Synthesis and characterization of novel mesoporous carbon material". (Oral presentation) **P. Karandikar,** B. Kakade, A. Mitra, K. R. Patil and A. J. Chandwadkar presented at **'National workshop on Catalysis for Energy' held at BHU'** during 23-25 Feb. 2006.

### d) Patents

1.      "An improved process for acceleration of hydrolyzing enzymes and production of alcohols" Asmita Prabhune, Asha Chandwadkar, Sulbha Karandikar, Saroj Pundle, **Prashant Karandikar, Patent filed.**

2.      "An improved process for the preparation of bimodal ordered mesoporous silica materials and mesoporous carbon materials thereafter" Asha J. Chandwadkar, Mangala S. Agashe, **Prashant R. Karandikar**, Nalini Edgar Jecob, Ratnesh Kumar Jha, Subramanian Sivasanker, **Patent no. 780/Del/2005.**